UNIVERSITÉ LIBRE DE BRUXELLES

vito

Thesis manuscript submitted in partial fulfillment of the requirements for the degree of engineering sciences: scientific doctorate

Development of Innovative Solutions to Identify and Manage Low-Voltage Distribution Grid Congestion

Thesis manuscript

Lionel Delchambre

Thesis submitted under the supervision of
Prof. Patrick Hendrick [ULB - ATM Dept.]

The co-supervision of
Prof. Pierre Henneaux [ULB - BEAMS Dept.]
Dr. Ir. Hamada Almasalma [VITO - WET Dept.]
Dr. Ir. Reinhilde D'hulst [VITO - WET Dept.]

Academic year
2025

In order to be awarded the Scientific doctorate in
Electromechanical Engineering

Acknowledgment

For me, a PhD thesis is not the result of solitary work; while the doctoral researcher is the driving force, it is shaped by a network of interactions and collaborations. This manuscript is therefore the product of a collective effort, and I would like to take a moment to express my gratitude to those who have contributed, in one way or another, to its completion.

First, I would like to thank the Université libre de Bruxelles and the Belgian Federal Public Service of Economy via the *Alexander* project for funding these four years of research. My sincere gratitude goes to Patrick Hendrick and Pierre Henneaux, my supervisor and co-supervisor. I also had the privilege of collaborating with VITO, where I was co-supervised by Hamada Almasalma and later by Reinhilde D'Hulst, to whom I extend my sincere thanks for her support in the final steps. I would like to thank my supervision team for their invaluable guidance. Their support was instrumental in shaping this work and allowing me to explore directions that would not have been possible otherwise.

Furthermore, as an engineer, I deeply value the link between research and real-world applications, and I would like to thank some persons at Sibelga who helped me integrate this research into some real applications, particularly Daphné, François, Tom, and the other persons with whom I had the opportunity to collaborate. In addition, I extend my appreciation to my colleagues whose discussions enriched my research, including Frédéric, Shahab, Rober, Elise, Marien Leticia and Jean-Luc from ULB side, as well as Koen, Juliano, Anibal, and Luciana from VITO side.

To be fully honest, I must also extend my gratitude to brupower, which played a significant role in my life during my PhD. It provided me with invaluable insights into the real-world challenges of the electricity sector, helping me to confront them more practically. A special thanks to Caroline, Stan, Chloé, Jan, and Sébastien, among others, for their support and shared experiences.

Beyond the intellectual effort, a PhD is also a personal journey. I am profoundly grateful to my grandparents, whose passion for mathematics was an early source of inspiration. I also wish to thank my family and friends for their unwavering support, especially during the final stages of this work. Finally, my deepest gratitude goes to someone truly special, whose patience and steadfast encouragement helped me persevere through the pressures and time constraints of this endeavor. Thank you, Marie.

Abstract

The ongoing energy transition, driven by Europe's ambitious climate goals and the regulatory framework of the Clean Energy Package, has significantly increased the penetration of distributed energy resources and electrified loads at the Low Voltage distribution grid level. Photovoltaic panels, electric vehicles, heat pumps, and residential energy storage systems are now commonplace among Low Voltage end-users. These developments, coupled with flexibility activities newly available at Low Voltage level, such as frequency control, present both opportunities and challenges for Distribution System Operators. However, the growing complexity and unpredictability of Low Voltage load profiles pose significant risks of grid congestion, potentially jeopardizing the safe operation of the Low Voltage grid. In this context, Distribution System Operators require innovative tools to identify and manage Low Voltage congestion effectively.

This manuscript addresses this critical need by developing and applying methodologies to identify and manage low voltage congestion. The first contribution is a comprehensive framework for identifying low voltage congestion risks under specific scenarios, such as the activation of low voltage assets by flexibility service providers for frequency control services. The second contribution focuses on determining the maximum flexibility that end users can safely provide without risking grid congestion, utilizing a relaxed Unbalanced Three-Phase Optimal Power Flow model to compute Operating Envelopes. These Operating Envelopes define safe operational boundaries for Low Voltage assets while accounting for uncertainties in load profiles and network constraints.

The research finally explores two practical applications where the congestion identification framework and Operating Envelopes can be integrated into Distribution System Operators processes to improve Low Voltage congestion management. The methodologies are validated through case studies on both benchmark grids and real-world Low Voltage feeders, demonstrating the effectiveness of the proposed solutions.

The findings highlight the potential of the congestion identification framework and Operating Envelopes as robust tools to address the growing complexity of Low Voltage grid management. They enable Distribution System Operators to safely harness flexibility from end users while maintaining grid reliability. This research provides Distribution System Operators with actionable insights and scalable methodologies to navigate the challenges of a rapidly evolving energy landscape.

List of Abbreviations

ADMS Advanced Distribution Management System. 53

aFRR automatic Frequency Restoration Reserve. x, 4, 19–21, 69–72, 78–80, 117–120, 126

ARMA Auto-Regressive Moving Average. xiv, 71, 73, 75–78, 80

ASM Active System Management. 28

BFM Branch Flow Model. xiv, 37, 88, 89, 111

BFS Backward-forward sweep. xiv, 34–36, 59–61, 65–67

BIM Bus Injection Model. 37, 88

CBA Cost-Benefit Analysis. 17

CEER Council of European Energy Regulators. 11

CEP Clean Energy for All Europeans Package. 3, 4, 6, 69

CIM Current Injection Method. 34, 36

CREG Commission de Régulation de l'Électricité et du Gaz. 4

CRI Congestion Risk Identification. 21, 120, 123

DOE Dynamic Operating Envelope. xiv, 28, 31, 86, 87, 103–109, 117, 127

DSO Distribution System Operator. xiii, xv, 3, 4, 6, 9–14, 17–24, 27, 28, 30, 31, 39, 40, 42, 44, 45, 50, 53–55, 58, 67, 69, 70, 73, 75–77, 79, 80, 85, 87, 103, 113–128

E.DSO European Federations of Distribution System Operators. 28

EHV Extra High Voltage. 11

ENTSO-E European Network of Transmission System Operators. 28

EV Electric Vehicles. 5, 6, 16, 19, 45, 60, 70, 110, 118, 127

FCR Frequency Containment Reserve. x, xiv, 4, 19–21, 69–80, 117–120, 126

FRR Frequency Restoration Reserve. 20

FSP Flexibility Service Provider. xiii, 4, 5, 18, 19, 21, 30, 70, 74, 79, 114–124, 127

GIS Geographic Information System. 45

HELM Holomorphic Embedding Methods. 35, 36

HP Heat pumps. 5, 6, 16, 19, 45, 70, 127

HV High Voltage. 9–11, 18, 30, 118, 120, 123

IEMD Internal Electricity Market Directive. 4, 18, 19, 30

KCL Kirchhoff's Circuit Law. 34, 37, 44

LP Linear Programming. 37, 38, 95

LV Low Voltage. ix, x, xiii–xv, xvii, 4–7, 9–20, 22–24, 27–34, 39–47, 49, 53–55, 57, 59–63, 65–67, 69–81, 85, 86, 93, 113, 115, 117–127

MAE Mean Absolute Error. xiv, 93, 94, 97

MC Monte Carlo. xiii, 55–57, 60

mFRR manual Frequency Restoration Reserve. 19, 20

MSE Mean Squared Error. 77

MV Medium Voltage. 11, 17, 22, 28, 30, 31, 41, 42, 44, 118

NFCA Non-Firm Connection Agreement. xv, 27, 30, 31, 86, 113–124, 127

NFS Network Flexibility Study. 119–121

NLP Non-Linear Programming. 37

OC Overcurrent. xiii, 24, 26, 32, 62, 63, 77, 80

OE Operating Envelope. x, xiv, xvii, 6, 7, 27, 28, 30, 31, 85–89, 91, 93–99, 102–106, 109–111, 113–117, 120, 121, 123–127

OLTC On-Load Tap Changer. 12

OPF Optimal Power Flow. 37

OT Overloarding of transformers. 24, 29

OV Overvoltage. xiii, 23–25, 63, 70, 77, 78, 80

PCC Pearson Correlation Coefficient. xvii, 75

PF Power Flow. 24, 34, 43, 44, 59, 61, 65, 66, 71, 126

PPF Probabilistic Power Flow. xiv, 54, 59–61, 67, 71, 72

PSD Positive Semi-Definite. 38, 92

PV Photovoltaic panels. 5, 6, 16, 17, 19, 23, 27, 57, 59, 60, 70, 71, 78, 87, 103, 105, 110, 125–127

REDII Renewable Energy Directive II. 3

RR Replacement Reserve. 20

SDP Semi-Definite Programming. 37–39, 95

SLP Synthetic Load Profiles. xiii, 53, 55–57

SOCP Second-Order Cone Programming. 37–39, 86, 88, 92, 95, 111

SOE Static Operating Envelope. xiv, 28, 31, 86, 103, 104

TSO Transmission System Operator. xiii, 4, 6, 9, 11, 12, 18–21, 27, 28, 30, 69, 70, 79, 80, 85, 114, 117, 118, 120–124, 127

UTOPF Unbalanced Three-Phase Optimal Power Flow. x, xiv, 37–39, 85–88, 93–99, 102–109, 111, 126

UTPF Unbalanced Three-phases Power Flow. x, xiv, 34, 37, 39, 54, 59–62, 71, 85–88, 93–96, 98, 99, 104, 105, 109, 111, 126

UV Undervoltage. 23, 24, 32, 63, 70, 77, 80

Contents

List of Figures

List of Tables

Part I

General Introduction

Chapter 1

Context and Contributions

Contents

1.1 Context

The European energy system is undergoing a profound transformation driven by the increasing integration of renewable energy, the electrification of transport and heating, and the advancement of digitalization. These changes require substantial investments in grid infrastructure to accommodate distributed and intermittent renewable sources while ensuring the reliability and efficiency of the electricity network.

DSOs play a central role in this transformation, shifting from a passive infrastructure provider to an active system operator. Their responsibilities now include ensuring cost-effective grid utilization, integrating renewable energy sources, and enabling active customer participation in energy markets. However, this transition presents several regulatory, economic, and technical challenges that DSOs must address.

This section provides an overview of the challenges faced by DSOs, examining regulatory, economic, and technical aspects. It concludes with a summary of the key challenges currently confronting DSOs.

1.1.1 Regulatory challenges

This subsection presents the regulatory framework, focusing on the DSOs' perspective and access to flexibility activities at the distribution level. It begins with the European context, narrows down to the Belgian federal level, and then explores the specifics of the Brussels region.

From a regulatory perspective, the role of DSOs has been progressively reinforced at the European level. The Electricity Directive 2009/72/EC [8], introduced under the 3rd Energy Package [9], initially defined DSOs' responsibilities, incorporating energy efficiency, demand-side management, and distributed generation into network operation and planning.

Building on this foundation, the Clean Energy for All Europeans Package (CEP) [10], adopted in 2019, established a legal framework to facilitate the energy system transition. It emphasizes DSOs' role in maintaining long-term system reliability, integrating renewable energy, and fostering flexibility services. Key directives include:

- The second revised Renewable Energy Directive II (REDII) [11], promoting cost-effective flexibility solutions;

- The Internal Electricity Market Directive (IEMD) [12], which mandates DSOs to procure ancillary services, collaborate with TSOs, and develop transparent network plans. [1]

Additionally, the CEP established the European DSO entity to enhance cooperation among DSOs and TSOs, facilitating the integration of distributed renewable resources at the distribution level.

More recently, the REPowerEU plan [13] was launched in response to geopolitical challenges, aiming to accelerate renewable energy deployment and electrification. This plan, supported by financial and legal measures, further expands DSOs' role in ensuring efficient network operations while advancing European energy independence and decarbonization goals.

In Belgium, these European directives must be transposed at both the federal and regional levels. The federal is competent for transmission networks (above 70 kV) and nuclear matters, while the regions oversee distribution networks and the integration of new energy sources, following the regionalization established by the Special Law of August 8, 1980, as modified by the Special Law of August 13, 1988 [14].

The Electricity Law of April 29, 1999 [15], alongside the Royal Decree of April 22, 2019 [16], governs electricity transmission in Belgium, defining the responsibilities of Elia (the Belgian TSO) and the federal energy regulator, Commission de Régulation de l'Électricité et du Gaz (CREG). In 2022, CREG introduced a behavioral code [17] setting conditions for offering ancillary services. In compliance with European regulations, since October 2022, federal law grants end-users the right to valorize their flexibility, with Elia managing the necessary flexibility data [18], enabling low-voltage consumers to participate in flexibility markets.

At the regional level, the regulators Vlaamse Nutsregulator (Flanders), CWaPE (Wallonia), and BRUGEL (Brussels) define technical regulations for DSOs and market participants. These technical regulations have introduced new provisions for LV flexibility, requiring DSOs to establish functional requirements, procedures, and contracts. To harmonize regional approaches, Synergrid, the federation of Belgian electricity and gas network operators, fosters collaboration among DSOs, producing standardized documents such as the Market Guide on Flexibility [19] and the Synergrid technical regulations C8/01 [20]. However, some regional differences remain.

In the Brussels Capital Region, the ordinance of February 8, 2022 [21], grants all end-users the right to participate in flexibility markets through their supplier or an FSP. DSOs may impose restrictions based on transparent technical criteria, and end-users are entitled to compensation in cases of unjustified curtailment. FSPs must sign contracts with DSOs, and for new service points, a grid study may be required based on Synergrid C8/01.

1.1.2 Economic challenges

In power systems, various market mechanisms are established to maintain the balance between electricity production and consumption. Prior to the new regulatory framework mentioned earlier, DSOs were largely insulated from market activities. However, with the emergence of new market opportunities at the LV level, DSOs now face challenges in adapting to and integrating these market activities, particularly in leveraging LV flexibility.

This research primarily focuses on market mechanisms related to frequency ancillary services, which, as discussed in the previous subsection, are now accessible at the LV level and are undergoing harmonization at the European level [22].

Subsequent sections of this manuscript will demonstrate that these activities can significantly alter traditional load profiles, increasing both variability and unpredictability. In particular, Part II investigates the impact of frequency ancillary services on LV distribution grids, while Part III proposes congestion management mechanisms designed to function independently of specific flexibility activities.

Although LV end-users can also participate in other market opportunities—such as the Day-Ahead Market through contracts with FSPs or dynamic agreements with suppliers (e.g., the dynamic tariff introduced by Engie in Flanders in 2024), a comprehensive analysis of these impacts on LV distribution grids is beyond the scope of this work.

[1] The coordination work is currently underway. In Belgium, DSOs and the TSO are collaborating through Synergrid to define a common framework. The rules for FCR and aFRR are still under discussion: a market guide, a contract template and technical specifications, are currently available on the Synergrid website: `https://www.synergrid.be/fr/concertation-du-marche/pdg-flexibilite`.

1.1.3 Technical challenges

Demand growth

Electricity demand is expected to increase significantly due to the electrification of mobility (Electric Vehicles (EV)s) and heating (Heat pumps (HP)s). At the European level, the REPowerEU initiative aims to deploy 30 million new HPs by 2030 [23], while the EU Mobility Strategy targets the deployment of 30 million zero-emission vehicles and 3 million public recharging points to reduce CO_2 emissions [24].

In Belgium, as illustrated in Figure 1.1, a recent report from EnergyVille estimates that the total final energy demand amounts to 375 TWh per year, considering the three main consuming sectors: Industry, Transport, and Residential and Commercial. The Residential and Commercial sector accounts for 122 TWh per year, of which 42 TWh is attributed to electrical demand and 80 TWh to non-electrical demand. Projections from EnergyVille suggest that by 2050, the total final energy demand from this sector will decrease from 122 TWh to 70 TWh per year. However, the share of electricity within this demand is expected to increase from 42 TWh to 59 TWh, depending on the scenario [1].

This underscores the fact that, despite a projected decline in total energy demand for the Residential and Commercial sector, electrical demand is anticipated to grow in absolute terms.

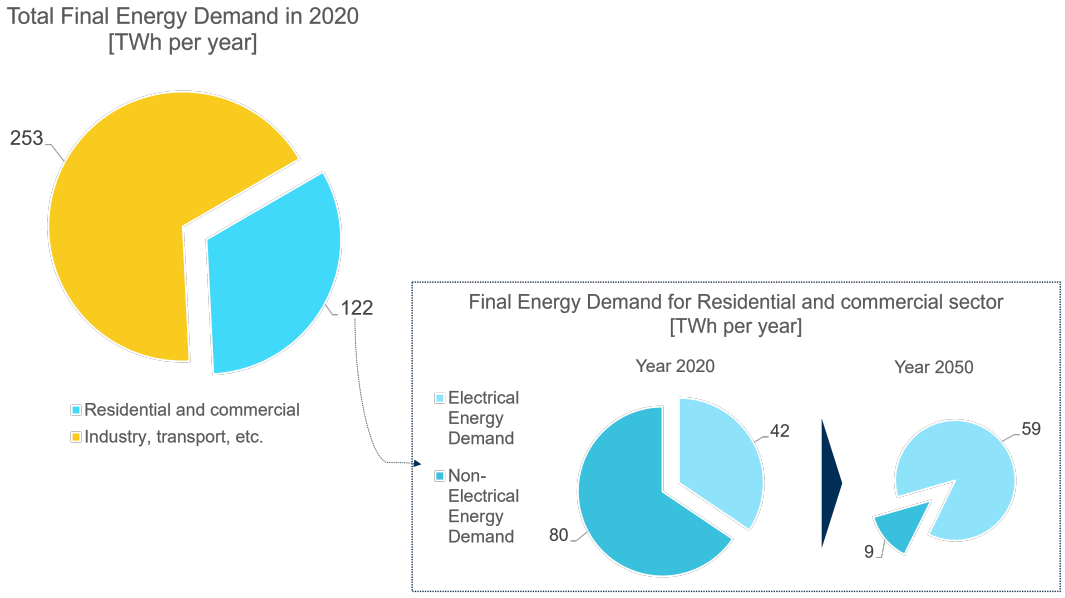

Figure 1.1: Final Energy Demand in Belgium for 2020, focus on Residential and Commercial Final Energy Demand for 2020 and its evolution towards 2050, source: [1]

Decentralization of generation and storage

Distributed generation and storage assets are becoming increasingly prevalent at the LV level, with growing adoption of residential Photovoltaic panels (PV) systems, V2G (vehicle-to-grid) technology, and home battery storage. The European Solar Rooftops Initiative mandates that all public and commercial buildings with a rooftop surface over 250 m^2 install solar panels by 2029, aiming to expand solar capacity from 260 GW to 600 GW by 2030 [25]. In Belgium, Elia reported 10.6 GWp of installed solar capacity by December 2024 [26], with EnergyVille projecting a fourfold increase by 2030 [1].

Flexibility access

Flexibility, defined as the ability to adjust consumption and production profiles, is gaining increasing relevance at the LV level. This document primarily examines how LV assets are being integrated into ancillary service market mechanisms. With more stakeholders—including prosumers, FSPs, traditional load profiles are becoming increasingly complex and harder to forecast.

1.1.4 Summary of distribution system operators challenges

At the LV distribution level (<1 kV), DSOs face multiple challenges as end-users adopt technologies such as PV systems, home batteries, EVs, and HPs. Additionally, European regulations (e.g., the Clean Energy Package [10]) enable new activities at this level, such as participation in frequency ancillary services mechanisms.

These developments modify established load profiles and introduce risks of grid congestion. Specifically, DSOs face challenges in three key areas:

1. **Regulatory and economic environment:** The emergence of new stakeholders and market activities at the LV level.
2. **Grid infrastructure:** Limited observability due to a lack of sensors (e.g., smart meters at transformers or end-users) and incomplete grid topology data.
3. **Load profile evolution:** Increased variability due to electrification, decentralization, and consumer-driven flexibility.

1.2 Scope and objectives

In that context, this research focuses on developing tools to assess and manage congestion risks in LV distribution grids, particularly in the context of increasing flexibility activities. The work is structured around three key objectives:

1. Impact Analysis of New Activities on the LV Grid - The first objective is to evaluate how emerging market activities, such as the participation of LV assets in frequency ancillary services, as enabled by the CEP [10], impact the LV distribution grid. This includes identifying potential congestion risks that arise when multiple end-users provide network services through aggregators. This objective will be addressed in Part II of this manuscript.
2. Calculation of Dynamic Grid Constraints Considering Load Uncertainty - The second objective is to determine the maximum flexibility that can be safely activated at the LV level while accounting for probabilistic load profiles and network constraints. Rather than simply identifying congestion risks, this phase integrates congestion as a constraint, ensuring that end-user flexibility remains within safe operational limits. This objective will be addressed in Part III of this manuscript.
3. TSO-DSO Integration and Market Design - The final objective explores the interaction TSOs and DSOs to develop mechanisms that maximize flexibility while maintaining secure grid operation. This involves incorporating the insights from the first two objectives into a market framework that enables dynamic pre-qualification of LV assets, ensuring congestion-free participation in flexibility markets. This objective will be addressed at the end of Part III of this manuscript.

1.3 Structure of the thesis

The remainder of this thesis is structured as follows:

- **Chapter 2** provides background on key concepts, including the characteristics of LV distribution grids and associated congestion challenges.
- **Chapter 3** presents the network models used as case studies throughout the manuscript.

Part II focuses on congestion identification and impact analysis:

- **Chapter 4** reviews methods for identifying congestion in LV distribution grids.
- **Chapter 5** examines the impact of LV assets providing ancillary services on the LV distribution grid.

Part III explores congestion management strategies:

- **Chapter 6** introduces the concept of the OE, a tool for preventing congestion in LV distribution grids.

- **Chapter 7** investigates specific applications of OE for LV congestion management, considering both market-based approaches and bilateral connection agreements.

Finally, **Chapter 8** concludes the thesis, summarizing key findings and outlining future research directions.

Chapter 2

Introduction to Low Voltage Distribution Congestion

Contents

This research focuses on tools for identifying and managing congestion at LV distribution level. This chapter deepens the key concepts discussed throughout the manuscript. It is organized into four main sections: the first section presents the characteristics of LV distribution grids ; the second introduces the concept of congestion as defined in this research ; the third provides an overview of the models utilized in subsequent parts of the manuscript; and the final section concludes the chapter.

2.1 The low voltage distribution grid today

Power systems are traditionally designed with a hierarchical structure. A High Voltage (HV) transmission grid connects centralized, geographically dispersed generation power plants to demand hubs such as urban areas or industrial hubs. At the interface with these demand hubs, the transmission network connects to lower-voltage networks, known as distribution grids, to distribute electricity directly to all end-users. These distribution grids, in contrast to transmission grids, have distinct structural features.

Understanding these differences is essential, as TSOs have developed active grid operation practices over several decades. In contrast, DSOs have historically had little need to actively manage their distribution networks—particularly at the LV level. This need has become increasingly urgent, as emphasized in the introduction, due to the new European regulatory framework and the anticipated changes in LV load profiles. Recognizing the distinctions between HV transmission grids and European LV distribution

grids is key to assessing which operational methods can be transposed from HV to LV. It also helps identify areas where further development is required to address the specific characteristics of LV distribution systems.

Key differences between LV distribution and transmission grids are outlined in Table 2.1. These differences will be elaborated upon in the following subsections. Specifically, the discussion will address: the general configuration and voltage levels of LV distribution grids, their components and the earthing configuration, the loads and their phase connections, and finally, the level of observability in LV distribution grids.

Criteria	Transmission grid	EU LV Distribution grid
General configuration	Meshed	Radial
Voltage level	36-400 kV	Hundreds of V
Impedance	$\frac{X}{R} >> 1$	$\frac{R}{X} \approx 1$, $\frac{R}{X} > 1$
Phase connection	Balanced three-phases delta and wye	Unbalanced delta/wye single, three or tetra-phases[2]
Earthing connection	Solid/Impedance grounding	TT mainly, IT, TN [1]
Load	Centralized	Widespread, highly stochastic, non-coincident
Visibility and observability	High	Low

Table 2.1: Comparison between Transmission grid and LV Distribution grid

The focus of this research is primarily on the European context, with particular attention given to Belgium and the Brussels region. Distribution network characteristics and challenges in other regions of the world fall outside the scope of this research.

2.1.1 General radial configuration and voltage levels

LV distribution networks generally have a radial configuration, in contrast to the meshed structure of HV transmission grids. Additionally, they consist of multiple lower voltage levels. This specific configuration and voltage levels not only influence the models used to represent the grid but also influence the choice of analytical tools employed to analyze electricity flows in this research.

Grid configuration

The Figure 2.1 shows the difference between meshed and radial configurations, respectively for HV transmission grid and distribution grid. In meshed grids, buses can be connected to multiple parent buses, whereas in radial configurations, each bus is connected to only a single parent bus. The parent bus refers to the upstream bus that is closer to the feeder's origin, typically the transformer.

In Brussels, to ensure redundancy during maintenance or in the event of damage, the MV feeders are configured in a loop. They originate from one secondary substation, connecting several MV/LV substations and ending at another secondary substation (not represented on the Figure). However, the network remains radial rather than meshed, with a single switch that opens the loop.

Similarly, LV feeders are also configured mainly radially. This radial configuration is a distinguishing characteristic of distribution networks. This important distribution characteristic will orient the choice of some models in the part 2.3.1, specifically regarding the Power Flow or Optimal Power Flow calculations. Throughout the remainder of this document, the term *feeder* will exclusively refer to LV feeders.

Distribution network categories

The DSO Observatory report [27] segments DSO into four categories based on the area covered, energy density, and number of customers. These characteristics, as defined in the report, are summarized in Table 2.2.

These categories are important because congestion behavior can vary across distribution grids depending on the type of DSO. This research will focus on grids operated by Urban DSO, as exemplified by

[1] The TT meaning will be further described in subsection 2.1.2

[2] Sibelga is naming tetra-phases a wye three-phases

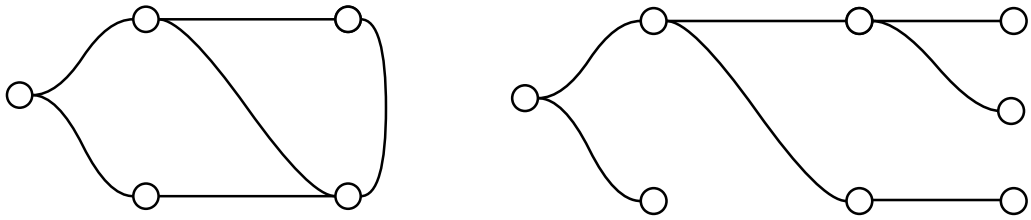

(a) Meshed HV configuration (b) Radial LV configuration

Figure 2.1: Illustration of meshed configuration for HV transmission grid and radial configuration for LV distribution grid

the Sibelga case study, as well as grids operated by Small and Medium DSOs for the benchmark analysis. The specific grids used as case studies will be detailed in Chapter III.

DSO category	Area $[km^2]$	Energy density $[GWh/km^2]$	Customers $[10^6]$
Small	> 1000	≤ 10	≤ 1
Medium	> 1000	≤ 10	> 1 and ≤ 10
Urban	≤ 1000	> 10	-
Big	> 1000	-	> 10

Table 2.2: DSO categories

Voltage levels

Regarding the voltage levels, the Council of European Energy Regulators (CEER) conducted a benchmark to identify how grids are designed across Europe [28]. The report highlights that Distribution grids include some of the four following voltage levels: LV, Medium Voltage (MV), HV and Extra High Voltage (EHV). These voltage levels can have different meanings across European countries.

For example, the British distribution networks consists of three voltage levels: LV ranges from 230V and 1.1kV, HV from 1.1kV up to 20kV and EHV reaching 132kV is still considered part of the distribution grid. In addition, voltage limits between transmission and distribution networks can sometimes become indistinct: for example in Belgium, part of the HV distribution grid can reach higher voltage limit (70kV) than the minimum voltage level managed by the TSO, which is 30kV.

Figure 2.2 displays a representation of the Brussels distribution grid. The interface between TSO and DSO is represented in black and operates mainly at 36kV. The distribution grid consists of two voltage levels: HV mainly set at 11kV represented in red and LV mainly set at 230V represented in blue.

2.1.2 Main components located on low voltage grid

The main components of the distribution grid structure are shown in Figure 2.2, that is aligned with reference book [4] and based on discussions with several European DSOs. These components are presented as they will be modeled in the subsequent chapters to study congestion on LV distribution grids.

Figure 2.2 shows the transformer interfacing the TSO and the DSO, which in this Brussels case is owned by the TSO. This transformer is connected to a secondary substation from which several MV feeders can originate. In the Figure, only one MV feeder is represented, connecting sequentially three MV/LV substations. An MV/LV substation can be either a customer substation, connecting for example a residential building or a big school, or a network substation. Several LV feeders leave from such network substation to connect homes, small apartments or small businesses. For each building, there is one connection point which can possibly connect several end-users if the building is divided into several entities.

In addition, there are three complementary components that are not represented on the figure:

- Protection - Substations must be protected against short-circuits. Traditionally, transformers are equipped with fuses on the HV side, and eventually a fuse for each feeder.

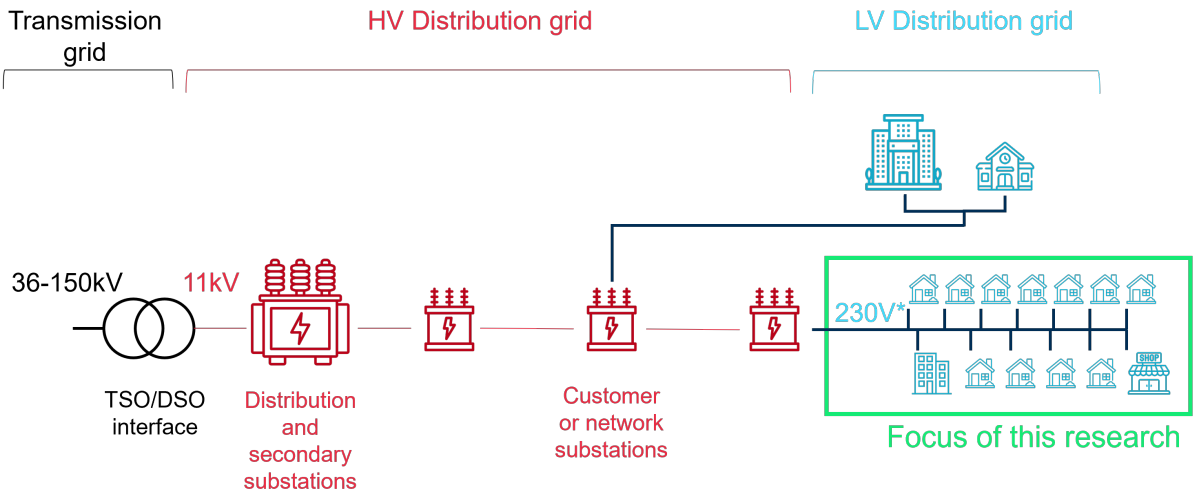

Figure 2.2: Simple distribution network representation

- Voltage regulation - Some transformers can be equipped with a voltage regulator to adjust the voltage based on the load on the feeder. These regulators can adapt voltage either at the high-voltage or low-voltage side, usually in incremental step of voltage. Transformers with On-Load Tap Changer (OLTC) can automatically adjust voltage in response to load variations.

- Metering - Each substation can be equipped with measurement devices to monitor physical parameters such as power, voltage or current.

Voltage regulation and metering are not represented on the figure because they are not yet fully implemented in Brussels. OLTCs, for instance, are more expensive than standard transformers, and the load evolution or voltage drop in the region has not justified their installation. In Wallonia, when overvoltage occurs, the Walloon DSO, ORES, deploys technical teams to manually adjust the voltage on the LV winding (decreasing voltage in April and increasing it in October).

To provide context, in Brussels in 2022, there are 46 TSO/DSO interfaces, 80 secondary substations, 5762 MV/LV substations, 215 980 connection points and 678 559 active end-users [29]. Regarding the metering, in 2023, Sibelga has installed 400 voltage meters on MV/LV substations and 150 current meters. For protection, substations are secured against short circuits, and each feeder is equipped with its own fuse.

Low voltage feeders

LV feeders configurations, material and sizes are highly heterogeneous, as they were implemented over several decades, during which technologies and DSO strategies evolved. For example, in the Volta neighborhood in Brussels, named after one of the city's first municipal power plants, the DSO still manages copper wires insulated with oil-impregnated paper that have never been replaced since their installation.

Each LV feeder consists of multiple conductors, as illustrated in Figure 2.3. Typically, there is one conductor per phase. Additionally, an LV feeder may include a neutral conductor (depending on the load and earthing configuration), a dedicated conductor for public lighting, and, in some cases, a mechanical support conductor.

Regarding the cables characteristics, data such as length, ampacity, or impedance are typically available or can be derived from technical datasheets as it will be explained in Section 3.2. However, determining the series impedance is a crucial step for conducting further analyses. The series impedance of a distribution line comprises the conductor resistance and inductance. The inductance of a specific conductor includes two components: its *self-inductance* and the *mutual inductance* with the other conductors in the system.

For LV feeders, the resistive effect of the lines generally dominates. Sibelga provided data on the most commonly used cable types, and their X/R ratios are presented in Table 2.3. This will influence the choice of models as described in 3.2.

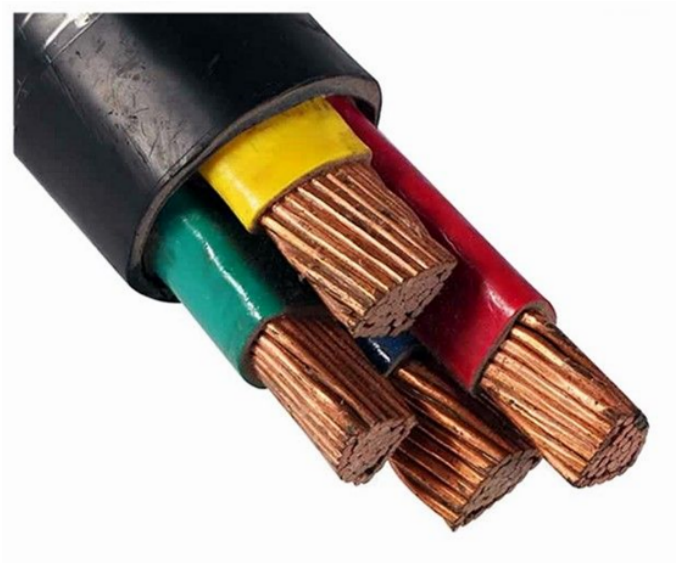

Figure 2.3: Picture of a LV feeder with four conductors extracted from lecture [2]

Cross-section-[mm^2]	R/X ratio for copper	R/X ratio for aluminium
10	13.06	18.62
16	8.86	12.47
25	5.99	8.38
35	4.56	6.39
50	3.59	5.04
70	2.62	3.66
95	1.94	2.72
120	1.58	2.21
150	1.31	1.84
185	1.08	1.51
240	0.83	1.17
300	0.68	0.96
400	0.55	0.76

Table 2.3: R/X ratio for Sibelga LV feeders

Phase connections

As illustrated previously, a LV feeder consists of several conductors for the different phases. At LV level, households or small buildings can be connected to a single-phase or to all three-phase, based on the strategy of the DSO. This leads to unbalanced power flowing through the different phases.

For transmission lines, two simplifying assumptions are commonly made:

1. The phases are considered equally loaded and balanced.

2. The lines are transposed (each phase occupies the same physical position along the structure for one-third of the line's length).

These assumptions allow the combination of self- and mutual impedance into a single-phase inductance. This will be further detailed in Section 3.2. In that context, a single line-to-neutral equivalent circuit can be used to model the HV segment line.

In contrast, LV distribution systems consist of three-phase lines connecting unbalanced loads. This results in different current flows through the conductors which can be attributed to several factors: a high number of houses or commercial building connected to a single phase, unbalanced loads behind the meter for end-users connected to all three phases and non-coincident load profiles among these end-users. Consequently, self- and mutual impedances must be computed for each individual wire and the simple single-line model cannot be used.

The model for calculating the series impedance matrix and reducing it is developed in more detail in the following section developing the grid data model.

When end-users are connected to a single phase, DSOs typically aim to distribute the load evenly across phases to reduce this unbalance effect. For instance, DSOs such as Sibelga use the *1-2-3 rule*, where the first house is connected to phase 1, the second to phase 2, the third to phase 3, and the fourth house is connected back to phase 1.

Another important characteristic of LV-level distribution grids is their phase connection configuration. These connections can be set up in either a wye configuration, commonly used across Europe, or a delta configuration, which is more prevalent in Brussels.

As illustrated in Figure 2.4, the wye connection (left) links each phase to the neutral. For instance, an end-user connected to a single phase a would be connected between phase a and the neutral. In contrast, the delta connection (right) does not include a neutral, so an end-user connected to a single phase would be connected between two phases, such as a and b. The implications of these configurations will be discussed further in the modeling section of this chapter.

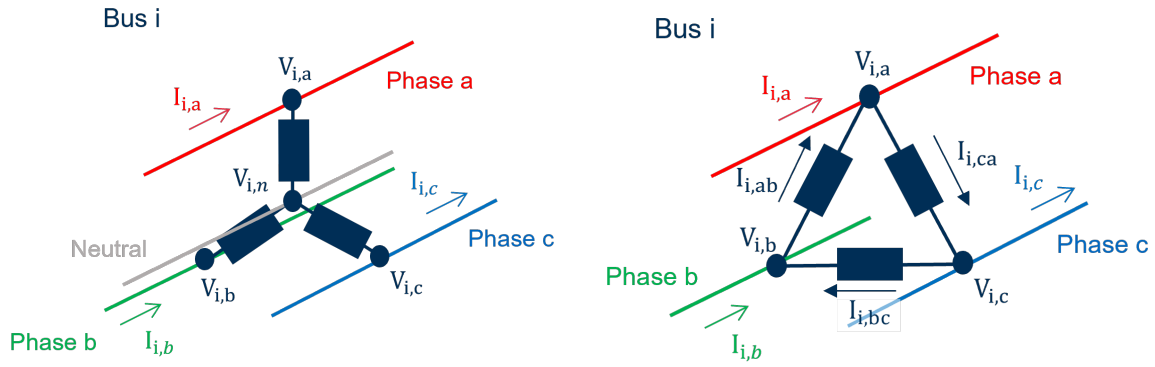

(a) Wye connection (b) Delta connection

Figure 2.4: Illustration of wye and delta connections for a single bus i, showing associated voltages and currents

Finally, when DSOs connect new households to the grid, they often do not keep track of which house is connected to which phases. This practice stems from the *fit-and-forget* approach, where DSOs focus on the immediate connection of new loads without monitoring their impact on phase balancing. In this approach, DSOs typically open the street, connect the household to a available cable, using for instance the *1-2-3 rule* for single-phase connection, and then close the street, without systematically recording phase assignments. This method was historically sufficient, as network planning was performed at the substation level, ensuring that each substation could distribute a predefined number of houses with an approximately balanced phase distribution.

However, due to this lack of tracking, the conventional *1-2-3 rule* may not always be consistently followed when integrating new single-phase connections. Over time, this can lead to unintentional phase imbalances, potentially impacting voltage stability, increasing losses, and exacerbating congestion issues at the low-voltage distribution level.

Earth connection

In power systems, regardless of voltage level, two key aspects of earthing must be addressed: (1) neutral earthing (how the transformer or generator neutral is connected to the earth) and (2) protection earthing (how equipment frames are connected to the earth) [30], [31], [32]. Earthing schemes are classified using two letters:

- Transformer Neutral Connection: T (neutral is directly connected to the earth) and I (neutral is isolated from the earth).
- Equipment Frame Connection: T (directly connected to the earth) and N (connected to the neutral, which is earthed at the installation origin).

The International Electrotechnical Commission (IEC 60364 [33]) standard defines three configurations for LV distribution networks based on these classifications, enumerated hereafter and are illustrated in Figure 2.5 (for TT and IT configuration).

1. TT - The transformer neutral is directly earthed at the head of the feeder, equipment frames and end-users are earthed locally without connection to the neutral. It requires multiple earthing points for protection, increasing construction costs. It is common in systems with distributed equipment (e.g., street lighting, billboards).
2. IT - The transformer neutral is not earthed or is indirectly earthed (via a high impedance), and equipment frames are earthed locally. It requires an overvoltage limiter to prevent overvoltage transmitted by the primary winding of the transformer to LV windings. It is suitable for systems needing high reliability and safety (e.g. hospitals, mines). It does not support steady single-phase voltage under all conditions.
3. TN - The transformer neutral is directly earthed and equipment frames are connected to the neutral via conductors.

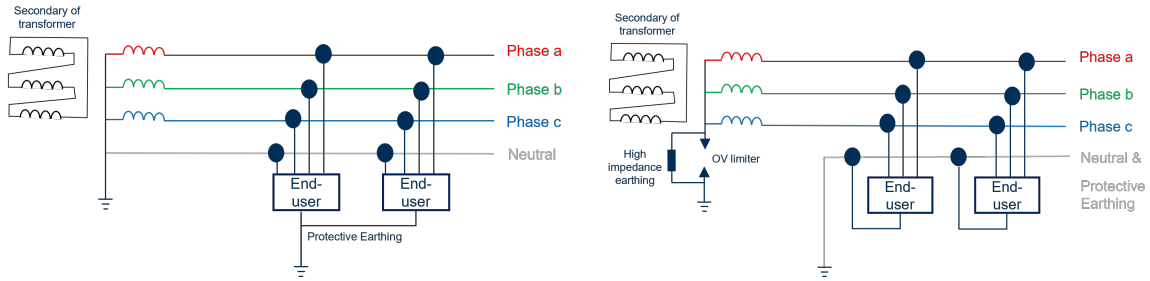

(a) TT configuration (b) IT configuration

Figure 2.5: TT and IT earthing schemes

In general, TN and TT schemes are most applied in LV distribution grid for single phase power supply [31], with TT earthing that is predominant in Europe. LV earthing systems for some European countries are listed in Table 2.4 [6].

It is important to emphasize that in TT configuration, mainly used in Europe, neutral is earthed at the head of the feeder. This will be important for grid modeling in the following sections.

Countries	LV earthing system
Belgium (230/400V)	TT
Spain (230/400V)	TT
France (230/400V)	TT
Italy (230/400V)	TT
Norway (230/400V)	IT
Portugal (230/400V)	TT

Table 2.4: LV earthing system for some European countries [6]

2.1.3 Stochastic and non-coincident low voltage loads

Historically, the modeling and analysis of individual LV load profiles were not of primary concern, as aggregated load profiles were generally sufficient for tasks such as network planning and capacity assessment [34]. In these cases, the stochastic behavior of individual loads was typically addressed through the use of a *simultaneity factor*, which accounted for the likelihood that not all consumers would simultaneously demand electricity at peak times.

However, with the growing emphasis on congestion management and grid optimization at the LV distribution level, the traditional approach of aggregated load profiling is no longer sufficient. The increasing complexity of energy systems, driven by the deployment of new technologies and shifting

consumption patterns, necessitates a more detailed and accurate understanding of individual LV load profiles. As a result, it becomes critical to account for the specific characteristics of each individual end-user's consumption and production patterns to address localized grid constraints effectively.

As outlined in the introduction, the deployment of distributed energy resources and new technologies, such as EVs and HPs, is contributing to the growing stochasticity of LV loads, while residential PV systems increase simultaneity pattern. As more prosumers (consumers who also produce energy) become integrated into the grid, their behavior introduces additional uncertainty in both energy consumption and production. The flexibility provided by these new assets, which can adjust their load profiles in real-time, adds an additional layer of variability to the system. This flexibility leads to both spatial and temporal fluctuations in the load profiles of individual households or small buildings.

Spatial stochasticity refers to the variations in load profiles across different locations within the same grid. For instance, one household may choose to use high-power appliances such as an oven or a dryer at a particular time, while a neighboring household may not. These discrepancies are further exacerbated by factors like household size, appliance usage patterns, and the presence of prosumers with PV systems or EVs.

On the other hand, temporal stochasticity is the variability in load patterns over time. This variation can occur not only throughout the day but also from one day to the next, influenced by external factors such as weekday versus weekend consumption habits, holiday seasons, or even evolving societal trends like the rise of remote working. For example, a household's electricity consumption may be higher on weekdays due to work-related activities, but it may drop on weekends when fewer appliances are used.

The increasing presence of stochasticity in LV load profiles significantly complicates grid operations and forecasting. As individual consumption patterns become less predictable and more diverse, the challenges of congestion management and grid optimization intensify. The integration of these more flexible and decentralized energy resources, combined with the growing influence of prosumers, makes it increasingly difficult to rely on traditional, aggregated models. Instead, detailed, individualized load profiles that account for both spatial and temporal variability are required for accurate assessments and efficient grid management.

These stochastic effects are illustrated in Figure 2.6. Spatial stochasticity is highlighted by comparing the blue and red curves, which represent the distinct consumption patterns of two different end-users. Temporal stochasticity is observed when examining a single curve over two consecutive days, showing variations in energy usage from one day to the next, even for the same consumer.

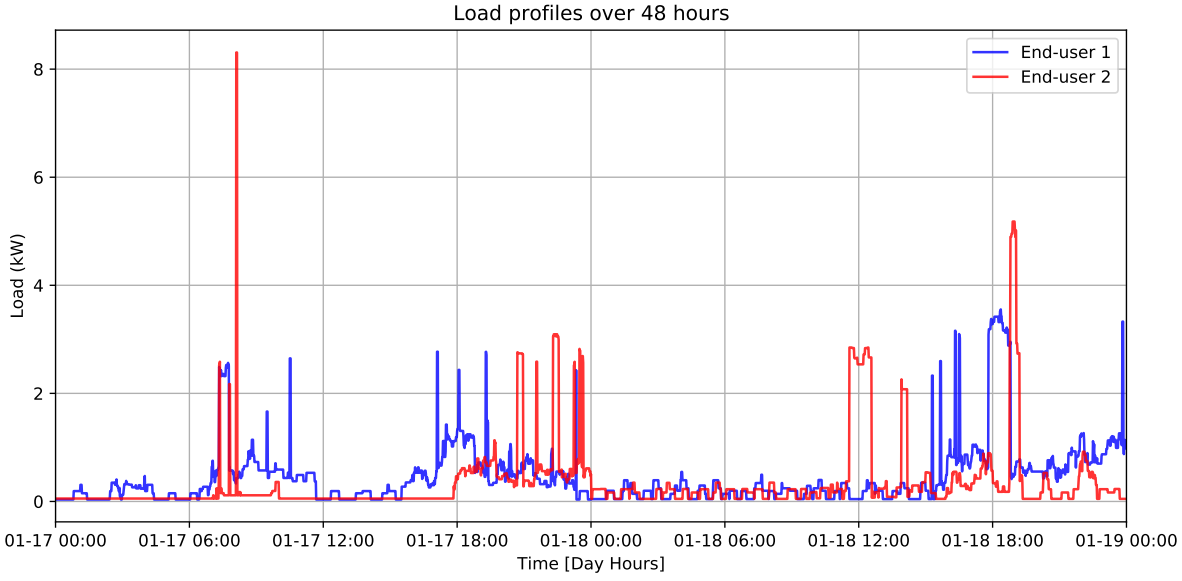

Figure 2.6: Load profiles of two end-users along two days from [3]

2.1.4 Unbalanced distribution grid

For the purposes of this manuscript, the term *unbalanced* will refer to the disparity in current or power flow among the different phases. This characteristic is fundamental, as its consideration complexifies the

models used to analyze congestion on the LV distribution grid. However, as will be presented in subsequent chapters, the simplifying assumptions typically applied to transmission lines, as presented earlier, do not hold for LV distribution grids.

Several factors contribute to the unbalanced current flowing through the conductors:

1. Typology evolution - When DSOs connect new households to the grid, they may not keep track of which house is connected to which phases due to the *fit-and-forget* approach. As a result, the *1-2-3 rule* may not be consistently followed when adding new single-phase connections.

2. Heterogeneity of load profiles - LV end-users often have varied assets, and these assets are distributed unevenly along the feeder. This variation in load profiles can lead to unbalanced power flow across phases. For instance, the installation of solar panels may depend on factors such as household investment capacity, roof ownership, or orientation. If only one house out of three installs solar panels, the electrical production will be injected in an unbalanced manner onto the grid.

3. Non-coincident load profiles - Since LV end-users do not consume power simultaneously, the power flow across different phases of the feeder becomes unbalanced due to non-coincident load profiles.

2.1.5 Data availability: visibility and observability

Visibility for grid data

Historically, DSOs have connected households and buildings using the *fit-and-forget* approach. This strategy involved installing lines, opening streets for underground installations, connecting houses to different phases as outlined above, and then closing the streets without maintaining detailed records. This approach was sufficient at the time, as ensuring the transformer was adequately sized for the load reliably prevented grid damage. However, it resulted in low grid visibility. In many cases, there are no clear records of which house is connected to which phase, feeder, or even MV/LV substation if switches status are unknown.

Throughout the remainder of this document, the term *lack of visibility* or *topological unawareness* will refer to the lack of data available on grid configuration. The grid is described as having low visibility when its configuration is not well known. Full visibility implies that the grid configuration, including phase connections, is completely known.

Observability for measurement data

Smart meters, in this research, refer to devices installed at end-user premises, distinct from the metering equipment described earlier as part of the distribution network components. These meters provide detailed end-users measurements of electricity consumption and, in some cases, production (e.g., from PV production).

The deployment of smart meters is driven by two EU Directives mentioned in the introduction: (EU) 2009/72/EC [8] and 2019/944 [12]. Briefly, Directive 2019/944, Article 19, paragraph 2, mandates that EU Member States must ensure a smart meter roll-out if a Cost-Benefit Analysis (CBA) proves favorable. If the CBA is positive, Member States are required to achieve 80% smart meter deployment. According to the DSO Observatory 2022 [27], as of 2022, 45% of Member States had completed a full roll-out.

Smart meters are expected to enhance decision-making and optimize grid operations by enabling functionalities such as congestion identification and management [27]. They measure a variety of electrical parameters, typically at intervals ranging from 1 to 15 minutes, depending on the regulatory framework and the technical capabilities of the meters.

The key data points collected by smart meters could include: active power consumption and injection, reactive power measurement or voltage and frequency monitoring, crucial for detecting anomalies and maintaining grid stability.

In Belgium, the CBA for smart meter deployment yielded inconclusive results, leading to delays in implementation. Unlike some EU countries that pursued an aggressive roll-out, Belgium adopted a phased approach, prioritizing installations for specific consumer groups, such as prosumers, high-consumption households, and newly built or renovated homes.

In Brussels, approximately 65,000 smart meters have been installed so far, with a goal of reaching 80% deployment among end-users by 2030 [35]. However, data collection granularity remains relatively low, typically in daily or 15-minute intervals, depending on the meter type and consumer contract.

The delayed and fragmented roll-out of smart meters in Belgium, and more specifically in Brussels, has significant implications for DSOs, as limited data availability hampers their ability to monitor and manage the grid effectively.

In this research, this lack of access to measurement data is referred to as *low observability*. Low observability can arise from various factors, including incomplete smart meter deployment, regulatory constraints on data access, or the absence of monitoring devices at critical network points.

2.1.6 Overview of Flexibility value chain Relevant to This Research

As outlined in the introduction, new activities are emerging in the LV distribution grid, and an increasing number of stakeholders are seeking access to flexibility from LV assets. This section provides a brief overview of the key stakeholders relevant to this research, including end-users and energy communities, system operators and FSPs. It also summarizes the sources of flexibility available at the LV level and presents a simplified overview of the flexibility services considered in this study.

The flexibility value chain is generally illustrated in Figure 2.7, focusing on the perspectives of DSOs and TSOs, while end-users and energy communities are not specifically categorized under the beneficiaries column. This reflects the focus of this research on the impact of flexibility on system operators. However, this general representation does not explicitly depict the specific relationships between the FSP, DSOs, and TSOs.

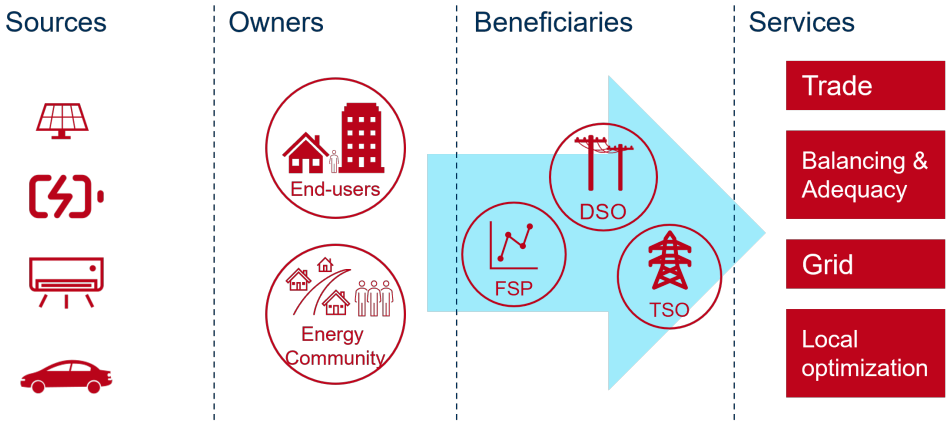

Figure 2.7: Flexibility Value Chain with Key Market Stakeholders and Flexible LV assets Relevant to this Research

Key Market Stakeholders

The European energy market design defines several distinct roles in the IEMD [12]. This research focuses on the roles illustrated in Figure 2.8, which are selected for their relevance to the objectives of the study. The roles are further defined based on European definition.

Figure 2.8: Market stakeholders considered in this research: TSO, DSO, FSP, TSO, end-users and energy community

- System operators: DSOs are responsible for operating and maintaining the distribution network as defined in this chapter, ensuring a reliable power supply and integrating decentralized energy resources. TSOs manage the HV transmission network, balancing electricity supply and demand in real time and ensuring system stability.

- FSP: A market participant that aggregates, manages, and trades the flexibility of distributed energy resources, including demand-side response, energy storage, and distributed generation. In this research, the focus is on the provision of frequency control to system operators. The role of the FSP, as considered here, combines the functions of an Aggregator and a Balancing Service Provider, following the framework established by USEF [36].

- LV end-users: Residential, commercial, or small industrial consumers connected to the LV distribution grid. They consume electricity and, in some cases, generate energy (e.g., via PV) and can provide flexibility services through demand response or energy storage. They include the *customer*, *active customer*, *final customer* as defined in IEMD if connected to the LV Distribution grid.

- Energy communities represent a new type of entity introduced by the IEMD, characterized by specific membership structures, governance rules, and objectives. They are governed by a defined set of principles and can engage in various activities, including the provision of flexibility services.

Flexible LV assets

This research focuses on the LV distribution grid and, accordingly, on the owners of flexible assets connected at this voltage level — namely, households and small to medium-sized enterprises.

The flexibility originates from distributed energy assets, already mentioned in the introduction, which are being promoted at the European level to support decarbonization goals. While these assets contribute to decarbonizing sectors such as heating and mobility, they can also provide valuable flexibility services to the grid. In particular, the LV assets considered in this study include photovoltaic systems (PV), electric vehicles (EV), heat pumps (HP), and residential batteries, all of which are increasingly present in the LV distribution grid, as outlined in the introduction.

Although it is important to accurately identify and model the various LV assets providing flexibility, from a DSO perspective, it is also necessary to assess whether detailed modeling is truly required. The DSO is responsible for the deployment and operation of the grid up to, but not beyond, the smart meter; the management of assets behind-the-meter, owned by end-users or energy communities, lies outside the DSO's scope. As such, congestion management solutions should be designed to be applicable even when the DSO does not have direct control over, or observability of, these assets. This approach defines the concept of technology-neutrality discussed in Chapter 7: if a congestion management method does not require data from behind-the-meter assets, it can be considered technology-neutral.

Flexibility services and focus on frequency control

Flexibility can be utilized to provide a variety of services, including:

- Energy trading services, where stakeholders buy and sell energy across different energy markets (e.g., Day-Ahead, Intraday, Imbalance markets);

- Balancing and adequacy services, such as the provision of FCR, aFRR, manual Frequency Restoration Reserve (mFRR), or participation in mechanisms like capacity reserves;

- Local optimization services, aimed at increasing self-consumption within a specific area — ranging from individual households through Home Energy Management Systems (HEMS) to larger-scale initiatives like neighborhood or regional energy sharing via energy communities;

- Grid support services, helping maintain system stability through congestion management, voltage control, or specialized services like black start capability, which enables system restoration following a blackout.

As illustrated in Figure 2.9, this research primarily focuses on balancing services. These services are provided to TSOs to ensure secure network operations. A key point to note is that, although LV assets are located within the distribution grid operated by DSOs, the primary beneficiaries of the balancing services are the TSOs (and, to some extent, the FSPs). These services are mainly supplied by third parties but can also be delivered directly by TSOs themselves via topology changes or integrated network components.

Among these services, there are balancing or frequency services. Frequency services, defined as reserves and procured in the Continental European common market [37], are detailed below:

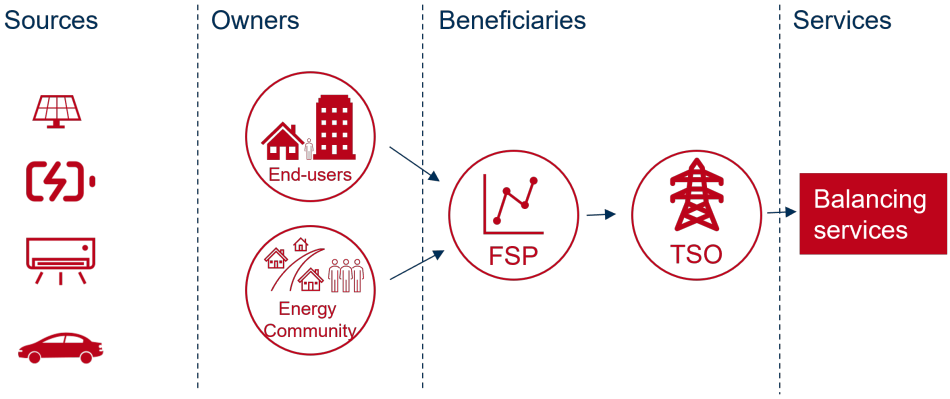

Figure 2.9: Value chain for LV assets providing frequency control

- **FCR** – Activated within 30 seconds to stabilize the grid frequency. Flexible assets participating in FCR adjust their output power in proportion to the frequency deviation from the nominal 50Hz (in continental Europe). The maximum power is activated when the deviation reaches a predefined limit (200mHz in continental Europe), and activation must occur within 30 seconds till the subsequent reserve is activated[1]. A deadband of 10mHz is defined to avoid excessive activation around the 50Hz setpoint.

- **Frequency Restoration Reserve (FRR)** – Activated more gradually to restore the frequency to 50Hz within 5 minutes for aFRR[2], and within 15 minutes for manual mFRR. These are asymmetric products, meaning assets can separately contract to either inject or consume electricity. In Belgium, aFRR is designed as a daily product with activation over specific 4-hour periods, defined from t_{start} to t_{end} [38]. In this manuscript, specific [38] products are identified using a letter (P or N) to indicate whether the product is for injection or offtake, respectively, followed by a number (1 to 6) representing the product period. Period 1 spans from midnight to 04:00, while Period 3 covers 08:00 to 12:00. For example, submitting an asset for Period P4 means the asset may be activated for injection between 12:00 and 16:00. An important constraint for flexible assets with limited reservoirs providing FRR for Elia is that the aggregator must ensure full activation of the contracted power throughout the entire 4-hour period [38]. This can be managed in two ways: either the aggregator limits the maximum power based on the available energy per asset, or it activates full power for FRR and, once the reservoir is depleted, shifts activation to other assets within its portfolio.

- **Replacement Reserve (RR)** – Some European TSOs procure additional slower reserves, known as Replacement Reserves, to support or relieve FRR activation.

This research focuses more specifically on FCR due to its fast and automatic activation and on aFRR due to its relatively fast activation and significant procurement volumes (which are approximately ten times larger than those for FCR). Additionally, FCR and aFRR are particularly relevant because they are the first reserves being opened to LV assets. The Commission Regulation 2017/2195, art. 15 [22], encourages TSOs to cooperate with DSOs to facilitate the provision of these reserves where relevant.

European member states are currently implementing mechanisms to allow LV assets to provide FCR and FRR. For instance, in Belgium, LV assets have been eligible to provide FCR since 2022, and discussions regarding aFRR participation are ongoing. As of now, Belgium's available FCR capacity reaches 87 MW, with 6 to 8 MW already provided at the LV level, while aFRR capacity reaches 145 MW [39].

Other reserves, such as RR or faster reserves like the fast frequency reserve implemented in Nordic countries, are not considered in this research.

Similarly to the discussion on ensuring that congestion management mechanisms are technology-neutral, it may also be necessary to develop congestion management approaches that are independent of the specific type of flexibility service used. This would enhance the robustness of the congestion

[1]Subsequent Section 2.2 highlights that congestion is typically assessed over a 15-minute timeframe. However, more *instantaneous* variations in power flows can also lead to voltage congestion. As a result, assets activated as part of the FCR, even if their activation lasts less than five minutes, remain important to consider in the analysis.

[2]The full activation time for aFRR was reduced from 7.5 minutes to 5 minutes on December 4th, 2024, by Elia: `https://www.elia.be/en/electricity-market-and-system/system-services/keeping-the-balance/afrr`

management solutions. In this research, such approaches are referred to as flexibility service-neutral mechanisms, as discussed in Chapter 7 and in the conclusion.

Simplified market process for FCR and aFRR

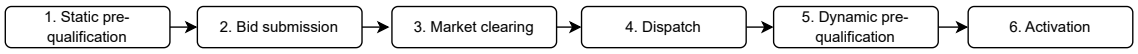

Figure 2.10: Relevant steps on FCR and aFRR design

Figure 2.10 present the six steps for FCR and aFRR design that are relevant for this research. Each step is based on Elia's process, but aligned with European harmonization of frequency control. Each step is further described below with the current roles for market stakeholders.

1. Static pre-qualification [40, 41, 42] - The asset undergoes technical testing to ensure it meets the performance criteria for providing FCR. This includes verifying the asset's response time, capacity, and ability to maintain frequency stability. This step aims to establish whether the asset can reliably provide FCR services over the long term. The FSP submits documentation and undergoes testing coordinated by the TSO.

2. Bid submission [41, 42] - The FSP submits offers to the balancing markets, detailing the reserve capacity they can provide [MW] and their bid price [€ per MW]. The TSO is in charge to operate the market platform, while the FSP submit bids within market deadlines.

3. Market clearing [40, 43] - The TSO evaluates all bids and selects the most cost-effective ones to meet the system's requirements. Selected bids are awarded contracts. This step aims to secure the reserves at the lowest price while maintaining grid reliability.

4. Dispatch [43, 41, 42] - The TSO notifies the FSP that their asset must maintain availability during the specified operating period. No energy is yet delivered; the asset remains on standby. For aFRR, the volumes dispatched can be activated for other purposes like redispatching in case of imbalances resolution. This step aims to ensure resources are ready to respond to frequency deviations.

5. Dynamic pre-qualification [44] - The TSO conducts continuous and dynamic testing for specific operational purposes. In Belgium, for example, this process is used to manage congestion risks related to aFRR activation. If one of the ten designated zones approaches congestion, Elia labels the Congestion Risk Identification (CRI) as high. As a result, the FSP is prohibited from activating assets for aFRR within that zone. The FSP must then either reallocate the activation to another zone or, if that is not possible, fails to deliver the service—leading to a redispatch through system imbalances. This mechanism ensures that frequency control activations do not compromise grid stability or cause potential damage. So far, the DSO does not implement any dynamic pre-qualification mechanism.

6. Activation [41] - In case of frequency deviation, FCR and aFRR service are automatically triggered, respectively within 30 seconds and 5 minutes. The asset portfolio adjusts its output or consumption (e.g., increasing generation or reducing demand) to help contain and restore grid frequency. The TSO sends the signal for activation and the FSP delivers the commited service within the required timeframe.

2.2 Low voltage distribution congestion

With the context of grid structure, load profiles, and the regulatory framework now established, this section will further explore the concept of congestion risks.

2.2.1 Formal congestion definition

Formal definition of Congestion in the EU regulation

According to the Regulation (EU) 2015 /1222 [45], congestion is defined as:

- *Market congestion* means a situation in which the economic surplus for single day-ahead or intraday coupling has been limited by cross-zonal capacity or allocation constraint;

- *Physical congestion* means any network situation where forecasted or realized power flows violate the thermal limits of the elements of the grid and voltage stability, or the angle stability limits of the power system;

The Regulation (EU) 2019/943 [46] of the European Parliament and the Council of 5 June 2019 on the internal market for electricity defines congestion as:

- *congestion* means a situation in which all requests from market participants to trade between network areas cannot be accommodated because they would significantly affect the physical flows on network elements which cannot accommodate those flows;

- *structural congestion* means congestion in the transmission system that is capable of being unambiguously defined, is predictable, is geographically stable over time, and frequently reoccurs under normal electricity system conditions.

These regulatory definitions highlight several types of congestion: market congestion, which is related to limitations within the market, and technical congestion, which relates to physical operational risks, or even structural congestion. A study conducted by Tractebel [47] suggests interdependence betwen the physical, market, and structural forms of congestion.

Nevertheless, when analyzing congestion in distribution grids, only a few market-based mechanisms at DSO level for DSO congestion have been implemented, with most efforts focusing primarily on the MV level [48]. Since this research focuses on congestion at the LV level, market mechanisms for congestion management are not considered as part of the congestion management strategies.

This manuscript focuses on the study of technical congestion, specifically examining the four types of congestion as follows:

- Unvervoltage (UV) - Congestion occurs when the voltage at any bus in the LV feeder drops below a predefined threshold. This is expressed either in [V] or as a per-unit value [p.u.].

- Overvoltage (OV) - Congestion occurs when the voltage at any bus in the LV feeder exceeds a predefined threshold. This is expressed either in [V] or as a per-unit value [p.u.].

- Overcurrent (OC) - Congestion occurs when the current flowing through any line exceeds the maximum ampacity of that line. This is expressed either as an absolute value in [A], or as a percentage of the maximum ampacity [%].

- Overloading of transformers (OT) - Congestion occurs when the substation is overloaded, which is represented as a percentage of the maximum capacity.

Norms and standards

Technical committees define standards to be applied in the industrial sector within a given geographical scope (e.g., CEN-CENELEC at the European level, ISO at the international level). For low-voltage network congestion indices, there are two standards of interest:

1. EN50160 Voltage characteristics of Public Distribution system - This standard focuses on the operation of the distribution grid and defines indices from the grid perspective ;

2. EN61000 Electromagnetic compatibility - This standard focuses more on the assets connected to the grid, specifically end-users assets located beyond the meter.

Some voltage characteristic indices defined in the previous standards are presented in Table 2.5.

Parameter	EN50160	EN61000
Voltage magnitude variations	LV,MV: ± 10% for 95% of week	± 10% applied for 15 minutes
Rapid voltage changes	LV: 5% normal, 10% infrequently	3% normal and 4% maximum

Table 2.5: Summary of LV congestion thresholds from CEN-CENELEC standards

In addition, due to thermal inertia, currents are not required to stay below the branch rating at all times. They must remain below the rating over a 15-minute period, as explained below.

However, in contrast to current limits, voltages must be maintained within specific limits at all times, *instantaneously*, meaning on a 10-second granularity. For instance, in Belgium, generating units connected to the distribution grid (e.g., PV) must be disconnected if the voltage exceeds 15% of its nominal value. The *instantaneous* voltage limits within these 15-minute periods (e.g., every 10 seconds) are adjusted to 1.15 p.u. for OV and 0.85 p.u. for Undervoltage (UV). This will be further discussed in Chapter5.

Additional considerations on congestion indices

There might be additional consideration when setting the congestion indices. For instance, DSO can have their own habits, possibly more conservative or precise than the thresholds defined in European standards.

DSO habits[3] **-** After reviewing the technical requirements from Synergrid, three documents are relevant for defining congestion indices:

- C1/107, which provides some information on the starting currents of certain equipment relative to the distance on an LV feeder.
- C1/111, which addresses overcurrent criteria depending on the type of cable.
- C10/11, which defines the voltage ranges within which electricity generation installations can operate.

Scientific literature - Some studies in the scientific literature propose different limit values than those specified in the standards and norms. This is often done to highlight the use of a particular congestion management technique, sometimes intentionally inducing more congestion for analysis purposes. Other studies may use a slightly modified version of the standard, such as a variation of voltage deviation or a percentage of simulation results. The distinction here lies in the difference between simulation practices and field measurements.

For example, [49] uses three indicators to assess congestion:

- Node voltage – voltage at a node and deviation from nominal value (threshold: 1.03 p.u.)
- Branch load - ratio of a branch's load to its nominal current (threshold: 0.5 p.u.)
- Transformer load – ratio of transformer load to rated capacity (threshold: 0.3 p.u.)

Paper [50] uses the three following indicators to asses congestion:

- Nodes voltage deviations – Deviation of the node voltages compared to specified value (critical node: more than 3% deviation for 20% of simulations)
- Branch overloading – Ratio of branch's current to rated thermal capacity (critical branch: branch overloading 100% for 20% of simulations)
- Transformers overloading – Ratio of transformer power to rated capacity (critical transformer overloading: transformer overloading 100% for 20% of simulations)

Summary of congestion thresholds used in this research

In this research, the following congestion types and thresholds are considered to ensure that no congestion occurs for *continuous* values:

- OV and UV congestion thresholds - These thresholds are set at ±10% of the nominal voltage. Thus, the OV threshold corresponds to 1.1 p.u., while the UV threshold is 0.9.

[3]DSOs also have management practices that could impact the calculations. Congestion limits remain unchanged, but thresholds might be adapted in the models. For instance, they may define voltage setpoints at the substation level for the LV feeder that vary based on the network topology (e.g., setting 1.05 p.u. in rural areas and 1.01 p.u. in urban areas) or depending on the season. For example, ORES set lowers voltage thresholds from May to October for certain particularly long feeders where a lot of PV systems are implemented.

- OC congestion threshold - Current values will be expressed as percentage, defined as the ratio of the current on a specific branch to the maximum ampacity of that same branch. The OC threshold is reached when this ratio exceeds 100%.
- Overloarding of transformers (OT) congestion threshold - The transformer load will be expressed as a percentage, computed as the ratio of the total power flowing through the feeders connected to the transformer to its maximum capacity. The OT threshold is reached when this ratio exceeds 100%. It will only be computed when several feeders are connected to the transformer.

In addition, the *instantaneous* voltage limits within these 15-minute periods (e.g., every 10 seconds) are adjusted to 1.15 p.u. for OV and 0.85 p.u. for UV. A more in-depth discussion regarding the time period for applying these thresholds will be provided in Chapter 5.

2.2.2 How congestion works

The effects of LV network congestion are becoming increasingly evident, given the evolving context described in the introduction. For instance, during the summer in Wallonia, newly installed solar panels generate a significant amount of electricity due to the abundant sunlight. When excess electricity flows into the grid, the voltage level can exceed the maximum threshold, leading to grid congestion. In such cases, the inverter activates its safety mode and disconnects the panels [51].

Congestion can be modeled and predicted using Power Flow (PF) calculations, which are explained further in the manuscript. Two examples presented below illustrate two types of congestion.

In both examples, a simplified grid is considered and depicted in Figure 2.11, with a nominal LV level of 400 V. The grid consists of 20 buses, evenly distributed.

The buses are interconnected using different cable types:

- Between the Grid Connection and bus 0, a cable is used, with an ampacity of 400A.
- Between the remaining buses, cables are modeled, with a lower ampacity of 125A.

This configuration highlights the impact of cable selection on grid performance, particularly regarding current loading and congestion behavior.

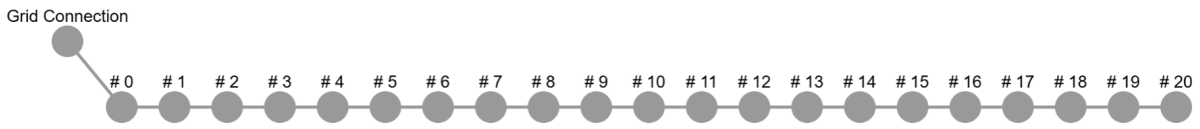

Figure 2.11: Representation of a simple grid with 20 busses

In the first example, each bus is spaced 100 meters apart, with a single end-user injecting 1 kW and 0.5 kVAR per bus. Figure 2.12 presents the voltage values at each bus (above) and the current values for each branch (below). The figure highlights that at bus 12, the voltage exceeds the maximum threshold, indicating OV congestion. However, in this case study, the current values remain below 20% of the maximum capacity.

A noteworthy observation is that line 0 presents a lower current loading percentage compared to subsequent lines, despite expectations of higher current on line 0. This discrepancy arises because line 0 has a higher ampacity (400A vs. 125A), as a larger cable is used for this segment. This shows how cable characteristics influence current congestion.

Additionally, this example illustrates an OV congestion scenario in a rural distribution grid, which is relevant for a medium or large DSO. The assumption of 100-meter spacing between end-users reflects a rural setting, where households are more spread out. An arrangement that would not typically be found in urban environments.

The second example considers the same grid configuration as shown in Figure 2.11, but in an urban context. The key differences are the reduced distance between buses (now 10 meters) and the load profile, where multiple end-users are connected to each bus. The aggregated consumption is set at 10 kW per bus (with reactive power remaining at 0.5 kVAR).

Figure 2.13 presents the voltage values at each bus and the current values for each branch. In this scenario, voltage decreases slightly rather than increasing, as end-users are consuming power instead of injecting it. While voltage limits are not exceeded, current limits are, leading to OC congestion.

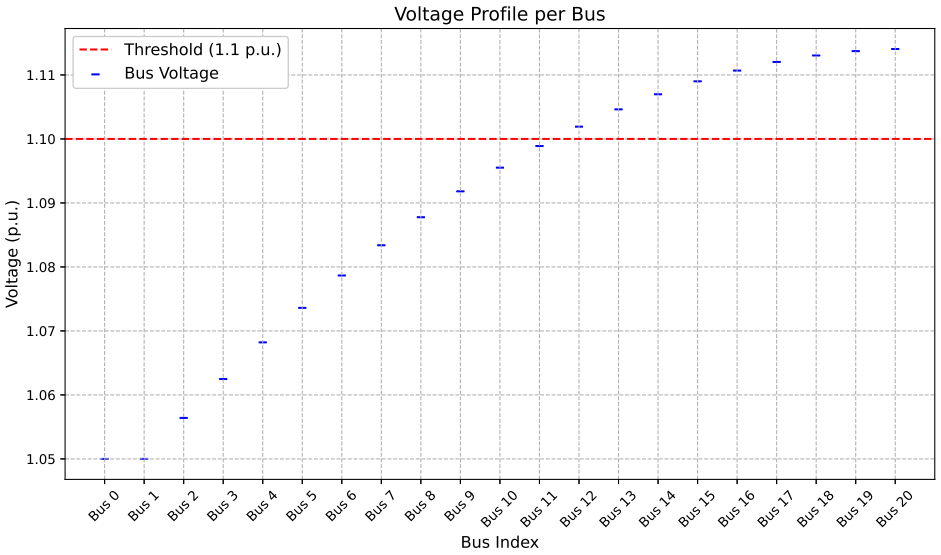

(a) Voltage values

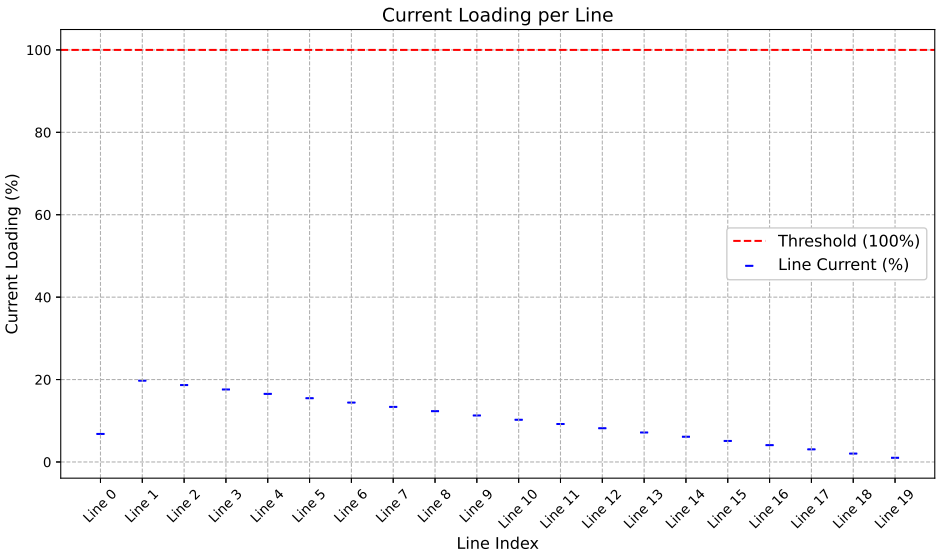

(b) Current values

Figure 2.12: Example of OV congestion on a simple rural grid (100m between end-users and one household per connection point)

These two examples illustrate the differences between voltage congestion and current congestion, emphasizing how grid configuration (rural vs. urban) influences the type of congestion observed. Additionally, it is worth noting that Line 0 does not experience congestion, as its higher ampacity prevents overloading, unlike Line 1.

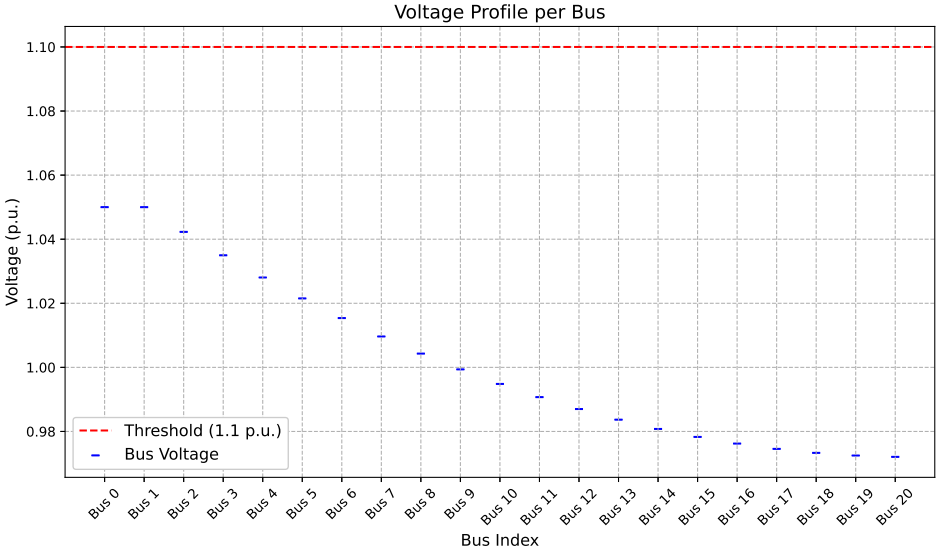

(a) Voltage values

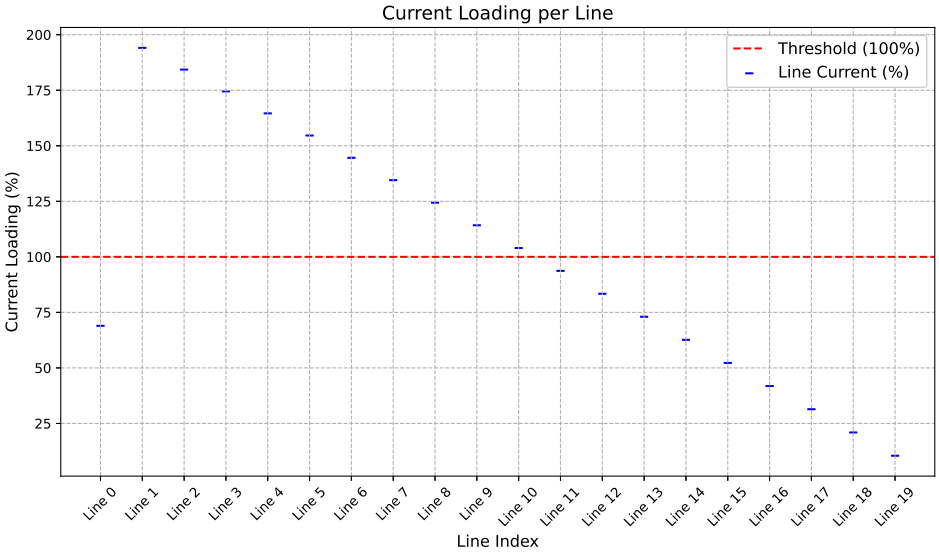

(b) Current values

Figure 2.13: Example of OC congestion on a simple grid (10m between end-users and several households per connection point)

2.2.3 Operating Envelope concept

Introduction to the concept

One approach used by DSOs to anticipate or manage congestion risks at the LV level involves computing the OE for each end-user. The OE represents the injection and offtake limits allocated to an end-user based on the available capacity of the local network or the overall power system [52]. In other words, it defines the maximum power that can be simultaneously consumed or produced by each LV end-user (illustrated in green in Figure 2.14) while ensuring the safe operation of the entire LV feeder or distribution grid.

The concept is applied in Australia through the EDGE project [53] to ensure the safe operation of the LV grid by limiting excess residential PV production. It can be used additionally in Europe to define limits in non-firm connection agreements NFCA in countries like Germany, Hungary, Sweden, and the Netherlands [48]. For example, the NFCA limit is set to 5 kW in Australia [54] and 4.2 kW in Germany [55], restricting end-users' production or consumption in exchange for reduced distribution tariffs. However, using the OE to define these NFCA limits could potentially unlock additional LV flexibility.

In Figure 2.14, the light-yellow bars indicate the maximum connection capacity for both injection and offtake. This capacity is primarily determined by factors such as the number of connected phases (single-phase or three-phase), the network configuration (delta or star), the nominal voltage, and the connection's ampacity. These parameters are largely independent of the end-user's preferences or behaviour.

The green bar represents the OE. The values P_{min} and P_{max} denote the minimum and maximum power that the end-user can inject into or draw from the grid, which may exceed the defined OE limits.

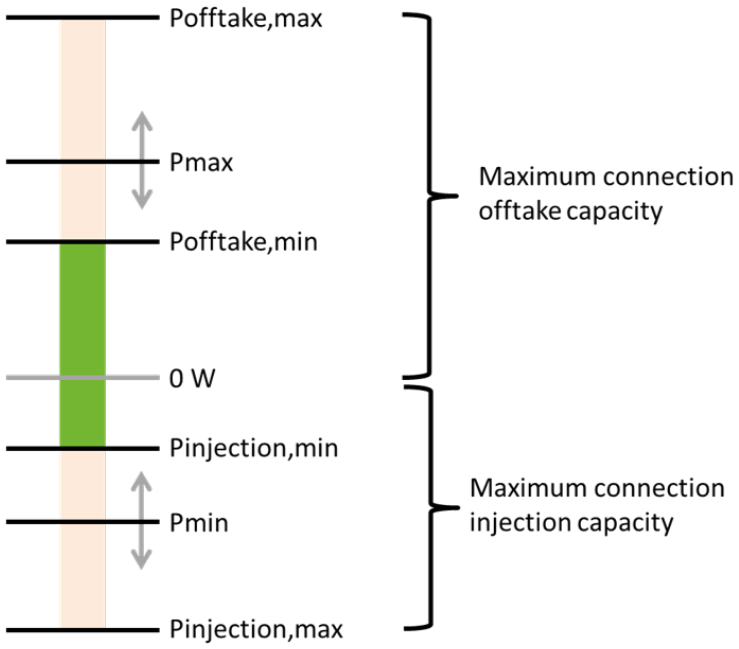

Figure 2.14: Representation of the OE concept for one end-user

This concept will be briefly discussed in the following subsection when embedded for congestion management mechanisms and further explored in detail in Chapter 6. Its application within a TSO-DSO coordination mechanism will be deepened in Chapter 7.

Characteristics of Operating Envelopes

OEs can exhibit different characteristics, including:

- *Optimal or Fair Distribution:* OEs can be assigned uniformly to all end-users or adjusted based on specific factors, such as the power-to-connection-capacity ratio. DSOs must ensure non-discriminatory treatment of end-users, as required by regulatory authorities. If OEs are implemented in congestion

management mechanisms, fairness must be demonstrated. However, fairness can be defined and applied in multiple ways.

- *Static or Dynamic:* OEs can be either static (SOE) or dynamic (DOE), depending on whether their import and export limits vary over time. A DOE continuously adjusts limits based on real-time or forecasted grid conditions, while a SOE maintains fixed limits.

- *Geographical Scope:* The application of OEs can vary in scope. In the Sibelga case study discussed in Part III of this manuscript, OEs are computed at the feeder level. However, for feasibility or acceptability, they could also be determined at the MV feeder level or even across an entire region.

The implementation of these characteristics and their influence on congestion management will be examined further in Part III of this manuscript.

2.2.4 Congestion management mechanisms

This subsection aims to provide an overview of the broad mechanisms that DSO's can implement to manage LV congestion. These mechanisms will be further deepened in part III of this manuscript, especially related to the computation of OE.

In general, a congestion management mechanism must ensure that no congestion occurs on the grid. Chapter 7 will first present solutions for preventing congestion on the LV distribution grid, and will then focus more specifically on addressing congestion caused by LV assets providing frequency control services, as illustrated in Figure 2.15.

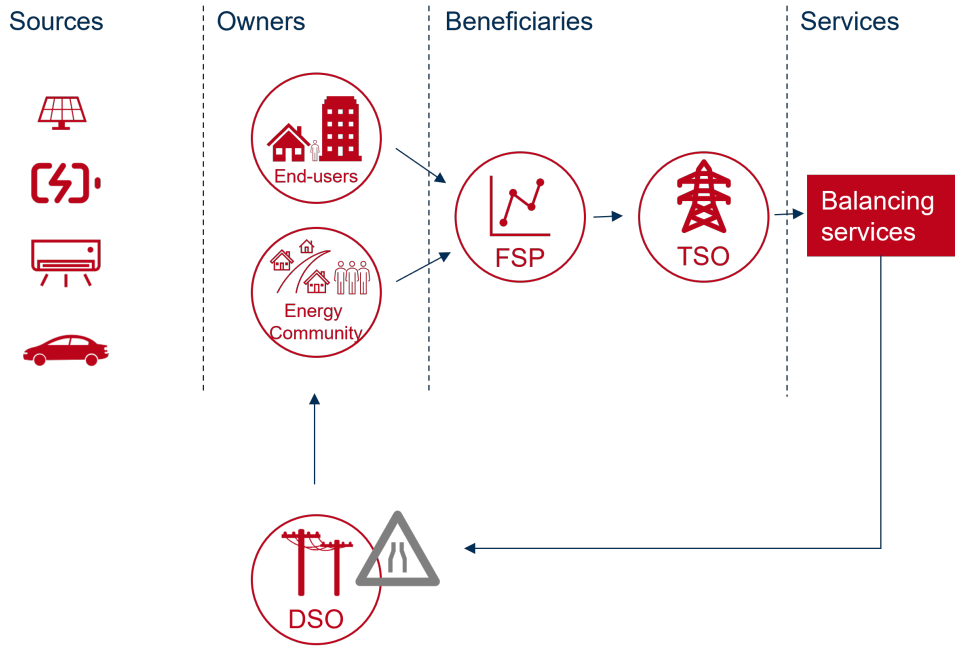

Figure 2.15: Illustration of LV Congestion Mechanism to be activated to prevent Congestion caused by LV assets providing frequency control

The European Network of Transmission System Operators (ENTSO-E) and European Feederations of Distribution System Operators (European Federations of Distribution System Operators (E.DSO), cedec, eurelectric, geode) define Active System Management (ASM) as a set of tools and strategies used by DSOs and TSOs to efficiently manage power systems and optimize costs [56], [57].

Within the ASM, they identify five main congestion management mechanisms for DSOs to implement, namely technical solutions, tariff solutions, market-based solutions, connection agreements, and rule-based approaches, DSOs can effectively manage LV congestion while balancing investment costs. Each solution offers unique benefits tailored to specific grid conditions and economic considerations, briefly presented below.

Technical solutions

Technical solutions for congestion management involve modifying grid topology or reinforcing the network to address constraints. These solutions can include:

- **Increasing maximum load limits on assets:** This can involve modifying connection capacities for end-users, such as upgrading from single-phase to three-phase connections or reinforcing the link between the LV feeder and the end-user connection point.
- **Reinforcing LV feeders:** This may include increasing the ampacity of cables or reducing their resistance, which enhances the ampacity, decreases voltage drops between buses, and mitigates risks of current and voltage congestion. Essentially, this approach involves replacing existing cables with larger ones or with cables made from more conductive materials.
- **Switch reconfiguration:** Adjust the switches to reconfigure topologies and optimize network capacity utilization.
- **Replacing transformers:** Upgrading transformers to increase their capacity helps accommodate higher demand and reduce OT.

Technical solutions are generally treated as a benchmark to compare the cost and performance of other congestion management mechanisms. However, they are typically considered as a last resort due to their high cost and time-consuming nature. For instance, based on discussions with Sibelga, it appears that they reinforce approximately 2% of its grid annually.

Tariff solutions

Tariff solutions aim to adjust distribution tariffs to provide implicit flexibility by incentivizing behavioral changes among end-users to avoid LV congestion.

To provide background, electricity bills typically consist of three components:

- The **commodity price**, representing the cost of electricity production and balancing;
- **Taxes**, including VAT and green certificates;
- **System operator tariffs**, covering transmission and distribution costs.

In this approach, only the distribution tariff is modulated to influence consumer behavior. For effective implementation, these tariffs must be cost-reflective, transparent, and non-discriminatory as controlled by the regulator.

They are designed with consideration of:

- **Tariff basis:** Volumetric (€ per kWh) or capacity-based (€ per kW).
- **Timing:** Fixed, dynamic, or time-of-use (ToU).
- **Location:** Area-specific or locational tariffs.

The effectiveness of tariff solutions may vary depending on the electricity market design. In unbundled markets, where system operator tariffs constitute a relatively small portion of the total electricity price (e.g., one-sixth), the impact of ToU tariffs may be counteracted by other dynamic pricing components, such as commodity prices.

Example: A ToU distribution tariff might be implemented to discourages solar injection between 10:00 and 16:00. However, if a dynamic commodity price incentivizes maximum injection due to insufficient wind generation, conflicting price signals may undermine the desired behavioral change.

In contrast, vertically integrated markets, such as Switzerland, allow for electricity prices to be designed to reflect system operator priorities.

Brussels plans to implement a voluntary ToU tariff system with three price steps by 2028, enabling a small-scale test of consumer responses to ToU pricing. [58]

Market-based solutions

Market-based solutions for congestion management involve establishing markets to procure congestion management products. These markets must be designed to ensure sufficient liquidity by offering prices higher than competing market prices.

Nevertheless, when analyzing congestion in distribution grids, only a few market-based mechanisms have been implemented, with most efforts focusing primarily on the MV level [48]. Since this research focuses on congestion at the LV level, market mechanisms for congestion management are not considered as part of the congestion management strategies.

Flanders is currently implementing such a market design, while Wallonia is in the design phase. Detailed discussions on the market design will be provided in Part III of this manuscript.

Connection agreement solutions

Connection agreement solutions also known as *variable network access*, *flexible connection agreements* or NFCA, is a connection contracts agreed between a system operator and an end-user that limit the end-users to export or import their full capacity [48], under specific conditions that will be described hereafter. This type of congestion management is promoted into the new IEMD directive [59] to foster collaboration between TSO and DSO. Compared to other congestion management methods, NFCAs offer the advantage of not requiring DSOs to directly control behind-the-meter assets, which can be restricted by regulators in vertically integrated power systems. Additionally, NFCAs do not necessitate third-party, such as aggregators or FSPs, access to network data [54].

NFCAs have been implemented for several years by DSOs, primarily at the MV and HV distribution levels, to regulate injections from renewable energy sources. At the LV level, this principle has recently been implemented for example in Australia through the EDGE project [60], while in Europe currently under implementation in Germany, Hungary, Sweden, and Netherlands [48]. For instance, the limit is set up to 5 kW in Australia [54] and suggested to be 4.2 kW in Germany [55]. This means that when NFCA is activated by DSO, each end-user having contract is limited to produce or consume a maximum of 5 kW in Australia and 4.2 kW in Germany.

There is a need to develop methodologies objectifying these guaranteed values, as described in [61]. This is how OE and NFCA can articulate: OE can be computed to define the maximum guaranteed values, operating the LV distribution grid at its optimal point and leveraging the maximum flexibility while preventing any congestion.

Figure 2.16 illustrates the articulation between guaranteed capacity available and OE at the end-user level. The OE is represented in green, the maximum connection capacity in black (for injection and offtake), and the NFCA limits are represented in blue.

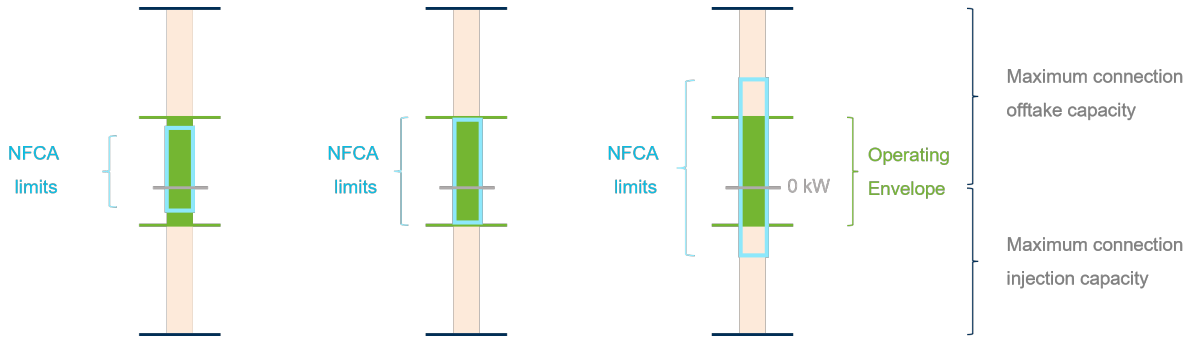

Figure 2.16: Representation of the articulation of OE and three NFCA limits for one end-user

Under normal conditions, end-users can utilize anywhere from the minimum to the maximum of their connection capacity. However, when NFCAs are activated, their usage is restricted to the guaranteed capacity, as indicated by the blue bar.

In the left figure, the blue bar is shorter than the OE, indicating an underutilization of the available LV grid capacity. In this case, the DSO could safely increase the capacity guaranteed to each end-user, thereby unlocking additional flexibility without risking grid congestion. In the central figure, the OE values and NFCA limits are equal, ensuring that each end-user is guaranteed access to the maximum grid capacity that can be provided without causing congestion. In the right figure, the NFCA limits exceed the OE, allowing end-users to access their guaranteed capacity at the risk of overloading the grid.

NFCAs can exhibit various characteristics the will be further deepened in part III:

- Permanent or Temporary Activation: NFCAs can either be activated permanently, effectively redefining connection capacity limits, or temporarily, under specific conditions such as a high risk of congestion. Temporary activation is more common, allowing end-users to utilize their maximum consumption or production capacities under normal conditions, with restrictions only during congestion risks. Some countries include provisions to reassure end-users, specifying the frequency and duration of activation (e.g., an NFCA may be activated up to ten times a year for a maximum of one hour each time).

- Optimal or Fair Distribution: similarly to OE, NFCA can apply uniform limits to all end-users or vary based on specific factors. DSOs are required to demonstrate non-discriminatory treatment of end-users to regulatory authorities. If OEs are used to define NFCAs guaranteed limits, fair OEs must be considered. And similarly, fairness principle can be implemented in various ways, resulting of the DSO choice and regulator approval.

- Static or Dynamic: Limits imposed by NFCAs can either be static, remaining constant regardless of time, or dynamic, changing based on temporal factors. Dynamic limits offer flexibility and can be tailored using various configurations, such as daily or seasonal time-of-use, 15-minute intervals, or even 1-minute intervals. The difference between static and dynamic NFCA is similar to the difference between SOE and DOE discussed previously in the chapter. Additional considerations must be addressed when deciding between static and dynamic features, such as the technical feasibility of implementing a time-varying contract and its acceptability to end-users.

- Geographical scope - The scope of the NFCAs application is another key consideration. In the Sibelga example, OEs are computed fairly per feeder; however, for feasibility or acceptability, OEs could also be computed across an MV feeder or an entire region.

NFCAs are implemented to ensure that LV distribution networks operate within voltage and current limits, safeguarding the reliability and safety of the LV distribution grid. When NFCAs are configured for temporary activation under conditions of high congestion risk, they serve as a last resort measure for DSOs to prevent LV congestion.

Finally, the NFCA can be contracted with only a subset of end-users, rather than involving all of them. Further details on connection agreement solutions will be explored in Part III of this manuscript.

Rule-based solutions

Rule-based solutions impose mandatory flexibility measures, such as PV curtailment, in situations where market-based mechanisms are insufficient or unavailable. These rules act as a fallback mechanism to ensure grid stability.

2.3 Overview of models to study low voltage distribution congestion

This section provides a concise overview of the models employed throughout the manuscript to study congestion on LV distribution grid. It does not aim to offer an exhaustive treatment of the subject, entire reference books are dedicated to these topics [4], but rather to present the key components and tools essential for understanding the analysis conducted in subsequent chapters.

An important assumption made in this research is that all analyses are conducted under *steady-state* operating conditions. This implies that all current and voltage variables have periodic waveforms over time. Short-circuit analyses or harmonic distortion caused by electronic converters or inverters are beyond the scope of this research.

The section is organized into four subsections, covering: grid models, load profile models, power flow analysis, and optimal power flow analysis. Each of these models will be explored in greater detail in the relevant sections or chapters that follow.

2.3.1 Distribution grid models

Subsection 2.1.1 introduced the structure of LV distribution grids, highlighting their key components and associated challenges. Building on that foundation, this subsection focuses on how LV distribution grids can be modeled for congestion analysis.

This subsection is structured as follows: first, it provides an overview of different grid types; second, it explores methods for approximating phase imbalance. The specific grid models used as case studies throughout this manuscript will be detailed in Chapter 3.

Distribution grid model types

Several grid layouts can be used to identify congestion, regarding the available data, as well as their quality. Paper [62] reviews publicly available distribution datasets. It also characterizes (incl. methodologies, intentions, data origins, etc.) how grid datasets are compiled. Finally, it presents the several distribution network types, among which three are used in this manuscript and defined in Table 2.6.

Grid types	**Recommended application**
Synthetic grid	No real grid model, or obtained by simplifying/modifying a real grid.
Example and test grid	Grid used for testing, validation or demonstration of a specific case.
Benchmark grid	Model used to compare the efficiency or validity of algorithms (more interest for the algorithm than for the grid).

Table 2.6: Grid typologies definition

In the previous subsection 2.2.2, the two grids used to illustrate UV and OC congestion mechanisms on rural and urban configurations are therefore synthetic grids. In the subsequent sections of this manuscript, two distribution grids are used for case studies:

1. The reduced IEEE LV European Testfeeder benchmark grid [63], which is used to ensure reproducibility of results since its dataset is publicly available. This grid is also simpler than the Sibelga test grid, fostering the explanation of key concepts.[4]
2. Sibelga Test Grid, a more complex dataset consisting of 49 real LV feeders provided by Sibelga in Brussels. This grid offers more realistic data and is studied to demonstrate the scalability of the proposed methods and to illustrate unique characteristics of real, urban distribution networks.

Load profiles models

The modeling and analysis of power systems are influenced by the characteristics of the load. This research focuses on analyzing congestion problems under steady-state operation. However, steady loads are an idealization; in reality, LV loads fluctuate continuously. This variability is particularly pronounced in LV feeders, as detailed in Table 2.1, where LV end-users exhibit stochastic and non-coincident behavior. Additionally, load profiles in this context encompass both active and reactive power, which can be either consumed or injected into the grid. This is due to the presence of decentralized generation, such as solar panels, but also other flexible assets, at the LV feeder level.

This subsection outlines the approach to modeling LV loads, with more sophisticated models for load forecasting and analysis developed in later sections of this manuscript.

Theses LV load characteristics form the base for analyzing and simulating LV distribution loads

In the context of this research, loads are modeled as constant power, applied to a wye connection at a specific bus i and for a specific time step, expressed in eq. 2.1. Note that if an end-user is connected to single-phase a, $I_{i,b}$ and $I_{i,c}$ would be set to zero.

$$s_{wye,i} = \begin{bmatrix} V_{i,an}(I_{i,a})^* \\ V_{i,bn}(I_{i,b})^* \\ V_{i,cn}(I_{i,c})^* \end{bmatrix} \tag{2.1}$$

[4]The benchmark grids are not arbitrarily designed: they are the results of two decades of efforts by the IEEE Power and Energy Society's Test Feeder Working Group under the Distribution System Analysis Subcommittee. These publicly available grids are available here: `https://site.ieee.org/pes-testfeeders/resources/`. Originally developed to assess the robustness of distribution system analysis software, these benchmark grids are therefore well-suited for testing the algorithms and methods studied in this research.

where $V_{i,an}$ represents the voltage difference between voltage for phase a $V_{i,a}$ and voltage neutral at bus i $V_{i,n}$, both at bus i.

Similarly, the same constant power load profile applied to a delta-connection is given by eq. 2.2. Note that if end-user is connected in single-phase between a and b, $I_{i,bc}$ and $I_{i,ca}$ would be set to zero.

$$s_{\Delta,i} = \begin{bmatrix} (V_{i,a} - V_{i,b})(I_{i,ab})* \\ (V_{i,b} - V_{i,c})(I_{i,bc})^* \\ (V_{i,c} - V_{i,a})(I_{i,ca})^* \end{bmatrix} \tag{2.2}$$

Let's define a variable χ_i as given by eq. 2.3 and a wye-delta transformation matrix Γ provided in eq. 2.4.

$$\chi_i = \begin{bmatrix} V_{i,a}(I_{i,ab})^* & V_{i,a}(I_{i,bc})^* & V_{i,a}(I_{i,ca})^* \\ V_{i,b}(I_{i,ab})^* & V_{i,b}(I_{i,bc})^* & V_{i,b}(I_{i,bc})^* \\ V_{i,c}(I_{i,ab})^* & V_{i,c}(I_{i,bc})^* & V_{i,c}(I_{i,ca})^* \end{bmatrix} \tag{2.3}$$

$$\Gamma = \begin{bmatrix} 1 & -1 & 0 \\ 0 & 1 & -1 \\ -1 & 0 & 1 \end{bmatrix} \tag{2.4}$$

These are useful for transposing equivalent power between delta and wye connections, or vice versa. Indeed, combining χ_i and Γ provides the power either in the wye or delta representations. For example, the power as wye connection equivalent is expressed as eq. 2.5, and similarly for the power as delta connection equivalent provided by eq. 2.6.

$$s_{wye,i} = diag(\chi_i \Gamma) \tag{2.5}$$

$$s_{\Delta,i} = diag(\Gamma \chi_i) \tag{2.6}$$

Several key criteria define load characteristics at the LV level.

Average power over time period - In real-world scenarios, the complex power consumed or injected by end-users fluctuates instantaneously. However, for modeling purposes, load profiles are typically represented by discretizing the instantaneous power consumption into fixed time intervals (e.g., 15 minutes), as illustrated in Figure 2.17. In this figure, the orange curve depicts an *instantaneous* load profile[5], while the blue curve represents the time-averaged load profile, which is generally used in the subsequent models of this research, unless explicitly stated otherwise. It is important to note that this averaging process can lead to the loss of some variability information, and may slightly dampen the peak values of the load profiles. Load profiles data are extracted from the IEEE LV testfeeder that will be described in subsequent sections.

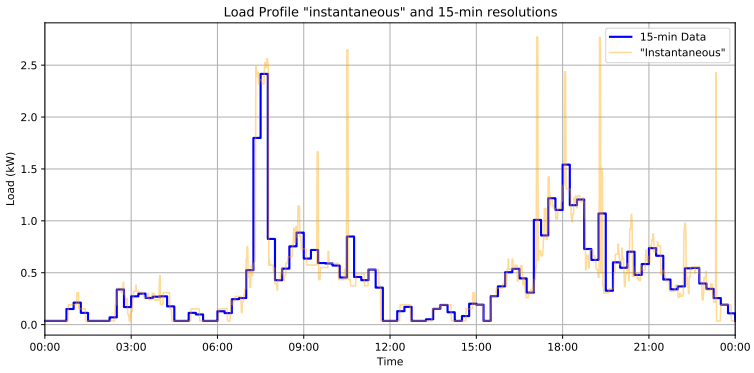

Figure 2.17: End-user load profiles for one day

This approach accounts for practical constraints such as metering—smart meters in Brussels, for example, record power consumption at 15-minute intervals. It also addresses computational limitations encountered during time-step simulations.

[5]While the load profile is not truly instantaneous, as power data is recorded over a specific time interval, the term instantaneous is used here for pedagogical purposes to illustrate the concept. In this illustrative case, the data is acquired over a 1-minute period.

Wye or Delta connection - Loads are modeled as either wye-connected or delta-connected, as discussed in earlier sections.

Phase connection - Load models must account for the number of phases to which loads are connected. For two-phase or single-phase connections, unconnected phases are represented by setting their currents to zero.

Voltage dependency - Load models vary based on how the load responds to changes in voltage magnitude. Common models include constant impedance (where load $\propto V^2$), constant current (where load $\propto V$), constant power (where load is independent from V), or a combination of these characteristics. In this research, loads are modeled as independent of voltage (constant power), as this assumption aligns well with the behavior of many LV modern devices, such as computers, LED lights, and household appliances.

2.3.2 Power Flow analysis

The analysis of a power system under steady-state operation typically involves PF analysis. It is a tool used to compute voltages, currents, and angles across all buses and branches of the network during normal operation. It relies on network topology, component models, and load profiles. It is the tool that is used to compute voltage and current in Figures 2.12 and 2.13 for the synthetic LV feeder.

Key outputs of PF analysis include [4]:

- Voltage magnitudes and angles at all feeder busses
- Line flow in each branch (measured in kW, kvar, amps or power factor)
- Power losses in each section
- Total feeder input and power losses
- Load kW and kvar based on specified load models

Focusing on the LV distribution level, the UTPF problem forms the basis for distribution network analysis. Its objective is to determine voltage and current values across the LV grid.

To perform such analysis, key inputs are required: the three-phase voltages at the substation, load models, and the electrical parameters of the feeder. These elements are introduced in Subsections 2.3.1 and 2.3.1, which describe the modeling of both series components and loads.

Formulating a UTPF problem begins by translating the physical principles governing power systems into mathematical expressions. Two fundamental laws apply: Kirchhoff's Circuit Law (KCL), which ensures current conservation by stating that the algebraic sum of currents at any node is zero, and Ohm's Law, which relates voltage (V), current (I), and impedance (Z) under steady-state conditions. These laws form the macroscopic foundation for describing power flow behavior.

Once the system variables are explicitly defined using KCL and Ohm's Law, various algorithms can be employed to solve the UTPF in radial networks. Classical methods developed for transmission systems are typically avoided due to poor convergence in radial topologies [4, 64]. Instead, specialized algorithms tailored for distribution systems are preferred, including:

- BFS method or ladder iterative technique [4], [65], [66] - This method begins with known initial voltage values and assumes initial branch currents and power losses are zero. The backward sweep starts from the last bus and computes branch currents towards the substation, adding contributions from child nodes to parent branches. The forward sweep propagates voltages from the substation, updating the voltage at all downstream buses based on branch currents and impedance. This iterative process continues until the differences between phases voltages at all buses fall below a predefined tolerance. BFS leverages the radial topology to avoid matrix inversion, thus reducing computational time. It is easy to implement and handles unbalanced systems efficiently but may converge slowly in networks with high R/X ratios.
- Current Injection Method (CIM) with Newton-Raphson [67], [68] - This method computes initial current injections based on specified powers and given initial voltages. A mismatch current vector is calculated from the voltage profile, and a linear system is solved iteratively to update the voltage vector. The iteration continues until power mismatches at all buses are within a specified tolerance. CIM is simple and efficient for radial networks, but for large networks, forming and inverting the admittance matrix can be computationally intensive, and convergence may be slower than BFS.

- Holomorphic Embedding Methods (HELM) [69] - HELM uses holomorphic functions[6] to reformulate the nonlinear power flow equations through an embedding parameter, λ, expressing solutions as a power series in λ. HELM provides a unique solution without requiring iterative processes. However, the mathematical models are more complex, and the computational effort is higher due to the need for holomorphic transformations and series expansions.

The three methods are compared in the table 2.7. Due to its simplicity and computational efficiency, BFS is chosen for this research and the model will be further described in subsequent sections.

[6] Complex functions presenting specific characteristics, e.g. complex differentiable at every point in its domain

Feature	BFS	CIM	HELM
Topology Suitability	Primarily designed for radial networks	Can handle both radial and meshed networks	Suitable for both radial and meshed networks
Unbalanced Systems	Well-suited for unbalanced systems	Handles unbalanced systems effectively	Not typically designed for unbalanced systems
Computational Complexity	Low (no matrix inversion)	Moderate to high	High due to holomorphic transformation
Convergence Characteristics	Reliable in radial networks	May face issues in poorly conditioned systems	Globally convergent for solvable cases
Implementation Complexity	Simple and intuitive	Moderate (Jacobian required)	High (advanced mathematical principles)
Speed	Fast for radial systems	Moderate, depends on system size	Slower due to complex calculations
Scalability	Highly scalable for radial systems	Scalable but computationally intensive	Limited by computation requirements
Robustness	Robust for radial networks	Good, depends on initialization	Highly robust for solvable systems
Handling of High R/X Ratios	May face challenges (higher number of iteration than CIM when R/X Ratios increase)	Increase number of iteration with higher R/X ratio	Handles effectively
Algorithm Type	Iterative (two-step sweep)	Iterative (linearized equations)	Non-iterative (holomorphic functions)

Table 2.7: Comparison of Power Flow Methods: BFS, CIM, and HELM

2.3.3 Optimal Power Flow analysis

The previous subsection introduced the UTPF, focusing on analyzing unbalanced power systems under steady-state operation while considering grid constraints. When the objective shifts to determining the optimal operation of such systems under grid constraints, Optimal Power Flow (OPF) analysis becomes necessary. In the case of unbalanced systems, this tool is referred to as UTOPF.

This subsection introduces general optimization concepts and outlines the two primary steps involved in applying these principles to UTOPF: the formulation of the UTOPF and the implementation of the optimization process. While it does not provide a comprehensive discussion of optimization or UTOPF, it focuses on the fundamental principles necessary to understand the critical steps and decisions required to effectively implement UTOPF. The UTOPF used for this research is further explained in the subsequent part III.

Brief overview on optimization

To provide general background about optimization, the term *feasible set* refers to the solution space formed by the intersection of all constraints, encompassing all solutions that satisfy the constraints. The optimization problem involves finding the solution that minimizes or maximizes the objective function, within the feasible set, depending on the specific goal. Importantly, a minimization problem can be reformulated as a maximization problem (and vice versa) by changing the sign of the objective function.

Optimization problems are categorized as convex or non-convex. Convex problems, characterized by convex objective functions and feasible sets, ensure that any local optimal solution is also globally optimal [70]. This property enables the use of fast and reliable algorithms. In contrast, non-convex problems may have multiple local optima, making it difficult or impossible to guarantee a global optimal solution.

Several classes of optimization problems exist within the convex domain, each with distinct properties and complexities, such as Linear Programming (LP), Second-Order Cone Programming (SOCP), Semi-Definite Programming (SDP), and Non-Linear Programming (NLP). OPF, including UTOPF, is inherently a non-convex, nonlinear problem[7]. To address this complexity, approximations and relaxations are often employed to simplify the problem and make it computationally tractable. These general principles (convexity and programming classes) guide the formulation of optimization problems.

The following paragraphs elaborate on the application of general optimization principles to unbalanced power systems, with a focus on the two critical steps required to formulate and implement an UTOPF.

Optimal Power Flow problem formulation

Similarly to the UTPF formulation, the first step in power flow modeling involves translating the physical behavior of power systems into mathematical expressions, primarily using KCL and Ohm's Law.

Apparent power (S) is a non-convex quadratic function of current and voltage, given by $S = UI^*$, where I^* is the complex conjugate of current. The inclusion of this relationship in network modeling introduces quadratic constraints. Since power networks are designed to transport power, components such as loads and generators are typically modeled by imposing constraints on their power consumption or generation, leading to the problem's non-convexity.

To formulate the UTOPF, two categories of variables (flow variables and voltage variables) and the mathematical frameworks to model the lines must be defined. Flow variables can represent power (S), current (I), or lifted current (L). Voltage variables can take the form of standard voltage (V) or lifted voltage (W). The concept of lifted variables will be briefly introduced below.

Two primary mathematical frameworks to model the lines are used to describe the network:

- BFM: Introduces explicit series current variables to describe the network.
- Bus Injection Model (BIM): Substitutes all current variables and expresses active and reactive power as functions of voltage differences between connected buses.

The choice of variables and line mathematical frameworks significantly affects the complexity and tractability of the optimization problem.

When current is selected as the flow variable, KCL is used directly, requiring that the sum of currents at each bus equals zero ($\sum I = 0$). This is referred to as the *current balance* constraint. Conversely, when power is used as the flow variable, Kirchhoff's law is adapted by multiplying each term by the corresponding voltage variable, resulting in a *power balance* constraint ($U \sum I^* = \sum UI^* = \sum S = 0$).

[7] Except for certain cases where loads are modeled as constant impedance, the problem may become convex.

The current and power balance constraints are illustrated in Figure 2.18, which depicts a single line for two buses: the parent bus, indexed as π, and one connected bus. The left-hand side of the figure illustrates current (I) and voltage (V) variable spaces with Kirchhoff's current law, while the right-hand side represents power (S) and voltage (V) variable spaces using the power balance constraint. Additionally, branch power is represented with a capital S, while end-user loads are denoted with a lowercase s. It is also noteworthy that only three phases are shown in the diagram (excluding the neutral), as the line segment incorporates the reduced series impedance described in Section 3.2.3.

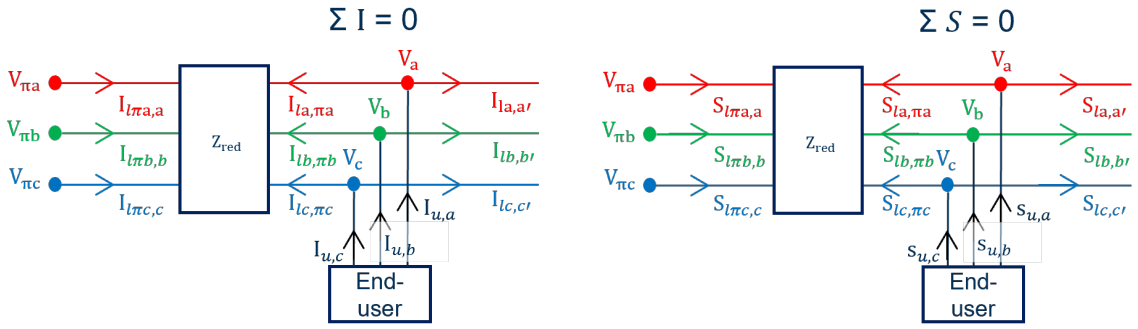

(a) Line in IV variable space (b) Line in SV variable space

Figure 2.18: Representation of a single branch with two buses and the reduced series impedance

Lifted current and voltage variables, used in subsequent parts of this manuscript, replace respectively standard current and voltage by increasing dimensions of these variables. Lifted variables are defined as the outer product of voltage phasors $W_i = V_i * V_i^H$ and current phasors $L_n = I_n * I_n^H$, where H denotes the Hermitian transpose[8].

Lifted variables enable the linearisation of some constraints and reduce overall complexity of the problem. However, this approach expands the feasible set, potentially leading to solutions outside the original set. To ensure the original problem's solution can be recovered, two constraints must be added: the Positive Semi-Definite (PSD) given by eq. (2.7) and rank-1 constraints given by eq. (2.8) [71]. The PSD constraint ensures the solution space remains convex by requiring matrix variables to be PSD. The rank-1 constraint is non-convex and is needed to retain consistency with the original feasible set.

$$W_i \succeq 0 \quad and \quad L_n \succeq 0 \tag{2.7}$$

$$rank(W_i) = 1 \quad and \quad rank(L_n) = 1 \tag{2.8}$$

Further development on these formulations are presented in subsequent sections when presenting the optimization problem considered in this research.

Optimal Power Flow implementation

The implementation of UTOPF involves choices across five layers:

1. *Models* – Selecting variables, parameters, line models, and complexity levels determines the class of optimization problem (e.g., LP, SOCP, SDP). Criteria include tractability, complexity, and solution exactness.

2. *Modeling Language* – Common languages applied to power systems include Matlab, Python, GAMS, and Julia. Selection depends on access (open-source vs. licensed), community support, existing libraries, and user expertise.

3. *Optimization Modeling Language* – Layers like YALMIP, Pyomo/CVXPY, or JuMP provide support for implementing optimization problems. Compatibility and relevance to the problem's requirements

[8]The Hermitian transpose of a matrix is obtained by taking the transpose of the matrix and then replacing each element with its complex conjugate.

are key factors. Regarding compatibility, certain optimization modeling languages are inherently tied to specific modeling languages. For example, YALMIP is designed for use with Matlab, while Pyomo and CVXPY are commonly used with Python, regardless of the solver being employed. Conversely, some optimization modeling languages are linked directly to a specific solver rather than a modeling language. For instance, Gurobi solver can be implemented with either Python or Matlab. In terms of relevance, it is essential to ensure that the chosen optimization modeling language supports the required mathematical operators. For example, CVXPY supports the SDP operator (critical for the SOCP relaxation of UTOPF), whereas in Pyomo, such operators may need to be explicitly implemented.

4. *Solvers* – Solvers like Gurobi or CPLEX are chosen based on access (open-source vs. licensed) and compatibility with mathematical operations, models, and optimization modeling languages.

5. *Algorithms* – Solvers may use specific algorithms (e.g., simplex, interior point) or custom algorithms optimized for particular problem classes.

The modeling engineer's role is to navigate these choices to achieve the optimal solution. While existing tools often provide predefined solutions, unique features or requirements may necessitate developing or customizing tools. A non-exhaustive list of existing tools, as well as the UTOPF developed in this research, are presented in Table 2.8 and will be further detailed in Part III.

Feature	**Model suggested**	**PMD [72]**	**Open-DSOPF [73]**	**Pandapower [74]**
Model	BFM (SW) with SOCP relaxation	BFM and BIM (SV) supporting NLP, SDP, SOC, and LP	BFM (SV) supporting LP, NLP, or QP	Interface with PMD for OPF models
Modeling language	Python	Julia	Python	Python
Optimization modeling language	CVXPY	JuMP & MOI	Pyomo	Pyomo
Solvers	Mosek	Depending on the problem (Ipopt, Gurobi)	Knitro	Depending on the problem (Ipopt, GLPK, Gurobi, CPLEX, Mosek)

Table 2.8: Comparison of some existing UTOPF toolboxes

2.4 Conclusions

This chapter provided an overview of the LV distribution grid, describing its structure and the technical, regulatory, and economic challenges it faces. It introduced the concept of LV congestion, explaining how it arises in today's grids and how its occurrence is expected to grow with increasing electrification of heating and mobility, as well as the participation of LV assets in new economic activities. The chapter also outlined models used to analyze the grid's steady-state operation UTPF and optimal operation UTOPF, forming the basis for understanding and addressing congestion.

LV congestion is a growing challenge for DSOs, driven by the electrification, the decentralized production and the digitization. These technologies, while beneficial, can strain the network and lead to operational bottlenecks. To address these challenges, DSOs require effective tools to analyze, identify, and manage congestion.

This research is focused on providing such tools. The rest of this PhD thesis is structured as follows: Part II introduces a congestion identification approach, including the innovative contribution of evaluating how LV assets providing frequency control impact grid congestion. Part III proposes a new method to calculate operating envelopes that can help mitigate congestion proactively. These solutions aim to

support DSOs in managing LV grid congestion effectively, ensuring reliable and efficient grid operation amidst a rapidly evolving energy landscape.

Chapter 3

Presentation of case studies

Contents

This chapter presents the grid models used as case studies throughout this manuscript. The first section introduces two case studies: a benchmark grid and a real-world Sibelga grid. The second section details the process of transforming raw data, provided by the Testfeeder working groups, for the benchmark grid, or directly by Sibelga, for the real grid, into a usable grid model. As it will be discussed in subsequent parts, this step is fundamental for studying and managing congestion in LV distribution grids.

3.1 Case Studies considered in this research

As described in 2.3.1, different types of grid models exist. This study focuses on two LV distribution grid types: a benchmark grid and a real-world dataset. These grids are detailed below:

1. The reduced IEEE LV European Testfeeder [63] serves as the benchmark grid. Its publicly available dataset ensures reproducibility of results. Additionally, its relatively simple structure facilitates the explanation of key concepts.

2. The Sibelga Test Grid is a more complex dataset comprising 49 real LV feeders from the Brussels distribution network, provided by Sibelga. This dataset provides realistic conditions to assess the scalability of the proposed methods and to analyze the characteristics of real urban distribution grids.

The reduced IEEE European LV Testfeeder is illustrated in Figure 3.1, featuring 55 end-users with predefined phase connections. Each end-user is connected with a maximum power capacity of ±9.2 kVA.

Figure 3.2 presents the Sibelga LV distribution grid, which includes three MV feeders (11 kV) distributing 49 LV feeders at a nominal voltage of 230 V. This grid comprises 712 connection points and 2,267 end-users, meaning multiple end-users may share a single connection point.

End-users can be single-phase or three-phase connected, all using delta connections. Their maximum connection capacities range from 3.7 kVA (single-phase, 16A) to 25.1 kVA (three-phase, 63A). These users are unevenly distributed across feeders and phases, and some have PV systems with known installed and inverter capacities.

The grid is located in an urban environment, with an average distance of 13 m between connection points.

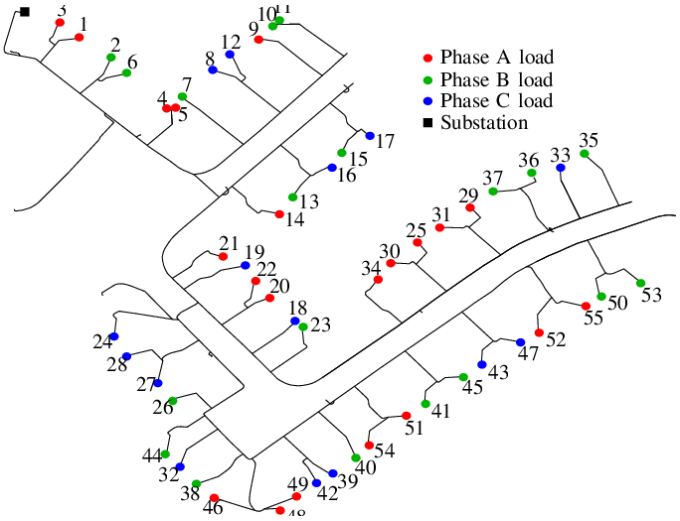

Figure 3.1: Reduced IEEE European LV Testfeeder with phase connections

3.2 From Raw Data to LV Grid Models

This section addresses the process of transforming raw data from a study group (for benchmark grids) or DSOs into models that accurately represent the physical characteristics of LV grids, including branches, buses, and end-user connections. While the task of modeling LV grids might appear straightforward, the datasets provided by DSOs often require extensive parsing and preprocessing to make them suitable for modeling purposes.

The structure and format of DSO data are typically influenced by historical operational strategies, leading to significant variability and a lack of standardization across organizations. Although the observations presented here are drawn from the specific Brussels case and may not generalize to all DSOs, they underscore the common challenges faced by engineers when developing precise and reliable LV grid models.

This section first presents the format needed for data to be used in the further LV congestion identification tool, second it presents the structure of Sibelga data and third it presents how the match can be made with assumptions regarding lack of data.

3.2.1 Structure of LV Grid model

Specific data is required to accurately model physical congestion on the LV distribution grid. This modeling focuses exclusively on the LV distribution grid, spanning from the MV/LV transformer to the final bus, without explicitly representing the MV grid. The grid model consists of six primary components, each characterized as listed below. Each characteristic is defined, along with its relevance to the subsequent PF or OPF. Identity characteristics are necessary for constructing the feeder graph, which connects, for a given LV feeder, each bus to its respective branch, each end-user and devices (if present) to its corresponding bus. The architecture of the grid model, along with the intrinsic characteristics of each component, is summarized in Fig. 3.3.

MV/LV substation

This component includes the MV/LV transformer and its technical characteristics, serving as the connection point between the MV and LV grids.

LV Feeder

The LV feeder provides information on individual feeders, including:

- LV feeder identity: Identifies the specific LV feeder.
- Connection configuration: Specifies whether end-users are connected via delta or wye configurations. It is needed to model load injections and offtakes, as described in the introduction.

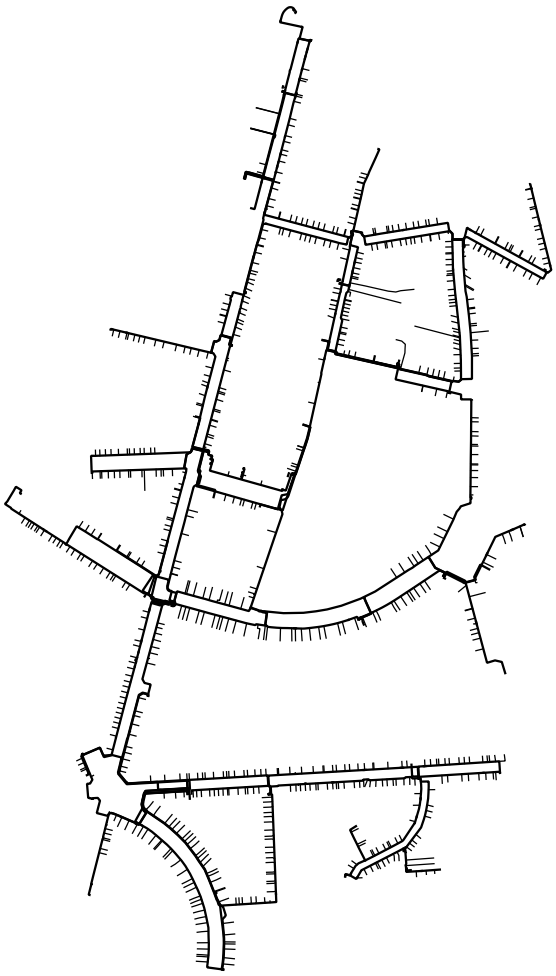

Figure 3.2: 49 Sibelga LV feeders

- Nominal line voltage and nominal capacity: used to normalize power, current, and voltage values into p.u. values. Additionally, these parameters help define congestion limits for the feeder.
- Transformer identity: Indicates the transformer to which the feeder is connected.

Each feeder consists of buses and branches. Since LV feeders are mainly radial (as outlined in 2.1.1), the number of buses equals the number of branches plus one. Each bus is connected to only one upper branch, while multiple child branches may originate from the same parent bus.

Bus Characteristics

Each bus is defined by:

- Bus identity: A unique identifier for the bus.
- Bus type: Specifies whether a bus is a slack bus or a load bus (PQ bus). For the slack bus, both voltage magnitude (V) and phase angle (ϕ) are predefined, serving as a reference point to initialize the PF problem. In contrast, for load buses (PQ buses), active power (P) and reactive power (Q) are known, while voltage magnitude and phase angle remain unknown. This classification aligns with the load modeling approach described in Section 2.3.1, where loads are assumed to be proportional to constant power.

Branch Characteristics

Branches are characterized by:

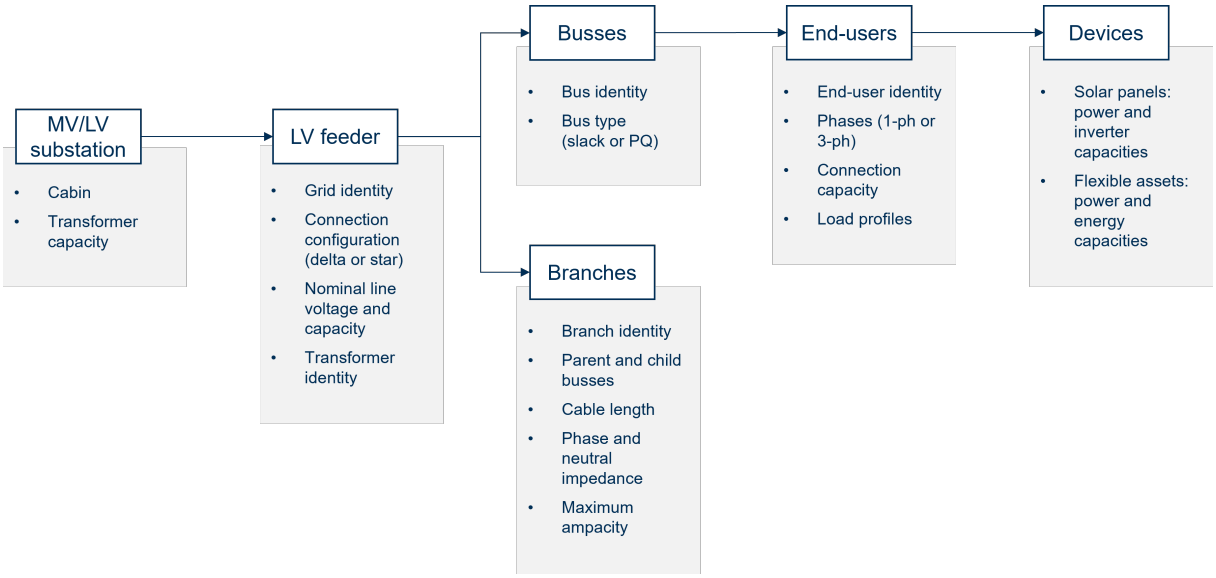

Figure 3.3: Components model hierarchy with the relevant characteristics

- Branch identity: A unique identifier for the branch.
- Parent (upper) bus and child (lower) bus: The specific buses the branch connects, with one parent branch per child bus.
- Cable length: Expressed in meters.
- Cable type: Details the material and configuration of the branch wiring.
- Phase and neutral impedance: Calculated per branch.
- Maximum ampacity: The branch's current-carrying capacity.

The cable length, cable type, and phase and neutral impedance are needed for calculating the impedance of each branch. As outlined in the introduction—and further detailed in PF equations, series impedances are necessary for applying Ohm's law and KCL to compute voltage drops and power losses. The maximum ampacity is needed to define congestion thresholds. For simplification purposes, it is important to note that shunt admittances are neglected, as demonstrated in [4].

End-Users

Buses may or may not connect end-users. When they do, the bus is referred to as a connection point. Multiple end-users can share the same bus, which is common in urban settings like Brussels. For instance, when a new apartment building is connected to the LV grid instead of a dedicated MV/LV transformer, up to 20 end-users might share one bus. End-users are defined by:

- Customer identity and bus identity: Links the end-user to a specific bus.
- Phases: Specifies whether the connection is single-phase or three-phase, and for single-phase, the exact phase connected. This information is required in the unbalanced models to determine the specific phase(s) to which each end-user is connected.
- Connection capacity: Represents the intrinsic characteristics of the connection, based on cable ampacity and the number of connected phases. The connection capacity introduces additional constraints to make PF more realistic, as the maximum power injected into or consumed from the grid cannot exceed this capacity. In real-world scenarios, exceeding the connection capacity would trigger the household's protection mechanisms (e.g. fuses, circuit breakers, inverter protections)
- Load profile: DSOs may have access to the yearly load profile for further refining consumption estimates, which is discussed in the next section.

Behind-the-Meter Devices

In certain cases, DSOs may access data beyond the meter when justified by regulatory approval. Examples include:

- Solar panels: Information includes end-user identity, installed capacity, and inverter capacity (to convert DC electricity from solar panels to AC).
- Flexible assets: Relevant for services like batteries, HP, or EV. Key data points include end-user identity, available flexibility power, and energy capacity.

This information is required to refine the computation of the load profiles as it will be explained in the next section.

3.2.2 Available data illustrated by Sibelga grid

While the previous subsection focused on the information required to model power flow within the feeder, this section briefly outlines how data is structured in the Sibelga dataset and the process of parsing it into the required format.

Although this task might appear straightforward, significant effort was dedicated to interpreting and applying the raw data to create a realistic model.[1]

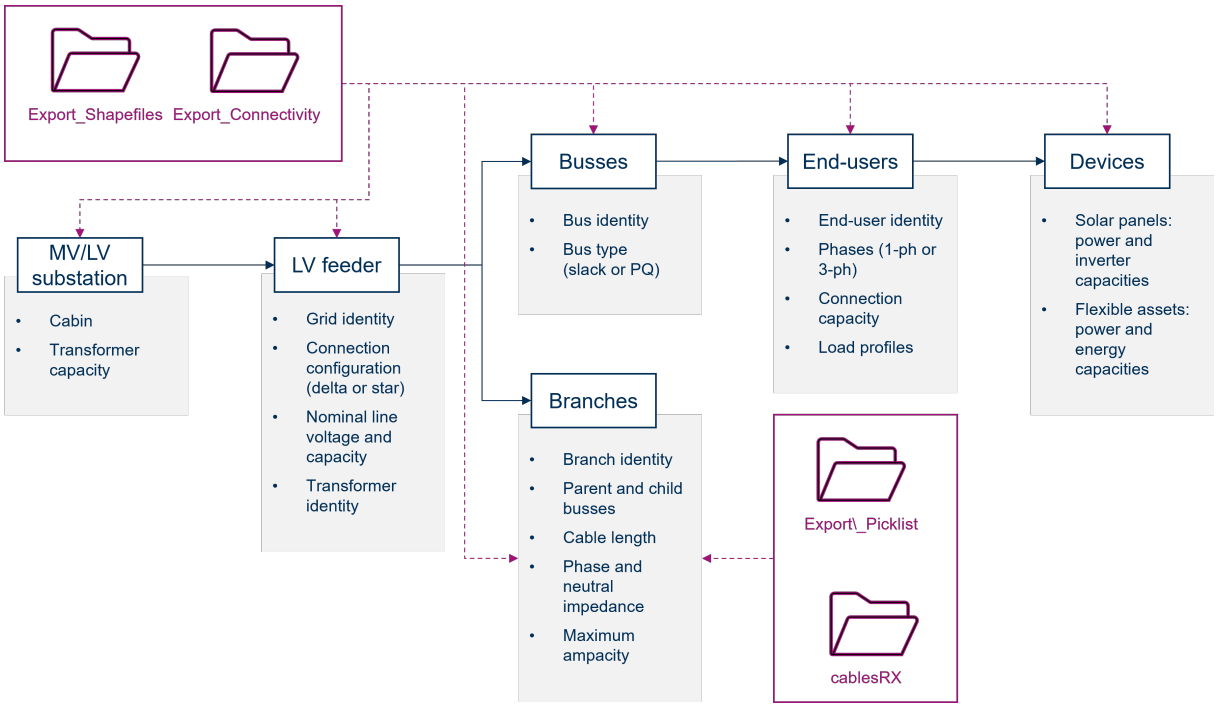

Figure 3.4: Components model hierarchy with relevant characteristics and raw data used as inputs into the model

Sibelga provided four main datasets, summarized below. The figure (3.4) illustrates how these datasets contribute to the grid model, detailing the connections between raw data and the required model inputs. The datasets are based on five files, with the primary documents briefly described for clarity. Note that additional documents not listed here may also exist but are omitted for brevity.

1. **Export_Shapefiles**: This dataset, compatible with Geographic Information System (GIS) readers, provides geographic information such as cable lengths.
2. **Export_Connectivity**: This file contains connectivity data for LV feeders, buses, branches, and end-users. Key documents include:

[1] While the majority of this work was conducted by colleagues from VITO, the PhD student contributed by leveraging expertise on Sibelga's data structure and adapting parsed data for specific studies.

- A document detailing the paths of assets, where each LV feeder (referred to as a *demi-boucle*) includes branch segment connectivity information.
- A document listing tens of thousands of end-users, specifying their connected substation, connection point, ampacity, phase connectivity, and annual consumption.

3. **Export_Picklist**: This dataset provides intrinsic characteristics of branches (e.g., branch labels, conductor number and size, nominal current, and maximum ampacity) and transformer details. However, it lacks sufficient information to compute branch impedance using Carson's equations, as detailed spatial data (e.g., inter-conductor distances) is missing.

4. **cablesRX**: This file complements the Picklist dataset by providing branch impedance information. It includes information extracted from the Eupen cables technical handbook:

   - Resistance values for specific cable labels.
   - Resistance-to-reactance ratios for various cable materials and sections, enabling the calculation of branch impedance.

The term "demi-boucle" reflects Sibelga's conceptualization of the LV distribution grid. As noted in the introduction, while the LV grid is modeled as radial, it is configured as an open loop (referred to as a *demi-boucle* in French) in practice. This loop extends from one substation to another and contains switches with normally one open and the other closed, effectively dividing the loop into two radial networks (or demi-boucles).

This terminology difference underscores the complexity of parsing and modeling specific LV grids, as even the semantic definitions can vary between stakeholders. For example, what Sibelga terms a *demi-boucle* corresponds to a LV feeder in other contexts.

The process of parsing Sibelga's raw data to populate the grid model is illustrated focusing on the single feeder 1002714281 with 5 busses. Fig. 3.5 shows the GIS representation of the LV feeder, derived from the shapefile provided by Sibelga, as well as the five first busses. Fig. 3.6 illustrates the parsing of this raw data into the model configuration, detailing the buses, branches, end-users with their respective phases, and any devices connected to the end-users, all arranged in the appropriate configuration. It is important to note that buses may connect to zero or multiple end-users and that these end-users can be connected in either single-phase or three-phase configurations.

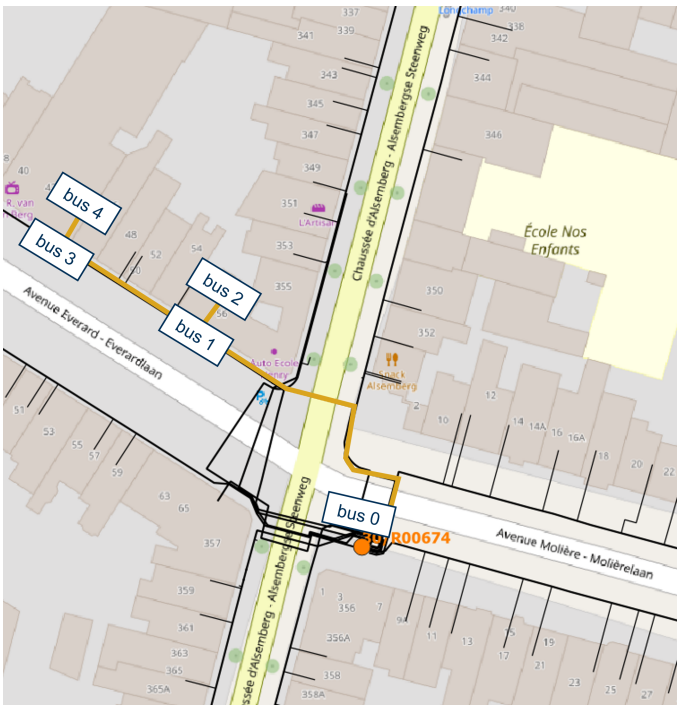

Figure 3.5: Illustration of the single LV feeder 1002714281 from the Sibelga dataset with the five buses and the representation on a map

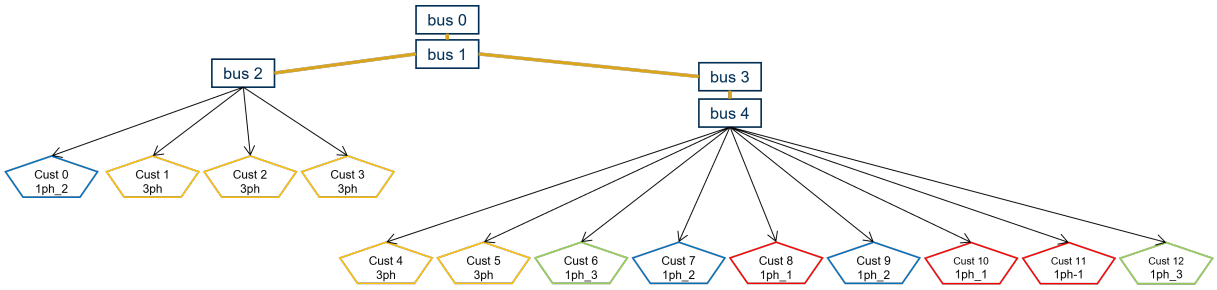

Figure 3.6: Illustration the corresponding model architecture of the single LV feeder 1002714281

3.2.3 Series impedance matrix

As outlined in the introduction, the series impedance of a distribution line comprises the conductor resistance, as well as the self- and mutual inductive reactances caused by the magnetic fields surrounding the conductors. In addition, for LV distribution feeder, the line cannot be considered as balanced and the inductance influence of each wire must be modeled individually.

General series impedance computation

In 1926, John Carson developed a set of equations to calculate self- and mutual impedances for distribution lines, accounting for the return path of current through the ground [75]. His work primarily addressed the problem of wave propagation along a transmission system consisting of a wire parallel to the Earth's surface, with applications in antenna and railway systems. These impedances are illustrated in Fig. 3.7 for two conductors. Carson's approach uses the concept of conductor images, where each conductor (shown in red and blue in the figure) at a specific height above the ground has an equivalent image conductor located at the same distance below the ground (depicted in lighter shades in the figure).

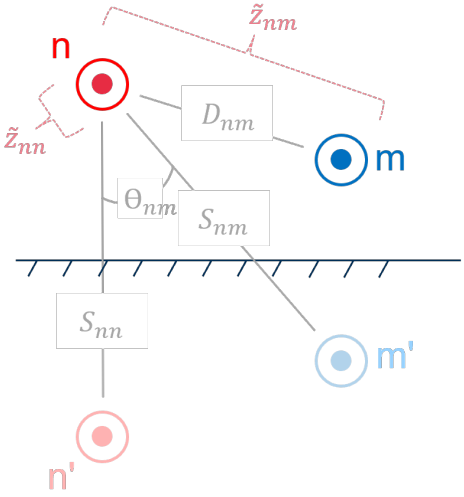

Figure 3.7: Representation of self and mutual impedances, as well as the conductor images [4]

Carson's equations to compute self- and mutual impedances are respectively given by Equation (3.1) and (3.2).

$$\tilde{z}_{ii} = r_i + 4\omega P_{ii} G + j\left(X_i + 2\omega G \ln \frac{S_{ii}}{RD_i} + 4\omega Q_{ii} G\right) \quad \Omega/mile \tag{3.1}$$

$$\tilde{z}_{ij} = 4\omega P_{ij} G + j\left(2\omega G \ln \frac{S_{ij}}{D_{ij}} + 4\omega Q_{ij} G\right) \quad \Omega/mile \tag{3.2}$$

with:

$$X_i = 2\omega G \ln \frac{RD_i}{GMR_i} \quad \Omega/mile \tag{3.3}$$

$$P_{ij} = \frac{\pi}{8} - \frac{1}{3\sqrt{2}} k_{ij} \cos\theta_{ij} + \frac{k_{ij}^2}{16} \cos(2\theta_{ij}) \left(0.6728 + \ln \frac{2}{k_{ij}}\right) \tag{3.4}$$

$$Q_{ij} = -0.0386 + \frac{1}{2} ln \frac{2}{k_{ij}} + \frac{1}{3\sqrt{2}} k_{ij} cos(\theta_{ij}) \tag{3.5}$$

$$k_{ij} = 8.565 \times 10^{-4} S_{ij} \sqrt{\frac{f}{\rho}} \tag{3.6}$$

where:

$\tilde{z}_{ii}$ is the self-impedance of conductor n [$\Omega/mile$],

$\tilde{z}_{ij}$ is the mutual impedance between conductor n and m [$\Omega/mile$],

r_n is the resistance of conductor i [$\Omega/mile$],

$\omega = 2\pi f$ is the system frequency [rad/s],

$G = 0.1609347 \times 10^{-3}$ [$\Omega/mile$],

RD_i is the radius of conductor i [ft],

GMR_i is the geometric mean radius of conductor i [ft],

f is the system frequency [Hz],

ρ is the resistivity of earth [Ωm],

D_{ij} is the distance between conductors i and j [ft] (cf. fig. 3.7),

S_{ij} is the distance between conductor i and image j [ft] (cf. fig. 3.7),

θ_{ij} is the angle between a pair of lines drawn from conductor i to its own image and to the image of conductor j (cf. fig. 3.7).

Carson's equations are inherently complex but can be simplified using the approximations provided in Equation (3.7) and (3.8) suggested by [4]. A 2011 study compared the original and modified Carson's equations and found that the error introduced by the simplification was less than 1% [76]. This level of accuracy can be considered acceptable, making the modified equations a practical choice for most applications.

$$P_{ij} = \frac{\pi}{8} \tag{3.7}$$

$$Q_{ij} = -0.0386 + \frac{1}{2} ln \frac{2}{k_{ij}} \tag{3.8}$$

These equations are used to compute the elements of the primitive impedance matrix. For instance, a four-wire distribution line segment, illustrated in fig. 3.8, will result in the 4×4 matrix given by Equation (3.9), represented in its full form and then in its partitioned form.

$$\begin{aligned} [\tilde{z}_{primitive}] &= \begin{bmatrix} \tilde{z}_{aa} & \tilde{z}_{ab} & \tilde{z}_{ac} & \tilde{z}_{an} \\ \tilde{z}_{ba} & \tilde{z}_{bb} & \tilde{z}_{bc} & \tilde{z}_{bn} \\ \tilde{z}_{ca} & \tilde{z}_{cb} & \tilde{z}_{cc} & \tilde{z}_{cn} \\ \tilde{z}_{na} & \tilde{z}_{nb} & \tilde{z}_{nc} & \tilde{z}_{nn} \end{bmatrix} \\ &= \begin{bmatrix} [\tilde{z}_{ij}] & [\tilde{z}_{in}] \\ [\tilde{z}_{nj}] & [\tilde{z}_{nn}] \end{bmatrix} \end{aligned} \tag{3.9}$$

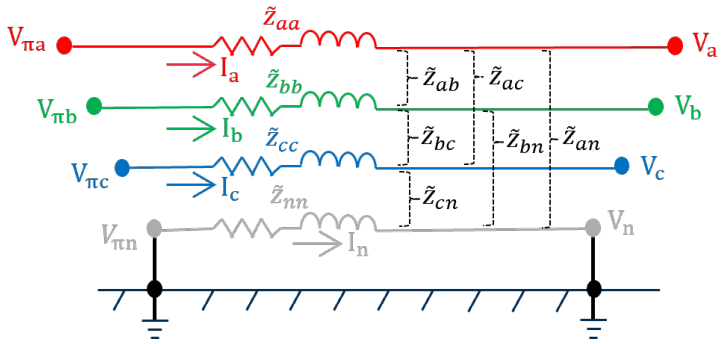

Figure 3.8: Representation of a four-wire distribution line segment with self- and mutual impedances and each neutral grounded [4]

Series impedance matrix reduction

Nevertheless, for most applications, the primitive impedance matrix must be reduced to a 3×3 matrix to reduce complexity. A widely used method for this purpose is Kron's reduction [77]. Kron's reduction is a method used in power system analysis to simplify impedance matrices. It is particularly useful for simplifying the primitive impedance matrix of an unbalanced series impedance model in distribution networks.

While effective, this approach assumes a distribution network with a grounded neutral at every bus, as illustrated in fig. 3.8. However, as discussed in subsection 2.1.2, European distribution networks predominantly employ TT configurations, where only the neutral at the feeder head is grounded. This configuration is depicted in Fig. 3.9.

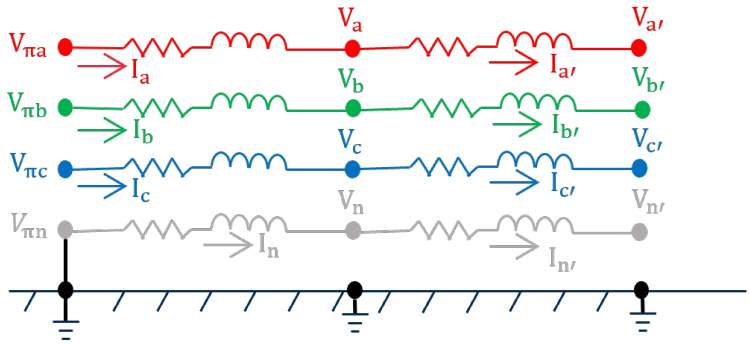

Figure 3.9: Representation of a four-wire distribution line segment with TT earth connection [5]

A reduction technique adapted to the sequence impedance modeling of European distribution feeders with TT earthing connections is introduced in [5]. This method formulates a three-wire equivalent considering neutral effect for the four-wire TT-grounded European LV networks.

In European LV distribution feeders, the return path is the neutral conductor, the effect of ground return does not exist. The mutual resistance term expressed in Carson's equation becomes zero. In addition, because R/X ratio is high, the mutual inductance term can be neglected. Finally, for simplification purposes, it is important to note that shunt admittances are neglected, as demonstrated in [4]. Equation (3.10) provides the reduced matrix.

$$[\tilde{z}_{reduced}] = \begin{bmatrix} \tilde{z}_{aa} + \tilde{z}_{nn} & \tilde{z}_{nn} & \tilde{z}_{nn} \\ \tilde{z}_{nn} & \tilde{z}_{bb} + \tilde{z}_{nn} & \tilde{z}_{nn} \\ \tilde{z}_{nn} & \tilde{z}_{nn} & \tilde{z}_{cc} + \tilde{z}_{nn} \end{bmatrix} \tag{3.10}$$

The proposed model produces more accurate power flow results compared to Kron's reduction when applied to the benchmark IEEE LV test feeder, and more generally to European TT grounded LV feeders, without adding computational complexity [5]. Consequently, line segments in this work will be modeled using Carson's equations or empirical data combined with the new reduced sequence impedance model for European LV feeders.

3.3 Conclusions

This chapter first presents the two grid case studies that are used throughout the entire manuscript: the IEEE European LV Test Feeder and 49 LV feeders provided by Sibelga. It also illustrates how raw data, provided either by the benchmark working group or by a real DSO, must be processed in order to be used as a grid model for further congestion identification and management tools.

Part II

Congestion Identification

Chapter 4

General Congestion Identification framework

Contents

4.1 Introduction to the Congestion Identification framework

Part I introduced the challenges faced by DSOs, the state of LV distribution grids, and the concept of congestion, illustrated through a simple example. It also provided an overview of the tools used to model LV distribution grids and presented the two case studies, explaining how they can be modeled using existing raw data.

Addressing these challenges requires effective tools to ensure grid safety and reliability [78]. However, most commercial Advanced Distribution Management System (ADMS) tools do not explicitly offer congestion analysis (e.g., the Network Manager ADMS from Hitachi Energy [79], the Spectrum Power ADMS from Siemens [80], and the ADMS from Schneider Electric [81]). To fill this gap, a congestion identification framework can be structured around four key components [49, 50], as outlined below and summarized in Figure 4.1.

1. LV grid model: Provides the structural and topological details of the LV distribution grid. Chapter 3 explains how raw data from DSOs or benchmark working groups can be used to build this model. This chapter will not repeat those details.

2. Probabilistic loads and generation profiles: Incorporates the stochastic nature of demand and distributed generation using probabilistic methods, and, where applicable, forecasting. The probabilistic load profile model for each end-user consists of sub-models (e.g., solar production, non-flexible load profiles), which, when aggregated, form the complete probabilistic load profile. As shown in the figure, several data sources are necessary to develop these models: data from DSOs (e.g., yearly consumption, connection capacity), weather data (e.g., solar irradiance forecasts), and aggregated data from System Operators (e.g., SLP).

3. PPF: Evaluates the electrical behavior of the grid under uncertainty to assess performance and risks. As highlighted in the figure, the probabilistic power flow receives input data from both the grid model and the probabilistic load profile models.

4. Congestion indicators: Define metrics to quantify and detect grid congestion, as summarized in subsection 2.2.1. As shown in the figure, this component also requires data from the DSO.

Finally, the figure illustrates the perimeter of the UTPF, which is important for Chapter III.

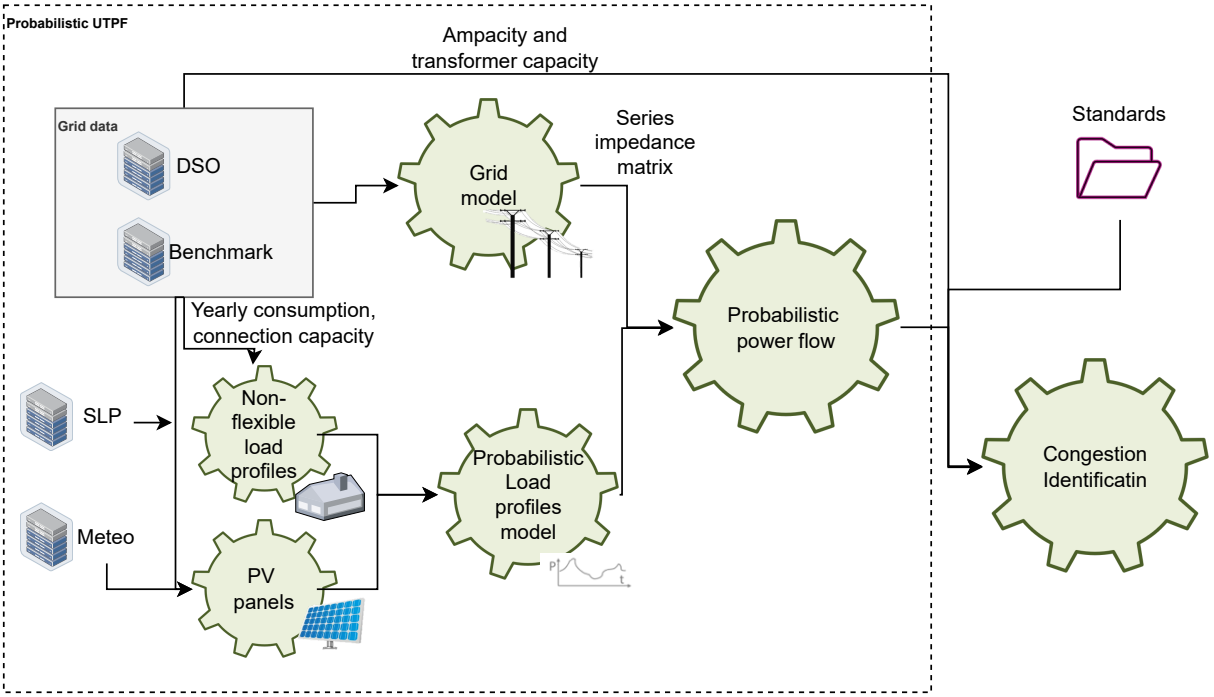

Figure 4.1: Overview of the building blocks for a congestion identifier

Part II presents a tool developed for DSOs to identify congestion in LV distribution grids, structured around the four components outlined earlier[1]. Building upon the foundational concepts introduced in Part I, this section is organized as follows:

- Chapter 4 - Introduces the general Congestion Identification framework and expands the current grid model by incorporating two key components: probabilistic LV load profiles and PPF analysis. Together, these components form a comprehensive tool for analyzing congestion in LV distribution grids.

- Chapter 5 - Applies this tool to a specific case study from this PhD research, focusing on the impact of LV assets providing frequency ancillary services on the LV distribution grid.

The remainder of this chapter provides a detailed analysis of the two remaining components of the framework, which were briefly introduced earlier.

4.2 Probabilistic load profiles

Probabilistic techniques are essential for accurately capturing the high variability in load and generation, limited data availability, and stochastic behavior characteristic of LV load profiles [34]. Additionally, emerging technologies like energy storage and electric vehicles further disrupt traditional load patterns, making probabilistic approaches indispensable [82].

A foundational overview of probabilistic forecasting methods is provided in [83], offering insights into general methodologies that, while not specific to energy forecasting, are applicable to this domain.

Numerous approaches exist for probabilistically modeling LV load profiles. For instance, [84] reviews various probabilistic load forecasting methods, such as Multiple Linear Regression and Artificial Neural

[1]This work is influenced by research developed by VITO over the past decade.

Networks. While these methods are primarily designed for transmission grids, they provide valuable insights for LV systems. Similarly, [85] examines bottom-up modeling techniques for residential electricity consumption, highlighting approaches such as conditional demand analysis, ANN, and probabilistic models. Furthermore, [86] proposes two techniques to generate realistic LV load profiles without historical data: the first using expert knowledge, the second using machine learning.

4.2.1 Simple probabilistic modeling of non-flexible low voltage load profiles

As highlighted previously, numerous methods exist to probabilistically model LV load profiles. This subsection describes the generation of non-flexible LV load profiles used throughout this manuscript.

In this research, non-flexible LV load profiles refer to consumption patterns that exclude models for PV production, batteries, EVs, and heat pumps. These profiles encompass, though not exhaustively, appliances such as refrigerators, dishwashers, lighting, and ovens. While these loads could theoretically be controlled to provide flexibility, their available power or energy is significantly lower compared to EVs, batteries, or heat pumps. Moreover, achieving controllability for these appliances presents greater challenges, as it often requires additional hardware. In contrast, batteries and EVs already incorporate control devices to manage charging effectively, simplifying their integration into flexibility strategies.

The literature presents several approaches to capture load variability for non-flexible load profiles. In [87], synthetic load profiles are employed, generated using a model described in [88], which simulates household profiles for two occupants. In [50], a normal distribution is assumed without extensive justification for this choice. A 2021 review [18] indicates that normal distributions are commonly used to model aggregated loads in LV networks, often based on synthetic profiles (e.g., Synergrid [89]), historical data fitting, or μ derived from historical data and variance set arbitrarily such as $\sigma = 0.07\mu$. In [50], μ is derived from forecasts, and σ is set arbitrarily at 0.1.

The method employed in this work for non-flexible load modeling is based on limited DSO data availability, specifically SLP, connection capacity (P_c^{max}), and yearly energy consumption (E_c^{year}). These inputs are provided for each end-user. While this method is not benchmarked against alternative approaches, it aims to capture the stochastic nature of LV load profiles using the available data from Sibelga, aligned with the SLP approach in [87]. Probabilistic load profiles in this study span four dimensions: end-user ID, timestep, power, and MC scenario.

The approach involves generating random non-flexible LV profiles derived from Synthetic load profiles published by the regulator or system operators (see [89] for Belgium). These profiles are scaled by the yearly consumption of each end-user. Since SLPs represent average behaviors and do not account for stochastic variations, additional variability is introduced while ensuring two constraints are met:

- The maximum power for each end-user does not exceed the connection capacity $p_c \leq P_c^{max}$.
- The average load profiles across MC scenarios conform to the desired SLP.

The process begins by extracting two attributes for each end-user from grid data: yearly consumption (E_c^{year}), which scales the load profile, and connection capacity (P_c^{max}).

The base mean active load profiles are calculated by scaling the SLP values SLP_{ts} with yearly consumption factors. These mean profiles are replicated for each of the MC scenarios m_c.

$$P_{c,ts}^{avg} = E_{year}^{c} \cdot SLP_{ts} \tag{4.1}$$

To introduce stochasticity, random perturbations P_{c,ts,m_c}^{var} are generated from a normal distribution with a mean of 0 and a standard deviation proportional to the connection capacity P_c^{max}, scaled by a variability factor β. Random perturbation are computed for each end-user, for each time-step, for each MC scenario.

$$P_{c,ts,m_c}^{var} \sim \mathcal{N}(0, \beta \cdot P_c^{max}) \tag{4.2}$$

Finally, the perturbations P_{c,ts,m_c}^{var} are added to the base load profiles $P_{c,ts}^{avg}$ to produce the final probabilistic load profiles P_{c,ts,m_c}.

$$P_{c,ts,m_c} = P_{c,ts}^{avg} + P_{c,ts,m_c}^{var} \tag{4.3}$$

To ensure physical plausibility, the generated load profile values are clipped to remain within realistic bounds, specifically constrained between 0 and the connection capacity of each end-user. This guarantees that the profiles are both non-negative and do not exceed the maximum allowable power. Reactive power

are computed by defining a constant power factor that will be defined and discussed in the subsequent case studies.

Probabilistic load profiles are generated for the 55 end-users of the benchmark grid, spanning 96 time steps and multiple MC scenarios. Figure 4.2 illustrates examples of four load profiles. For end-user 0 (blue) and end-user 1 (red), profiles are shown for two different MC scenarios (solid and dashed lines). Additionally, the modulated SLP is displayed for comparison.

The figure demonstrates that the generated load profiles exhibit significant variability. The profiles differ across end-users, vary over time, and fluctuate across MC scenarios.

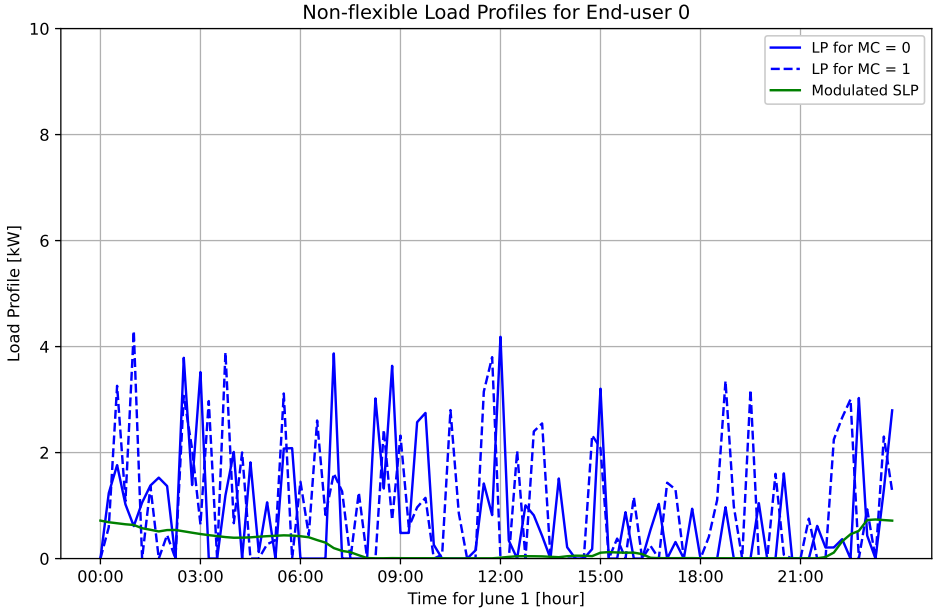

(a) Load Profiles for end-user 0 and two MC scenarios

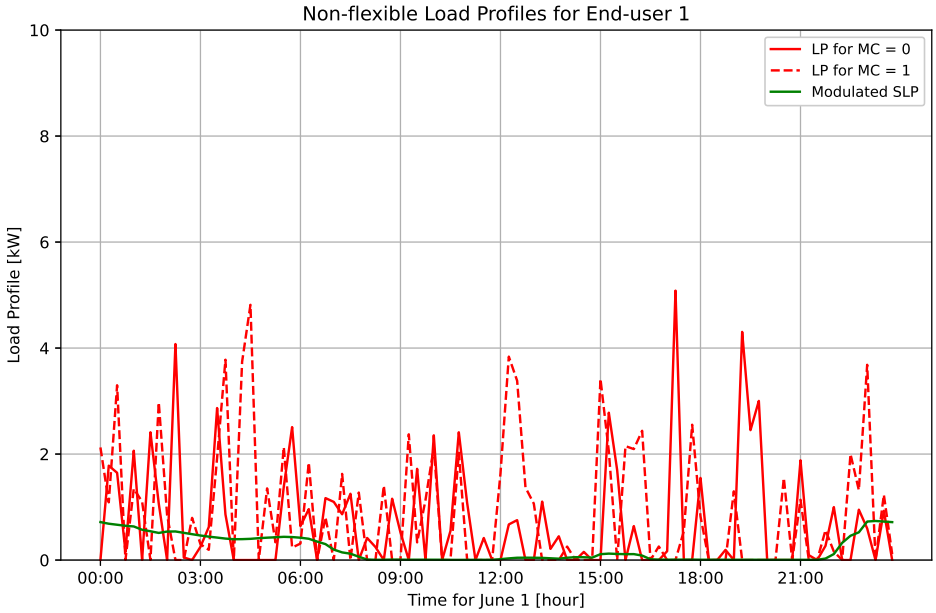

(b) Load Profiles for end-user 1 and two MC scenarios

Figure 4.2: Examples of generated load profiles for two end-users and two MC scenarios.

Figure 4.3 provides an overview of load profiles generated for all end-users, represented in light grey. The average load profiles, shown in blue, are compared to the SLP represented in green. The average load profiles exhibit some variability across MC scenarios, highlighting the stochastic nature of the generation

process. While the average profiles deviate slightly from the SLP, they retain the same overall daily pattern.

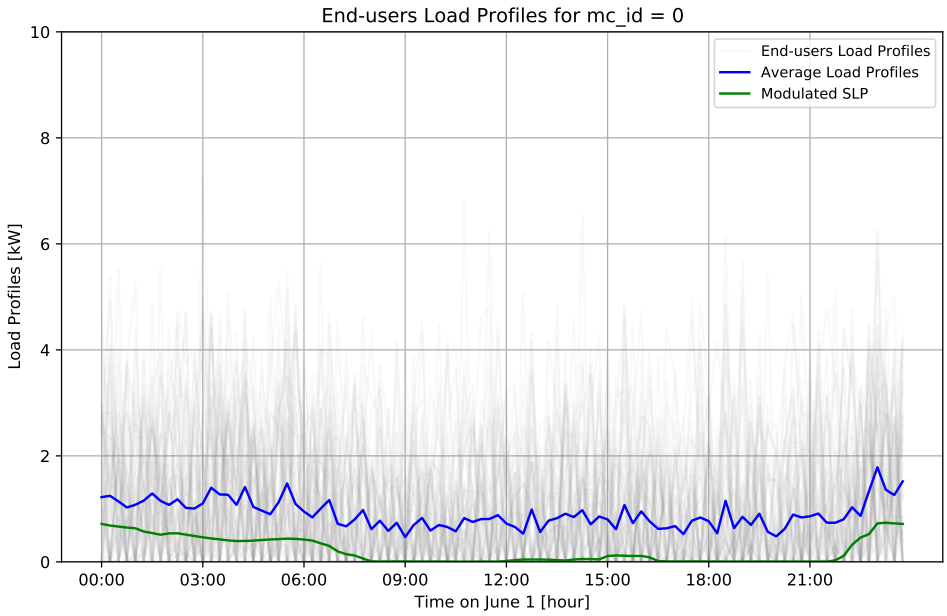

(a) Averaged Load Profiles and SLP for MC = 0

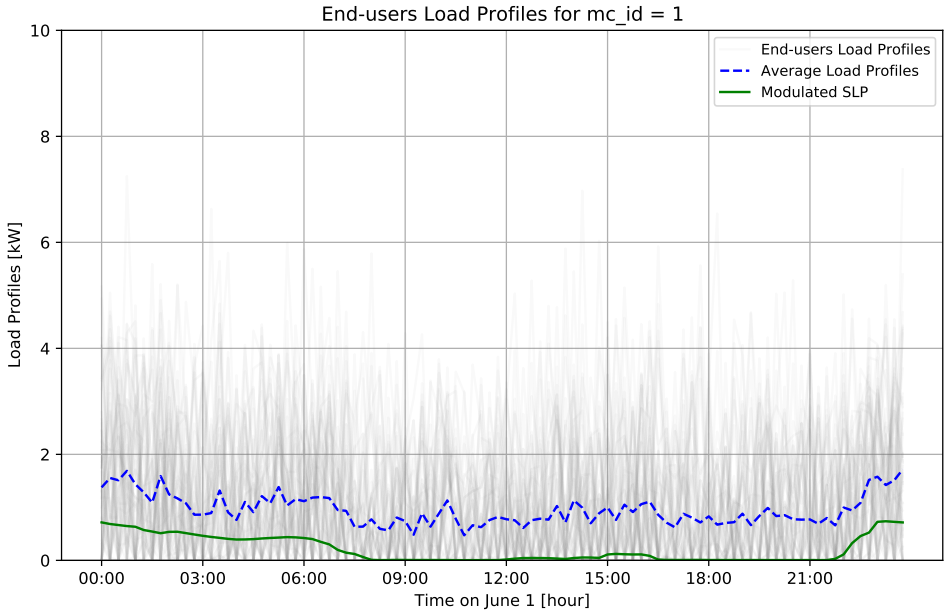

(b) Averaged Load Profiles and SLP for MC = 1

Figure 4.3: Averaged load profiles for all end-users, compared to the SLP, across two MC scenarios.

Although further refinement of the model parameters could enhance the realism of the generated load profiles, such improvements fall outside the scope of this manuscript. The primary objective was to generate stochastic load profiles that incorporate available data from Sibelga, specifically connection capacities and yearly consumption, while maintaining a behavior comparable to the SLP.

4.2.2 Simple modeling of phovoltaic production

The introductory section on LV load profiles probabilistic modeling also highlights several approaches for modeling or predicting PV production. However, as with LV non-flexible load profiles, solar forecasting

is not a primary contribution of this research. Instead, a probabilistic model for solar production is introduced to support the broader scope of this study.

The PV production profiles are defined by equation (4.4). The installed capacities of solar panels, $P_{panels,b}$, and inverters, $P_{inv,b}$, are assumed to be known parameters, provided by the DSO. For each scenario, irradiation profiles $I_{c,t}$ are randomly selected from a private dataset of historical solar irradiation measurements collected by VITO over the past six years in Genk. These profiles drive the production of all PV installations over 96 time steps. The efficiency coefficient η_{eff}, is applied to convert solar irradiation into energy production, expressed in $\frac{kWh}{kW}$ per time period.

$$S^{pv}_{c,t} = I_{c,t} \cdot \eta_{eff} \cdot \min(P_{panels,c}, P_{inv,c}) \tag{4.4}$$

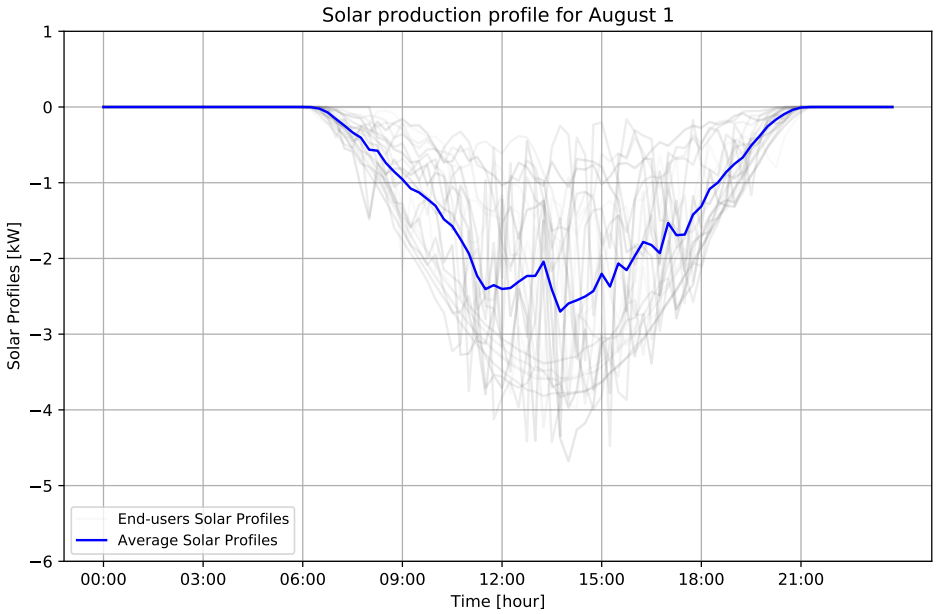

(a) PV production profiles for August 1

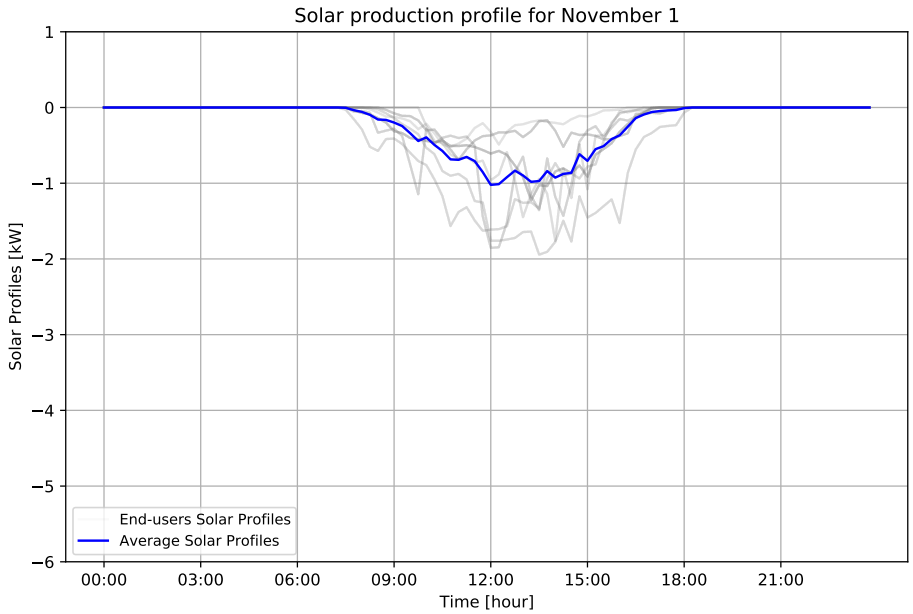

(b) PV production profiles for November 1

Figure 4.4: PV production profiles for two days in the year, August and November 1

Solar production profiles for two specific days of the year, August 1 and November 1, are illustrated

in Figure 4.4. These profiles represent the production of all end-users equipped with PV installations, assuming inverter and panel capacities of 5kVA and 5kWp, respectively. To facilitate comparison, average solar production profiles are shown in blue for each day.

As expected, solar panels produce significantly more electricity on August 1 compared to November 1 due to seasonal variations in solar irradiation. It is important to note that, in this part, solar production profiles are treated as negative values, whereas non-flexible load profiles are positive. This convention reflects the reference framework used: grid injections are defined as negative, while electricity consumption from the grid is defined as positive.

4.3 Probabilistic Power Flow calculation

The preceding sections introduced the grid model and probabilistic LV load profiles, which together form the inputs for the PPF. This PPF method determines the probabilistic distribution of the voltage and current at each bus and branch within the LV distribution grid, accounting for the uncertainty in LV load profiles.

Many probabilistic methods still rely on a deterministic load flow solution as part of the process [90]. Accordingly, this section is structured in two parts: first, the deterministic PF computation is presented, followed by its integration into a probabilistic framework. The equations governing the PF model are detailed, showing how the grid and load profile models are utilized in the calculations.

4.3.1 Deterministic Power Flow – Backward-Forward Sweep

As introduced earlier, three commonly used methods for PF computation include the BFS method, the Current Injection method, and the Holomorphic Embedding method. Among these, the BFS method is selected for this research due to its simplicity and computational efficiency, as outlined in the introduction.

The implemented PF model is an UTPF solved using the BFS method, as detailed in [4, 66].

This subsection presents the UTPF using the BFS method for deterministic analysis. The BFS algorithm is demonstrated on a simplified LV grid, illustrated in Figure 4.5. The grid assumes a single end-user per bus for simplicity, although in reality, there could be multiple or no end-users per bus. Additionally, the figure does not represent multiple branches originating from a single parent bus, which is possible in real systems. The model can be generalized to include these complexities, such as multiple end-users per bus or multiple child branches from a single parent bus. Finally, for clarity, individual phases of the grid are not depicted.

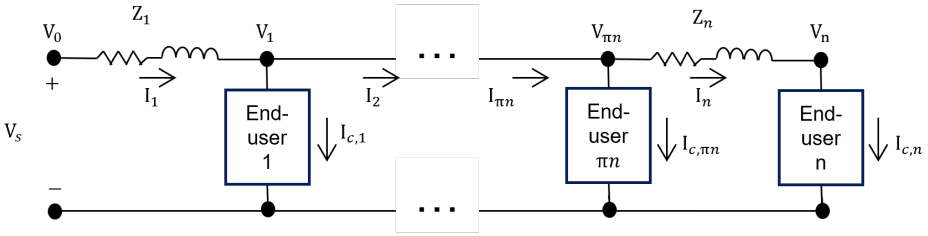

Figure 4.5: Representation of simplified LV distribution grid adapted from [4]

This approach considers a known voltage source value V_s^t. It initializes the computation progressing in a forward sweep towards the terminal bus $V_n^{k,t}$, assuming no load conditions. Under these assumptions, line currents $I_n^{k,t}$ and load currents $I_{c,n}^{k,t}$ are set to zero, resulting in $V_n^{k,t} = V_s^t$. Here, n, k, and t denote the branch, iteration index, and time step index, respectively. It is important to note that V_s^t can be time-varying, as in the case of an On-Load Tap Changer (OLTC).

The backward sweep begins at the terminal bus by computing the load current at the final bus with equation (4.5). Kirchhoff's voltage law is then applied iteratively to compute parent bus voltages, progressing toward the transformer using equation (4.6). In these equations, S_n^t represents the complex apparent power derived from the previously introduced load profile models, and z_n is the series impedance matrix described in the grid data model. Together, these equations establish the connection between the previously described models and the PF method. Both S_n^t and z_n are independent of the iteration index k, although S_n^t evolves with time, consistent with time-varying load profiles.

$$I_{c,n}^{k,t} = \left(\frac{S_n^t}{V_n^{k,t}} \right)^* \tag{4.5}$$

$$V_{\pi n}^{k,t} = V_n^{k,t} + z_n \cdot I_n^{k,t} \tag{4.6}$$

During the backward sweep, load currents are computed using Kirchhoff's current law, incorporating contributions from child branches and end-user loads. The parent branch currents are updated iteratively, as expressed in equation (4.7).

$$I_{\pi n}^{k,t} = I_n^{k,t} + I_{c,\pi n}^{k,t} \tag{4.7}$$

After completing the backward sweep, the voltage at the transformer, V_0, is determined. This voltage will be different from V_s. Another forward sweep is initiated to propagate updated voltages from the transformer to the terminal busses. This process works but requires time to converge.

An alternative method consists of performing a forward sweep computing the node voltage bus using the line current from the previous backward sweep, and not the current from the load. Child bus voltage is recalculated based on the parent branch current and impedance, as shown in equation (4.8). In this equation, bus voltage computations utilize the line currents obtained from the preceding backward sweep. Similarly, the next backward sweep relies on bus voltages calculated during the preceding forward sweep. This iterative exchange between the forward and backward sweeps typically requires a greater number of iterations for convergence but achieves this with reduced computational time compared to methods where the initial load current are used.

$$V_n^{k+1,t} = V_{n-1}^{k+1,t} - z_n I_n^{k,t} \tag{4.8}$$

This iterative process continues until the differences between phases voltages at the $k-1$ and k iterations at all buses fall below a predefined tolerance, as specified in equation (4.9).

$$\frac{||V_b^{k+1,t}| - |V_b^{k,t}||}{V_{\text{nom}}} \leq \text{tolerance} \tag{4.9}$$

The BFS UTPF algorithm is then executed iteratively for each time step, enabling the analysis of voltage and current distributions under daily load conditions.

4.3.2 Probabilistic Power Flow - Numerical sampling based method

Reference [91] categorizes probabilistic PPF methods into two main approaches: numerical, such as MC simulations, and analytical, including convolution methods. The paper also explores specific scenarios, such as nonlinear equations, changes in network configuration, and interdependence between stochastic variables. Applications discussed include grid planning, voltage control, integration of decentralized generation, three-phase imbalances, and harmonic studies. More recently, [90] provides a comprehensive review of PPF methods in distribution grids with PV and EV integration, focusing on three key components: uncertainty modeling, correlation modeling (e.g., autocorrelation or cross-correlation between assets), and calculation methods (numerical, analytical, and approximation). This review highlights the relevance of PPF methods for handling specific LV load profiles and distributed energy resources.

Based on these reviews, PPF implementation methods can be categorized into:

- Numerical - Estimate the output probability distribution through repeated sampling of input probability distributions and solving the power flow (e.g., MC simulations). Iterations continue until a predefined threshold, such as the number of iterations, is met.
- Analytical - Perform direct arithmetic operations on input probability density functions (PDFs) without iterative computation.
- Approximation - Use data from a limited number of sample points and their associated weights (representing input PDFs) to estimate the output statistics.

MC simulations are recognized for their accuracy in PPF analysis and are generally the easiest to implement among these methods. While the main drawback is their computational intensity, the tool provided by VITO operates efficiently within acceptable timeframes. For this reason, the numerical method using MC simulation has been selected for this research. A brief description of its implementation follows.

This subsection introduces the PPF framework used in this research. Specifically, PPF is used to account for the stochastic nature of variables when assessing voltage and current in the LV grid.

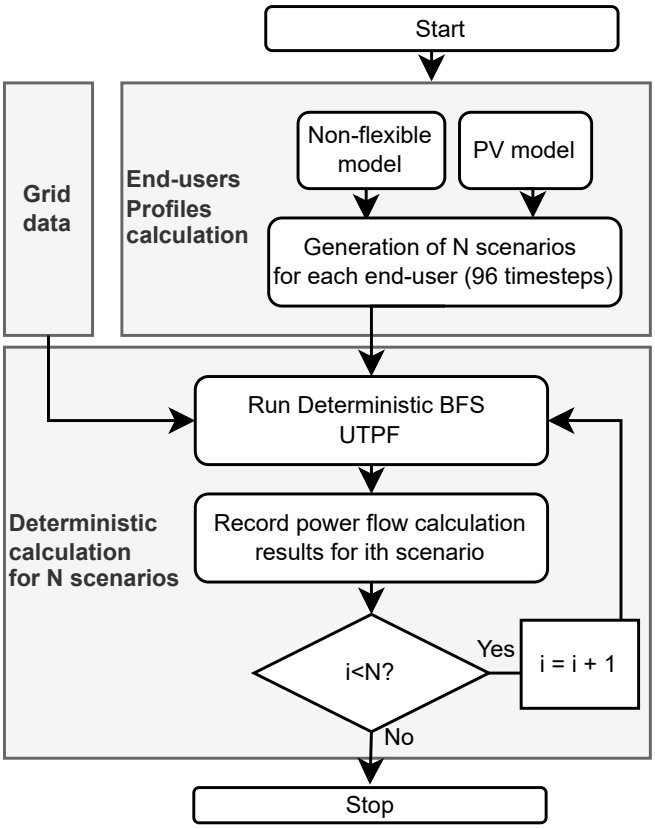

Figure 4.6: Framework of the PPF implemented in this research

The approach to implement the PPF using the previous grid model, LV probabilistic load profiles the UTPF BFS is illustrated in Figure 4.6. The approach starts by extracting grid data and generates probabilistic daily load profiles (96 time steps) for the number of scenarios required. The UTPF BFS is then computed for each scenario deterministically. The values of voltage and currents for each bus and branch are saved and till there is remaining scenario, the BFS is computed iteratively. The PPF computations consist in several deterministic UTPF BFS, computed using random values for the input variables. The values are for instance drawn from the PDFs deduced at the previous step, for every iteration.

The approach stops when all the N scenarios are computed with each of the N load profiles generated. Note that the grid data are the same for each scenario.

After performing PF computations for N scenarios, probabilistic current and voltage values can be analyzed for specific branches or buses. Figure 4.7 illustrates these probabilistic values, where currents and voltages are represented for each phase. These values were computed for a system with 18 solar panels installed on the IEEE LV distribution grid, each with a power capacity of 5 kWp and an inverter capacity of 5 kVA.

The probabilistic loading of the transformer can also be determined by summing the branch power flowing through Branch 0. This is depicted in Figure 4.8.

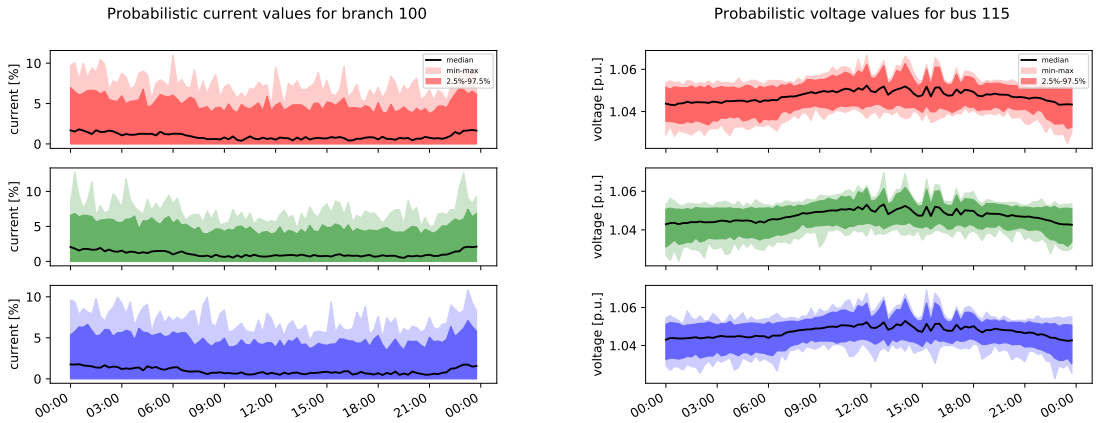

(a) Probabilistic current values for branch 100 (b) Probabilistic voltage values for bus 115

Figure 4.7: Probabilistic current and voltage values for a selected branch and bus across all phases.

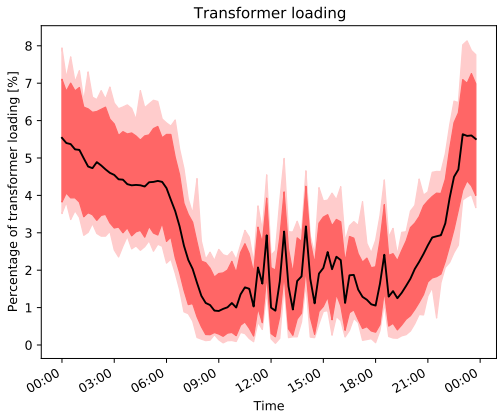

Figure 4.8: Probabilistic transformer loading values based on the sum of branch power flows.

4.4 Congestion limits

The previous sections introduced the modules for constructing a probabilistic LV UTPF model, which calculates voltage and current values while considering LV grid characteristics like high R/X ratios, radial configuration, phase imbalance, and stochastic load profiles. This section expands on the congestion identification tool by introducing congestion thresholds summarized in subsection 2.2.1.

4.4.1 Defining congestion thresholds

For each type of congestion outlined in the introduction (overvoltage (OV), undervoltage (UV), overcurrent (OC), and overloading of transformers (OT)) a corresponding threshold must be defined, as presented in subsection 2.2.1.

By comparing the computed voltage, current, and transformer loading values against these thresholds, it becomes possible to identify potential congestion events under the specified grid conditions and probabilistic LV load profiles.

The EN50160 standard, as mentioned in the introduction, sets the voltage congestion threshold at $\pm 10\%$ of the nominal voltage for continuous operation. Although voltage variations under 15-minute granularity are important, they will be addressed in the following chapter and are beyond the scope of this discussion.

For current congestion, the current values are expressed as a percentage of the branch ampacity, i.e., the ratio of computed current values to the branch's current-carrying capacity. A branch is considered congested OC when this ratio exceeds 100%.

For transformer loading, a threshold of 100% of its rated loading capacity is used to assess potential overloading conditions.

For this analysis, these thresholds are directly included in the Figures 4.9. Furthermore, rather than analyzing congestion bus by bus or branch by branch, the analysis focuses on the entire feeder. Therefore, maximum values (e.g., maximum voltage or current) across the feeder are compared against the thresholds, rather than examining specific locations individually.

4.4.2 Congestion analysis

The impact of congestion thresholds is illustrated using two case studies:

- Base Case: A system with 18 solar panels distributed across the LV grid, each with a capacity of 5 kWp and 5 kVA.
- High Solar Penetration Case: A system with increased solar penetration, featuring 40 solar panels, each with a capacity of 10 kWp and 10 kVA.

These case studies are consistent across all types of congestion (voltage, current, and transformer loading) to enable comparative analysis under identical grid configurations.

For voltage congestion, the computed maximum voltage values across the feeder are compared against the threshold defined by the EN50160 standard (±10% of nominal voltage). The figures for both case studies 4.9 demonstrate that in the high solar penetration scenario, the overvoltage threshold is reached, indicating a potential congestion event. These thresholds provide a clear basis for identifying and mitigating voltage congestion in LV grids under varying conditions.

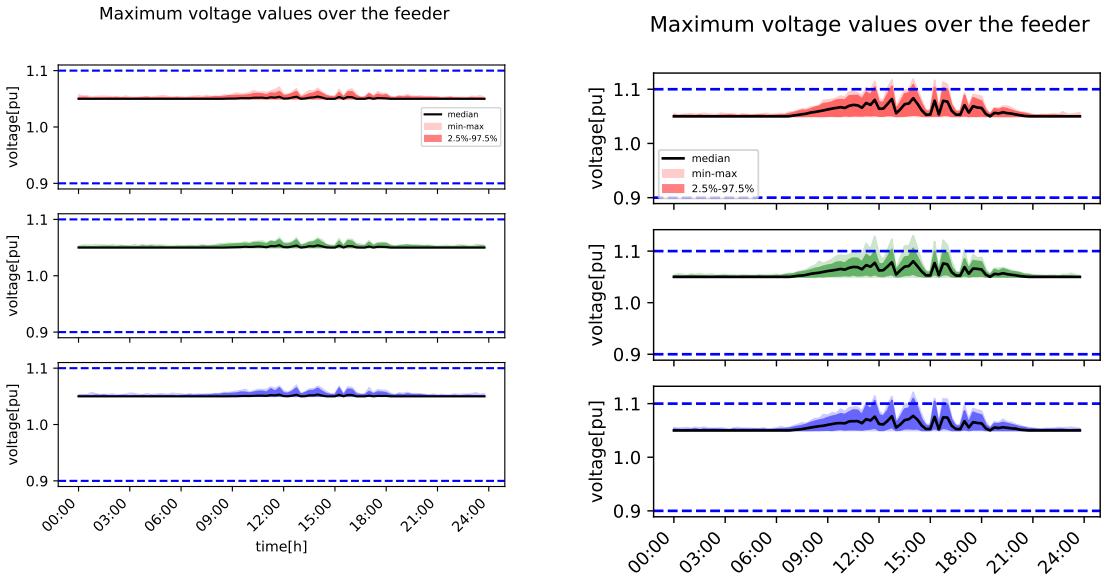

(a) Base case (b) High Solar Penetration Case

Figure 4.9: Comparison of maximum voltage values with OV congestion

Similar to voltage analysis, the current figures 4.10 represent the maximum current value across the feeder, rather than focusing on a single branch. The results show that similarly to OV, there is observable OC risks around noon, caused by solar production.

The congestion probabilities can be effectively summarized in a single figure that highlights the probabilities of OV, UV and OC, across the day for the entire feeder and all three phases. This is illustrated in Figure 4.11, which provides a comprehensive overview of the likelihood of congestion risks throughout the day. Each type of congestion is represented using a distinct color for clarity. Consistent with the earlier results, only OV and OC probabilities are visible, occurring between 12:00 and 18:00, when excess photovoltaic (PV) production is at its peak.

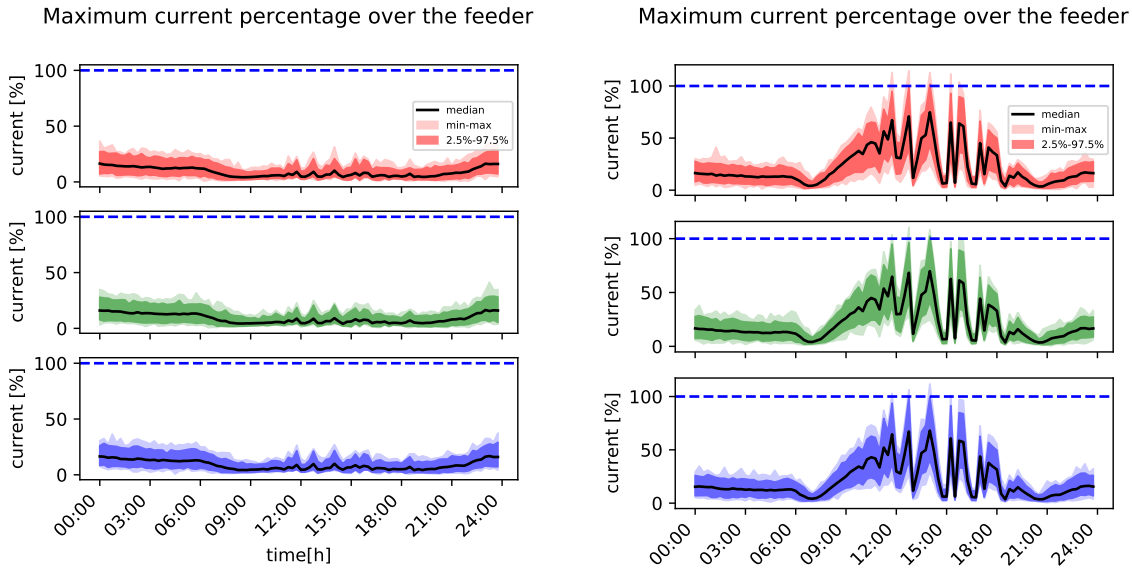

(a) Base case (b) High Solar Penetration Case

Figure 4.10: Comparison of maximum current values

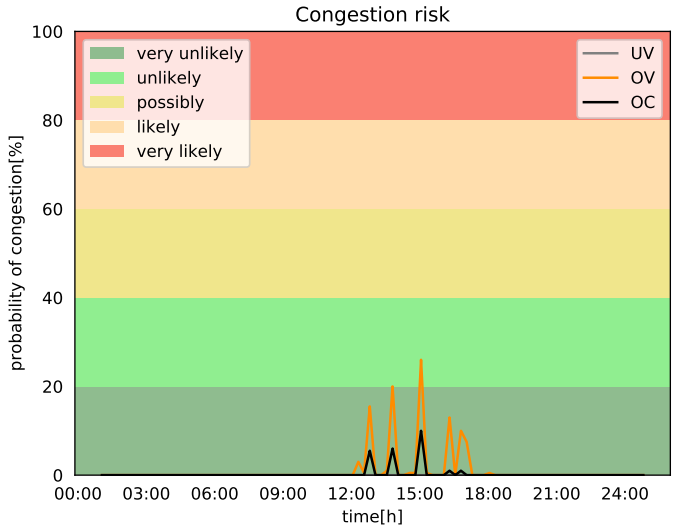

Figure 4.11: Probability of congestion risk (OV, UV, OC) along the day for the entire grid and across the three phases for the High Solar Penetration case

4.5 Model validation

The previous sections introduced the individual models comprising the congestion identifier framework. However, once the grid is modeled, validation becomes a critical step. The conclusions drawn from the results presented in subsequent chapters depend on the validity of these models and require clear identification of their limits.

This section provides an overview of the model validation process. Both benchmark grid and real grid validations are discussed, as each requires distinct techniques and considerations.

4.5.1 Benchmark grid validation

This subsection details the validation process using a benchmark grid. As a reminder, benchmark grids are not arbitrarily constructed; they are the result of decades of effort by working groups, such as the IEEE Power and Energy Society's Test Feeder Working Group under the Distribution System Analysis Subcommittee. These grids are rigorously validated and purpose-built to test algorithms and methods, ensuring their reliability for research applications.

To validate the proposed algorithm, the benchmark grid supplies grid data, deterministic load profiles, and voltage profiles for three end-users on the grid: end-user 1 (phase 1), end-user 32 (phase 3), and end-user 53 (phase 2). These profiles are obtained from PF calculations using GridLab-D, an open-source simulation tool for modeling power systems, including PF analyses [92].

The presented model is tested under the same conditions as those defined by the IEEE committee. Specifically, the grid data provided by the IEEE committee is extracted and translated into the model's architecture. Similarly, the deterministic load profiles provided by the benchmark are incorporated. A notable difference is that these profiles are specified at a 1-minute resolution, rather than the 15-minute resolution presented previously in the BFS model. The BFS PF model is then executed using these inputs and adapted to consider 1-minute resolution, and the resulting voltage profiles for the three end-users are compared.

Figure 4.12 illustrates this comparison. The upper graph presents the voltage profiles for each end-user over 1440 one-minute time steps generated by the BFS model. The middle graph displays the voltage profiles provided by the IEEE benchmark grid, validated using GridLab-D. The lower graph shows the error between the two sets of voltage profiles, calculated for each end-user and time step. The error remains below 0.2%, confirming the validity of the BFS model in capturing the physical behavior of a LV electrical feeder. This low error margin demonstrates consistency with the IEEE-validated benchmark model, providing confidence in the proposed approach.

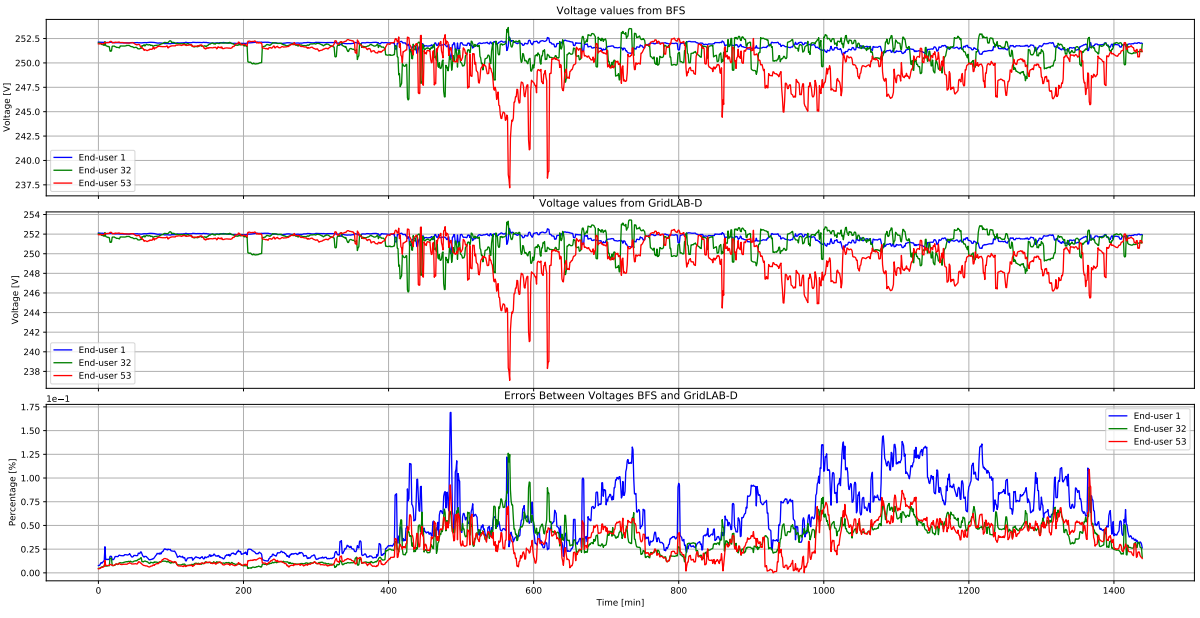

Figure 4.12: Validation of the grid model and the BFS PF presented in the research

4.5.2 Real grid validation

Validating the model against real grid data is also a crucial step. Although this task primarily falls under the responsibility of colleagues at VITO and is outside the direct scope of this PhD work, a brief overview of the validation methodology is provided here. While the grid architecture model and BFS PF model appear to be validated based on benchmark grid data, it is essential to compare the model outputs to real-world datasets, including both grid data and LV load profiles.

Access to measured data is indispensable for this validation. As mentioned in the introduction, Sibelga's access to smart meter data is limited. However, current metering devices installed in MV/LV cabins provide measurements that allow for the validation of modeled currents at the head of LV feeders. While individual end-user probabilistic load profiles cannot be independently validated due to data limitations, aggregated current measurements at the feeder head serve for assessing the model's accuracy.

The validation process involves comparing measured currents provided by Sibelga with modeled currents computed using the validated grid architecture and the BFS PF model, and probabilistic load profiles generated from Sibelga's grid data. By assessing the probabilistic current outputs at the feeder head against real measurements, the accuracy and reliability of the grid model can be evaluated.

This comparison is illustrated in Figure 4.13 for a specific LV feeder operated by Sibelga. The figure shows the probabilistic current curves at the feeder head for January 23 to 28, 2014. The black curve represents the median of the probabilistic values, the dark red region denotes the 25th to 75th percentiles, and the light red region encompasses the minimum and maximum values. The blue curve corresponds to the measured current data provided by Sibelga over the same period.

The measured data generally lies within the probabilistic range, and the trends in the modeled and measured currents are consistent. This suggests that the probabilistic modeling approach presented in the previous sections is reasonably accurate. However, discrepancies may arise due to factors beyond the grid data model itself, such as inaccuracies in the load profile models (as individual LV load profiles could not be validated) or potential inaccuracies in the provided grid data.

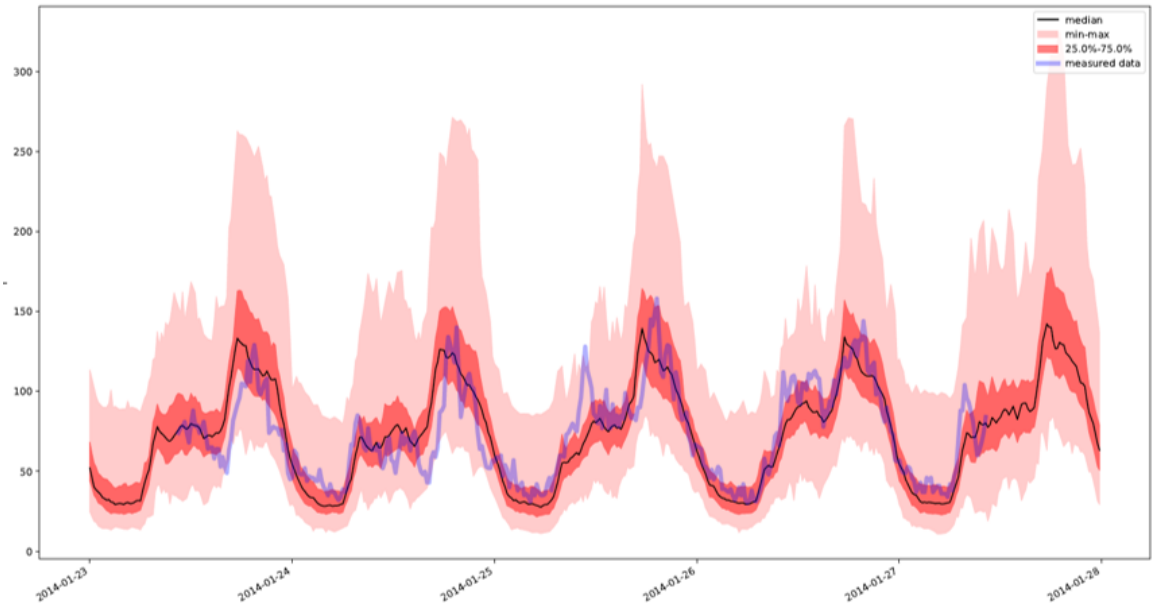

Figure 4.13: Illustration of grid data validation using modeled probabilistic current data (red) and measured current data (blue)

4.6 Conclusions

This chapter has detailed the methodology for analyzing congestion on a LV distribution feeder. The specific characteristics of LV grids have been thoroughly considered to ensure the methodology's applicability and accuracy. Key aspects addressed include:

- High R/X Ratio and Radial Topology: the BFS to perform power flow analysis is chosen due to

the high resistance-to-reactance (R/X) ratio and radial topology of LV networks. This approach ensures computational efficiency for such networks.

- Phase Imbalance: The inherent imbalance among phases in LV grids makes it necessary to consider self- and mutual inductance in the computation of the series impedance matrix. The model can therefore capture the unbalanced power flowing across different phases of the LV distribution grid.
- Stochasticity of LV load profiles: The high variability in LV load profiles requires the adoption of probabilistic models to accurately reflect the uncertainty and randomness in load patterns. Consequently, a PPF method was implemented to analyze the evolution of voltages and currents along the feeder under uncertain conditions.
- Congestion Thresholds: The identification of congestion relies on well-defined thresholds:
  - For voltage, the EN50160 standard specifies a $\pm 10\%$ threshold relative to the nominal voltage.
  - For current and transformer loading, thresholds are derived from technical handbooks, industry practices, and DSO conventions.
- Model Validation: A dedicated section was included to validate the model. First, deterministic results were benchmarked against reference data, ensuring the accuracy of the implementation of the grid and BFS models. Subsequently, insights were provided using real data from the Sibelga dataset, demonstrating the model's performance in real-world scenarios.

This chapter has not only highlighted and explained these critical steps but also justified their implementation as part as an LV congestion identification tool. By addressing the unique characteristics of LV grids, the methodology provides a comprehensive framework for analyzing congestion at LV distribution grid.

In the next chapter, this methodology will be applied to specific case studies that align with the operational challenges faced by DSOs. These case studies will demonstrate the practical utility of the congestion analysis framework, providing insights into its real-world applications and effectiveness in mitigating congestion in LV distribution systems.

Chapter 5

Congestion caused by LV assets providing ancillary services

Contents

5.1 Introduction

The previous chapter introduced a methodology to identify congestion risks in LV distribution grids for end-users with non-flexible assets and solar panels. However, it did not consider LV assets providing frequency control, now enabled by the CEP, nor their impact on the LV grid.

Regulatory developments increasingly encourage LV assets to provide flexibility services, such as frequency control. In the European regulatory framework, TSOs are encouraged to rely on flexible assets connected to distribution grids for system balancing [22].

However, activating or deactivating LV flexible assets for frequency control can lead to operational limit violations (e.g., voltage and current constraints) at the distribution level, thereby increasing congestion risks for DSOs. Consequently, it is essential for DSOs to assess the congestion risk associated with frequency control activation to ensure system operation remains within safe limits.

Therefore, this chapter focuses on the impact on LV distribution grid caused by LV assets activated for frequency control. More specifically, it focuses on FCR due to its rapid and automatic activation, and on aFRR due to its slightly slower but still fast activation and larger volume requirements. These reserves are defined as applied for Continental Europe [22] and previously outlined in Subsection 2.1.6. The focus on FCR and aFRR is particularly relevant since they are the first reserves accessible to LV assets in Europe. Fo example: since 2024, LV assets in Belgium are eligible for both FCR and aFRR services, comprising 10% of the assets pre-qualified for FCR [39]. Other frequency reserves, such as Replacement Reserve (RR) or faster reserves like the fast frequency reserve used in Nordic countries, are not considered in this study.

5.1.1 Time granularity on congestion limits for frequency services

This chapter aims to demonstrate the use of *continuous* congestion limits for 15-minute averages of frequency, voltage, and current, while also considering *instantaneous* voltage limits under full activation of LV assets providing FCR. This approach enables DSOs to accurately and safely estimate congestion caused by LV assets providing frequency control on the LV distribution grid. As a result, DSOs can avoid both overly restricting access to LV flexible assets for frequency control and making unnecessary grid reinforcement investments.

As outlined in the introduction, quantifying the risk of congestion requires first identifying the relevant operational limits that must be maintained. As presented in Subsection 2.2.1, at the distribution level, two electrical variables must stay within specific limits: the voltages at various busses and the currents on distribution elements (such as lines and transformers). Due to thermal inertia, currents are not required to remain below the branch rating at all times. However, they must remain below the rating on a 15-minute basis. Similarly, according to the EN 50160 standard, the average RMS values over 10 minutes should remain within -10% and +10% of the nominal voltage for 95% of the week.

In contrast to the current limits, voltages must also be maintained within specific limits at all times, *instantaneously*, meaning on a 10-second granularity. For example, in Belgium, generating units connected to the distribution grid (e.g., PV) must be disconnected if the voltage exceeds 15% of its nominal value. As a result, assessing the congestion risk associated with frequency control necessitates estimating (as outlined in Subsection 2.2.1):

- *continuous* congestion limits for 15-minute average values of currents and voltages
- *Instantaneous* voltage values within these 15-minute periods (e.g., every 10 seconds), with congestion limits adjusted to 1.15 p.u. for OV and 0.85 p.u. for UV

The rationale to consider instantaneous congestion limits when studying frequency services, compared to the non flexible load profiles and the PV production, is driven by the following three factors. They highlight the need to further investigate the impact of instantaneous frequency deviations on LV distribution grids:

- Fast and automatic activation: Once a bid is submitted, cleared, and dispatched, the TSO can send an activation signal. The assets must respond fastly and automatically, regardless of the potential risks to local LV congestion.
- Magnitude of volumes involved: The Belgian FCR market clears approximately 87 MW daily (with 6 to 8 MW already located at the LV level), while the aFRR clears around 145 MW [39]. These power magnitudes, when decentralized, are significant compared to the profiles typically observable on LV distribution grids.
- Activation coincidences: Unlike traditional, non-flexible load profiles, the activation of LV assets for frequency control may occur simultaneously if the entire reserve is called upon, which increases the risk of congestion challenges.

Compared to PV production profiles, LV assets providing frequency control are far less predictable, as their behavior depends on numerous external factors, including e.g. grid frequency deviations, economic considerations (e.g., market dispatch), or the strategies of FSPs. In contrast, solar panel output is primarily determined by irradiance, which is well forecasted with today's advanced prediction models, as outlined in the previous chapter.

5.1.2 Existing research and literature gap

Several methods have been proposed to assess the risk of congestion in LV distribution grids due to flexible LV assets. For instance, [93] and [94] assess the impact on a LV distribution grid of LV assets such as EV, HP and PV, and [95] studies the impact of HP and PV on a Belgian LV feeder. Furthermore, [96] analyses the impact of LV assets (batteries, PV, EVs) on a real Norway grid for market-oriented activities, such as P2P and local markets.

However, to the best of the authors' knowledge, only a very limited number of works consider LV assets providing frequency control and their impact caused on the LV distribution grid. Reference [97] studies the congestion of a European LV network caused by batteries providing self-consumption combined with other activities, such as frequency reserves. Nevertheless, this works deal only with average values of

currents and voltages over *continuous* congestion period (i.e. 15 minutes), and none of them deal with *instantaneous* values of voltages within these time periods (i.e. 10-seconds). It is thus inadequate to estimate the risk of congestion due to activation of frequency response services.

In North America, the transient response of LV aggregate loads providing frequency control is investigated in [98]. The study focuses on the surge currents due to building Heating Ventilation and Air-Conditioning (HVAC) loads when they are asked to increase their consumption (inrush/starting currents of induction motors). These surge currents, lasting typically a few hundreds of milliseconds, can have severe adverse effect on protection systems (unwanted trips). Although that work deals with instantaneous values of electrical quantities, it focuses on a problem very specific to induction motors and the approach cannot be transposed to the risk of congestion for all assets providing frequency control.

Thus, existing studies either focus only on average values or address very specific transient effects, making them inadequate for a comprehensive congestion risk assessment due to frequency control.

5.1.3 Contribution of this Chapter

This chapter adresses this gap and extends previous work published in CIRED 2023 [99], where a deterministic model assessed the impact of randomly distributed batteries providing frequency reserves on an LV feeder. The present work improves this methodology by:

- Enhancing congestion indicators to consider both *continuous* (15-minute) and *instantaneous* (10 seconds) voltage variations, enabling a more accurate risk assessment.
- Integrating an ARMA model to better capture high-resolution frequency variations, refining the probabilistic approach.
- Expanding the case study to evaluate the method under broader and more realistic conditions.
- Assessing the impact of aggregator activation strategies for aFRR, contrasting portfolio-based activation with a limited-reservoir approach.

The key contribution of this chapter is the integration of ARMA-based frequency modeling into the PPF framework, enhancing the estimation of *continuous* current and voltage variations and improving congestion risk assessment for LV assets providing frequency control. Additionally, the ARMA model validates the use of extreme frequency deviation inputs solely for assessing *instantaneous* voltage variations. These advancements are submitted for publication at PowerTech 2025.

The remainder of the chapter is structured as follows: Section 5.2 introduces the extended Congestion Identification framework, integrating LV assets providing frequency services. Section 5.3 delves deeper into the modeling of LV assets providing FCR services, with a focus on the ARMA model to capture the probabilistic nature of frequency deviations, supported by numerical results. The section also demonstrates the use of extreme frequency deviation input to study the impact of *instantaneous* voltage congestion. Section 5.4 presents the model for LV assets providing aFRR services, accompanied by numerical results. Finally, Section 5.5 summarizes the key conclusions of this chapter.

5.2 Congestion Framework extended to frequency services

The PPF methodology builds on the previous congestion identifier and is illustrated in Fig. 5.1. It is used to analyze the congestion probability in an LV distribution grid caused by LV assets providing frequency control.

The process starts by generating N probabilistic daily load profiles (96 time steps, corresponding to 15-minute intervals over a 24-hour period) for both non-flexible loads and PV production. Additionally, frequency profiles are modeled for end-users with LV flexible assets participating in frequency services.

For each scenario, a deterministic UTPF is computed iteratively until all N scenarios are completed. Each deterministic PF simulation uses random input values drawn from probability distributions established in the previous step, or determined by the frequency ARMA model. The voltage and current results are then evaluated against congestion thresholds to assess the probability of congestion.

As illustrated in fig. 5.1, stochastic load profiles assigned to each end-user are built on three probabilistic models: a model for LV assets providing frequency control $S^t_{flex,b}$ that will be particularly deepened in the subsequent subsections, a stochastic model for non-flexible loads $S^t_{nonflex,b}$ and a stochastic model for PV production $S^t_{pv,b}$. Note that $S^t_{nonflex,b}$ and $S^t_{pv,b}$ are discussed in the previous chapter and will

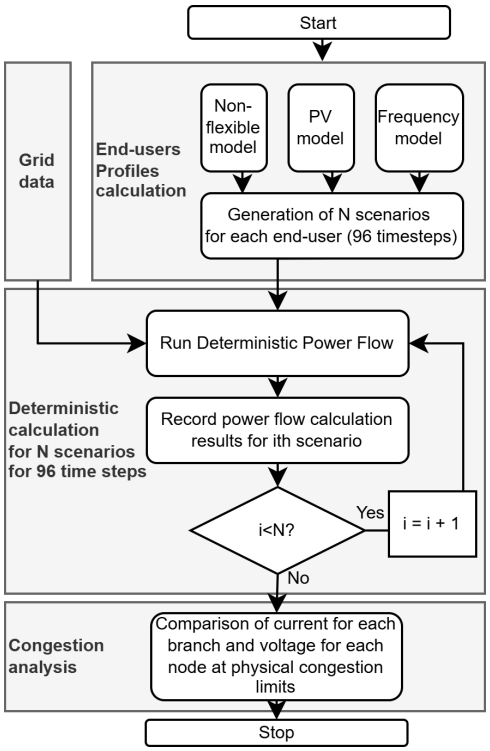

Figure 5.1: Flow chart of the PPF including LV assets providing frequency services

not be further defined in this chapter. The terms *load*, *load profile* or *profile* refer to both consumption and production, modeled as constant complex power given by Equation (5.1) for each timestep t and for each scenario N.

$$S_b^t = S_{flex,b}^t + S_{nonflex,b}^t + S_{pv,b}^t \tag{5.1}$$

The two following sections will describe the modeling of $S_{flex,b}^t$, differentiating based on whether the LV assets provide FCR or aFRR services.

5.3 LV assets providing FCR services

This section outlines the modeling approach for LV assets providing FCR. The following subsections are presenting:

1. The model to compute the power output of LV assets providing FCR based on the grid frequency deviation.
2. The motivation and implementation of using an ARMA model to forecast frequency, using the *continuous* congestion indicators.
3. The rationale for considering extreme frequency deviation as inputs for the LV assets with *instantaneous* congestion indicators, ensuring DSOs to remain conservative, as introduced in this chapter.
4. The presentation of numerical results.

5.3.1 LV assets providing FCR profiles based on the grid frequency deviation

LV load profiles providing FCR are modeled as proportional to the global system frequency deviation Δf^t, as defined in Equation (5.2). In this context, $S_{max,c}$ represents the maximum power reserved by each end-user for FCR. The frequency deviation Δf^t is calculated using 10-second frequency values f^t.

To model *continuous* FCR, values are averaged over each 15-minute time step into f^t_{avg} to compute the normalized average frequency deviation Δf^t. The computation, detailed in Equation (5.3), accounts for a maximum frequency deviation Δf_{max} of ±200 mHz, a deadband Δf_{db} of 10 mHz, and a nominal frequency f_{nom} of 50 Hz. It is important to note that Δf^t is uniform across all end-users at each time step, while $P_{max,c}$ varies between individual end-users.

$$S^t_{flex,c} = S_{max,c}\Delta f^t \tag{5.2}$$

$$\Delta f^t = \begin{cases} \frac{f_{nom} - f^t_{avg}}{\Delta f_{max}} & \text{if } \Delta f_{db} < |f^t_{avg} - f_{nom}| < \Delta f_{max} \\ 1 & \text{if } (f_{nom} - f^t_{avg}) \geq \Delta f_{max} \\ -1 & \text{if } (f_{nom} - f^t_{avg}) \leq \Delta f_{max} \\ 0 & \text{otherwise} \end{cases} \tag{5.3}$$

The power output of an LV asset providing FCR in response to a steadily increasing frequency signal over time is illustrated in Fig. 5.2. The maximum frequency deviation Δf_{max} is represented in green and the deadband Δf_{db} in orange.

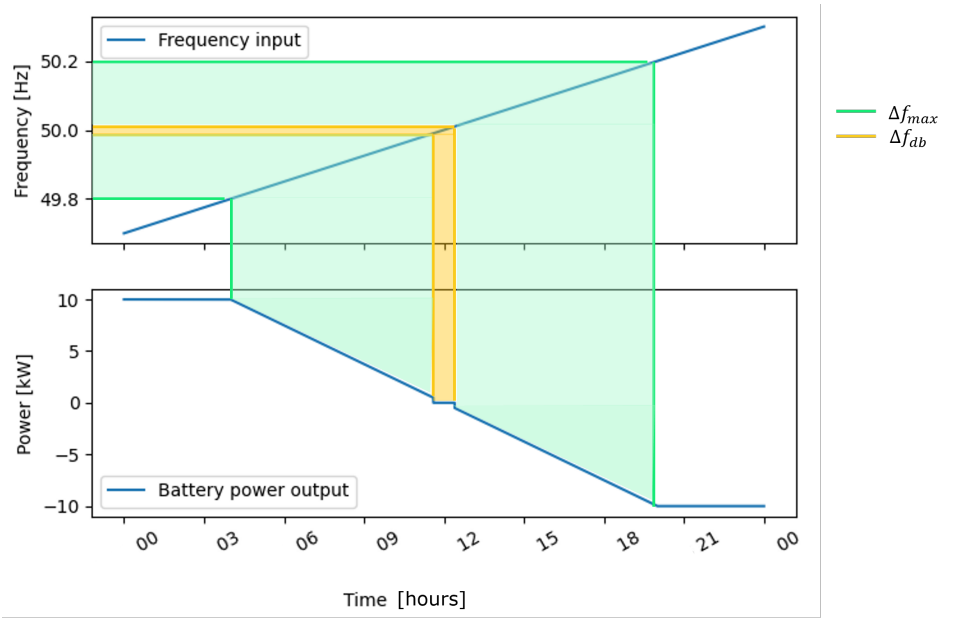

Figure 5.2: Power profile for a 10kW LV asset providing FCR to a steadily increasing frequency signal

For flexible LV assets with limited reservoirs, such as batteries, their capacity to provide frequency control must account for energy constraints. At any given time t, the available energy in the flexible asset is represented by $E^t_{flex,c}$, while $S^t_{flex,c}$ denotes the power consumed or injected during the timestep T_s, with the efficiency coefficient η_c. The energy in the asset must always remain within its operational limits: it cannot drop below a minimum threshold $E_{min,c}$ nor exceed its maximum capacity $E_{max,c}$.

$$E^{t+1}_{flex,c} = E^t_{flex,c} - \eta_c \cdot S^t_{flex,c} \cdot T_s \tag{5.4}$$

$$E_{min,c} \leq E^t_{flex,c} \leq E_{max,c} \tag{5.5}$$

The model does not include a mechanism for recharging batteries once depleted, as the focus is solely on the impact of LV assets providing frequency control. While FSPs must ensure sufficient capacity when assets are activated, their strategy for maintaining adequate charge levels is beyond the scope of this research.

The deterministic frequency deviation on January 8, 2021, along with the power output of a 10 kW/10 kWh battery providing FCR and its available energy is illustrated in fig. 5.3. This highlights the relationship between grid frequency and the power and energy response of a flexible LV asset with limited reservoir to frequency deviations.

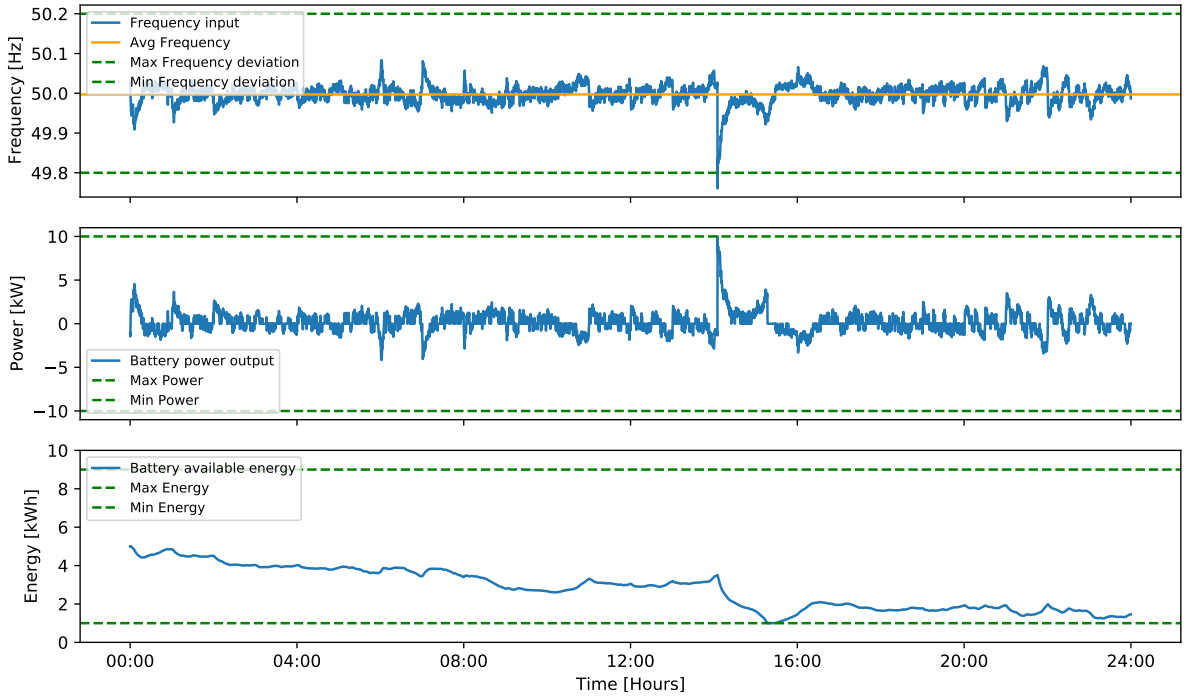

Figure 5.3: Frequency profiles, Power and energy outputs for a 10kW/10kWh LV asset providing FCR during January 8, 2021

5.3.2 Auto-Regressive Moving Average to model frequency for *continuous* FCR

Using the maximum positive or negative frequency deviation at each time step to compute a power profile proportional to FCR deviation can lead to overestimating congestion on the LV distribution grid. grid. Consequently, DSOs might either overly restrict access to LV flexible assets for frequency control to ensure its safe operation, or overinvest in grid reinforcement.

In practice, such extreme deviations are rare, with notable exceptions, such as January 8, 2021. To precisely identify congestion, this research incorporates the ARMA model, which accurately captures the frequency behavior and helps avoid unrealistic worst-case scenarios. The frequency deviation Δf^t is calculated using 10-second frequency values f^t, which are predicted from an ARMA model trained on 10-second historical data available on Elia's open data platform [100].

However, to ensure a safe operation of the LV distribution grid, the unrealistic case of extreme events considering a worst-case scenario activating full FCR will not be overlooked and will be discussed in the next subsection.

Motivation to use ARMA model

Scientific literature identifies two main approaches to study and forecast frequency behaviour: statistical models and machine learning techniques [101]. In [101], an Auto-Regressive method is used to predict grid frequency for both small-scale microgrids and the UK power grid, with forecast horizons between 10 and 200 seconds. Reference [102] compares two methods for predicting frequency in three U.S. power grids (Eastern, Western, and Texas) over 5 to 30 minutes: an ARMA model and a kernel regression (similar to K-nearest neighbors). The study suggests that while machine learning (kernel regression) performs better for longer horizons (30 minutes), both ARMA and kernel methods provide similar results for shorter forecasts, depending on the grid. In [103], a long short-term memory (LSTM) neural network forecasts short-term frequency (0.1 to 1 second) on the UK power grid. Lastly, [104] applies a weighted nearest neighbor method to predict frequency in Continental Europe, Great Britain, and Nordic grids for multiple horizons (15, 30, and 60 minutes).

Based on this recent literature review, no single method clearly outperforms the others. In this research, an ARMA model is chosen due to its demonstrated effectiveness in prior studies, suitability for forecasting highly self-correlated time series (i.e., correlation between a signal and its lagged versions [105, 106]), and ease of implementation.

Indeed, [105] highlights that ARMA is relevant to characterize or forecast a time series when its self-correlation is high. Using frequency historical data from Elia's open data platform [100], Figure 5.4 illustrates the 10-second frequency autocorrelation for January 2021, highlighting the high self-correlation observed in the time series. Note that this period is specifically chosen to emphasize the three outlier points deviating from the curve, corresponding to the unexpected event on January 8, 2021, when the maximum frequency deviation was reached, fully activating the FCR.

The autocorrelation can be further quantified using the PCC, defined in Equation (5.6).

$$\rho_{X,Y} = \frac{cov(X,Y)}{\sigma_X \sigma_Y} \tag{5.6}$$

where *cov* is the covariance and σ_A the standard deviation of the random variable A.

A PCC close to 1 indicates strong positive correlation, meaning the frequency amplitude at time t is similar to that at t+1. A PCC close to 0 implies little to no correlation. Table 5.1 presents PCC values for different lagging times for the 10-second frequency signal in January 2021 provided by Elia.

Table 5.1: PCC for lagging times for the 10-second frequency signal in January 2021.

	t	t+1	t+2	t+3
t	1.0000	0.9489	0.8897	0.8513

Figure 5.4 and the high PCC values demonstrates the strong autocorrelation shown by historical grid frequency data, thereby justifying the use of an ARMA model for frequency prediction.

ARMA implementation

The methodology for forecasting time series with strong autocorrelation, known as the ARMA model, is presented in [105]. In general, this model assumes that an observable time series z_t, where values are

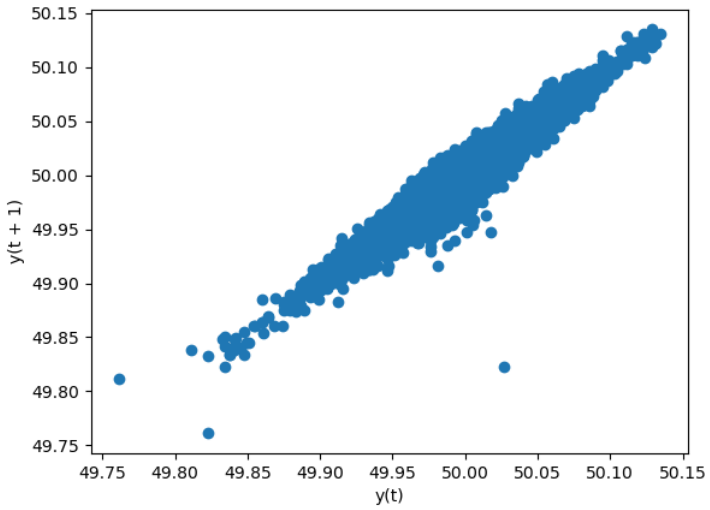

Figure 5.4: Autocorrelation for the 10-second frequency signal in January 2021

Table 5.2: ARMA parameters estimation

Unknowns	**Coefficient**	**Std error**
ϕ_1	0.92	0.005
θ_1	0.22	0.012
μ	49.99	0.001
σ_a^2	2.46 e-05	3.01 e-07

highly dependent, can be represented as a combination of a finite linear aggregation of lagged values and random shocks a_t. The general form of the ARMA (p,q) model is:

$$\tilde{z}_t = \phi_1 \tilde{z}_{t-1} + ... + \phi_p \tilde{z}_{t-p} + a_t - \theta_1 a_{t-1} - ... - \theta_q a_{t-q} \tag{5.7}$$

The model consists of $p+q+2$ unknown parameters: $\phi_1, ..., \phi_p, \theta_1, ..., \theta_q, \mu$ and σ_a^2.

The results presented in this manuscript focus on forecasting general frequency variations, as well as frequency variations for a specific dayJ anuary 8, 2021, involving an unexpected event. The ARMA model is trained using 10-seconds data collected from January 1 to January 7. The first step in defining the model is to determine the orders p and q. The complete methodology for modeling frequency using ARMA is detailed in Annex A.1, leading to the selection of an ARMA (1,1) model meaning that $p = 1$ and $q = 1$.

For this ARMA (1,1) model, the corresponding unknown parameters are computed, and the results are presented in Table 5.2, along with the steady-state error of the prediction interval.

Now that the ARMA model is defined, it can be used to predict frequency, which will serve as an input for LV assets providing FCR. In addition, as it will be discussed in the next subsection, the same ARMA model can be used to forecast frequency to verify that, following an extreme event, the frequency tends to return to its average value within less than 15-minute period.

5.3.3 Full activation to model frequency for *instantaneous* FCR

In contrast to the previous subsection, this section emphasizes the importance of considering the impact of maximum frequency deviations on LV congestion. Although such events are currently rare, DSOs can still be impacted for these extreme scenarios when assessing the congestion impact on their distribution grids. To evaluate these deviations, a worst-case scenario is considered, where LV assets are modeled as $S_{fcr,b}^t = P_{max,b}$.

In the event of unexpected extreme frequency deviations, i.e., when the frequency deviation reaches the maximum limit Δf_{max} over a few 10-second time steps, extreme load activation could occur simultaneously, potentially causing instantaneous LV network congestion. Since frequency deviations are averaged over 15-minute periods in the *continuous* model, this worst-case scenario, and its corresponding load profiles, are not fully captured in the averaged data.

While such extreme events are inherently unpredictable, the evolution of the frequency signal following the event can still be anticipated. Evaluating this impact involves assessing the transmission grid's ability to contain and restore frequency after these extreme events and determining whether DSOs should account for such deviations in both *continuous* and *instantaneous* congestion models. This will be explored further in the case studies presented in a subsequent section.

However, when studying such events, the case study aims to demonstrate that it is possible to consider only voltage congestion, adapting the voltage limits to 0.85 p.u. for UV and 1.15 p.u. for UV, rather than the presented 0.9 p.u. and 1.1 p.u. This approach helps DSOs to more accurately assess the impact of extreme frequency events on their distribution grid, while avoiding the overestimation of voltage congestion.

5.3.4 Numerical results - Distinguishing between *continuous* and *Instantaneous* FCR models

This subsection outlines the rationale for adapting FCR load profiles for *continuous* and *instantaneous* congestion thresholds. As presented previously, frequency deviation is presented to be computed with an ARMA model for *continuous* FCR and considering a maximum frequency deviation for *instantaneous* FCR.

In this case study, the ARMA mode is used to predict frequency behavior following an unexpected extreme event. The model's performance is validated against historical frequency data from January 8, 2021, when the frequency dropped to 49.8 Hz.

To evaluate its performance, the ARMA model is benchmarked against a naive predictor that assumes frequency variations follow a normal distribution fitted to historical data. For January 2021, the naive predictor is fitted to an average frequency of 49.9942 Hz with a standard deviation of 0.0199 Hz for Continental Europe.

Figure 5.5 illustrates the frequency behavior post-extreme event, comparing historical data (blue and green) with the ARMA probabilistic prediction (average in orange, 99.9% prediction interval in light orange) and the naive persistent model (purple). Blue data are used to train ARMA model and green data to validate it. Over a 15-minute period, ARMA achieves a lower Mean Squared Error (MSE) of 0.24 compared to 0.30 for the naive model, confirming ARMA's superior predictive accuracy at a 10-second granularity, after the occurrence of an extreme frequency event.

The predicted average frequency returns to the historical frequency within 6 minutes 10 seconds. This finding is important, as overcurrent OC must last longer than 15 minutes to damage network components like cables or transformers due to their thermal inertia. Furthermore, voltage congestion (OV and UV) are defined differently for *continuous* and *instantaneous* voltage variations. These results validate the use of 15-minute averaged predicted frequency data using the ARMA model for assessing *continuous* congestion thresholds, as frequency is restored well within the averaging period.

However, for instantaneous congestion thresholds, relying solely on 15-minute averages may overlook instantaneous frequency peaks and FCR model is suggested to be adapted in the form $S^t_{fcr,b} = P_{max,b}$ considering only voltage limits with adapted congestion thresholds set to 0.85 p.u. and 1.15 p.u.

Note that the model is validated based on a single extreme event, which limits its reproducibility. To strengthen the robustness of these numerical results, further validation should be performed on additional datasets featuring extreme events, either from different time periods in Europe or from other regions around the world. However, the authors consider it valuable to question the applicability of using only frequency predicted with ARMA with *continuous* LV congestion indicators in the context of LV assets providing frequency control.

5.3.5 Numerical results - Impact of LV assets providing FCR

Regarding grid data, the reduced IEEE European LV Testfeeder is chosen for the benchmark grid case study [63]. As outlined in 3, this grid connects 55 end-users and their initial phase connections are given. Each end-user is connected to the grid with a maximum power capacity (in this case: $\pm$ 9.2 kVA). Voltage at slack bus is set at 1.05 p.u.

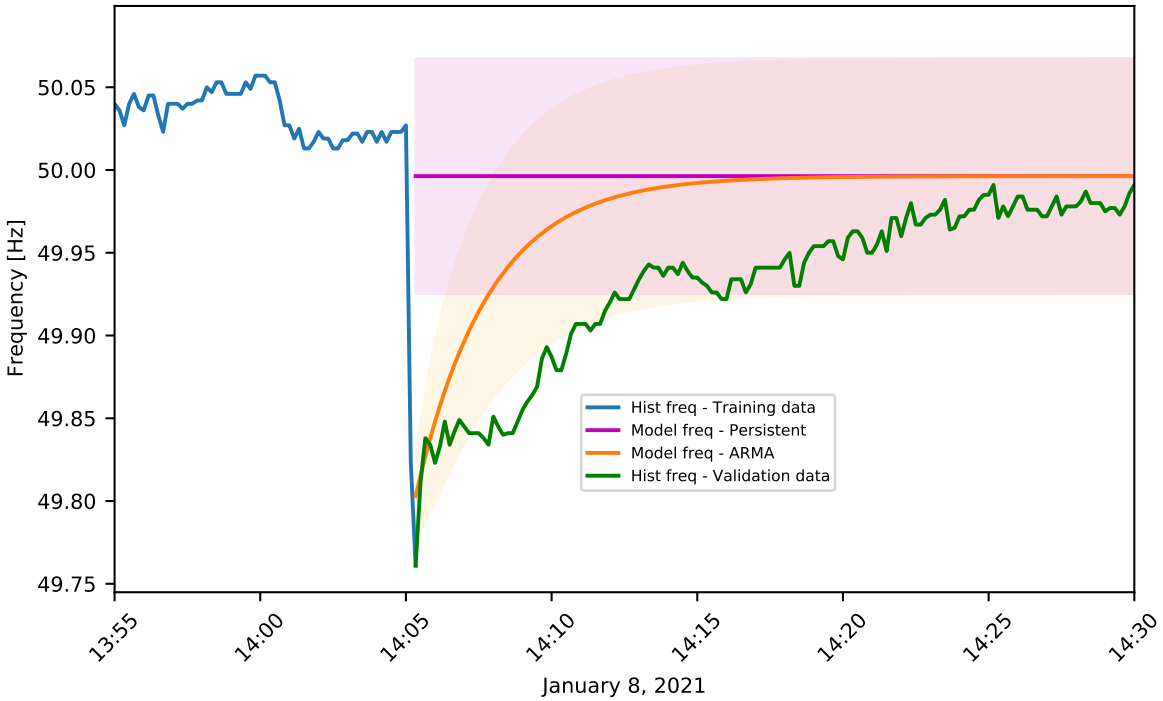

Figure 5.5: Part of historic trained frequency data at 10 seconds granularity till January 8, 2021, at 14:05:20 in blue, forecast frequency data with ARMA model in orange and with persistant model in purple, historic frequency data to validate from January 8, 2021 at 14:05:20 in green

Regarding load profiles, half of the end-users are assumed to own LV assets providing flexibility, as well as solar panels. These assets are distributed such that one out of every two end-users is equipped.

Each end-user with flexible LV assets is assumed to contribute up to 10 kW/20 kWh for FCR or aFRR services. Consequently, $P_{max,b}$ for FCR is set at 10 kW per end-user with flexible assets.

Non-flexible load profiles and PV production profiles are derived from historical data, as described in Chapter 4. The mean SLP_t for non-flexible load profile is derived from the 2023 Belgian synthetic load profiles, as published by Synergrid, the system operator federation in [89]. Yearly energy is set to 3500kWh. The summer solstice is selected as the reference day for sampling, ensuring there is solar irradiance for PV production. Each PV system is configured with an inverter capacity of 5 kVA and a peak installed power of 5 kWp.

Fig. 5.6 shows the probability distribution of voltages [p.u.] per phase for the most loaded bus (bus 80 connecting end-user 36) on the summer solstice. The left panel represents the scenario where LV assets providing FCR follow an averaged probabilistic frequency signal for the 15-minutes analysis. In this case, voltages remain below the *continuous* OV congestion threshold (red dotted line), indicating no congestion.

The right part of the figure depicts the voltages per phase for the instantaneous analysis. In this scenario, LV assets are modeled to deliver maximum power as a response to an unexpected extreme frequency event. Consequently to consider instantaneous congestion, the OV congestion threshold is raised to 1.15 p.u. The figure shows that while voltages may momentarily exceed the *continuous* congestion threshold during the extreme event (light dotted line), they remain below the instantaneous congestion threshold (red dotted line). As a result, no *instantaneous* congestion occurs in this scenario.

Therefore, this result highlights the importance of using consistent congestion thresholds to avoid overestimating the congestion caused by FCR on the LV distribution grid. This approach helps increase the access of LV flexibility for frequency control.

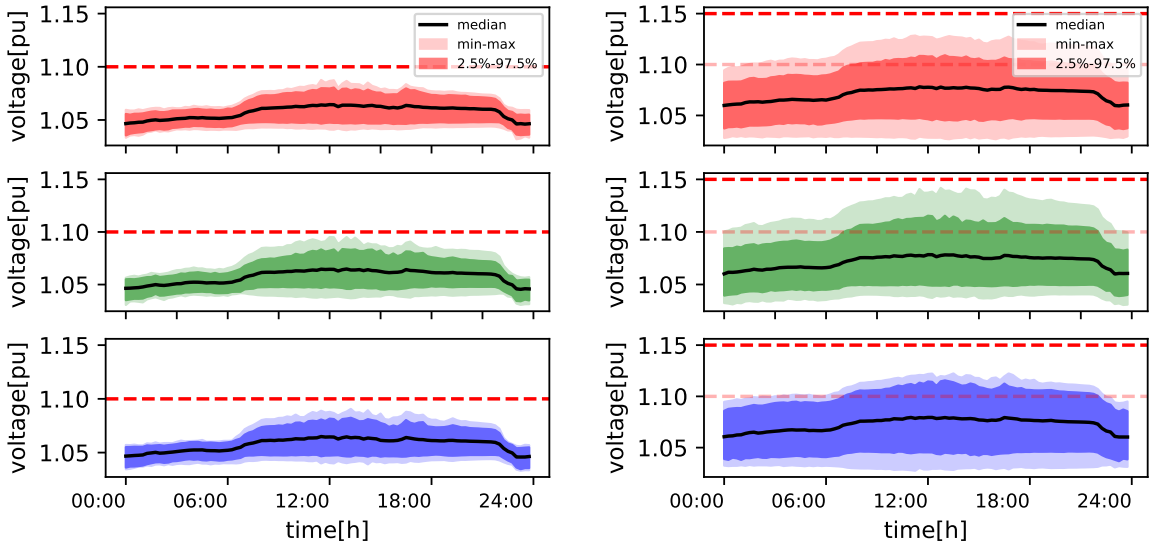

(a) LV assets following probabilistic frequency signal for continuous congestion threshold

(b) LV assets following worst case frequency signal for instantaneous congestion threshold

Figure 5.6: Case study I - LV assets providing FCR

5.4 LV assets providing aFRR services

5.4.1 Methodology

For the aFRR services, several papers study the design strategy of aggregators to optimally define their bids for the auction mechanism [107, 108]. However, DSOs are not expected to know the specific design strategies of aggregators owning flexible assets located on their local grid.

In this context, this research does not consider the FSPs' own design strategy but focuses on the possible impact of the LV assets providing aFRR if dispatched and fully activated by TSO. When the LV assets provide aFRR, LV assets are considered to provide full power activation for each product (positive or negative) beginning at the starting time of the possible activation of the product t_{start} and at the ending time t_{end} as represented in Equation (5.8). Hence, maximum deterministic power profile is considered when LV asset provide aFRR for a specific product.

$$S^{t}_{flex,b} = \begin{cases} \pm P^{T}_{afrrmax,b} & \text{for T in } [t_{start}, t_{end}] \\ 0 & \text{otherwise} \end{cases} \tag{5.8}$$

In Belgium, flexible assets with a limited reservoir providing aFRR must ensure full activation of contracted power over a 4-hour period [38]. Two scenarios are analyzed: (1) the limited reservoir approach, where maximum power is constrained by each asset's available energy, and (2) the portfolio approach, where full power is considered to be activated during the full product 4h period. These approaches are evaluated in the case studies to assess aFRR's impact on the LV distribution grid.

5.4.2 Numerical results - Impact of LV assets providing aFRR

For aFRR, two scenarios are analyzed: (1) the limited reservoir approach where the maximum power is constrained by the energy capacity of 20 kWh, limiting $P_{afrrmax,b}$ to 5 kW, and (2) the portfolio approach where residential batteries can deliver maximum power regardless of their individual energy capacity, setting $P_{afrrmax,b}$ to 10 kW. The case study examines the aFRR P4 product, where LV assets inject power into the grid from 12:00 to 16:00 when activated.

As outlined in 2.1.6, specific [38] products are identified using a letter (P or N) to indicate whether the product is for injection or offtake, respectively, followed by a number (1 to 6) representing the product period. In this example, submitting an asset for Period P4 means the asset may be activated for injection between 12:00 and 16:00.

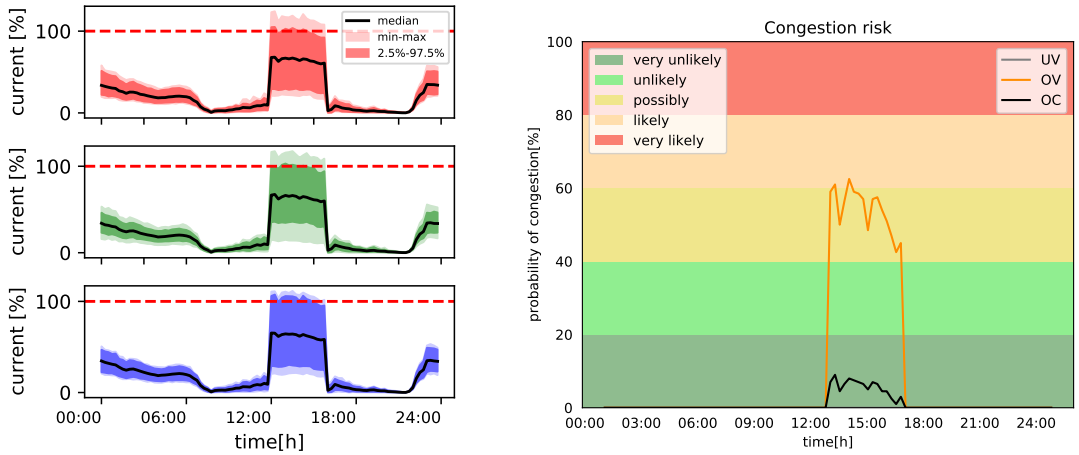

(a) Current probability along the day per phase on branch 0

(b) Congestion probability along the day for the full feeder

Figure 5.7: Case study II - LV assets providing aFRR P4 in a portfolio approach

Congestion is absent in the limited reservoir approach but exceeds 0% in the portfolio approach, with OV and OC probabilities arising from P4 activation between 12:00 and 16:00. Congestion caused by limited reservoir approach for this case study is therefore not represented.

Figure 5.7 shows the congestion probability distribution for branch 0 on the summer solstice when the LV assets are providing aFRR for the P4 product. The left figure presents the current probability distribution per phase and per time step at branch 0. The right figure displays the two congestion probabilities, OV and OC, occurring on the LV distribution grid. The figure clearly shows a step increase in current yielded between 12:00 and 16:00 corresponding to the modeling of the activation of LV assets providing aFRR P4.

This raises important considerations for discussions between DSOs and TSOs regarding activation approaches for LV assets in aFRR. While LV assets offer significant potential for frequency reserve participation, their activation must be carefully managed to prevent congestion on the LV network. In this case study, the scenario considering limited reservoir approach results in no congestion on the LV distribution grid, whereas the scenario considering portfolio approach leads to OV and OC congestion.

5.5 Conclusions

In conclusion, this chapter completes the methodology outlined in the previous chapter by presenting a model of congestion caused by LV assets on the LV network when providing frequency control, specifically FCR and aFRR. The impact of FCR is analyzed for both a *continuous* case, with 15-minute granularity, and an *instantaneous* case, with 10-seconds granularity.

Three key results are highlighted:

- A probabilistic ARMA model for frequency control more accurately predicts the output power of LV assets providing FCR following an extreme frequency event compared to a simple normal distribution.
- The model demonstrates that frequency data predicted with an ARMA model can be used to study the impact of *continuous* congestion thresholds. However, extreme frequency events should also be evaluated, but with *instantaneous* adapted congestion thresholds to avoid overestimating FCR-induced LV congestion. Specifically, this supports the recommendation that DSOs, when assessing the impact of LV assets providing frequency control, could consider probabilistic frequency forecasts in their *continuous* model, with current and voltage congestion limits set at 0.9 p.u. for UV and 1.1 p.u. for OV. Additionally, they should account for maximum frequency deviation (or full asset activation) and adapt the congestion limits to 0.85 p.u. for UV and 1.15 p.u. for OV.
- The modeling approach used by the DSO to assess the impact of LV assets providing aFRR significantly influences the results. If aFRR activation is modeled using a worst-case scenario where

aggregators rely on a portfolio-based approach, the analysis shows greater LV congestion compared to a modeling approach where the worst-case scenario considers a limited-reservoir approach.

Part III

Operating Envelopes to manage LV congestion

Chapter 6

Operating Envelope concept

Contents

Section 2.2 introduced the concept of the OE and outlined five mechanisms that DSOs can implement to manage LV congestion: technical solutions, tariff-based solutions, market-based solutions, connection agreements, and rule-based solutions. The OE can be applied across several of these mechanisms. This chapter focuses on developing new methods for computing the OE, elaborating on its definition, analysis, and computation. The subsequent chapter explores its application within various TSO/DSO coordination mechanisms.

Specifically, this chapter introduces an innovative approach to calculate the maximum flexibility for each end-user, ensuring safe grid operation. The proposed method is based on a relaxed unbalanced three-phase optimal power flow UTOPF, and is benchmarked against a conventional non-optimised approach. The methodology is applied to both grids presented in the introduction, i.e. the IEEE EU LV Test Feeder and 49 real-world delta-connected LV feeders in Brussels. Results demonstrate that the optimal solution improves the available flexibility by 7% to 10% compared to traditional methods, unlocking significant flexibility while ensuring grid safety.

The remainder of this chapter is organized as follows: Section 6.1 introduces the OE concept, outlines methods for its computation, and highlights the chapter's main contributions. Section 6.2 presents the relaxed UTOPF considered, with discussion on the objective function to consider fairness and the exactness of the solution. The UTPF that is used as benchmark is also introduced. Section 6.3 presents the results and discussions and the last section ends with the conclusion.

6.1 Introduction to Operating Envelopes

6.1.1 Motivations

As outlined in the introduction, one approach used by DSOs to manage congestion risks at LV level involves computing the OE for each end-user, i.e. the value that indicates injection and offtake limits per end-user based on the available capacity of the local network or power system as a whole [52]. This is represented in green in Figure 6.1, while the sand-yellow part indicates the maximum connection capacity.

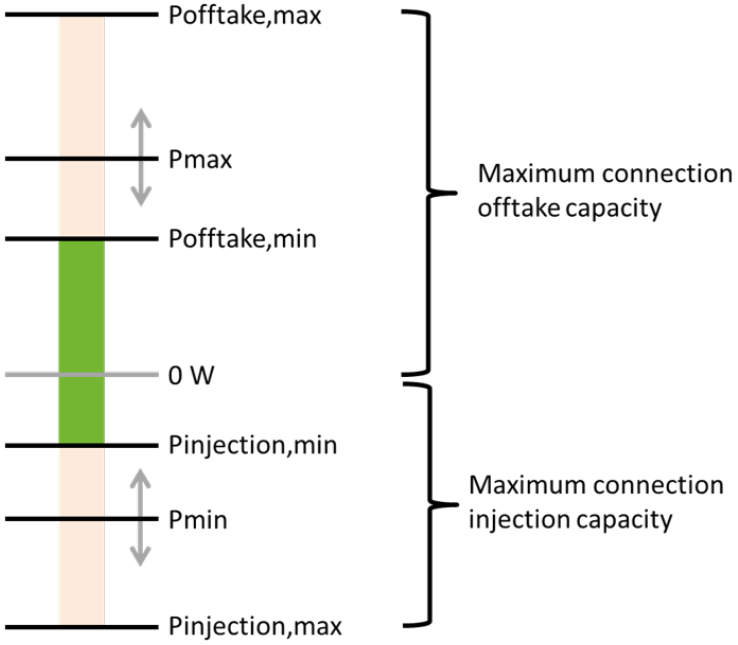

Figure 6.1: Representation of the OE concept for one end-user

As a reminder, the OE can be characterized as dynamic (DOE) when import and export limits vary over time. If not, the OE is static (SOE). This feature will be further discussed in this chapter.

As outlined in Subsection 2.2.3, the concept is currently applied in Australia with the EDGE project [53], and could be used to define limits of NFCA in several countries in Europe [48]. Nevertheless, there is a need to provide methodologies that that objectively determine this guaranteed value. Compared to other congestion management methods, the concept of setting OEs offers the advantage of not requiring DSOs to directly control behind-the-meter assets, which can be restricted by regulators in vertically integrated power systems. Additionally, a NFCA does not necessitate third-party, such as aggregators or flexibility service providers, access to network data.

As outlined in the introduction, several features must be considered to compute OEs. First, fairness is critical, as DSOs must ensure non-discriminatory treatment of end-users. Fairness concepts are reviewed in [109] for congestion management in distribution networks. In [110] and [111], fairness is considered by modifying the objective function when computing OEs. Second, a single-line approximation to compute OEs is inadequate, because LV distribution grid unbalances cannot be neglected as outlined in Subsection 2.1.2. Indeed, a phase voltage sensitivity analysis of OE computation on an unbalanced distribution network is performed in [112]. The study concludes that imbalances cannot be ignored when calculating OEs for LV distribution grids. Third, active power variations and influences of topological structures on OE are studied.

6.1.2 Contributions

This chapter contributes to the existing literature by presenting for the first time an algorithm using the UTOPF with Second-Order Cone Programming (SOCP) relaxation to compute OEs, rather than the commonly approach using linear UTOPF or UTPF. This approach demonstrates to offer more efficient use of network capacity compared to algorithms with UTPF and provides a quasi exact solution, avoiding the inaccuracies associated with linear UTOPF. Additionally, unlike machine learning techniques, the

proposed method does not rely on smart meter data for constructing the electrical model, that are currently not available by DSOs. Load profiles are required solely for the computation of Dynamic OEs (DOEs) that will be further described in the next chapter, and can be extrapolated from aggregated grid-level datasets when individual smart meter data is not available. This characteristic is particularly relevant in regions such as Brussels (Belgium), where the deployment of smart meters remains limited, and Sibelga, the Brussels DSO, face restricted access to such data.

Furthermore, this chapter contributes to the literature by extending the model to consider delta connections, in addition to the more usual wye connection of LV end-users. This is necessary because most of the LV distribution grids connect end-users via delta connections in Brussels. Such connections require additional variables and complementary equations that are explicitly presented hereafter. This Chapter presents the OE calculation methodology applied to a benchmark grid but also to part of the delta-connected real-grid with 2267 LV end-users provided by Sibelga. Finally, the results are compared with those from a UTPF, demonstrating the advantages of the suggested relaxed UTOPF.

6.2 Operating Envelopes calculation methods

This section begins by outlining the background of calculating OEs, followed by a summary of existing methods. It then presents two approaches in more detail: a novel algorithm based on the relaxed UTOPF model, which represents the main contribution of this chapter, and a benchmark algorithm using the UTPF model. First, the relaxed UTOPF model is described, followed by its integration into an OE calculation algorithm. The benchmark algorithm using the UTPF model is then introduced. Finally, a subsection covers the implementation process, emphasizing key design choices that, while seemingly simple, provide valuable insights for engineers seeking to implement such models.

6.2.1 Background on the computation methods

To provide background, to the best of authors' knowledge, the concept of computing operational limits was introduced for the first time in [113].The paper aims to characterize the flexibility needed to include wind turbine generation in the California grid, with the well-known intermittent challenge. Therefore, it presents a methodology to assess the necessary operational flexibility of power systems and introduces the concept of a geometric approach to define flexibility with three parameters: ramp rate (i.e. technical curve to reach maximum power versus time), maximum power and available energy. Makarov's team publishes two years later a new paper considering load uncertainty in the model [114]. In that paper, flexibility is defined as the ability to modify the production and/or consumption profiles and the same definition of flexibility is considered for this research.

Makarov's papers focus on flexibility needed to integrate power generators with uncertainty into the grid. The concept of guaranteed operating capacity was further refined in 2012 in [115] presenting a method for assessing the *available* operational flexibility of a power system, compared to the previous concept of *needed* flexibility. This available flexibility is defined as the maximum technical capability of a single power system unit to modulate power and energy into the grid. Nevertheless, the paper uses the same parameters (ramp rate, maximum power and energy) as those presented previously. The grid is considered as a copper plate and hence, internal constraints are not yet taken into account. It also extents the considered loads and generators (i.e. solar PV, controllable loads at high voltage level).

The OE was more formally defined in [116] as the possible capacity of the system to provide flexible power over future time steps, where flexibility is represented in the form of a cone when plotted as power versus time.

The concept of using OEs was adapted from the transmission to distribution network in [110] and [111], where they are computed using a linear optimal power flow (OPF) on a three-bus network and on a pseudo distribution network. The papers [117] and [54] present a linear Unbalanced Three-phases OPF (UTOPF) to compute OEs for distribution grids in Australia, focusing mainly on residential PV export. Due to the unavailability of public LV grid data in Australia, pseudo-LV feeders are modeled following the methodology outlined in [118]. This approach involves distributing end-users uniformly along the feeder and assigning them to single-phase connections. While this method provides a more realistic representation compared to using lumped load models, it still represents a significantly simplified approximation of real-world LV network conditions.

6.2.2 Summary and selection of the computing methods

Reference [119] recently reviewed three types of techniques to compute OEs: UTPF, UTOPF and machine learning techniques, as illustrated in Figure 6.2.

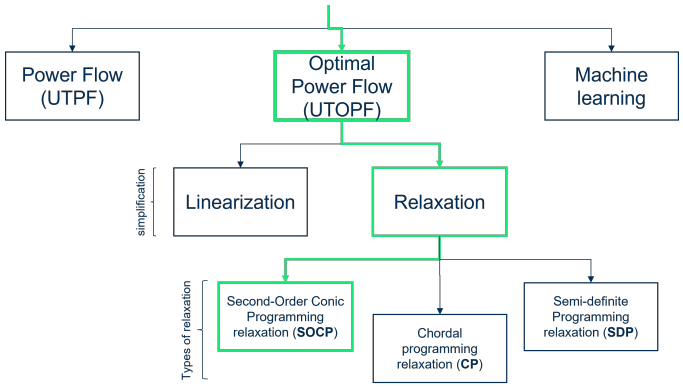

Figure 6.2: Overview of models from literature to compute OEs with focus on relaxation techniques

First, the UTPF with grid data, voltage at the reference bus and load profiles of passive customers as inputs is used to compute the OE by incrementing iteratively the power levels of active consumers while congestion limits are respected (i.e. overvoltage (OV), undervoltage (UV), or overcurrent (OC)) [112, 60]. Here, active customers refer to customers who agree to implement the OE, and passive customers refer to those who do not. This method is computationally efficient. However, it may result in an underutilization of the network's capacity because it does not aim to find the optimal operating state of the grid.

In a second approach, an UTOPF is defined where PF equations and congestion limits are implemented as constraints of an optimization problem where the objective function aims to maximize the sum of individual OEs. This method can improve the network capacity utilization. However, because PF equations are non-linear and non-convex, solving the UTOPF is computationally demanding and tractability might be a challenge. Several methods exist in the literature to simplify the OPF equations [120]: approximation as well as relaxation methods [121]. Literature shows several examples of the use of approximated UTOPF to compute OEs [54, 117, 118]. However, the papers show that linearization can introduce significant errors due to the inherent inaccuracy of the approximation. To the author's knowledge, literature does not show any use of relaxed UTOPF to compute OEs.

Thirdly, machine learning-based techniques are recently applied to compute OEs [122], [123]. However, these methods presented in the papers require high observability of consumer connection data: historic records of active and reactive power consumption from each end-user at 5 minutes granularity as well as grid topology. The paper highlights that accuracy can increase if voltage at the head of the LV feeder is also known. However, as highlighted in Chapter 3, the Sibelga case study exhibits low observability. Since the necessary load profile data to develop machine learning-based methods are unavailable, these techniques are not considered in the subsequent parts of this manuscript.

The UTOPF with SOCP relaxation is novel and not found in existing literature, making it a key focus of this research. The UTPF method, due to its simplicity, is used as a benchmark. Machine learning techniques are excluded due to the lack of sufficient load profile data provided by the case studies.

6.2.3 UTOPF with relaxed Extended Branch Flow Model formulation

One key contribution of this research focuses on a relaxed UTOPF using the Extended Branch Flow Model (EBFM) with SOCP relaxation. The model presented hereafter includes the extended model considering delta-connected loads. Sets, parameters, variables and extended constraints are adapted from the OPF extended BFM presented in [124].

A Branch Flow Model (BFM) is to be preferred over a Bus Injection Model (BIM) because it is numerically more stable [121]. For a radial network, a SOCP relaxation should always be preferred because the solution is exact under specific conditions, discussed later in this Section (see the discussion on the objective function), and it is the tightest and simplest relaxation out of SOCP, chordal and semi-definite positive relaxation [125].

Figure 6.3 illustrates the Branch Flow Model (BFM) for a single main branch. The four wye variables per branch are highlighted in orange, along with one end-user connected to bus i and two departing

branches.

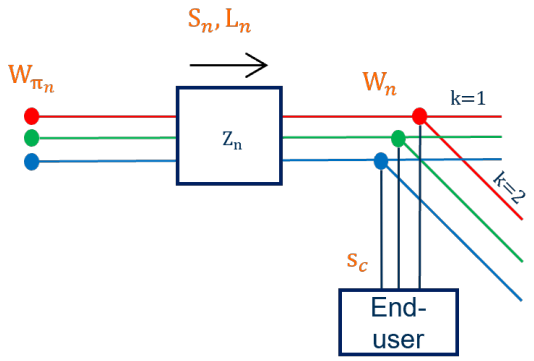

Figure 6.3: Representation of the BFM with one main branch and two departing branches, the four wye variables in orange, the relevant sets and the z_n parameter

In the following paragraphs, first, sets are presents, then the parameters, the variables, the constraints and finally the objective function with a discussion on the exactness of the solution.

Sets - Five sets are considered in the proposed optimization model, as outlined in Table 6.1. As a reminder, for radial networks, the number of busses equals the number of branches plus one: $\{\mathcal{B}\} = \{\mathcal{N}\} + 1$. This makes it possible to reference busses connected to a specific branch n using the branch index with π_n as a parent bus and n as the downward bus. Furthermore, in radial networks, several branches can originate from the same bus, referenced here with the k index.

In addition, note that multiple end-users, denoted as c, may be connected to the same bus i, while some buses may have no end-users at all. Therefore, these sets are distinct. Finally, Λ represents the set of possible λ parameters required to compute exact OEs using the novel algorithm.

To improve legibility of the equations presented, the phases ϕ are omitted throughout the paper, except in cases where phase information is essential.

Table 6.1: Sets and indices

Phases	$\phi \in \mathcal{P} = \{a, b, c\}$
Branches	$n \in \mathcal{N}$
Branches originating from bus n	$k \in \mathcal{N}$
Busses	$i \in \mathcal{B}$
Parent bus index	$\pi_n \in \mathcal{N}$
End-users	$c \in \mathcal{C}$
Exactness Parameter Set	$\lambda \in \Lambda$

Parameters - Parameters used in the algorithm are summarized in table 6.2. The maximum and minimum bus voltage magnitude V_i^{min}, V_i^{max} are provided by DSO habits aligned with relevant standards (EN50160 or EN61000) as outlined in subsection 2.2.1. Branch current rating $I_n^{ampacity}$ depends on the characteristics of the feeders.

One important parameter is the branch series impedance matrix z_n which characterizes the self and mutual impedance of the cables of the feeder. The reduced model presented in [5] an described in 3.2.3 is applied to represent z_n.

The end-user active and reactive power boundaries, P_c^{min}, P_c^{max}, Q_c^{min}, and Q_c^{max}, are determined per end-user and depend on the connection characteristics, such as the number and configuration of phases, as well as the type of connection.

The matrix Γ is a matrix convenient to transpose delta-connected powers into their equivalent wye model, as it will be shown in Equations (6.11) and (6.12) [124]:

$$\Gamma = \begin{bmatrix} 1 & -1 & 0 \\ 0 & 1 & -1 \\ -1 & 0 & 1 \end{bmatrix} \tag{6.1}$$

Finally, the parameter λ will be further discussed when describing the objective function.

Table 6.2: Parameters

Bus voltage magnitude min./max. (V)	$V_i^{min}, V_i^{max} \in \mathbb{R}^{\lvert\mathcal{P}\rvert\times 1}$
Branch current rating (A)	$I_n^{ampacity} \in \mathbb{R}^{\lvert\mathcal{P}\rvert\times 1}$
Branch apparent power rating (VA)	$S_n^{rate} \in \mathbb{R}^{\lvert\mathcal{P}\rvert\times 1}$
Branch series impedance (Ω)	$z_n \in \mathbb{R}^{\lvert\mathcal{P}\rvert\times\lvert\mathcal{P}\rvert}$
End-user active power bound (W)	$P_c^{min}, P_c^{max} \in \mathbb{R}^{\lvert\mathcal{P}\rvert\times 1}$
End-user reactive power bound (var)	$Q_c^{min}, Q_c^{max} \in \mathbb{R}^{\lvert\mathcal{P}\rvert\times 1}$
End-user load profile (W)	$p_{c,lp}, q_{c,lp} \in \mathbb{R}^{\lvert\mathcal{P}\rvert\times 1}$
Wye-delta transpose matrix	Γ
Exactness parameter	λ

Variables - Six complex variables per branch are defined for the problem and resulting in twelve variables in the real domain (see Table 6.3)[1].

Table 6.3: Optimization variables

	Complex domain	Real domain
Operating Envelope (W)	$OE_c \in \mathbb{C}^{\lvert\mathcal{P}\rvert\times 1}$	$OE_c^{Re}, OE_c^{Im} \in \mathbb{R}^{\lvert\mathcal{P}\rvert\times 1}$
Power branch (W)	$S_n \in \mathbb{C}^{\lvert\mathcal{P}\rvert\times\lvert\mathcal{P}\rvert}$	$P_n, Q_n \in \mathbb{R}^{\lvert\mathcal{P}\rvert\times\lvert\mathcal{P}\rvert}$
Bus lifted voltage (V^2)	$W_i = V_i * V_i^H \in \mathbb{C}^{\lvert\mathcal{P}\rvert\times\lvert\mathcal{P}\rvert}$	$W_i^{Re}, W_i^{Im} \in \mathbb{H}^{\lvert\mathcal{P}\rvert\times\lvert\mathcal{P}\rvert}$
Branch lifted current (A^2)	$L_n = I_n * I_n^H \in \mathbb{C}^{\lvert\mathcal{P}\rvert\times\lvert\mathcal{P}\rvert}$	$L_n^{Re}, L_n^{Im} \in \mathbb{H}^{\lvert\mathcal{P}\rvert\times\lvert\mathcal{P}\rvert}$
Delta lifted current (A^2)	$\rho_n = I_{\Delta,n} * I_{\Delta,n}^H \in \mathbb{C}^{\lvert\mathcal{P}\rvert\times\lvert\mathcal{P}\rvert}$	$\rho_n^{Re}, \rho_n^{Im} \in \mathbb{H}^{\lvert\mathcal{P}\rvert\times\lvert\mathcal{P}\rvert}$
Voltage and delta current product (W)	$\chi_c \in \mathbb{C}^{\lvert\mathcal{P}\rvert\times\lvert\mathcal{P}\rvert}$	$\chi_c^{Re}, \chi_c^{Im} \in \mathbb{H}^{\lvert\mathcal{P}\rvert\times\lvert\mathcal{P}\rvert}$

The complex variable OE_c denotes the maximum power that can be consumed or produced by each LV end-user, while ensuring the safe operation of the grid. It is described in Equation (6.2).

$$OE_c = \begin{bmatrix} OE_{c,a} \\ OE_{c,b} \\ OE_{c,c} \end{bmatrix} = OE_c^{Re} + jOE_c^{Im} \tag{6.2}$$

It is important to note that the generator convention is applied for the optimization problem, in contrast to the methods presented in previous Part II: i.e. a positive $OE_c^{Re} > 0$ indicates that the end-user is injecting power into the grid, while a negative $OE_c^{Re} < 0$ signifies power consumption.

The variable S_n denotes the power flowing into the branches and is expressed in Equation (6.3).

$$S_n = \begin{bmatrix} S_{n,aa} & S_{n,ab} & S_{n,ac} \\ S_{n,ab} & S_{n,bb} & S_{n,bc} \\ S_{n,ac} & S_{n,bc} & S_{n,cc} \end{bmatrix} = P_n + jQ_n \tag{6.3}$$

The subsequent variables considered in the problem are not the voltage V_i, current I_n and delta current $I_{\Delta,n}$, but the lifted variables, i.e. the outer product of voltage phasors $W_i = V_i * V_i^H$, current phasors $L_n = I_n * I_n^H$, delta current phasors $\rho_n = I_{\Delta,n} * I_{\Delta,n}^H$ where H denotes the Hermitian transpose. These higher-dimensional lifted variables are introduced to simplify certain model constraints, as detailed in the constraints presentation. However, their use requires the addition of complementary constraints described in eqs. (6.5) and (6.8), which will also be discussed in detail in the constraints section.

The lifted variable for the voltage satisfies (6.4) and (6.5).

$$W_i = W_i^{re} + jW_i^{im} = V_i(V_i)^H \tag{6.4}$$

$$W_i \succeq 0, rank(W_i) = 1. \tag{6.5}$$

The structure of W_i as a real-valued matrix in rectangular coordinates is expressed as in (6.6). Note that 9 unique scalar variables are required for each complex matrix variable.

$$W_i = \begin{bmatrix} W_{i,aa}^{re} & W_{i,ab}^{re} & W_{i,ac}^{re} \\ W_{i,ab}^{re} & W_{i,bb}^{re} & W_{i,bc}^{re} \\ W_{i,ac}^{re} & W_{i,bc}^{re} & W_{i,cc}^{re} \end{bmatrix} + j \begin{bmatrix} 0 & W_{i,ab}^{im} & W_{i,ac}^{im} \\ -W_{i,ab}^{im} & 0 & W_{i,bc}^{im} \\ -W_{i,ac}^{im} & -W_{i,bc}^{im} & 0 \end{bmatrix} \tag{6.6}$$

[1] $\mathbb{H}$ is the Hermitian symmetric space which at every point has an inversion symmetry preserving the Hermitian structure

Similarly, the auxiliary variables for the current satisfies equations (6.7) and (6.8) and can be expressed in the real domain as equation (6.9).

$$L_n = L_n^{re} + jL_n^{im} = I_n(I_n)^H, \tag{6.7}$$

$$L_n \succeq 0, rank(L_n) = 1. \tag{6.8}$$

$$L_n = \begin{bmatrix} L_{n,aa}^{re} & L_{n,ab}^{re} & L_{n,ac}^{re} \\ L_{n,ab}^{re} & L_{n,bb}^{re} & L_{n,bc}^{re} \\ L_{n,ac}^{re} & L_{n,bc}^{re} & L_{n,cc}^{re} \end{bmatrix} + j \begin{bmatrix} 0 & L_{n,ab}^{im} & L_{n,ac}^{im} \\ -L_{n,ab}^{im} & 0 & L_{n,bc}^{im} \\ -L_{n,ac}^{im} & -L_{n,bc}^{im} & 0 \end{bmatrix} \tag{6.9}$$

Other lifted variables satisfy similar equations that are not further described in this manuscript. The complex variables χ_c and ρ_n are implemented to consider delta-connected loads. The variable χ_c expresses the voltage and current product, and is defined by (6.10). Figure 6.4 reminds how the current and voltage variables are defined for a wye and a delta connection.

$$\chi_c = \begin{bmatrix} V_{i,a}(I_{c,ab})^* & V_{i,a}(I_{c,bc})^* & V_{i,a}(I_{c,ca})^* \\ V_{i,b}(I_{c,ab})^* & V_{i,b}(I_{c,bc})^* & V_{i,b}(I_{c,bc})^* \\ V_{i,c}(I_{c,ab})^* & V_{i,c}(I_{c,bc})^* & V_{i,c}(I_{c,ca})^* \end{bmatrix} \tag{6.10}$$

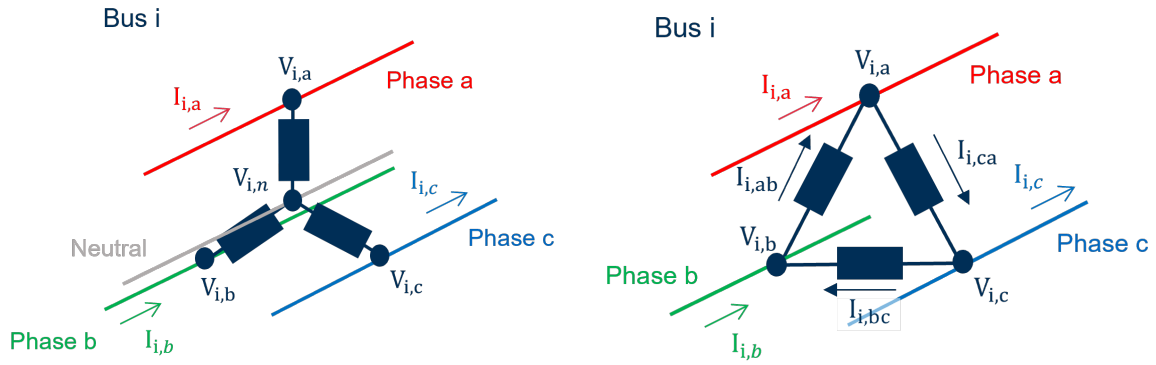

(a) Wye connection (b) Delta connection

Figure 6.4: Illustration of wye and delta connections for a single bus i, showing associated voltages and currents

Combining χ_c and Γ provides the wye-connection equivalent of the power consumed by a wye end-user c in Equation (6.11) or a delta-connected end-user c in Equation (6.12).

$$s_{wye,c} = diag(\chi_c \Gamma) = \begin{bmatrix} V_{i,a}(I_{c,ab} - I_{c,ca})^* \\ V_{i,b}(I_{c,bc} - I_{c,ab})^* \\ V_{i,c}(I_{c,ca} - I_{c,bc})^* \end{bmatrix} \tag{6.11}$$

$$s_{\Delta,c} = diag(\Gamma \chi_c) = \begin{bmatrix} (V_{i,a} - V_{i,b})(I_{c,ab})^* \\ (V_{i,b} - V_{i,c})(I_{c,bc})^* \\ (V_{i,c} - V_{i,a})(I_{c,ca})^* \end{bmatrix} \tag{6.12}$$

Constraints - Following constraints are considered to compute OEs. First, Ohm's law is expressed in the complex domain as 6.13. The equivalent real expressions are written after, for real voltage in (6.14) and imaginary voltage in (6.15).

$$W_n = W_{\pi_n} + z_n L_n z_n^H - S_n z_n^H - z_n S_n^H \tag{6.13}$$

$$\begin{aligned} W_{\pi_n}^{re} = W_n^{re} - P_n(r_n)^\intercal - Q_n(x_n)^\intercal - r_n(P_n)^\intercal - x_n(Q_n)^\intercal \\ + r_n L_n^{re}(r_n)^\intercal - x_n L_n^{im}(r_n)^\intercal + x_n L_n^{re}(x_n)^\intercal + r_n L_n^{im}(x_n)^\intercal \end{aligned} \tag{6.14}$$

$$W_{\pi_n}^{im} = W_n^{im} - Q_n(r_n)^\intercal + P_n(x_n)^\intercal - x_n(P_n)^\intercal + r_n(Q_n)^\intercal + x_n L_n^{re}(r_n)^\intercal - r_n L_n^{im}(r_n)^\intercal + r_n L_n^{re}(x_l)^\intercal + x_n L_n^{im}(x_n)^\intercal \quad (6.15)$$

Second, power balance equations are defined in (6.16) for the complex domain, and in (6.17) and (6.18) for the equivalent real and imaginary expressions, respectively.

$$diag(S_n - z_n L_n) + \sum_{c \in n} OE_c = \sum_{k:n \to k} diag(S_k) \quad (6.16)$$

$$dg(P_n - r_n L_n^{re} + x_n L_n^{im}) + \sum_{c \in n} OE_c^{Re} = \sum_{k:n \to k} dg(P_k) \quad (6.17)$$

$$dg(Q_n - x_n L_n^{re} - r_n L_n^{im}) + \sum_{c \in n} OE_c^{Im} = \sum_{k:n \to k} dg(Q_k) \quad (6.18)$$

It is important to note that several end-users can be connected to the same bus in (6.16), and that (6.13) and (6.16) are applied only to the diagonal elements. In these equations, the index π_n represents the parent bus on the network, i.e. the connected bus located closer to the transformer. For delta-connected loads, OE_c in (6.16) is defined as in (6.19).

$$OE_c = diag(\Gamma \chi_c) \quad (6.19)$$

In this model, variables are lifted to higher dimensions, expanding the original feasible set. While this facilitates optimization, the resulting solution may not necessarily belong to the original set. To ensure solution recovery, two types of auxiliary constraints are introduced. First, PSD constraints are applied to lifted voltages, currents, and power branches, by implementing constraint (6.20), ensuring the expanded feasible set remains convex [126]. Similarly, for delta configurations, PSD constraints are applied to lifted voltages, delta currents, and their products, as represented in (6.21) [124]. For both PSD constraints, auxiliary matrix constraints explicitly represent variables in the complex domain, and subsequently in terms of real and imaginary components following developments in [127].

$$M_n = \begin{bmatrix} W_{\pi_n} & S_n \\ S_n^* & L_n \end{bmatrix} = \begin{bmatrix} W_{\pi_n}^{re} & P_n & W_{\pi_n}^{im} & Q_n \\ (P_n)^\intercal & L_n^{re} & -(Q_n)^\intercal & L_n^{im} \\ -W_{\pi_n}^{im} & -Q_n & W_{\pi_n}^{re} & P_n \\ (Q_n)^\intercal & -L_n^{im} & (P_n)^\intercal & L_n^{re} \end{bmatrix} \succeq 0 \quad (6.20)$$

$$M_{\Delta,n} = \begin{bmatrix} W_{\pi_n} & \chi_n \\ \chi_n^* & \rho_n \end{bmatrix} = \begin{bmatrix} W_{\pi_n}^{Re} & \chi_n^{Re} & W_{\pi_n}^{Im} & \chi_n^{Im} \\ (\chi_n^{Re})^\intercal & \rho_n^{Re} & -(\chi_n^{Im})^\intercal & \rho_n^{Im} \\ -W_{\pi_n}^{Im} & -\chi_n^{Im} & W_{\pi_n}^{Re} & \chi_n^{Re} \\ (\chi_n^{Im})^\intercal & -\rho_n^{Im} & (\chi_n^{Re})^\intercal & \rho_n^{Re} \end{bmatrix} \succeq 0 \quad (6.21)$$

Second, a rank-1 constraint is typically imposed to maintain consistency with the original feasible set in (6.22) and (6.23). However, this constraint is non-convex and is omitted in the SOCP relaxation, as it is not always necessary to guarantee solution recovery under certain conditions [125].

$$rank(M_n) = 1. \quad (6.22)$$

$$rank(M_{\Delta,n}) = 1. \quad (6.23)$$

Connection capacity constraints are introduced into the problem using (6.24), (6.25), and (6.26).

$$0 \leq diag(S_n) \circ diag(S_n)^* \leq S_n^{rate} \circ S_n^{rate} \quad (6.24)$$

$$-P_c^{max} \leq OE_c^{Re} \leq P_c^{max} \quad (6.25)$$

$$-Q_c^{max} \leq OE_c^{Im} \leq Q_c^{max} \quad (6.26)$$

Network constraints are implemented respectively for voltage limits, with (6.27) and (6.28), and current limits, with (6.29) and (6.30).

$$V_i^{min} \circ V_i^{min} \leq diag(W_i^{re}) \leq V_i^{max} \circ V_i^{max} \tag{6.27}$$

$$-V_i^{max}(V_i^{max})^\top \leq W_i^{re}, W_i^{im} \leq V_i^{max}(V_i^{max})^\top \tag{6.28}$$

$$I_n^{min} \circ I_n^{min} \leq diag(L_n^{re}) \leq I_n^{max} \circ I_n^{max} \tag{6.29}$$

$$-I_n^{max}(I_n^{max})^\top \leq L_n^{re}, L_n^{im} \leq I_n^{max}(I_n^{max})^\top \tag{6.30}$$

Finally, to address the principle of fairness, the constraint in (6.31) is added. Implementing the constraint results in all end-users limited to the same ratio of OE relative to their connection capacity. Although more complex fairness criteria are discussed in the literature [109], a comprehensive exploration of these is beyond the scope of this research.

$$\frac{OE_c^{Re}}{P_c^{max}} = \frac{OE_{c+1}^{Re}}{P_{c+1}^{max}} \quad \forall c \in \mathcal{C} \tag{6.31}$$

Objective function - The objective function aims to optimize the sum of active powers per household to compute the OE. Nevertheless, when computing the OE by simply maximizing the sum of active power from households, the solution is inexact as demonstrated in [125]. One assumption for this relaxed OPF solution to be exact is that the objective function should be convex, strictly increasing in L, non decreasing in s and independent of branch flow S. This theorem is proven in [126].

When computing OEs, the condition of non decreasing s is not satisfied, and thus leading to an inexact solution. For example, the optimal solution might indicate residual currents in branches where none should exist in a real physical grid, such as currents on a phase on a branch connected to a household with no load on that phase.

This issue is recently addressed to some extent for single-line OPFs in [128]. Therefore, a second weighted term is added to the objective function in (6.32) to satisfy the sufficient exactness condition.

$$\max \sum_{c \in \mathcal{C}} OE_c^{Re} - \lambda \sum_{n \in \mathcal{N}} diag(r_n L_n^{Re}) \tag{6.32}$$

By adding a loss minimization term, it is ensured that the objective function is non decreasing in s. When λ is sufficiently high, both conditions are satisfied and an exact solution can be recovered.

The λ parameter appearing in (6.32) has to be chosen carefully: if the value is set too low, the solution will be inexact, while setting it too high excessively limits the OE. To find an optimal λ value, the UTOPF is run for several λ. The resulting active and reactive powers per branch computed for each λ are then used as inputs into the UTPF presented in Part II to compute voltage V_{pf_n} and current I_{pf_n}. Then, the MAE between UTOPF and UTPF results is computed for voltage and currents using the following equations:

$$\frac{1}{n} \sum_n |V_{pf_n} - V_{opf_n}| \tag{6.33}$$

$$\frac{1}{n} \sum_n |I_{pf_n} - I_{opf_n}| \tag{6.34}$$

The optimal λ, which must be selected, is the value of λ that simultaneously minimizes losses and maximizes the sum of the OEs. It is important to note that this optimal λ must be computed independently for each LV feeder.

6.2.4 Algorithm to compute OEs with the relaxed UTOPF

Algorithm (1) presents the algorithm to compute upper OEs with the relaxed UTOPF. The upper OEs represents the maximum guaranteed power injection per end-user, denoted as OE_c^{Re}. The algorithm begins by computing OEs for several λ. Subsequently, the results corresponding to the optimal λ, which minimizes losses while maximizing the OEs, are selected, ensuring solution exactness.

The algorithm is depicted in Figure 6.5, offering a clear representation of how the UTPF (introduced in Part II) and the UTOPF (introduced in Part III) are applied to determine the optimal value of λ.

Algorithm 1 Upper OE Computation with relaxed UTOPF

Input: Grid data (z_n, I_n^{ampacity}, $V_i^{\min}$, $V_i^{\max}$), connection capacities ($P_c^{\min}$, $P_c^{\max}$, $Q_c^{\min}$, $Q_c^{\max}$)
Output: OE per end-user with optimal λ_{opt} denoted as $OE_{c,opf,\lambda_{opt}}$ and $OE_{c,opf,\lambda_{opt}}$
for $\lambda \in \Lambda$ **do**
    Run UTOPF with objective:

$$\max \sum_{c \in \mathcal{C}} p_c - \lambda \sum_{n \in \mathcal{N}} \text{diag}(r_n L_n^{\text{Re}})$$

    Return $OE_{c,opf,\lambda}$, $OE_{c,opf,\lambda}$, $V_{i,opf,\lambda}$, and $I_{n,opf,\lambda}$
    Run UTPF with $OE_{c,opf,\lambda}$ and $OE_{c,opf,\lambda}$ as inputs
    Return $V_{i,pf,\lambda}$ and $I_{n,pf,\lambda}$
    Compute MAE between $V_{i,opf,\lambda}$, $I_{n,opf,\lambda}$ and $V_{i,pf,\lambda}$, $I_{n,pf,\lambda}$
    Return Optimal λ_{opt}
end for
Return $OE_{c,opf,\lambda_{opt}}$ and $OE_{c,opf,\lambda_{opt}}$

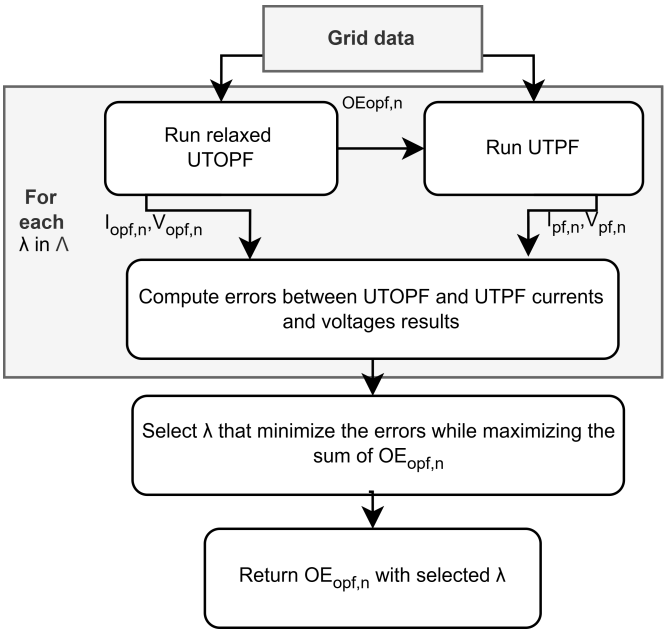

Figure 6.5: Algorithm to ensure exactness of OE computation with UTOPF

The process begins with incorporating grid data as parameters into the constraints of the relaxed UTOPF problem. The relaxed UTOPF is then solved for multiple λ values. For each λ, the UTOPF computes the operating envelope ($OE_{c,opf,\lambda}$) for each end-user, as well as branch currents ($I_{n,opf,\lambda}$) and bus voltages ($V_{i,opf,\lambda}$). These $OE_{c,opf,\lambda}$ values, along with grid data, are subsequently used as inputs to the UTPF model introduced in Part II, yielding branch currents ($I_{n,pf,\lambda}$) and bus voltages ($V_{i,pf,\lambda}$).

Finally, for each λ, the MAE between the UTOPF and UTPF results are calculated for both voltages and currents, allowing for the selection of the optimal λ.

To compute the lower OE, i.e. the maximum guaranteed power that can be consumed, the objective function needs to switch from maximization to minimization and the λ sign must be switched in the objective function.

6.2.5 Implementation of the relaxed UTOPF

The process of implementing a UTOPF, or more generally any optimization problem, can be broken down into five key layers, as described in Subsection 2.3.3. These layers involve making critical decisions regarding: the model, the modeling language, the optimization modeling language, the solver, and the algorithm.

The model, defined earlier, plays a crucial role in guiding the decisions made across these layers, as

detailed in the subsequent sections. One of the most important aspects of the model that will influence the choices in the next four layers is the implementation of the PSD constraint.

While the decisions presented here may seem straightforward, they require significant effort and provide added value for engineers seeking to implement the relaxed UTOPF model.

Modeling Language choice

The chosen modeling language is Python. This decision aligns with the fact that previous models (such as grid models and load profiles required for the UTPF) were implemented in Python. Moreover, Python offers a wealth of relevant libraries for optimization problems, and has an active community that can assist with potential implementation challenges.

Optimization Modeling Language choice

Once the modeling language is selected, it inherently limits the choice of the optimization modeling language. For example, optimization software like YALMIP or JuMP are only compatible with specific modeling languages, such as MATLAB and Julia, respectively.

The choice of optimization modeling language therefore depends on the available libraries, particularly those that provide specialized mathematical operators, such as the PSD operator. When the problem was implemented in 2024, neither Pyomo nor Gurobi included a PSD operator. However, Gurobi seems to be actively working on this issue, and it is possible that a more recent release may have integrated the PSD operator.

Given that CVXPY supports the PSD operator, it was selected as the optimization modeling language for implementing the relaxed UTOPF.

Solver choice

The selection of a solver is also constrained by the type of optimization problem being addressed. Table 6.4 summarizes the licenses and types of modeling supported by several solvers, as extracted from [7]. The available licenses are either EPL (Eclipse Public License), which is open-source, or commercial, which require payment for access. The various optimization problem types (e.g., LP, MILP, SOCP, SDP) were defined earlier in 2.3.3.

In this case, the key criteria for selecting a solver are its ability to handle SOCP problems and work with the SDP operator. These requirements led to the selection of the MOSEK solver, for which ULB holds a commercial license.

Table 6.4: Overview of Selected Solvers [7]

Solver	**License**	**Supports**
MOSEK	Commercial	LP, MILP, SOCP, MISOCP, SDP
Cbc	EPL	MILP
CPLEX	Commercial	LP, MILP, SOCP, MISOCP
Gurobi	Commercial	LP, MILP, SOCP, MISOCP
Ipopt	EPL	LP, QP, NLP

6.2.6 Using benchmark UTPF to compute OE

To benchmark the results obtained by the approach with the UTOPF method, an algorithm based on an UTPF model is used and described in this subsection. In [112], a dichotomic search is used to compute OEs using UTPF. In [60], OEs are computed by iteratively increasing power export/import while ensuring compliance with constraint limits.

The algorithm with the UTPF model used in this research combines elements of these two approaches. To compute the upper OE, active power is incrementally increased by a predefined value, ϵ, in each iteration. The UTPF, using the common backward/forward sweep PF model [65] for radial networks, is then run, updating voltage and current values until OV or OC conditions are reached within the grid. Conversely, to compute the lower OE, a similar algorithm is implemented, where ϵ is incrementally subtracted from the power in each iteration, and UV conditions are considered instead of OV.

Algorithm 2 presents the algorithm used to compute OE with UTPF model.

Algorithm 2 OE Computation with UTPF (Upper OE)

Input: Grid data (z_n, I_n^{ampacity}, $V_i^{\min}$, $V_i^{\max}$), connection capacities ($P_c^{\min}$, $P_c^{\max}$, $Q_c^{\min}$, $Q_c^{\max}$)
Output: OE per end-user OE_c^{Re}, OE_c^{Im} and voltage $V_{i,\text{pf}}$ and current $I_{n,\text{pf}}$ per branch
while $V_i^{\min} < V_i < V_i^{\max}$ and $I_n < I_n^{\text{ampacity}}$ **do**
    $OE_c^{Re} = min(OE_c^{Re} + \epsilon, P_c^{\max})$
    Run UTPF [65]
    Return V_i and I_n
end while
Return OE_c^{Re} and OE_c^{Im}

6.3 Results

6.3.1 Case studies description

Two case studies are discussed in this section: the first involves the benchmark grid, and the second uses the Sibelga grid presented in 2.3.1. Two distinct scenarios are considered, depending on whether the fairness principle is implemented:

1. The first scenario does not implement the constraint in (6.31), resulting in an optimal OE, though unfair, referred to as Optimal UTOPF.

2. The second scenario implements the constraint in (6.31), ensuring all end-users are limited to the same ratio of OE relative to their connection capacity, referred to as Fair UTOPF.

6.3.2 Case study 1 - IEEE European LV Testfeeder

The results begin by presenting the computation of the optimal exactness parameter λ implemented in the objective function (see Equation (6.32)). Figure 6.6 illustrates the voltage and current values per phase obtained using the UTOPF and UTPF methods for $\lambda = 0$. The figure clearly demonstrates a discrepancy between the two methods: voltage values are underestimated in the UTOPF results, while current values are overestimated.

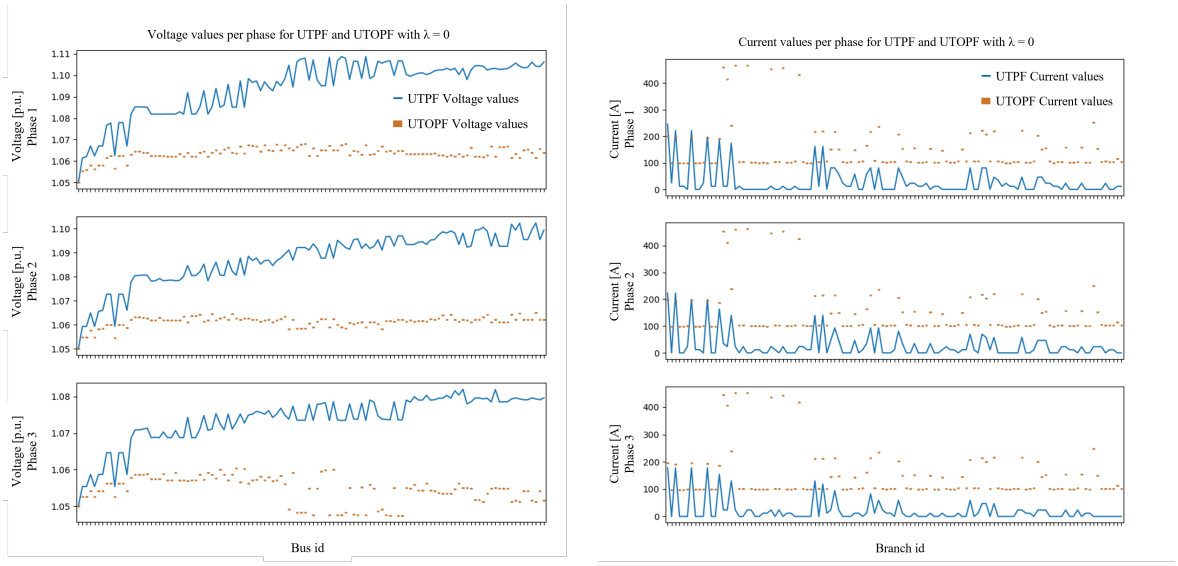

(a) Voltage values (b) Current values

Figure 6.6: Voltage and current values per phase for $\lambda = 0$

Figure 6.7 presents a similar analysis for $\lambda = 5$, showing the voltage and current values per phase obtained using the UTOPF and UTPF methods. This figure demonstrates a significant improvement in alignment between the voltage and current values computed by the two methods.

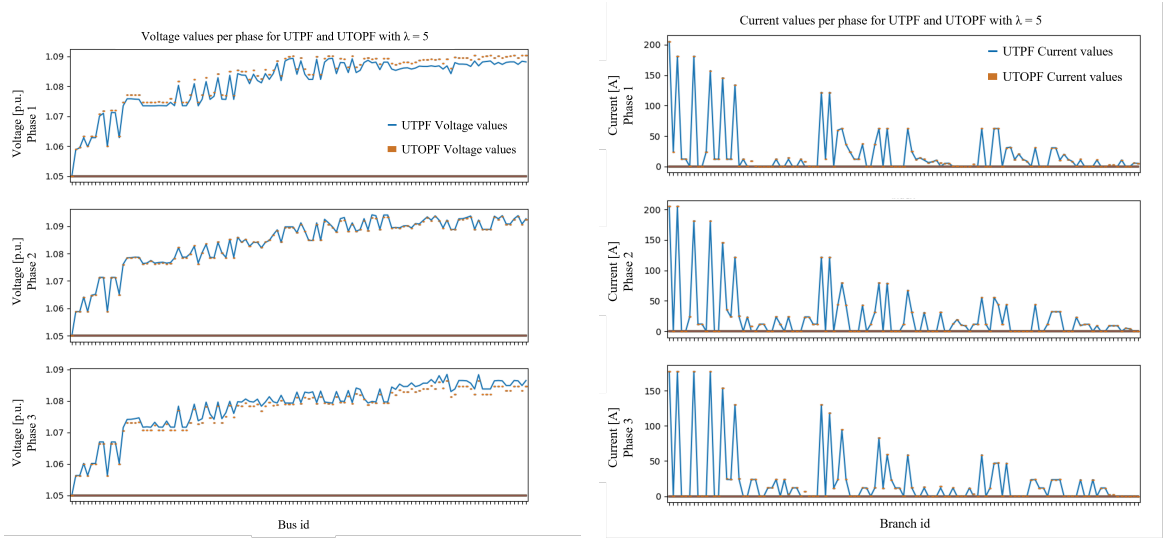

(a) Voltage values (b) Current values

Figure 6.7: Voltage and current values per phase for $\lambda = 5$

These two figures effectively illustrate the differences in current and voltage values per phase for different λ values. Figure 6.8 summarizes the results given by the multiple iterations in the Algorithm (1). More specifically, each dot represents the MAE across all phases and buses or branches for one iteration, while also comparing them with the aggregated OE for several λ values.

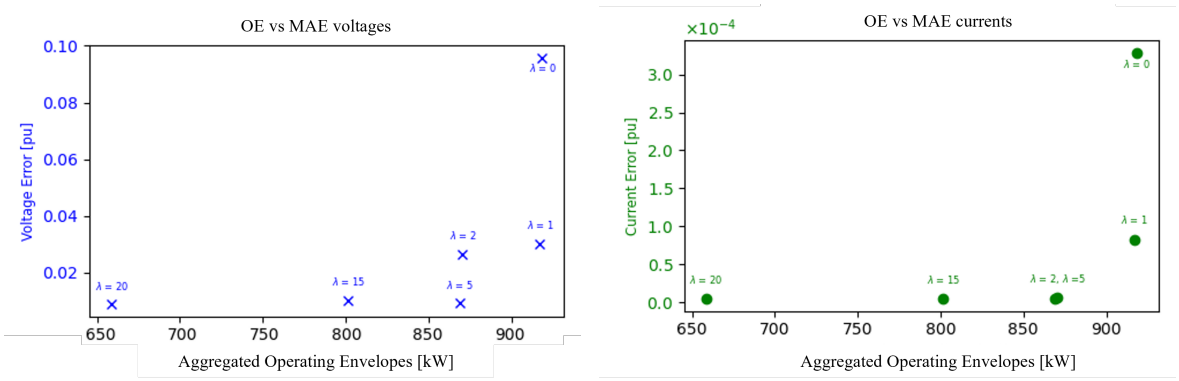

(a) Voltage values (b) Current values

Figure 6.8: Voltage and current values MAE compared to aggregated OEs for $\lambda = \{0,1,2,5,15,20\}$

More specifically, on Figure 6.8, each dot or cross represents an iteration for a specific λ value. In the figure, the x-axis represents the sum of OEs for all end-users, with the voltage MAE shown in blue and the current MAE in green. As outlined in Algorithm (1), the optimal λ is the λ value that minimizes MAE while maximizing the OEs. For this specific testfeeder, when $\lambda = 2$, the voltage MAE remains significant, whereas for $\lambda = 15$ results in a reduced OE with similar error levels compared to $\lambda = 5$. As a result, $\lambda = 5$ is selected as the optimal value: it is the value that minimizes the losses while maximizing the OEs. After finding the optimal λ, the OEs can be interpreted.

Figure 6.9 illustrates the resulting OEs per end-user, computed using the relaxed UTOPF on the IEEE EU LV testfeeder. In the figure, each pair of bars represents the OE limit for an end-user. The dark green bar represents the optimal OE per connection point, the light green bar represents the fair OE, and the light yellow bar represents the maximum connection capacity. Both the optimal and fair OEs cannot exceed the maximum connection capacity.

The results demonstrate that, with the Optimal UTOPF model, end-user 0, located near the trans-

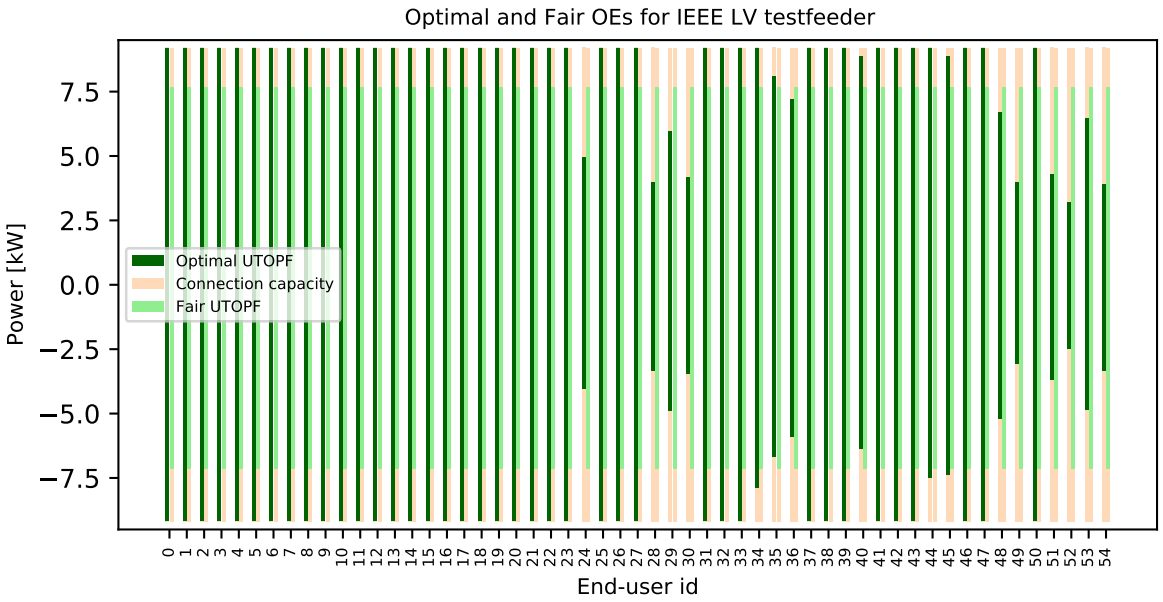

Figure 6.9: OE per end-user for Optimal and Fair relaxed UTOPF on the IEEE European LV Testfeeder

Table 6.5: Results comparison of Optimal and Fair OE for IEEE EU LV testfeeder

Metrics	**Optimal UTOPF**	**Fair UTOPF**	**Fair UTPF**
OE [kW]	[+ 457.86kW/- 439.15kW]	[+ 421.24kW/- 394.68kW]	[+ 421.85kW/- 391.60kW]
OE [%]	108	100	100
Fairness	No	Equal	Equal
Computation time [s]	70	60	3

former, has access to a significantly larger power range compared to end-user 54, who is located at the end of the feeder. The aggregated OEs for the Optimal UTOPF are 457.9 kW and -439.1 kW for the upper and lower bounds, respectively.

This disparity underscores the importance of incorporating fairness criteria for DSOs. In contrast, when considering the fairness constraint, the Fair UTOPF, as well as the UTPF method, ensure equal access for all users, setting each OE to 7.6 kW for the upper bound and -7.2 kW for the lower bound. This results in aggregated OEs of 421.2 kW and -394.7 kW for the upper and lower bounds, respectively. Fairness is needed, but it usually reduce the overall available flexibility.

These results are summarized in table 6.5 and in figure 6.10.

6.3.3 Case study 2 - Sibelga LV feeders

This subsection presents results for the OE on 49 Sibelga LV feeders, focusing on Optimal and Fair UTOPF methods. Figure 6.14 shows the OEs aggregated per LV Feeder for Optimal and Fair UTOPF methods. In addition, the aggregated connection capacity of all end-users is also shown in the figure. This analysis is used to categorize feeders. Just note that "end-user" refers to the aggregated group of end-users behind the same connection point, in contrast to IEEE results where end-user would be a single household. This is a difference between Urban and other types of grids as outlined in the introduction.

Feeders can be grouped into three types, each illustrated in Figures 6.11, 6.12 and 6.13, respectively for feeders of Type 1, Type 2 and Type 3.

- **Feeder type 1 – Oversized feeders.** These feeders are characterized by their maximum power not being constrained by grid cables capacity but rather by the connection capacities. They include oversized LV feeders that allows all end-users to access their maximum connection capacity without congestion risks. Fifteen feeders fall into this category (e.g. feeders 16, 17 or 47) characterized by short feeder lengths (58 to 227 meters) and few end-users (1 to 24). This behavior is illustrated

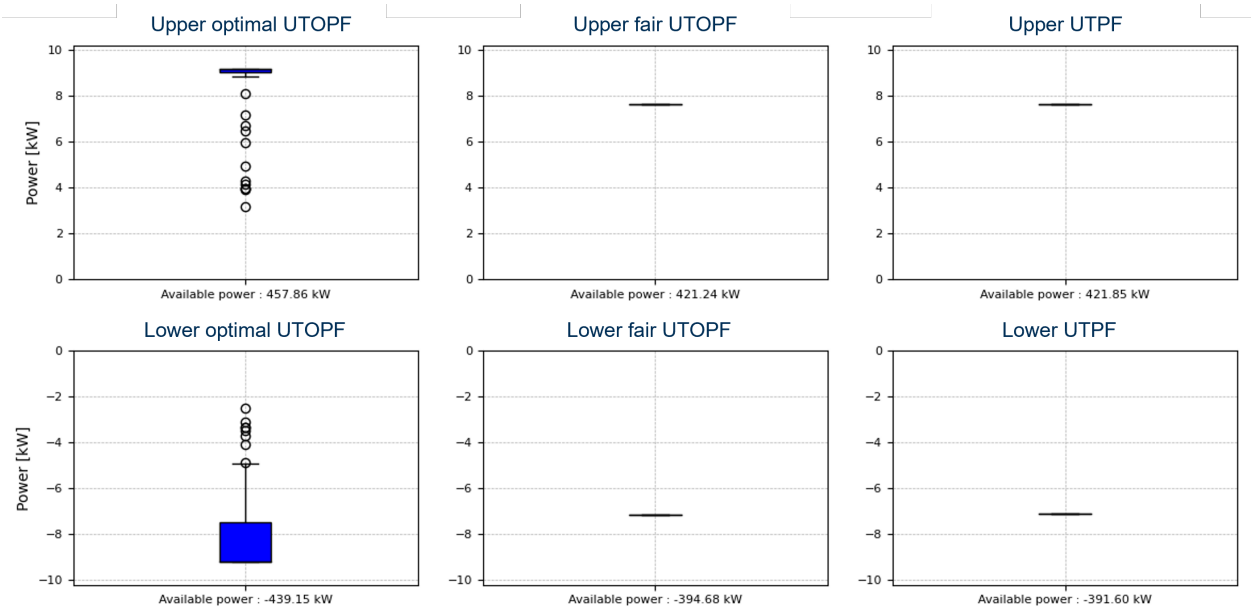

Figure 6.10: OE summary for Optimal and Fair relaxed UTOPF, and UTPF, on the IEEE European LV Testfeeder

in Figure 6.11, where both the Optimal and Fair OEs consistently reach the maximum connection capacity for feeder type 1.

- **Type 2 - Feeders where fairness does not reduce aggregated OEs.** This feeder category includes feeders where the aggregated OE for both Optimal and Fair methods is equal (e.g. feeders 0, 1 or 46). It is represented in Figure 6.12. In this case, the fairness principle does not reduce the total flexibility available on the feeder. While individual OEs for specific end-users may vary, the aggregated OE at the feeder level remains similar. For example, for end-user 0, located near the head of the feeder, the Optimal OE allows access to the maximum power, while the Fair OE reduces it. Conversely, for end-user 13, situated at the end of the feeder, the Optimal OE is more restricted compared to the Fair OE. Despite these individual variations, the total sum of OEs across all end-users on the feeder remains consistent between the Optimal and Fair methods.
- **Type 3 - Other feeders.** This category includes feeders that do not fit the characteristics of Types 1 or 2. One feeder of type 3 is represented in Figure 6.13.

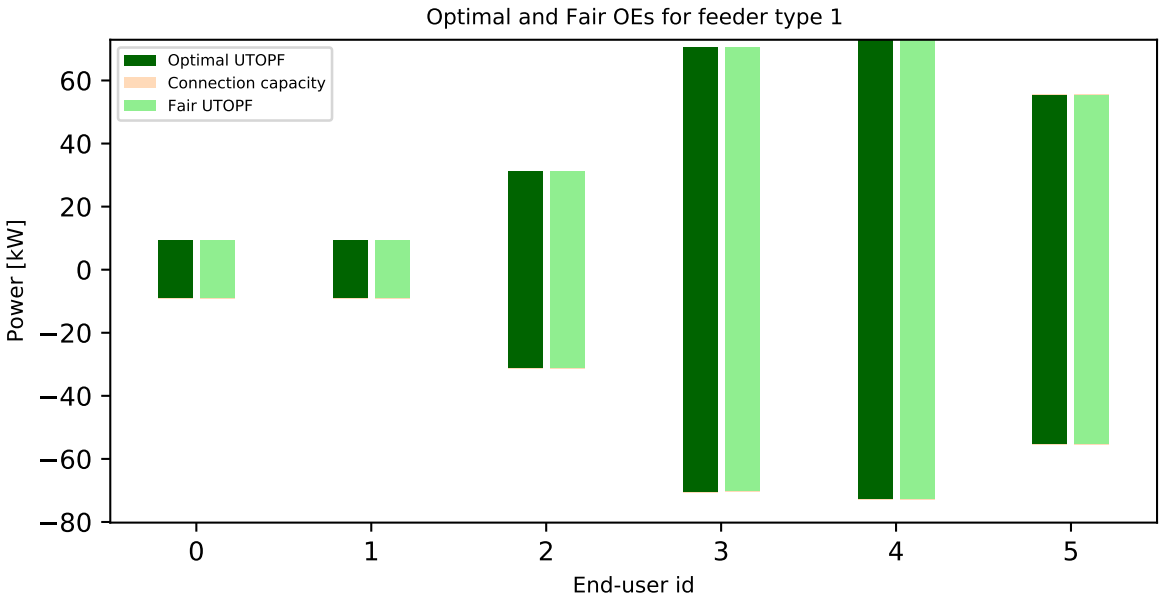

Figure 6.11: Feeder type 1

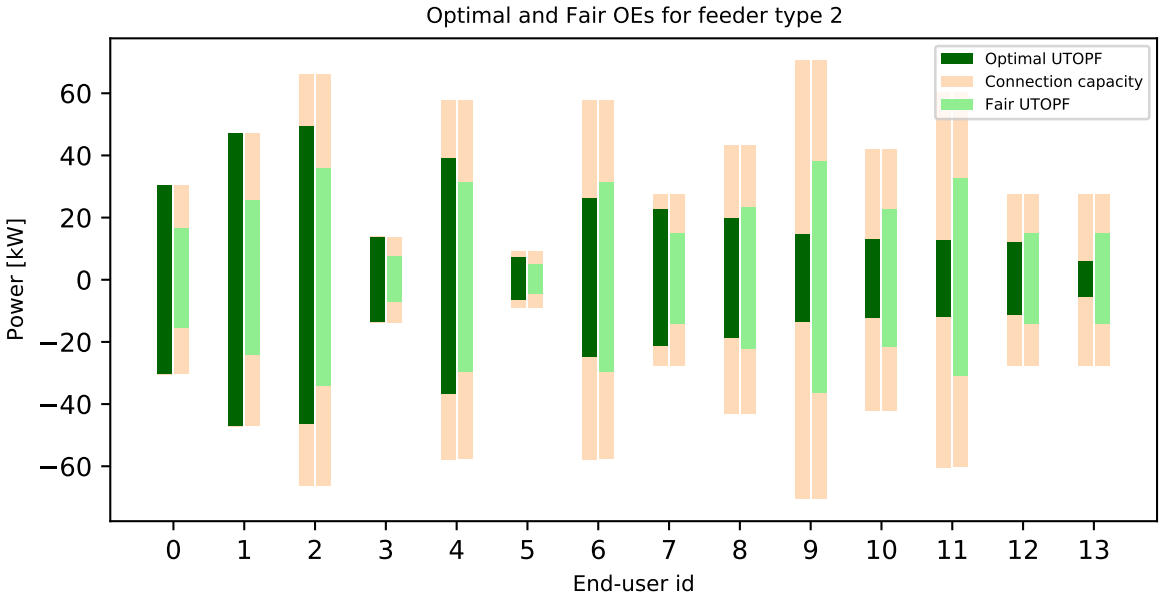

Figure 6.12: Feeder type 2

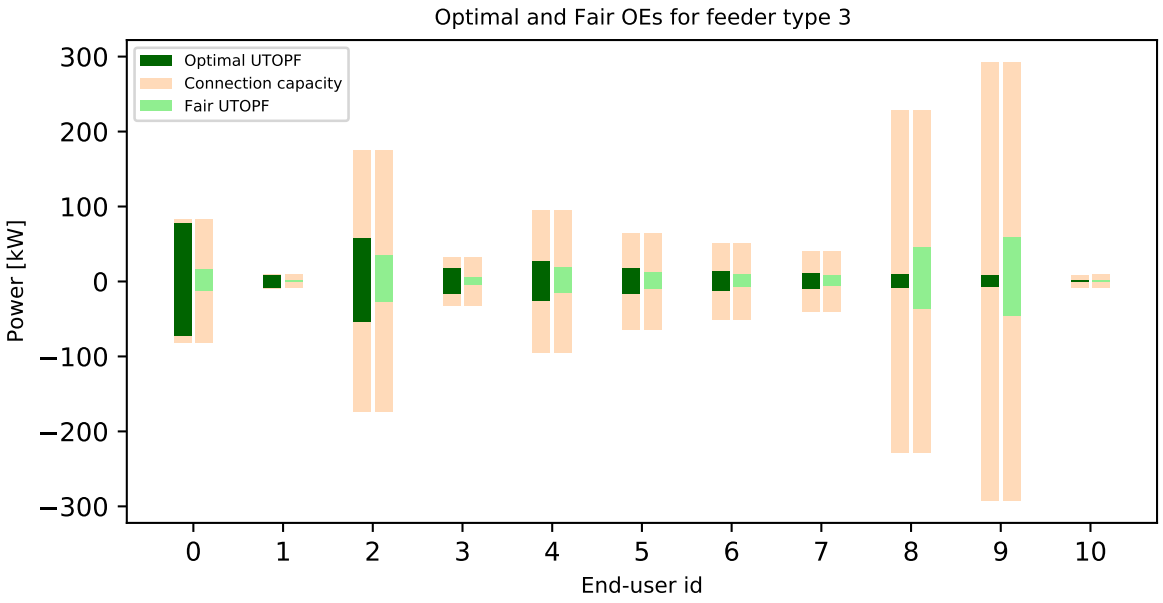

Figure 6.13: Feeder type 3

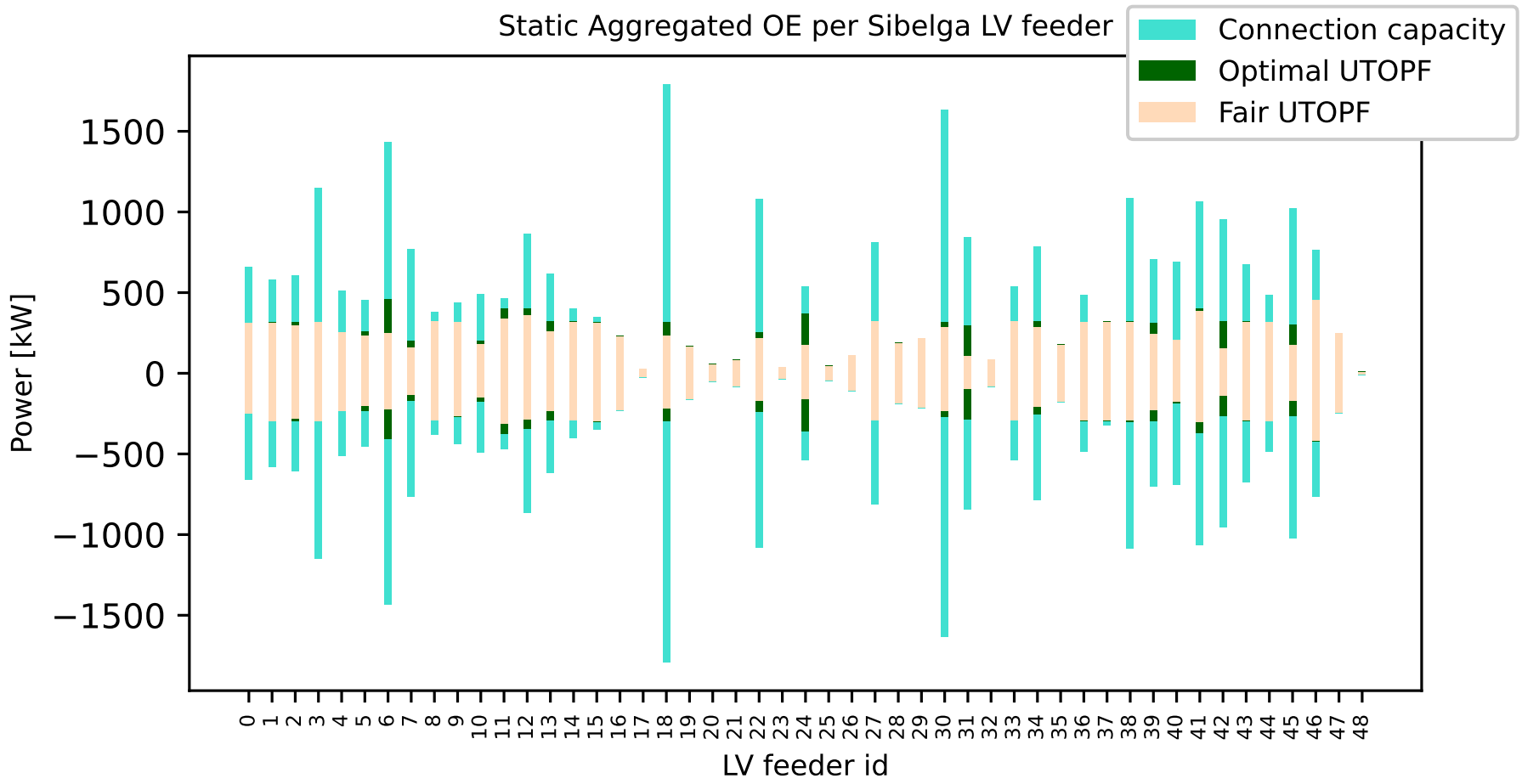

Figure 6.14: Aggregated OE per LV feeder for Optimal suggested UTOPF (green) and Fair suggested UTOPF (orange), with connection capacity (turquoise)

6.4 Influence of technical features on the Operating Envelope

So far, the OE principle is presented, methodologies discussed and chosen, two algorithms introduced, and results illustrated using the benchmark and Sibelga case studies. However, as outlined in subsection 2.2.3, some aspects remain unexplored. Specifically, load profiles have not yet been considered in the OE computation, which means the OEs presented so far are static.

This section will explore how different features affect the shape of the OE. One important principle, the fairness principle, was introduced in the previous Section due to its inherent connection with the OE and will not be revisited here.

The following complementary features are analyzed in this section:

1. Dynamic versus static assumptions
2. Unbalanced connections
3. Reactive power
4. Topological characteristics of the grid

These features are studied in detail to understand their impact on the shape of the OE.

6.4.1 Dynamic and Static Operating Envelopes

Introduction of the dynamic concept

As outlined in the introduction,OEs can be categorized as either dynamic DOE or static SOE, depending on whether their import and export limits vary over time. If the limits are time-varying, the OE is classified as dynamic; otherwise, it is static.

The computation of SOEs relies solely on the static, intrinsic characteristics of the grid. This means that SOEs are determined without incorporating load profiles, providing the maximum power that can be injected or consumed based purely on the grid's inherent characteristics. In the previous section, only SOE are therefore presented.

In contrast, DOEs leverage end-users' load profiles to unlock additional flexibility. These load profiles are determined by the DSO computing the OE. For example, if a DSO aims to maximize PV production, forecasted PV profiles can be integrated into the UTOPF model. This integration dynamically adjusts the individual DOEs, enabling higher energy offtake limits during sunny hours and thereby better utilizing solar production.

The distinction between DOE and SOE is illustrated in Fig. 6.15. The SOE for a specific end-user is highlighted in red, remaining constant over time. In contrast, the DOE is shown in green, with its shape varying over time. This example also includes a dashed blue curve representing an LV load profile, which combines the non-flexible load profile, typically represented by the well-known "duck curve"[2] and a solar production component.

It is important to note that the shape of an individual DOE depends not only on the end-user's load profile but also on the load profiles of other end-users on the same feeder. For instance, even if a particular end-user does not have solar panels, their DOE can still be influenced by the solar production profiles of neighboring end-users sharing the same feeder.

In summary, the DOE approach incorporates time-varying load profiles, allowing the OEs to adapt and enabling greater flexibility. These DOEs modify some constraints of the model: the power balance equations (6.35), as well as in the constraints limiting power injection and offtake (6.36) and (6.37).

However, implementing DOEs requires making assumptions about behind-the-meter assets. Access to such data by DSOs can be challenging, particularly given constraints related to market design and interactions with the regulator.

$$diag(S_n - z_n L_n) + \sum_{c \in n} (OE_c - s_{c,lp}) = \sum_{k:n \to k} diag(S_k) \tag{6.35}$$

$$-P_c^{max} \leq OE_c^{Re} - p_{c,lp} \leq P_c^{max} \tag{6.36}$$

[2]The "duck curve" describes a load profile where electricity demand from residential end-users follows a distinct pattern: it is high in the morning (around breakfast time), drops during the day due to reduced usage while people are at work, and then rises in the evening when people return home. This creates a dip in demand during midday hours, resembling the shape of a duck.

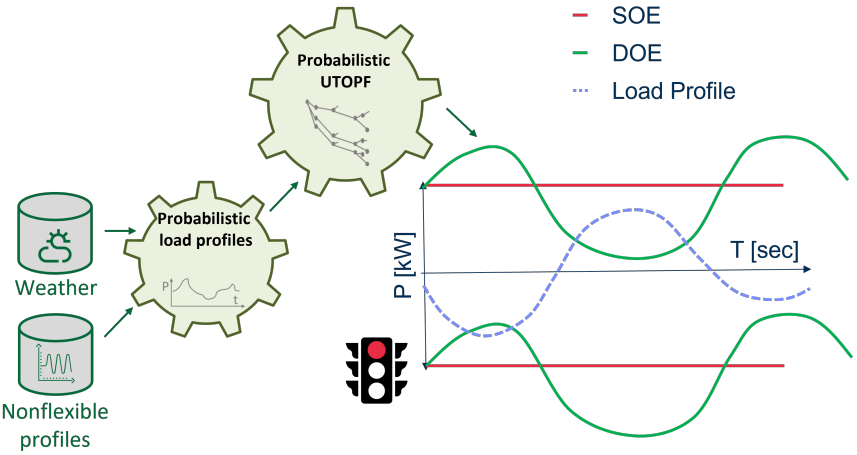

Figure 6.15: Illustration of SOE and DOE concepts

$$-Q_c^{max} \leq OE_c^{Im} - q_{c,lp} \leq Q_c^{max} \tag{6.37}$$

In addition, the fairness constraint in (6.38) is also adapted. As a reminder, implementing the fairness constraint results in all end-users limited to the same ratio of OE relative to their connection capacity. Importantly, the subset C^* which includes all end-users except those for whom $OE_c^{Re} - p_{c,lp} = p_c^{max}$, is used instead of the full set C. The rationale for using C^* is as follows: if the fairness criterion is applied to all end-users, the connection capacity of one single end-user could become the most restrictive limit, rather than the congestion limit. Therefore, the OEs of all other end-users might be unnecessarily constrained, leading to underutilization of grid capacity. This subtle distinction is illustrated in the case studies.

$$\frac{OE_i^{Re}}{P_i^{max}} = \frac{OE_{i+1}^{Re}}{P_{i+1}^{max}} \quad \forall i \in \mathcal{C}^* \tag{6.38}$$

Finally, the UTOPF and UTPF algorithms are adapted to include the dynamic feature of the OEs, respectively in Algorithm (3) and Algorithm (4).

In the proposed methodology, the value of λ is computed based on the SOE formulation and then reused for the DOE analysis. No additional recalculation of λ is performed for DOE.

Algorithm 3 Upper OE Computation with relaxed UTOPF

1: **Input:** Grid data (z_n, I_n^{ampacity}, $V_b^{\min}$, $V_b^{\max}$), connection capacities ($P_c^{\min}$, $P_c^{\max}$, $Q_c^{\min}$, $Q_c^{\max}$) and load profiles for DOE ($p_{c,lp}$ and $q_{c,lp}$)
2: **Output:** OE per end-user with optimal λ_{opt} denoted as $OE_{c,opf,\lambda_{opt}}$ and $OE_{c,opf,\lambda_{opt}}$
3: **for** $\lambda \in \Lambda$ **do**
4: Run UTOPF with objective:

$$\max \sum_{c \in \mathcal{C}} p_c - \lambda \sum_{n \in \mathcal{N}} \text{diag}(r_n L_n^{\text{Re}})$$

5: **Return** $OE_{c,opf,\lambda}$, $OE_{c,opf,\lambda}$, $V_{b,opf,\lambda}$, and $I_{n,opf,\lambda}$
6: Run UTPF with $OE_{c,opf,\lambda}$ and $OE_{c,opf,\lambda}$ as inputs
7: **Return** $V_{b,pf,\lambda}$ and $I_{n,pf,\lambda}$
8: Compute MAE between $V_{b,opf,\lambda}$, $I_{n,opf,\lambda}$ and $V_{b,pf,\lambda}$, $I_{n,pf,\lambda}$
9: **Return** Optimal λ_{opt}
10: **end for**
11: **Return** $OE_{c,opf,\lambda_{opt}}$ and $OE_{c,opf,\lambda_{opt}}$

Algorithm 4 OE Computation with UTPF (Upper OE)

1: **Input:** Grid data (z_n, I_n^{ampacity}, $V_b^{\min}$, $V_b^{\max}$), connection capacities ($P_c^{\min}$, $P_c^{\max}$, $Q_c^{\min}$, $Q_c^{\max}$) and load profiles for DOE ($p_{c,lp}$ and $q_{c,lp}$)
2: **Output:** OE per end-user OE_c^{Re}, OE_c^{Im} and voltage $V_{b,\text{pf}}$ and current $I_{n,\text{pf}}$ per branch
3: **while** $V_b^{\min} < V_b < V_b^{\max}$ and $I_n < I_n^{\text{ampacity}}$ **do**
4: $OE_c^{Re} = min(OE_c^{Re} + \epsilon, P_c^{\max})$
5: Run UTPF [65]
6: **Return** V_b and I_n
7: **end while**
8: **Return** OE_c^{Re} and OE_c^{Im}

Case studies

Dynamic results are applied on both the benchmark grid and some of the Sibelga LV feeders. The end-users load profiles (active and reactive power), considered in this paper are considered to be known. For the reduced IEEE EU LV Testfeeder, OEs are computed for a specific moment (12h00), respective load profiles are available in [63]. For the Sibelga data, the load profiles are based on the 2023 Belgian synthetic load profiles, as published by the system operator federation in [89], with data corresponding to the time step of June 1 at 12:00.

For both case studies, phase connections are assumed to be known, and the power factor is considered as constant. It is important to note that uncertainty regarding phase connections can alter the shape of the OE, as discussed in [129], and this topic will be further explored in the following subsection.

For the Sibelga case study, PV production is included as input into the load-profile to compute DOE. By including PV production as input, the resulting OE will reflect the influence of PV production, thereby unlocking greater downward flexibility.

Two scenario are considered related to fairness: (1) Not implementing the constraint in (6.31) resulting in an optimal OE, though unfair, referred to as Optimal UTOPF, and (2) Implementing the constraint in (6.31) resulting in all end-users limited to the same ratio of OE relative to their connection capacity (except if $OE_i^{Re} - p_{i,lp} = p_i^{max}$), and referred to as Fair UTOPF.

Case study 1 - IEEE European LV Testfeeder

The optimal exactness parameter λ is found based on methodology presented in Algorithm (1). When the optimal λ is selected, the OEs can be interpreted. Fig. 6.16 presents the resulting OEs per end-user that are computed with the different methods: the Optimal UTOPF, the Fair UTOPF and the benchmark UTPF. It shows that, with the Optimal UTOPF model, end-user 0 located near the transformer has access to larger power range than end-user 54 located at the end of the feeder. This variation highlights the importance of the fairness criterion to be considered by DSOs.

End-user 8 exhibits two noteworthy results. First, the upper optimal OE, i.e. the allowed injection limit, exceeds the maximum connection capacity (9.2 kVA). This is due to the high consumption of this end-user (3.6 kw) at the considered time (12:00), which shifts the OE up. This indicates that higher consumption enables this end-user to unlock more injection flexibility, aligning with the expectation that DOE increases upper flexibility by leveraging consumption. Second, the lower fair OE limit (-5.6 kw) differs from the lower limits of other end-users (-6.5 kw). This distinction arises because the OE for this end-user is constrained by his individual connection capacity (see Equation (6.36)) rather than by congestion limits. Consequently, other end-users do not share the same lower OE limit as end-user 8, as doing so would result in underutilizing grid capacity.

Table 6.6 shows for each method the comparison of the sum of aggregated upper and lower OEs, the qualitative evaluation of fairness, the computation time, as well as the voltage and currents MAE in p.u. The computation time is computed for UTOPF methods for one iteration once the λ value is parametrized and for 150 iterations for the UTPF method.

Fig. 6.16 and table 6.6 also show that Optimal UTOPF can unlock 10% more flexibility than Fair UTOPF or UTPF method. Fig. 6.17 shows the aggregated results at the feeder level.

Case study 2 - Sibelga LV feeders

As a reminder, the previous Section suggests to segment feeder types into three main categories. For type 1 feeders, dynamic OE analysis is irrelevant, because the connection capacity limits power

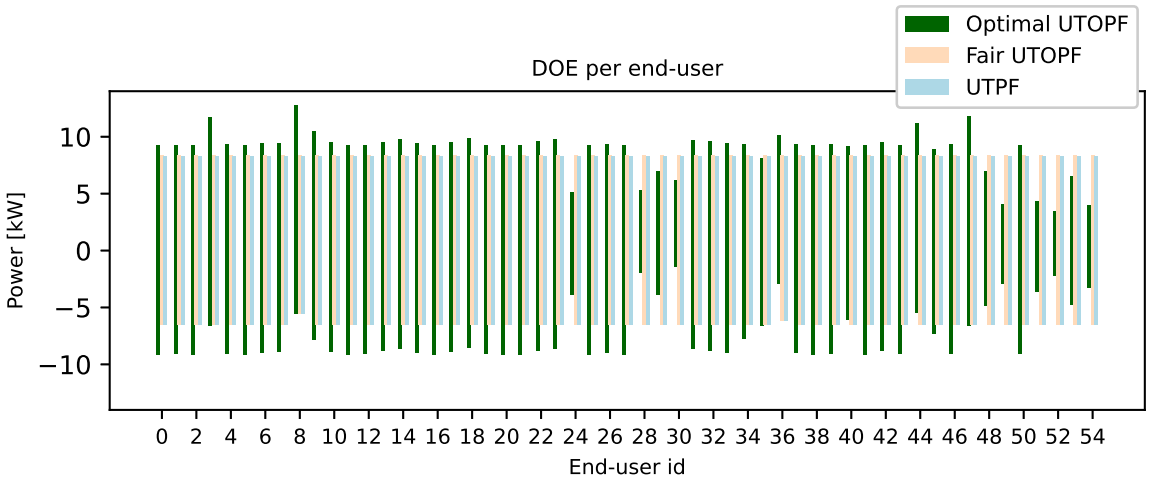

Figure 6.16: DOE (12h00) per end-user for Optimal suggested UTOPF (green), Fair suggested UTOPF (orange) and UTPF (blue) on the reduced IEEE European LV Testfeeder

Table 6.6: Results comparison for IEEE EU LV testfeeder

Metrics	**Optimal UTOPF**	**Fair UTOPF**	**UTPF**
DOE [%]	110.1	100.2	100
Fairness	No	Equal	Equal
Computation time [s]	38.1	34.5	0.7
Voltage MAE [p.u.]	0.004	0.013	NA
Current MAE [p.u.]	0.001	0.001	NA

consumption or injection, not the OE.

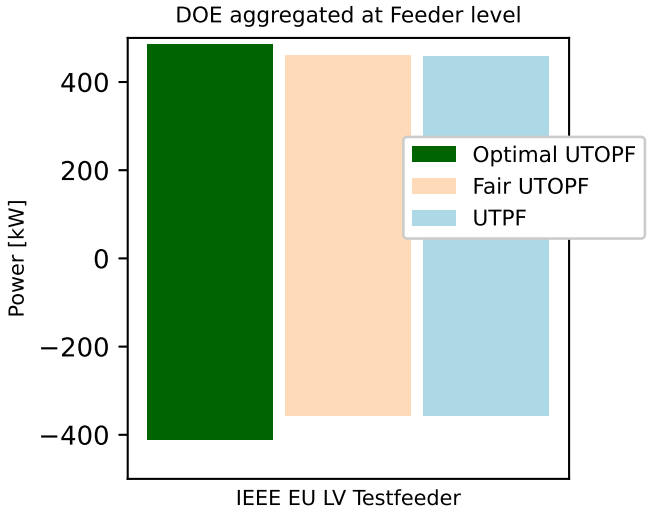

Figure 6.17: DOE (12h00) aggregated at LV feeder level for Optimal suggested UTOPF (green), Fair suggested UTOPF (orange) and UTPF (blue) on the reduced IEEE European LV Testfeeder

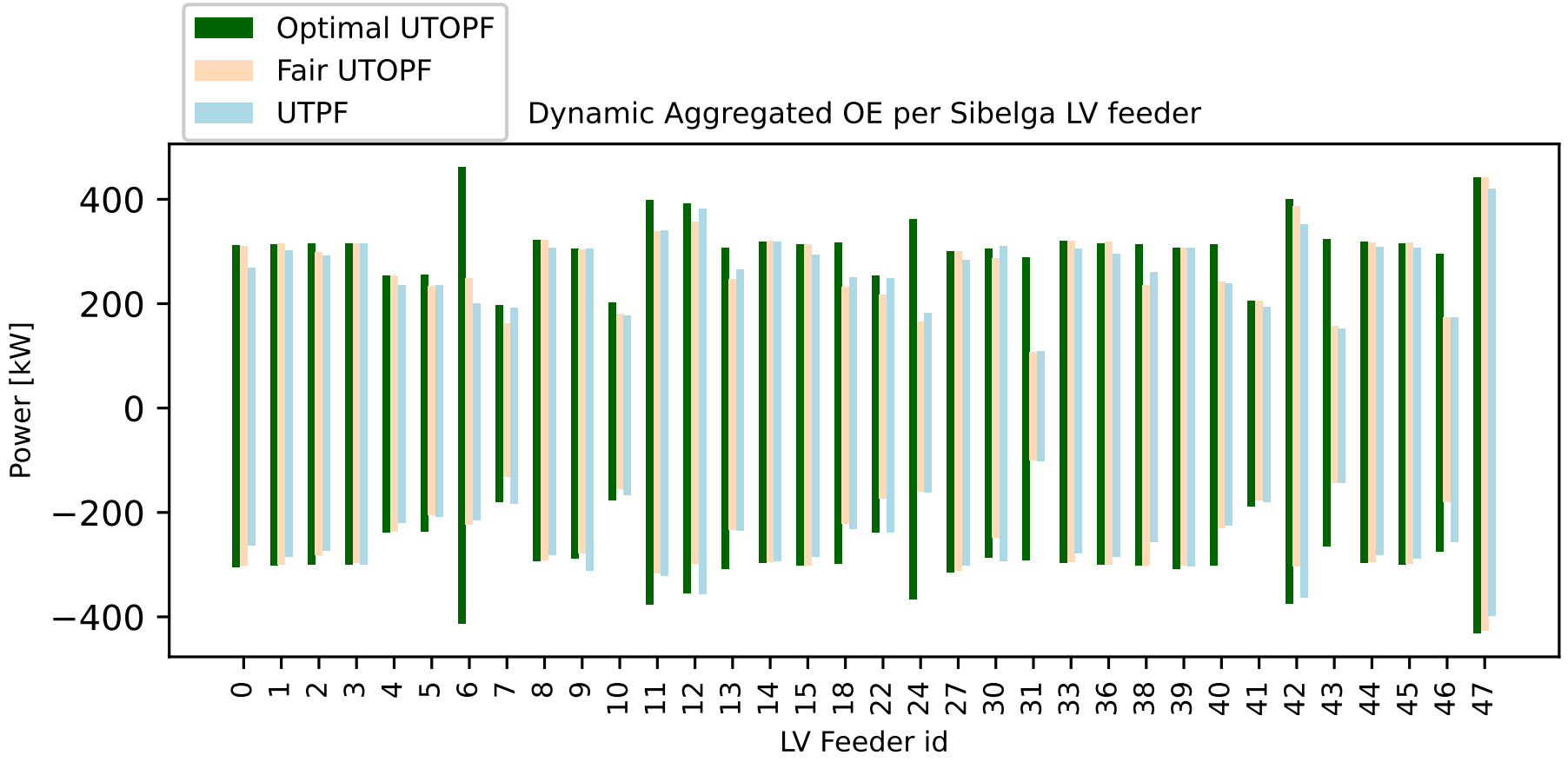

Figure 6.18: Aggregated DOE per LV feeder for Optimal suggested UTOPF (green), Fair suggested UTOPF (orange) and UTPF (blue)

Table 6.7: Results comparison for Sibelga LV testfeeder

Metrics	**Optimal UTOPF**	**Fair UTOPF**	**UTPF**
OE [%]	107.87	90.49	100
Fairness	No	Equal	Equal
Computation time [s]	1104.0	728.4	18.6
Avg. Voltage MAE [p.u.]	0.006	0.007	NA
Max. Voltage MAE [p.u.]	0.013 (feeder 24)	0.018 (feeder 7)	NA
Current MAE [p.u.]	0.000	0.000	NA

Fig. 6.18 illustrates the DOE for the 34 feeders selected for dynamic analysis (feeders of type 2 and 3), i.e. considering load profiles into the OE computation in (6.25) and (6.26). The feeder IDs are consistent between Fig. 6.14 and 6.18 to foster comparison. A summary of the findings, including a comparison of the aggregated OE across all LV feeders, computation times for the 34 LV feeder OE, and the average voltage and current MAE, as well as the maximum voltage error among the feeders, is provided in Table 6.7.

The results show similarly to the IEEE EU LV Testfeeder that the optimal UTOPF achieves a larger or similar DOE than the Fair UTOPF and the UTPF. The Optimal UTOPF can unlock 7% more flexibility than the UTPF method, and the Fair UTOPF can only unlock 9.5% less.

The comparison of the Fair UTOPF and the benchmark UTPF on Sibelga feeders reveals only minor differences, attributed to two key factors. When the Fair UTOPF results in higher OEs than the UTPF (e.g. feeders 0, 4 and 47), it is because the Fair UTOPF optimizes OEs at the end-user connection level, allowing three-phase end-users to distribute power unevenly across phases to achieve an optimal solution. In contrast, the UTPF increases power uniformly across phases. Conversely, when the UTPF yields higher OEs compared to the UTOPF (e.g. feeders 7, 12 and 24), this is due to relaxation-induced errors in the UTOPF model when recovering the quasi-exact solution. These errors can cause voltage overestimation for the upper OE (and underestimation for the lower OE), leading to over-constrained maximum power and a reduced OE.

6.4.2 Influence of Unbalance and Reactive Power on the OE

In previous analyses, OEs are computed assuming that end-users' connections were known based on case study data. However, as outlined in the introduction, DSOs may not always have precise knowledge of which end-users are connected to which phase. This subsection examines whether unbalanced connections among end-users influence the OE. In addition, this subsection studies whether constraining reactive power reduces the OE.

To investigate this, an extreme case study is devised to compare the OE of end-users distributed across different phases with a hypothetical, unrealistic scenario where all end-users are connected to the same phase.

Additionally, two assumptions regarding reactive power are analyzed:

- Variable Power Factor: Reactive power is treated as a variable and optimized to maximize the OE.
- Fixed Power Factor: Reactive power is constrained to a fixed value (e.g., power factor = 1, based on real grid data [130]).

Figure 6.19 show the OEs for each end-user under the variable and fixed Power Factor scenarios. When the Power Factor is variable, left figure, the reactive power is limited only by the maximum allowable current at the injection point. In this case, the blue curve (OE1) represents the scenario where end-users are evenly distributed across phases, while the green curve (OE2) represents the extreme case where all end-users are connected to a single phase. The comparison reveals a reduction in the OE when all end-users are connected to the same phase.

In contrast, the right figure shows the results under a fixed Power Factor. OE3 and OE4 represent the scenarios of distributed and single-phase connections, respectively. Summing the maximum and minimum power values for all end-users, the results are as follows:

- OE1: Maximum = 446 kW, Minimum = -384.2 kW;
- OE2: Maximum = 159.06 kW, Minimum = -151.18 kW;

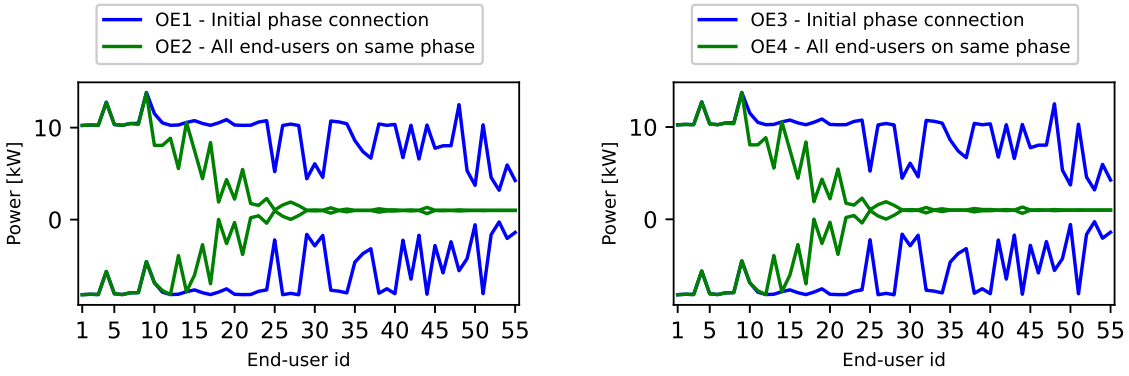

(a) Reactive power variable

(b) Reactive power fixed (Power Factor = 1)

Figure 6.19: Illustration of OE with variable or fixed Power Factor (Power Factor=1) where end-users are connected on different phases (blue) and to the same phase (green)

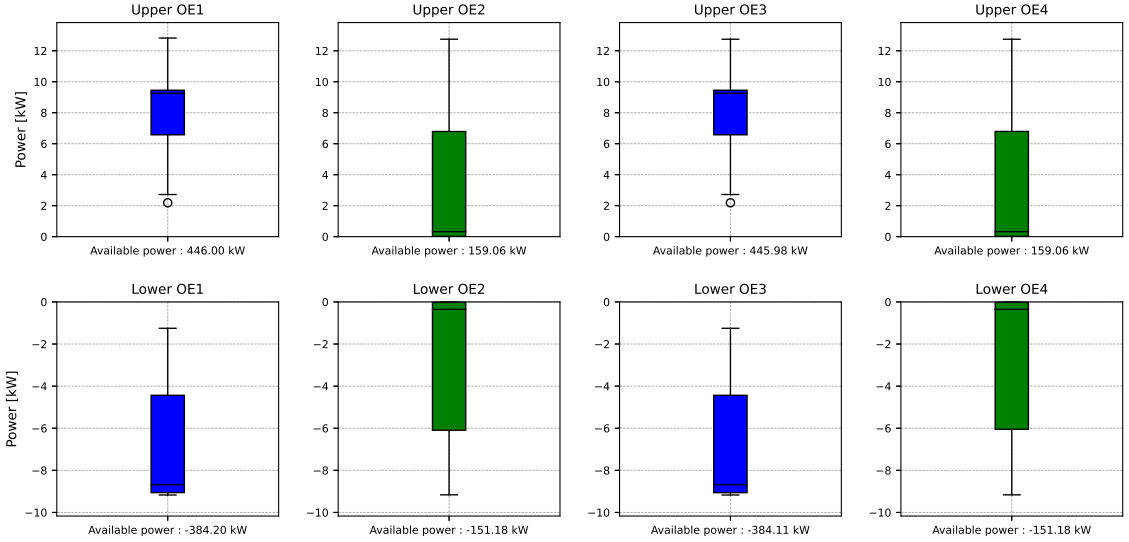

Figure 6.20: Summary of the four upper and lower OE

- OE3: Maximum = 445.98 kW, Minimum = -384.11 kW;
- OE4: Maximum = 159.06 kW, Minimum = -151.18 kW.

These results indicate that OE reductions under single-phase connections occur regardless of whether the Power Factor is fixed or variable.

The results also highlight the influence of grid topology and phase connections. For instance, end-users located at the farthest points of the feeder (e.g., users 52 and 55 on phase A, and 50 and 53 on phase B) face the most constrained OE values under OE1 and OE3.

When strong imbalances occur, end-users closer to the substation have greater flexibility compared to those further away. Thus, the farther end-users are from the substation, and the more loaded their phase, the more constrained their flexibility becomes.

This subsection also evaluates the influence of reactive power control on the OE. Modern end-user equipment, such as inverters for PV systems, EV, and domestic batteries, can adjust their reactive power. However, results show that even under fixed Power Factor assumptions, evenly distributed connections across phases yield similar flexibility levels to those with variable Power Factor. Therefore, reactive power control does not significantly enhance the OE or mitigate imbalances.

6.4.3 Influence of Grid Topology

Finally, this section ends by analyzing the influence of some grid characteristics over the OEs and the feeder types identified in the static case study over the Sibelga feeder in Subsection 6.3.3. As outlined, Feeder type 1 refers to feeders where the OE is constrained by the connection capacity before the distribution grid limits. Feeder type 2 consists of feeders where the Fair and Optimal OEs are similar. Feeder type 3 includes all other feeders that do not fall under the first two categories.

Several topological characteristics of the real Sibelga LV feeders are analyzed and compared with feeder types and the exactness parameter λ weighting the objective function of the UTOPF. The analyzed characteristics include the nominal capacity of the feeder [kVA], the total connection capacity [kVA] (TCC), the total feeder length [m] and the maximum branch length [m] (MBL). To evaluate the statistical significance of differences in these characteristics across feeder types, non-parametric tests are conducted.

The Kruskal-Wallis[3] test reveals that both the MBL (p=0.012) and TCC (p=0.006) exhibit significant differences across feeder types. Pairwise comparisons using the Mann-Whitney U test[4] show that for the MBL, a significant difference exists between Feeder Type 1 and Feeder Type 2 (p=0.005). For TCC, significant differences are observed between Feeder Type 1 and Feeder Type 2 (p=0.025) as well as between Feeder Type 1 and Feeder Type 3 (p=0.002).

Fig. 6.21 illustrates statistical distribution per feeder type. For MBL, Feeder type 1 has the highest median, with greater variability compared to Feeder types 2 and 3. In contrast, TCC is higher in Feeder types 2 and 3 compared to type 1, with type 3 showing the most consistent distribution. These findings emphasize that both features—Maximum Branch Length and Total Connection Capacity—are key in distinguishing feeder types and understanding their operational characteristics.

6.5 Conclusions

This chapter presents a novel method for computing optimal OEs in unbalanced LV distribution grids using the EBFM UTOPF framework with SOCP relaxation. A key contribution is the development of a new algorithm that integrates the relaxed UTOPF for OE computation, featuring a parametrization technique to recover a quasi-exact solution. Notably, the method is applied to both wye and delta connections, thereby broadening its applicability.

The proposed approach has been validated on the IEEE EU LV Testfeeder benchmark and 49 real-world delta-connected LV feeders in Brussels. Results demonstrate that the Optimal UTOPF consistently provides equal or greater flexibility compared to fairness-based methods while delivering near-exact solutions—critical for accurately defining the operational limits of the grid.

Several key features are also discussed. Regarding fairness, if the criterion is to be considered, the benchmark UTPF method is preferred over the UTOPF method, as it ensures equal OEs for the benchmark grid or higher OEs in the Sibelga case study while also offering lower computation times.

In addition, the chapter shows that unbalance impacts the shape of the OE, whereas the power factor does not appear to have any significant effect.

Furthermore, the analysis identifies three distinct feeder types, providing valuable insights into the relationship between network topology and OEs. Oversized feeders can reach their maximum OE without causing grid congestion, while Type 2 feeders shows that Fair and Optimal OE are similar. A brief statistical analysis indicates that maximum branch length and total connection capacity are key factors influencing a feeder's classification.

[3]The Kruskal-Wallis test is a non-parametric statistical method used to compare three or more independent groups to determine if they come from the same distribution.

[4]The Mann-Whitney U test is a non-parametric test used to compare differences between two independent groups. It evaluates whether the distributions of the two groups are different, specifically focusing on whether one group tends to have larger values than the other.

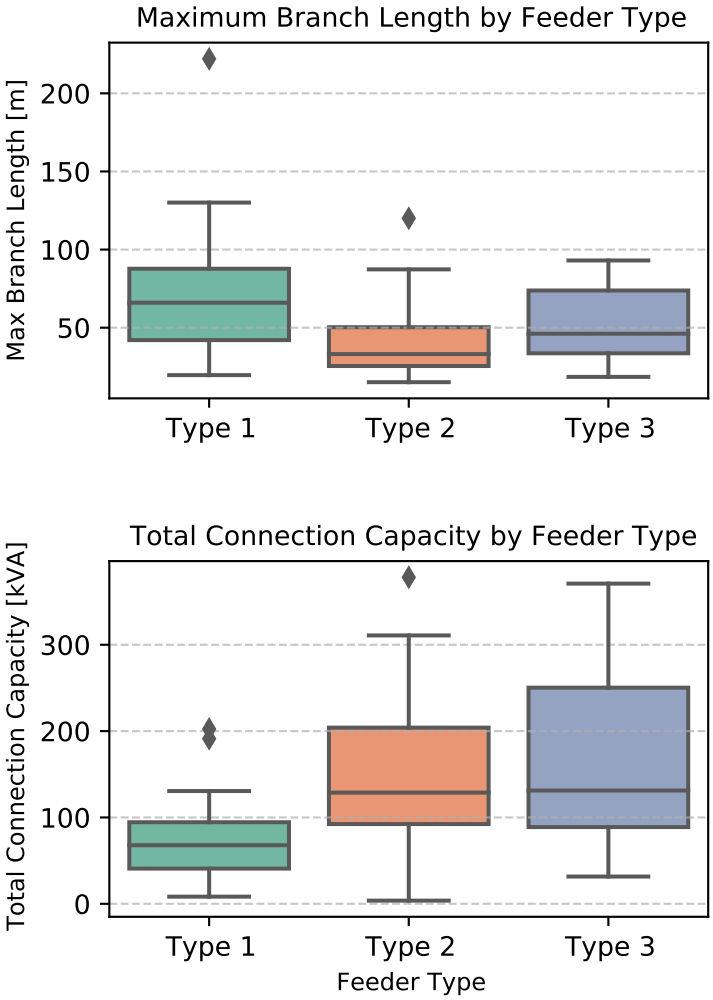

Figure 6.21: Boxplots for significant topological characteristics

Chapter 7

Application of Operating Envelopes for Congestion management

Contents

7.1 Introduction

As outlined in Subsection 2.2.2, DSOs can activate five mechanisms to effectively manage LV congestion: technical solutions, tariff-based solutions, market-based solutions, connection agreement solutions, and rule-based solutions.

This Chapter focuses on illustrating how OEs can be used within connection agreement solutions to prevent LV congestion, with a particular emphasis on the NFCA as presented in Subsection 2.2.2. It also introduces the use of the congestion identifier presented in Part II of this manuscript.

As a reminder, the Non-Firm Connection Agreement (NFCA) is a connection contract agreed between a system operator, here, the DSO, and an end-user, which limits the ability of the end-user to fully export or import their capacity [48]. It displays the following features: permanent or temporary activation, Optimal or Fair distribution, Static or Dynamic, geographical scope. These features are further discussed in the following sections, but some feature can be identified as similar as to the features analyzed when computing the OE (e.g. Optimal vs. Fair, Static vs. Dynamic).

In addition, the NFCA can be contracted with only a subset of end-users rather than involving all of them, as illustrated in Figure 7.1. The figure depicts the OE, whose limits are used for an NFCA, on the left side. Then, these contracts are established with only 16 of the end-users on the IEEE LV EU Test Feeder, represented by green houses.

Figure 7.2 illustrates the guaranteed capacity computed using the OE as a function of the number of end-users adhering to the NFCA for the benchmark grid. When only a portion of end-users agrees to adhere to the NFCA, those end-users are assumed to be located farthest from the transformer, adopting a conservative approach.

If all 55 end-users adhere to the NFCA, the guaranteed capacity is set to $\pm 7.5kW$. However, if only 22 end-users participate, the guaranteed capacity decreases to $\pm 5kW$. This demonstrates that as

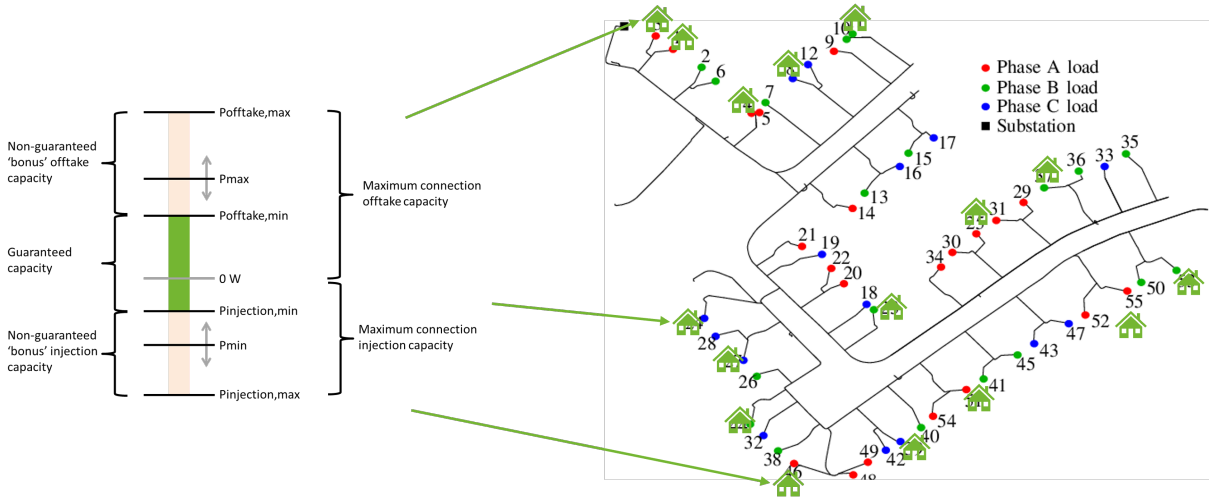

Figure 7.1: Representation of a NFCA contracted for 16 end-users on the IEEE LV EU Testfeeder

more end-users join the NFCA, the constraints on each individual end-user are reduced, highlighting the collective benefit of broader participation.

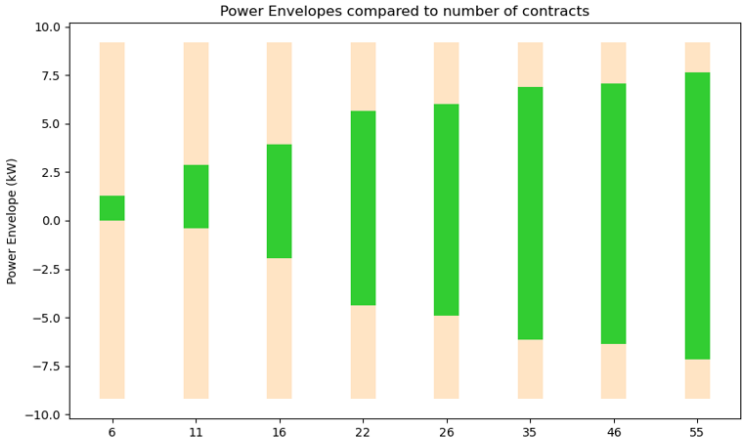

Figure 7.2: Guaranteed capacity compared to number of end-users adhering to the NFCA

This chapter first presents in Section 7.2, the application of the NFCA, using OEs as limits for the guaranteed capacity, to enable flexibility services within a simplified market design involving only the DSO, FSP, end-users, and energy communities. In Section 7.3, it then explores the impact of the NFCA on balancing services provided by flexibility providers to the TSO, highlighting how the proposed mechanisms support coordination across different system levels.

7.2 Simplified Framework for Non-Firm Connection Agreement Application

This section outlines the application of the NFCA concept within a DSO-driven process under a simplified market framework involving only end-users, energy communities, FSPs, and the DSO. It first introduces the simplified value chain, with a focus on operational actions, followed by a more detailed description of the NFCA flexibility process.

7.2.1 Simplified NFCA Value Chain and integration of tools developed in this research

The value chain is illustrated in Figure 7.3. This framework is not tied to a specific flexibility service and is thus well-suited for implicit flexibility schemes or local optimization. The integration of frequency control services is discussed in the next section.

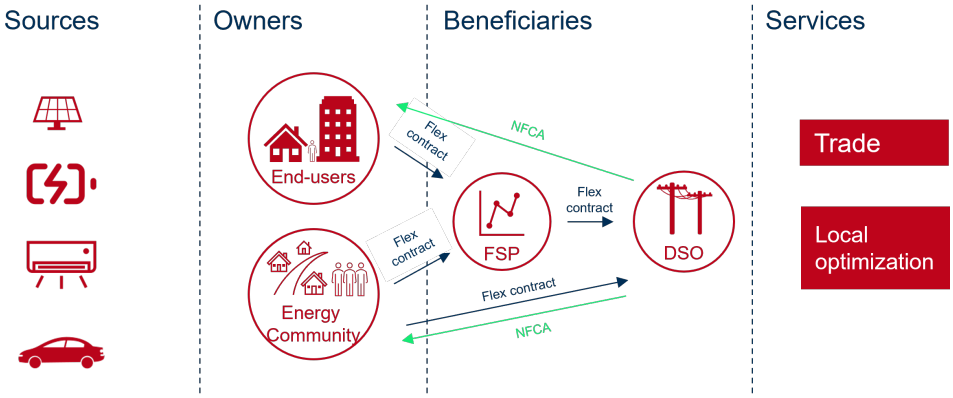

Figure 7.3: Simplified value chain with NFCA

In this setup, end-users and energy communities own flexible assets. To valorize flexibility, they may contract with an FSP, who in turn must establish a contractual agreement with the DSO to operate on the LV grid. Such contracts are available via the Synergrid platform in Belgium [131]. Alternatively, energy communities can act as aggregators and contract directly with the DSO.

According to section *5.3.3. Limitations sur demande du GRD* of the standard DSO–FSP flexibility contract, the DSO may restrict flexibility activations if they present a risk to distribution grid. This research proposes using the forecasting and optimization tools developed in Part II and Chapter 6 to assess congestion risks and define operating limits for flexibility. These limits can be enforced through an NFCA, ensuring that when congestion risks are high, the FSP or energy community is constrained to the OE boundary, thus avoiding grid violations.

This approach supports congestion-free grid operation while maximizing available flexibility, accounting for both technical constraints and fairness considerations. It provides a more targeted alternative to deactivating delivery points entirely when grid risks arise.

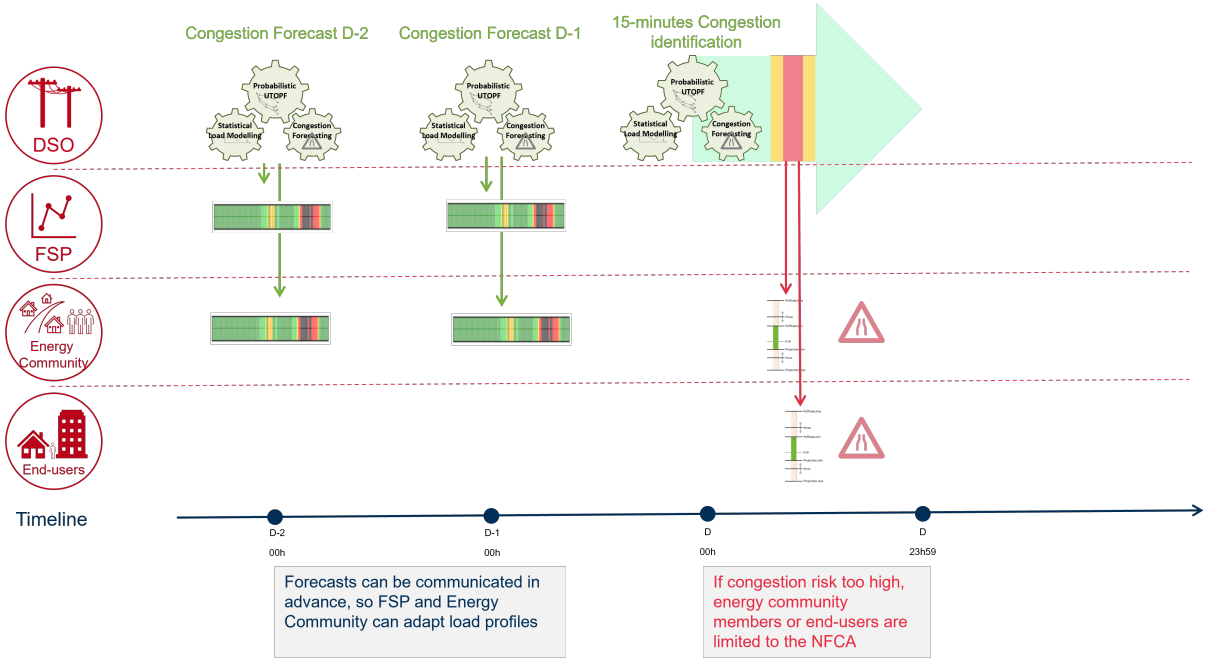

Figure 7.4: Operation of NFCA using tools developed in this research

Figure 7.4 illustrates the working flow of the NFCA during operate phase. The congestion identifier can be executed two days and/or one day ahead, using updated forecasts for solar generation and non-flexible loads. Based on this analysis, the FSP or energy community receives congestion risk signals and can adjust load profiles accordingly.

On the operating day, the DSO monitors congestion risks every 15 minutes. If the risk exceeds a defined threshold, the NFCA is activated, limiting the capacity of end-users or energy community members. When limits are derived from OE values, this ensures that no congestion occurs without requiring the DSO to control behind-the-meter assets. The approach maintains grid reliability while offering transparency and predictability for flexibility providers.

7.2.2 Simplified NFCA Flexibility Process

The flexibility activation process presented in the Synergrid guide [19] outlines standard coordination steps among market stakeholders. This research adapts that process to integrate the tools and methods developed in this research. While the original guide defines five stages, they are consolidated into three main phases for clarity and aligned with the simplified market context. These phases will be further detailed for frequency control applications in the next section.

The three steps of the simplified NFCA flexibility process are detailed below and illustrated in Figure 7.5.

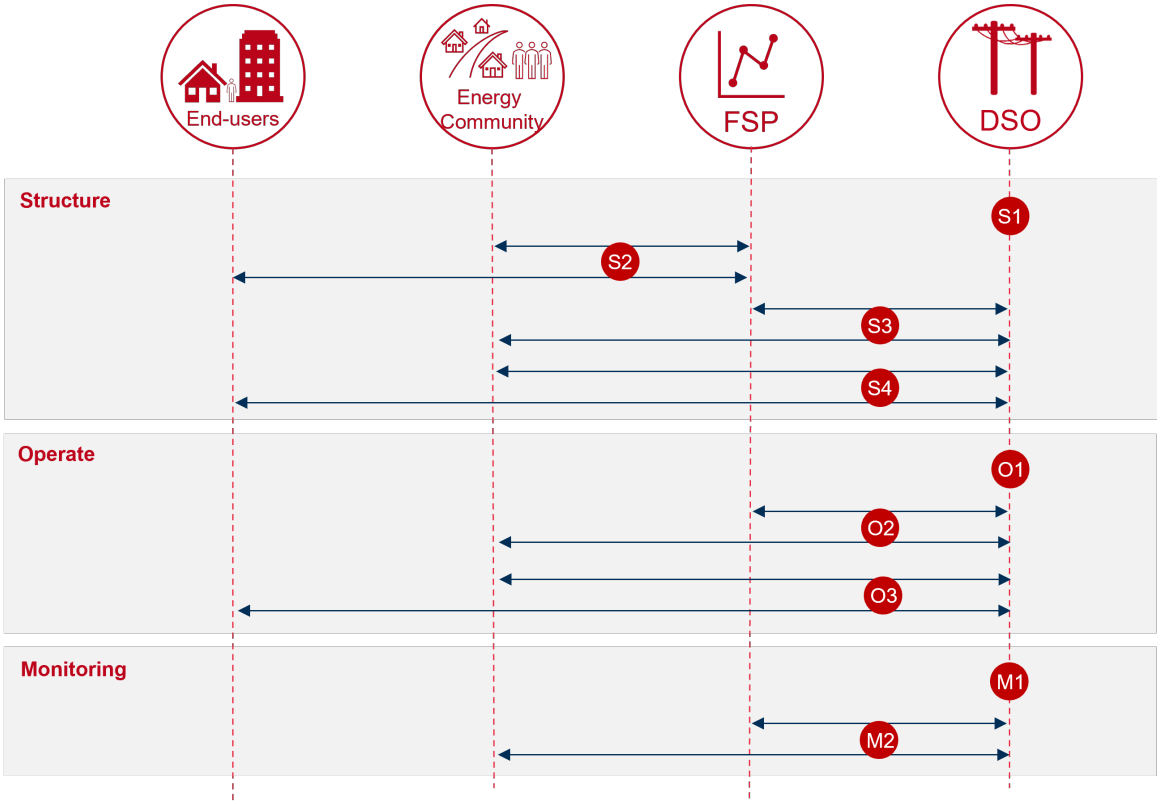

Figure 7.5: Information flow for NFCA

Structure

The structure phase occurs well before operational timelines, so the computation time required for OE is not a constraint.

[**S1**] In this initial phase, the DSO designs the NFCA based on technical and policy criteria, including whether the agreement is dynamic or static, the number or percentage of end-users expected to adhere, the fairness criterion, and the geographical scope of application. Using these design parameters, the DSO computes the OE as described in Chapter 6 of this manuscript. The computed OE values determine the capacity thresholds that prevent grid congestion.

[**S2**] From his side, the FSP is contracting flexibility with the end-users or the energy community.

[**S3**] The DSO and FSP sign a contract as flexibility will be activated on the distribution grid. The OE thresholds are used to configure the NFCA and can be formalized within the DSO–FSP flexibility contract. Communication channels and data exchange formats are then established. Upon contract signature, the flexibility service becomes active.

[**S4**] Finally, the NFCA can be signed between DSO and point connection owners. In practice, contracting with an aggregator or an energy community—rather than individual end-users—can improve scalability and stakeholder engagement. Indeed, a key consideration during this phase is that the DSO must establish a NFCA with the connection point owner—typically the end-user or an energy community. However, managing contracts with numerous stakeholders may exceed the DSO's current resource capacity. To address this, a default policy could be applied: flexibility at connection points on LV feeders is canceled when congestion risk is high, unless a NFCA is in place. In such cases, flexibility is allowed but limited to the terms of the contract (e.g. by the limits computed by the DSOs based on the OE). This shifts the incentive to contract NFCA with end-users from the DSO to the FSP, who ultimately benefits from flexibility activation and is also the party directly contracting with end-users. Energy communities add value in this context, as they both own the flexible assets and can directly engage with members in an NFCA contract, avoiding additional aggregation and contracting costs.

Operation

The *operation* phase spans from two days before real-time up to the end of each operating day, providing timely, actionable information to flexibility providers. This phased approach enables effective grid management while facilitating decentralized flexibility provision.

[**O1**] As shown in Figure 7.4, the congestion identification tool (detailed in Part II) can be used to predict congestion risks one or two days in advance.

[**O2**] These forecasts are shared with contracted parties (FSPs or energy communities) to support the possible planning adaptation. If a dynamic operating envelope (DOE) is implemented, it is also computed day-ahead using forecasted load profiles.

[**O3**] On the operating day, the DSO monitors grid conditions in real time on a 15-minutes basis. If congestion risk becomes critical, the NFCA is activated: contracted parties must reduce their injections or offtake to stay within defined limits. If OE is used to set up NFCA limits, this ensures congestion is avoided without requiring direct DSO control over behind-the-meter assets.

Monitoring and Evaluation

Throughout and after operation, the DSO evaluates NFCA performance using key performance indicators, including congestion occurrence, end-user adherence, and the effectiveness of guaranteed capacity limits. This analysis informs whether adjustments to the NFCA structure or OE computation are needed to reflect evolving grid conditions or behavioral changes. Additionally, it helps verify compliance: if participants exceed limits without justification, penalties may apply. Importantly, the DSO's role remains non-intrusive, limited to communicating constraints rather than controlling individual flexible assets. This monitoring phase requires visibility, and therefore end-users contracting NFCA must be equipped with smart meters.

[**M1**] Regarding data sharing, the DSO uses internal data such as grid parameters and, for DOE, the load profiles, to compute the operating envelopes.

[**M2**] These values are then shared exclusively with the contracted FSP or energy community, which are informed in advance of their respective flexibility limits. This approach minimizes the need for extensive coordination: the DSO independently calculates the envelopes, while the FSP or energy community is responsible for adapting load profiles when NFCA is activated.

7.3 Framework for Non-Firm Connection Agreement application combined with frequency control activation

This section aims to provide insights into the impact of activating NFCA on TSO operations when LV assets should provide frequency control. Specifically, it examines how NFCA may hinder the activation of LV assets for frequency control. Indeed, as outlined throughout the manuscript, and specifically in Subsection 2.1.6, FCR and aFRR are opened for LV flexibility assets in Belgium.

While NFCAs aim to maintain the local distribution network safety, they may inadvertently restrict the utilization of LV assets that have been pre-qualified and cleared to provide services in other markets,

such as frequency control. For example, consider an aggregator submitting a portfolio of LV assets, such as residential batteries or electric boilers, for a negative aFRR product between 16:00 and 20:00. If the portfolio is pre-qualified, cleared, and dispatched, the assets should be available for activation within this period. Now, imagine it's a high-demand day before a holiday, and several EVs are fast-charging in a specific LV feeder to prepare for travel (note that fast charging in this context represents 10 to 15kV compared to fast charging at the MV or HV level). This leads to increased LV network stress, prompting the DSO to activate NFCAs to avoid congestion. Simultaneously, a global frequency incident occurs, requiring the TSO to call upon the full secondary reserve. Due to the active NFCA, the FSP cannot activate the pre-qualified LV assets, limiting the available response capacity, potentially impacting grid stability during a critical event.

This scenario highlights the need to carefully balance network safety mechanisms like NFCAs with the operational flexibility required for integrating LV assets into broader energy markets in a TSO-DSO coordination scheme. In this scenario, the flexibility value chain includes end-users and energy communities owning flexible assets, similarly to the previous section. To valorize flexibility, they may contract with an FSP, who in turn must establish a contractual agreement with the DSO to operate on the LV grid. Again, energy communities can act as aggregators and contract directly with the DSO.

In addition, as illustrated in Figure 7.6 the FSP or the energy community can contract with the TSO to provide balancing services. And the DSO and TSO must coordinate to ensure that LV assets providing frequency control do not damage the distribution grid, while the overall system remains safe.

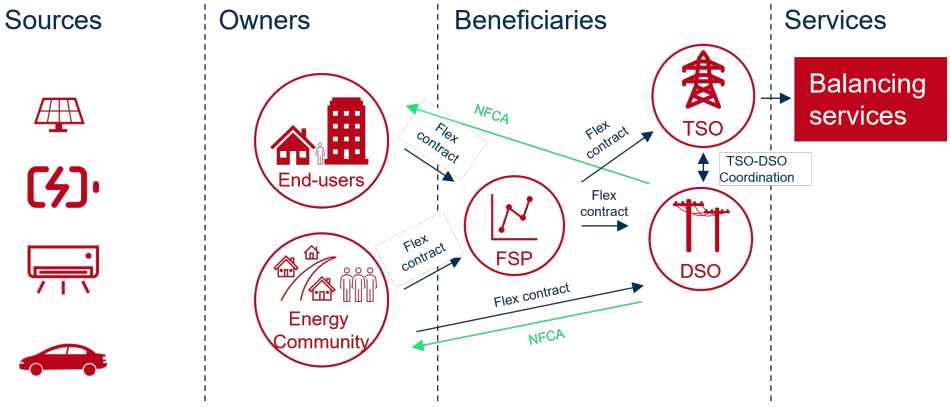

Figure 7.6: Value chain with NFCA combined with frequency control

The following subsections describe how the tools developed in this research contribute to managing LV congestion, unlocking maximum flexibility, and ensuring smooth coordination among stakeholders illustrated in Figure 7.6. The corresponding information flow is then presented.

7.3.1 NFCA combined with frequency control activation Value Chain and integration of tools developed in this research

Static pre-qualification through network flexibility study

The pre-qualification phase was briefly introduced in Subsection 2.1.6. In Belgium, only a static pre-qualification process currently exists at the distribution level, and the approach varies depending on the type of ancillary service being procured. For FCR, assets are exempt from pre-qualification, based on the assumption that FCR provision has minimal impact on the distribution grid.

However, as demonstrated by [99] and detailed in Chapter 5, LV assets providing FCR can, in fact, induce congestion in the LV distribution grid. Two operational scenarios should be considered in this context:

1. Decentralized response: Each LV asset individually compensates for frequency deviations. This case is analyzed in Chapter 5, showing a quantifiable risk of congestion when such assets are densely deployed.

2. Centralized portfolio optimization: The FSP distributes the frequency control effort across its asset portfolio. While this may reduce overall system imbalance, individual assets may still deliver their full contracted reserve capacity at once, independent of local constraints. This creates a risk similar

to the "unbounded aFRR" case discussed in Chapter 5, where uncoordinated activations can cause local grid stress.

In both cases, the exemption of static pre-qualification for FCR may overlook potentially significant risks to the distribution grid.

By contrast, for aFRR, DSOs in Belgium are authorized to carry out an Network Flexibility Study (NFS) [1] analysis prior to activation. This procedure allows the DSOs to assess the impact of activating flexibility services on local grid conditions, including potential congestion or power quality issues [132]. For the purposes of this discussion, such NFS assessments are treated as static pre-qualification mechanisms.

To improve the robustness of pre-qualification, this research proposes integrating the congestion identifier tool presented in Part II of this manuscript into the NFS process as illustrated in Figure 7.7. This would allow DSOs to evaluate, in advance, the likelihood that LV assets providing frequency control might trigger congestion. Based on this assessment:

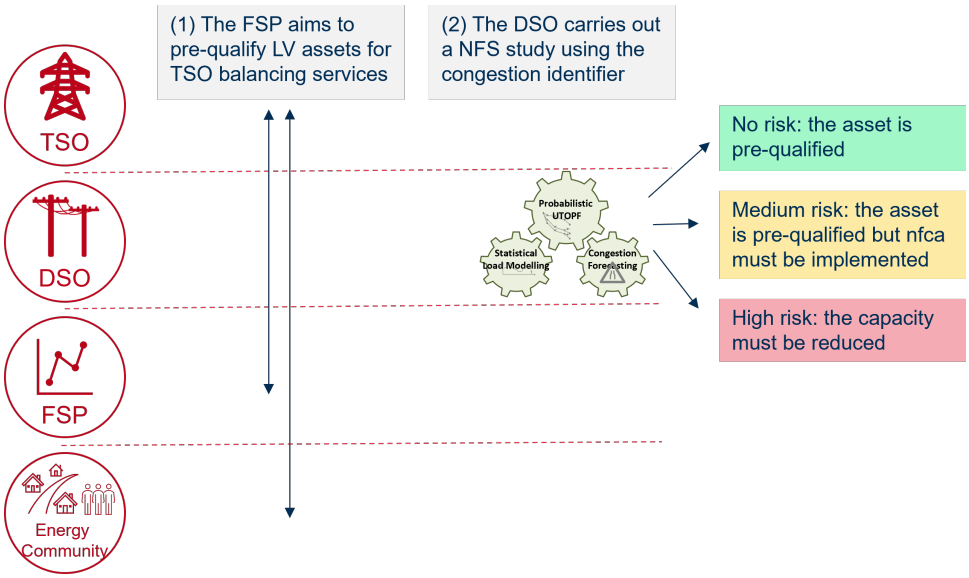

Figure 7.7: Structure process to pre-qualify LV assets providing balancing services through NFS using congestion identifier, from DSO perspective

- If the congestion risk is negligible, the asset can be pre-qualified.
- If the risk is moderate, the asset could still be accepted, provided a NFCA is in place to enforce capacity limitations.
- If the risk is high, pre-qualification should be denied or the reserve capacity reduced accordingly.

This structured approach enables risk-informed decisions that safeguard distribution network integrity while facilitating greater participation of LV assets in frequency control markets.

While static pre-qualification could be executed each time an FSP requests a prequalification for an asset located on a specific LV feeder, this could become resource-intensive. It might be better to perform static pre-qualification only when the LV feeder is identified as having a high risk of congestion, based on monitored data. Alternatively, it could be triggered when the NFS is achieved, in alignment with the existing operational processes implemented by Sibelga.

Extension of the Congestion Risk Indicator to LV distribution grid

So far, limiting the activation of LV assets providing frequency control to ensure LV distribution grid integrity has been a topic of discussion during Synergrid Working Group meetings, but to the author's knowledge, no formal decision is made on the matter. This subsection aims to propose a framework for

[1] The Net Flex Study (NFS) is a DSO-led qualification process used to assess whether activating flexibility at a connection point could impact the distribution grid. It is a required step for certain services as defined in the FSP-DSO contract, based on regulatory requirements. The DSO performs the analysis and shares the results with the FSP. [132]

implementing LV Congestion Risk Indicators (CRI), complementing the existing static prequalification (e.g. NFS) and building upon the existing congestion management mechanism implemented at the HV transmission grid.

Indeed, this section proposes using the congestion identifier and NFCAs as a dynamic limiting tool for LV assets. The concept presented here extends the existing CRI processes, currently applied to aFRR at the HV level, to LV assets providing aFRR (and eventually FCR). In addition to considering the transmission grid, this approach takes into account the congestion impact on the LV distribution grid.

The CRI is described in detail in [44]. It is a tool developed by Elia to monitor and mitigate congestion risks on the transmission grid, particularly during the activation of aFRR for frequency control. Such activations can generate additional power flows that risk overloading transmission lines or transformers. The CRI helps Elia assess whether these injections or offtakes may exceed the available capacity of grid infrastructure. It operates based on predefined thresholds that trigger alerts when congestion risks become significant. In response, Elia can take preventive actions—such as blocking the activation of specific assets within a cleared portfolio, if those assets are located in areas identified as congested. These congestion indicators are communicated to FSPs in advance, allowing them to anticipate possible activation restrictions. If an FSP plans to activate assets in a blocked zone, it must reallocate the activation within its portfolio. If reallocation is not possible, the FSP is liable for any resulting imbalances.

In the CRI used by Elia, ten congestion management zones are defined for the full Belgium. The idea proposed here is to increase the granularity of these zones by considering for example LV feeders as zones. This would allow for a more detailed measurement of congestion risk and, if necessary, the cancellation of assets activation that present an excessive risk to the system. The suggestion here is that, unlike HV congestion zones (where asset activation is entirely blocked) LV assets may still be activated, provided they remain within the limits defined by the NFCA. This enables partial activation under safe operational boundaries, thereby unlocking more flexibility while avoiding congestion on the distribution grid.

In that specific case, as shown in Figure 7.8, the NFCA may be activated at the same time as the TSO sends an activation signal to the same assets. In such a case, the assets are unable to fulfill their activation obligations, as represented by the red box. When this occurs, either the FSP reallocates the activation within its portfolio, or the resulting imbalance is managed through internal TSO mechanisms.

This mechanism clearly delineates the responsibilities of each market stakeholder. The DSO is responsible for computing the OE, contracting the NFCA, and continuously assessing congestion risk on its grid. When the risk becomes high, the NFCA is activated to ensure safe grid operation.

From the FSP perspective, full activation of flexibility is permitted when there is no congestion risk. However, when risk is detected on a given LV feeder, the FSP must reallocate reserve activation within its portfolio—similar to the approach used for aFRR on the HV grid. The FSP benefits from transparency and can identify feeders that are more prone to congestion, improving future dispatch strategies.

Unlike the binary blocking currently implemented for CRI in HV congestion zones, activation of LV assets can still occur under NFCA-defined limits. This partial activation increases available flexibility while ensuring grid security. The DSO does not need to compute behind-the-meter profiles but instead sets a limit at the connection point, allowing the FSP to optimize internally across assets.

Finally, the TSO simply sends the activation signal to the FSP, without accounting for distribution-level congestion. If activation would result in local congestion, the NFCA mechanism ensures the affected LV assets are constrained in advance, preventing unintended activation and preserving grid integrity. The FSP has the responsibility to reallocate within its portfolio.

Figure 7.8 illustrates the market steps for FCR and aFRR, highlighted in dark blue. These steps include the gate opening time (GOT), which occurs fourteen days (D-14) before the day of reserve activation for both FCR and aFRR, and the gate closing times (GCT), which are set at 08:00 (D-1) for FCR and 09:00 (D-1) for aFRR. Additionally, the publication of results takes place at 08:30 for FCR and 09:30 for aFRR. The figure illustrates the use of the Congestion Forecaster to communicate with flexibility providers, allowing them to adjust their bids accordingly.

It also shows the part of the operating day when a TSO first sends a signal to flexibility providers to activate flexibility. However, the assets that the flexibility providers aim to activate are located on a LV feeder, where the DSO detects a risk of congestion using the congestion identifier. In response, the DSO activates the NFCA. As a result, the flexibility provider must either reallocate the activation of their assets within their portfolio or pay for any resulting imbalances.

This approach ensures that LV assets are integrated into frequency control markets in a LV grid-safe manner, aligning with both technical requirements and market dynamics. By leveraging the proposed congestion identifier and the OE-based tools in NFCA for extended CRI methodology, the framework

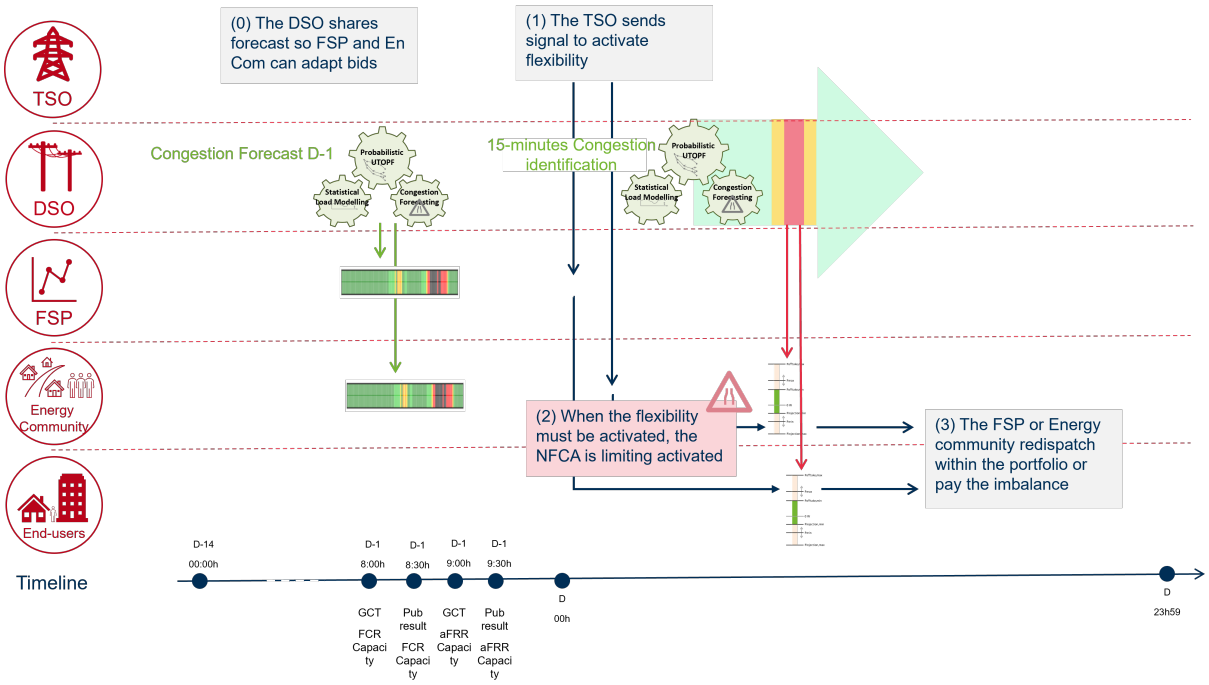

Figure 7.8: Ex-post correction of LV assets that were prevented from frequency control activation due to NFCA-based LV congestion management.

enhances LV asset participation while maintaining LV grid reliability.

7.3.2 NFCA Combined with Frequency Control Flexibility Process

As in the previous section, the flexibility activation process described below builds upon inputs from the Synergrid guide [19] and adapts them to incorporate the tools and methods developed in this research. The following phases will be further elaborated for frequency control applications in the next paragraphs.

The two steps of the simplified NFCA flexibility process are described below and illustrated in Figure 7.9. From the DSO perspective, the Monitoring phase is similar than the previous section and is not further described hereafter.

The coordination process between the TSO, DSO, and FSP regarding data exchange is structured as follows:

Structure

[S1] The first step involves the FSP accepting the general conditions set by the system operators requiring flexibility. As in the previous section, the DSO can compute the OE and integrate these values into the NFCA contract.

[S2] In parallel, the FSP contracts flexibility services with end-users or energy communities, following a similar approach to the one previously described.

[S3] The DSO then uses the congestion identifier within the NFS to assess whether the activation of flexible assets poses a risk to the grid. If the risk is acceptable, the assets are pre-qualified, and a flexibility contract can be signed between the DSO and the FSP. Finally, the NFCA is signed between the DSO and the point of connection owners, with similar incentive mechanisms from the DSO toward the FSP. Ex post and real-time data transmission procedures are configured.

[S4] The FSP can then sign a contract with the TSO, including all necessary product prequalification steps to ensure the service can be delivered reliably.

Operation

[O1] Once the market gate opens, the FSP submits its bids. One or two days in advance, the DSO communicates congestion forecasts, allowing the FSP to adjust its bids accordingly. After the gate closes, the market is cleared.

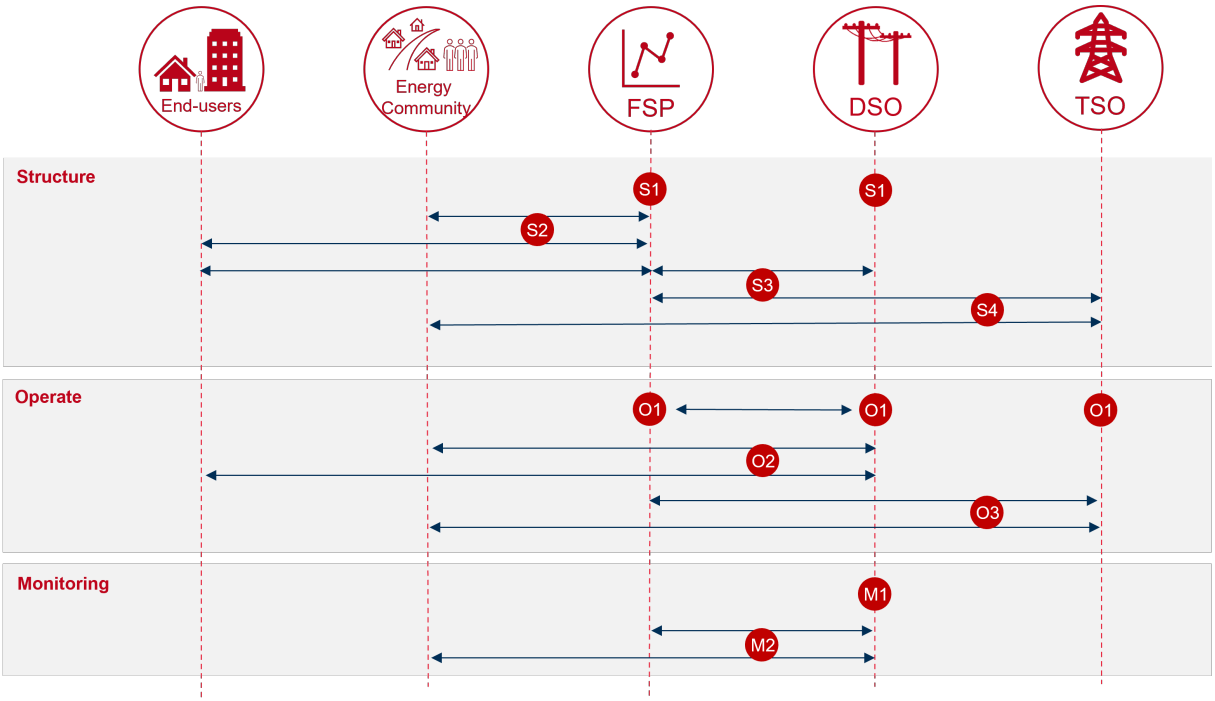

Figure 7.9: Information flow for NFCA combined with Frequency Control services

[**O2**] On the operating day, the DSO monitors grid conditions in real time, typically at 15-minute intervals. If the risk of congestion becomes critical, the NFCA is activated: contracted parties (connection owners) must then reduce their injections or offtake to remain within predefined limits.

[**O3**] If the TSO activates flexibility and the NFCA is also activated, the FSPs or energy communities can activate their assets within the limits defined by the NFCA. From the DSO's perspective, the process is the same as in the previous section. From the FSP's perspective, it receives advance notice and is aware of the NFCA limits, allowing it to reallocate activations within its portfolio. From the TSO's perspective, flexibility remains available without compromising the LV distribution grid. In this structure, flexibility activations do not need to be explicitly notified to the DSO, and the TSO does not need to know the DSO's grid constraints. This approach simplifies coordination while ensuring that each market participant retains its responsibilities. Moreover, the comparison of NFCA activation in both implicit and explicit flexibility mechanisms shows that it does not result in significant differences in their operational processes.

7.4 Operational Perspective of NFCA Activation

While the detailed operational implementation of NFCA activation lies beyond the scope of this research, this section offers insights into potential activation and remuneration mechanisms. These proposals require further exploration through additional research or pilot projects.

7.4.1 Activation Mechanism

The NFCA is activated through a signal sent by the DSO to the smart meter. This type of signaling is already possible with existing meters, for example when switching between day and night tariffs. The introduction of modern smart meters, as discussed in the introduction, simplifies and enhances this capability.

However, the critical question is: what should this signal trigger? If a consumption or production limit is defined and then exceeded, disconnecting the household is not a realistic or safe solution. While conservative, such disconnections pose safety risks to end-users (e.g., spoiled food due to refrigeration loss or someone trapped in a halted elevator). These risks could hamper end-users from entering into NFCA contracts. As highlighted in the introduction of this Chapter, widespread participation is key to the success of the NFCA scheme.

One alternative could be for the DSO to install a gateway behind the meter to control flexible assets via their inverter, smart controller, or energy management system. However, this approach would require

the DSO to control assets behind the meter, which falls outside its regulatory role and could introduce significant administrative and technical burdens.

A more suitable solution would be for the DSO to send the constraint signal—including the operational limit—to the smart meter and it is the FSP, who would then integrate it into its optimization algorithm. This approach aligns with market design principles by respecting the roles of different stakeholders. From an operational standpoint, the FSP is already managing behind-the-meter assets for flexibility provision and has established the required control systems and APIs. It is therefore reasonable to assign responsibility to the FSP to adjust the load profile accordingly, using historical consumption and production data as input.

Finally, in cases where multiple FSPs control assets behind the same meter, it remains their responsibility—not the DSO's—to coordinate and ensure the overall load stays within defined limits.

7.4.2 Remuneration Mechanism

Multiple remuneration models could be considered for NFCA implementation. One baseline approach is to be mandatory for all FSPs activating flexibility on the LV grid to have an agreement with asset owners. In this case, participation in NFCA is not directly remunerated. The rationale is that the entity benefiting from flexibility must ensure that its actions do not endanger grid stability. Traditionally, distribution grids have been over-dimensioned and rarely require such mechanisms. Without flexibility activation, the load profiles of end-users generally remain within safe operational limits. In contrast, flexibility activations introduce additional variability and potential congestion risks, and should thus be constrained. From a fairness standpoint, this approach treats all users equally in terms of access to the grid and flexibility opportunities.

Another remuneration model, as implemented in Germany, involves offering a reduced distribution tariff to end-users who voluntarily sign up for a NFCA. In this model, the compensation should be carefully calibrated. For example, the cost savings from deferring grid reinforcement investments through the use of NFCAs could be shared between the DSO and participating end-users.

Importantly, this incentive model should be available to all end-users, regardless of whether they own flexible assets. Consider a scenario where the OE is set at 7.5kW. An end-user with controllable assets can sign a NFCA, and the FSP or the user's energy management system can automatically limit the profiles to stay within limits when necessary. On the other hand, an end-user without flexible assets may still naturally remain below the 7.5kW threshold (even during peak usage, e.g., using an oven, washing machine, and dryer simultaneously). Thus, both types of users can help mitigate congestion: flexible users by adapting their load profiles actively, and others by staying within limits passively. It would be unfair to restrict tariff incentives only to users with flexible assets. All users contribute to congestion management, and the mechanism should reflect that inclusivity. This example is simplified and warrants further analysis, but it underscores the importance of fairness in designing DSO services.

In general, if a user exceeds their NFCA limit, the breach will be detected during monitoring, and penalties or fees can be applied accordingly.

Finally, implicit mechanisms such as dynamic tariffs based on real-time grid conditions could be considered. However, the purpose of the NFCA is to ensure that grid limits are not exceeded. Since the OE defines the operational limit of the grid, relying solely on price signals could lead to unpredictable behaviors and congestion risks. Thus, purely implicit mechanisms may not provide sufficient control and should be applied with caution.

7.5 Conclusions

This chapter introduces the concept of the NFCA, in which the congestion identifier and OEs are integrated into both DSO and TSO processes to enhance the management of LV congestion:

- The first application proposes the NFCA approach to congestion management, leveraging OEs to compute the guaranteed capacity and the congestion identifier to provide flexibility providers with transparent data.
- The second application explores the implications of NFCA on the activation of LV assets for frequency control. In this context, the congestion identifier serves both as a static pre-qualification tool and a mechanism for continuous monitoring of LV feeders, operating similarly to the Congestion Risk Indicator (CRI) used by Elia at the HV level. The NFCA continues to rely on OEs to ensure that flexibility activations do not cause LV congestion.

These contributions demonstrate the flexibility and practical relevance of the developed tools (i.e. the congestion identifier and OEs) in addressing LV congestion challenges, while aligning with both technical constraints and market mechanisms.

Finally, this chapter shows how DSOs can implement a simple yet effective coordination mechanism to enable the activation of LV assets across various flexibility services, while maintaining secure grid operation. The proposed use of OEs to define guaranteed capacity of NFCA at the LV level provides a lightweight solution that preserves the roles of each market actor and can be readily implemented using the tools developed in this research.

This chapter focuses exclusively on the interactions between the TSO, DSO, FSP, end-users, and energy communities, deliberately excluding other roles such as Balancing Responsible Parties and suppliers to avoid additional complexity in the model. The integration of these actors could be explored in future work. Nevertheless, the added value of the NFCA within the presented framework is clearly presented.

Chapter 8

General Conclusions and Future Work

This manuscript addresses the critical issue of congestion in LV distribution grids, presenting novel tools to identify and manage such congestion effectively. The primary contributions of this work are summarized as follows:

- Comprehensive Overview - A detailed examination of the technical, regulatory, and economic challenges faced by Distribution System Operators in managing LV distribution grids, compared to the high-voltage transmission grid. This includes practical insights into real-world constraints and differences between the two grid levels.
- General Framework for LV Congestion Identification extended to LV assets providings frequency control - The presentation and application of a general framework to identify LV congestion. This framework is demonstrated through a case study where LV assets participate in newly available activities such as Frequency Containment Reserve and automatic Frequency Restoration Reserve.
- Innovative UTOPF Tool for OE computation - The proposition of a relaxed Unbalanced Three-Phase Optimal Power Flow approach to compute Operating Envelopes for managing LV congestion. The tool's applicability is showcased through real-world case studies, highlighting its practicality.

The following section summarizes the general conclusions of the research, addressing when relevant the three research questions. Finally, suggestions for future work are presented, offering pathways for continued exploration and development in this domain.

8.1 General Conclusions

This manuscript addresses the growing challenge of congestion in LV distribution grids, a challenge that has become more prominent with the increasing electrification of heating, mobility, and the integration of photovoltaic PV panels. These developments pose new operational challenges for DSO, who must ensure the safe operation of the grid under higher loads and more dynamic conditions. The research presented in this manuscript focuses on developing methods and tools to identify and manage congestion in LV distribution grids, considering the regulatory, economic, and technical challenges posed by these new developments.

Chapter 2 provides background on LV grids and their key operational characteristics. It explains how LV congestion arises and how its impact is expected to grow with the increasing demand for electricity and the participation of LV assets in frequency control services. The chapter highlights the importance of understanding grid structure, phase imbalances, and load variability, which are essential for developing effective methods for identifying and managing congestion. The need for efficient tools to help DSOs manage congestion in the face of these challenges is clearly established.

Chapter 3 presents the case studies used throughout this research: the IEEE European LV Test Feeder and 49 LV feeders provided by Sibelga. The chapter details how raw data from both benchmark working groups and real-world DSOs must be processed into usable grid models. This data processing step is necessary for building accurate grid models for congestion analysis and management, ensuring that the tools developed in this thesis can be applied to real-world scenarios.

In Chapter 4, a methodology for identifying congestion in LV grids is introduced. The chapter explains how key characteristics of LV networks, such as the high R/X ratio and radial topology, are considered when selecting appropriate PF models for congestion analysis. A probabilistic approach is used to account for the stochastic nature of LV load profiles and PV production, which is critical given the variability of consumer demand. The chapter also outlines the criteria for defining congestion thresholds for voltage and current based on industry standards and technical handbooks. The model is validated using real-world data, showing its effectiveness in identifying congestion and supporting the development of tools for grid management.

Chapter 5 extends the congestion identification methodology by considering the impact of LV assets participating in frequency control services, such as FCR and aFRR. The chapter shows how participation in these services can exacerbate congestion in LV grids, particularly during extreme frequency events. It introduces a probabilistic model (ARMA) to first predict the behavior of LV assets providing FCR in general, and then predicting the frequency behaviour after extreme frequency deviation events, providing more accurate predictions than naive model. The chapter also discusses how congestion limits should be adapted for these extreme events to prevent overestimating the impact of frequency control. Additionally, it compares aggregation strategies for aFRR and demonstrates how a portfolio-based approach leads to greater congestion than a limited-reservoir approach.

Chapters 2 to 5 address the first research question: *How do the activities enabled by the new market design, as defined in the European Clean Energy Package ([10]), impact the low voltage grid?* The new market design enables LV assets to participate in ancillary services, such as frequency control. The increasing participation of LV assets in these services is likely to impact grid stability and congestion. The tools and methodologies presented in this thesis provide insights into how these activities affect LV grids and suggest ways to mitigate potential negative impacts. Three key results are highlighted:

- A probabilistic ARMA model for frequency ancillary services more accurately predicts the output power of LV assets providing FCR following an extreme frequency event, compared to a simple normal distribution.

- The model demonstrates that frequency data predicted with ARMA can be used to study the impact of *continuous* congestion thresholds, while extreme frequency events should only use *instantaneous* congestion thresholds to prevent overestimating FCR-induced LV congestion.

- The modeling approach used by the DSO to assess the impact of LV assets providing aFRR significantly influences the results. If aFRR activation is modeled using a worst-case scenario where aggregators rely on a portfolio-based approach, the analysis shows greater LV congestion compared to a modeling approach where the worst-case scenario considers a limited-reservoir approach.

Chapter 6 introduces a new method for calculating OE in unbalanced LV grids. The proposed approach uses a second-order cone programming (SOCP) relaxation technique integrated into the EBFM UTOPF framework. This method allows for accurate and efficient calculation of OEs, which are critical for mitigating congestion. The approach is validated on the IEEE European LV Test Feeder and 49 real-world feeders from Sibelga, showing that the optimal UTOPF method provides greater flexibility than fairness-based methods while maintaining computational efficiency. If the fairness criterion must be applied, the UTPF method is to be preferred to the UTOPF method, as it unlocks more flexibility under lower computation time. The chapter also demonstrates the impact of unbalance and power factor on the shape of the OE, providing valuable insights into how different feeder types behave and their capacity to handle congestion.

Chapter 6 addresses the second research question: *What is the maximum flexibility available on the low voltage grid, considering load profile uncertainty?* The results demonstrate that the Optimal UTOPF consistently provides equal or greater flexibility compared to fairness-based methods while delivering near-exact solutions—critical for accurately defining the operational limits of the grid.

Additionally, the analysis reveals three distinct feeder types, offering valuable insights into the interplay between network topology and OEs. Oversized feeders can reach their maximum OE without risking grid congestion, while Type 2 feeders highlight the trade-offs between fairness and optimal flexibility without diminishing the total aggregated OE.

The research also explores key factors influencing the design of OEs, providing DSOs with insights to tailor DSOs to their specific operational needs. The analysis focuses on several aspects, including the comparison of dynamic versus static OEs, the impact of load unbalance, the influence of reactive power, and variations in grid typology.

Chapter 7 demonstrates how the tools developed in this research can be applied in real operational frameworks. The congestion identifier is used either as a forecasting tool, enabling transparent data sharing with FSPs to help them adapt their flexibility profiles, or as a real-time monitoring tool during the operating day. The OE is employed to define guaranteed capacity limits within a NFCA, which can be activated when congestion risks become critical. This approach allows for the full activation of available flexibility under normal conditions, while ensuring grid safety by constraining flexibility when congestion risks arise. These tools are examined both for local optimization and implicit flexibility involving LV assets, as well as for scenarios where these assets provide frequency control services, with a focus on enhanced TSO-DSO coordination.

Chapter 7 addresses the third research question: *How can the articulation between TSOs and DSOs be optimized to implement mechanisms unlocking maximum flexibility while ensuring secure operation of the network?* This chapter builds upon the findings of the previous questions to propose a coordinated framework that enables high levels of flexibility while maintaining grid reliability. It illustrates how the integration of the congestion identifier and OE supports more effective interaction between TSOs and DSOs, offering practical mechanisms for secure, flexible grid management.

Overall, this thesis provides valuable insights and tools for managing congestion in LV grids, helping DSOs address the challenges posed by increasing electrification and the growing role of PV production. The methodologies developed in this work, including the congestion identification framework, probabilistic models for frequency control, and optimal operating envelope calculations, offer practical solutions for congestion management. These tools are designed to support DSOs in maintaining reliable and efficient grid operations while accommodating the increasing complexity and variability of modern LV networks.

8.2 Future Work

8.2.1 Future Work on LV Load Profile Forecasting

To refine the modeling of LV load profiles, integrating advanced forecasting techniques into the congestion identification framework and DOEs could significantly enhance the accuracy and reliability of the results presented in this manuscript. Additionally, studying the impact of other market activities, such as LV asset participation in the Day-Ahead Market, could provide a more comprehensive understanding of LV grid behavior.

However, the increasing complexity of LV load profiles calls for a reevaluation of forecasting approaches. This complexity arises from the growing number of behind-the-meter assets, such as EVs, HPs, and PV, and the multiplication of activities and stakeholders managing these assets. For example, a single household may have its PV system governed by an energy community, its EV controlled by a FSP, a part of its residential battery engaged in dynamic contracts with suppliers, and the remainder of its consumption managed under fixed-tariff agreements. This layering of activities and stakeholders creates significant challenges in forecasting and managing LV congestion.

Rather than focusing solely on developing increasingly sophisticated forecasting techniques, future tools could emphasize neutrality, i.e. remaining technology-neutral, activity-neutral, and stakeholder-neutral. Such tools would provide robust, adaptable solutions capable of managing the growing complexity of LV grids. OEs appear particularly promising in this regard, offering a scalable framework that can accommodate diverse scenarios while unlocking flexibility and grid safety.

8.2.2 Future Work on Operating Envelopes

Further research on the relaxation method used in the UTOPF model could explore alternative solution recovery techniques, aiming to improve computational efficiency and accuracy. Additionally, incorporating probabilistic approaches or robust optimization techniques to address uncertainties in LV load profiles could further enhance the model's practical relevance and reliability.

Expanding the application of OEs for and beyond congestion management is another promising direction. For instance, OEs could be used in rule-based or tariff-based solutions for LV congestion or adapted to support other grid activities. Exploring alternative fairness criteria would also be valuable, ensuring equitable access to flexibility resources for various grid users and fostering wider acceptance of OE-based solutions.

8.2.3 General Future Directions

Future work should prioritize the integration of these methods with real-time data to enhance their applicability in dynamic grid environments. Furthermore, the operational maturity of the tools developed in this research must be improved. While this manuscript highlights the potential and practicality of the proposed frameworks for DSOs, the current implementations remain at a preliminary stage, as expected in PhD research. Advancing these tools to a production-ready state will be critical for their adoption in real-world grid management.

Finally, collaboration with industry stakeholders and pilot testing in real LV grids will be essential to validate the scalability and robustness of the proposed approaches. Such efforts will ensure alignment with the evolving needs of DSOs and the broader energy ecosystem, paving the way for sustainable and efficient grid management solutions.

Appendix A

ARMA to model power grid frequency

A.1 ARMA model

This appendix presents how the ARMA is designed to model stochastic frequency used as inputs when LV assets provide FCR. This modeling process is based on [105] presenting a methodology to forecast time series based on historical data through a three-stage procedure: tentative model identification, estimation of model parameters and model checking and diagnostics.

The authors define a four steps approach to build a relevant model, with iterative procedures between step 4 and step 2.

1. Select a general class of model
2. Identify a model to be tested and entertained - where identification means that data can be used to suggest a subclass of parsimonious models worth entertaining
3. Estimate parameters in the test entertained model - i.e. effective use of data to make inferences about the conditional parameters and the fit of the chosen model
4. Diagnostic checking - check the fitted model related to the data with the aim of revealing model deficiencies and improving the model

The remainder of this appendix consists on presenting an overview of the ARMA model, then going step by step on the full process to model the frequency with the ARMA modeL.

A.1.1 Overview of the ARMA model

Auto-Regressive term (AR)

[105] based their time series predictions on the idea that an observable time series z_t in which the values are strongly dependent can be thought of as generated from a series of independent "shocks". The authors define the autoregressive (AR) model where the current value of the process is a finite and linear aggregation of the previous values and random shocks a_t. The autoregressive process of order p can be expressed as:

$$\tilde{z}_t = \phi_1 \tilde{z}_{t-1} + \phi_2 \tilde{z}_{t-2} + ... + \phi_p \tilde{z}_{t-p} + a_t \tag{A.1}$$

where:

- $t, t-1, t-2, etc.$ are the equal time steps
- $z_t, z_{t-1}, z_{t-2}, etc.$ are the values of a process for the specific time steps
- $\tilde{z}_t = z_t - \mu$ the series of deviation from μ

The equation is named autoregressive process because the following equation expresses the dependent variable z as a set of independent variables $x_1, x_2, ...$ plus a random error term a, named the regression model.

$$\tilde{z}_t = \phi_1 \tilde{x}_1 + \phi_2 \tilde{x}_2 + ... + \phi_p \tilde{x}_p + a \tag{A.2}$$

In the previous equation, the variable $\tilde{z}$ is regressed on previous values of itself. Let's define an autoregressive operator of order p in terms of backward shift operator B by the following equation:

$$\phi(B) = 1 - \phi_1 B - \phi_2 B^2 - ... - \phi_p B^p \tag{A.3}$$

Therefore, the autoregressive model can be expressed as:

$$\phi(B)\tilde{z}_t = a_t \tag{A.4}$$

The model contains $p+2$ unknown parameters: $\phi_1, \phi_2, ..., \phi_p, \mu$ and σ_a^2, the variance of the white noise process a_t.

Autoregressive processes can be stationary of nonstationary. For the process to be stationary, $\phi(B) = 1-\phi_1 B-\phi_2 B^2-...-\phi_p B^p$ considered as a polynomial in B of degree p, must have all roots of $\phi(B) = 0 > 1$.

Moving Average term (MA)

The moving average (MA) process of order q is another mathematical model particularly important and can be expressed as:

$$\tilde{z}_t = a_t - \theta_1 a_{t-1} - \theta_2 a_{t-2} - ... - \theta_q a_{t-q} \tag{A.5}$$

A moving average operator of order q can be expressed by:

$$\theta(B) = 1 - \theta_1 B - \theta_2 B^2 - ... - \theta_q B^q \tag{A.6}$$

Enabling to write the MA model as:

$$\tilde{z} = \theta(B) a_t \tag{A.7}$$

The model contains $q+2$ unknown parameters: $\theta_1, \theta_2, ..., \theta_q, \mu$ and σ_a^2, the variance of the white noise process a_t. The parameters will be estimated from the data.

Complete ARMA

It could be interesting to consider both AR and MA mathematical model to fit time series, leading to the autoregressive-moving average (ARMA) model:

$$\tilde{z}_t = \phi_1 \tilde{z}_{t-1} + ... + \phi_p \tilde{z}_{t-p} + a_t - \theta_1 a_{t-1} - ... - \theta_q a_{t-q} \tag{A.8}$$

The model contains $p+q+2$ unknown parameters: $\phi_1, ..., \phi_p, \theta_1, ..., \theta_q, \mu$ and σ_a^2. Indeed, if the process is a MA, the process could not be represented as a parsimonious representation of AR (and conversely for an AR, through a MA).

A.1.2 ARMA to model Frequency

The ARMA approach presented in [105] is used to forecast frequency based on historical data. The predicted frequency will then be used as input to the FCR model to better capture the power profile of LV assets providing FCR. The four steps applied to continental Europe grid frequency data in January 2021 with a granularity of 10 seconds, are summarized below

The following parts describe each step of the ARMA model for FCR.

Select a general class of Model and identify a model to be tested and entertained

The general AR(I)MA model is defined as:

$$\phi(B)(1-B)^d z_t = \theta_0 + \theta(B)a_t \tag{A.9}$$

where $\phi(B)$ is the autoregressive operator of order p and $\theta(B)$ is the moving average operator of order q, in terms of backward shift operator $B^k X_t = X_{t-k}$. d is the degree of differenciating when processes are non stationnary.

The first step aims to identify an appropriate subclass of models from the general AR(I)MA family where Equation A.9 represents a given time series.

The approach consists in: 1. assess z_t stationarity and if necessary, differentiate the the time series to ensure stationarity and 2. identify the remaining ARMA parameters.

d-parameter

To define d parameter, the Augmented Dickey-Fuller Statistic test can be used. If the ADF is negative, the time series can be considered as stationary. For the ADF, the function is used directly from the panda library.

The ADF tests result in -37.74. The d parameter of the AR(I)MA is therefore considered as 0 and the model considered is therefore an ARMA model (the integrated term is null).

p-parameter

The authors define the autoregressive (AR) model where the current value of the process is a finite and linear aggregation of the previous values. The autoregressive process of order p can be expressed with Equation A.10.

$$\tilde{z}_t = \phi_1 \tilde{z}_{t-1} + \phi_2 \tilde{z}_{t-2} + ... + \phi_p \tilde{z}_{t-p} + a_t \tag{A.10}$$

where:

- $t, t-1, t-2, etc.$ are the equal time steps
- $z_t, z_{t-1}, z_{t-2}, etc.$ are the values of a process for the specific time steps
- $\tilde{z}_t = z_t - \mu_{arma}$ the series of deviation from μ
- $\phi_1, \phi_2, ..., \phi_p, \mu_{arma}$ and σ_a^2, the variance of the white noise process a_t, are the $p+2$ unknown parameters.

The number of AR terms needed (i.e. the value of p) can be obtained thanks to the Partial Autocorrelation (PACF) plot. Partial Autocorrelation can be considered as the correlation between the series and its lag once contributions from intermediate lags are excluded. In [105], the authors demonstrates that when the autocorrelation function of an autoregressive process of order p stops, its partial autocorrelation function has a cutoff after lag p.

PACF of lag(k) of a series is the coefficient of that lag in Auto-Regression equation of Y, as expressed in Equation A.11.

$$Y_t = \alpha_0 + \alpha_1 Y_{t-1} + \alpha_2 Y_{t-2} + \alpha_3 Y_{t-3} + ... + \alpha_k Y_{t-k} \tag{A.11}$$

Based on the graphical approach (cf. Figure A.1), the PACF lag 1 seems more significant than other lag and the p-parameter is therefore set at 1.

q-parameter

The moving average (MA) process of order q can be expressed by the Equation A.12.

$$\tilde{z}_t = a_t - \theta_1 a_{t-1} - \theta_2 a_{t-2} - ... - \theta_q a_{t-q} \tag{A.12}$$

Where $\theta_1, \theta_2, ..., \theta_q, \mu$ and σ_a^2, the variance of the white noise process a_t, are the $q+2$ unknown parameters.

Similarly for the method to find the number of Auto-Regressive terms, we can use the ACF plot to find the q-parameter. Indeed, the autocorrelation function of a q-order moving average process has a cutoff after lag q, while its partial autocorrelation function stops. The ACF lag 1 seems the more significant in Figure A.2, so let's first consider the q-parameter set at 1.

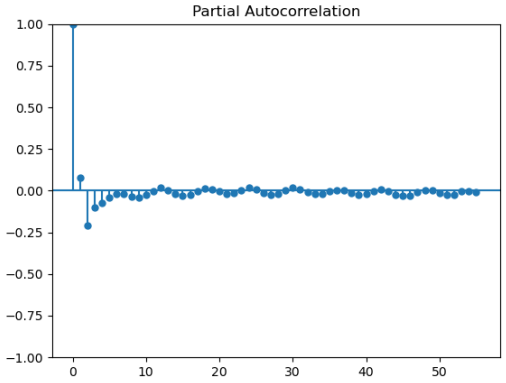

Figure A.1: Partial autocorrelation for the 10-second frequency signal in January 2021

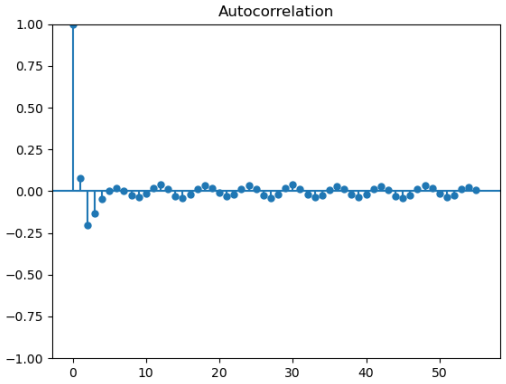

Figure A.2: Autocorrelation for the 10-second frequency signal in January 2021

Identify the model to be tested

The model to be tested will therefore be an ARMA (1, 1) model that can be represented by the following equation:

$$\tilde{z}_t = \phi_1 \tilde{z}_{t-1} + a_t - \theta_1 a_{t-1} \tag{A.13}$$

The model contains 4 $(p + q + 2)$ unknowns: ϕ_1, θ_1, μ_{arma} and σ_a^2, the variance of the white noise process a_t.

Estimate parameters in the test entertained model

The model is first trained with the 10 second frequency data of January 1. The unkwons are computed and result in data presented in Table A.1 with the steady error.

Table A.1: ARMA parameters estimation

Unknowns	**Coefficient**	**Std error**
ϕ_1	0.9175	0.005
θ_1	0.2164	0.012
μ	49.9968	0.001
σ_a^2	2.463 e-05	3.01 e-07

Table A.2: Log likehlihood for ARMA models with varying parameters

Log likelihood	**q = 1**	**q = 2**	**q = 3**	**q = 4**
p = 1	31879.93	32032.99	32078.56	32078.53
p = 2	31879.57	32059.46	32078.25	32078.20
p = 3	31294.98	32078.72	32080.53	32084.05
p = 4	32036.43	32081.29	31935.04	32083.10

Diagnostic checking

To check the order of the ARMA model, [105] suggests using the overfitting method and comparing the goodness of fit when the models are overfitted. To do this, the log-likelihood functions of the model with different parameters are calculated when varying the orders of the model and listed in table A.2. Data are in blue for the models where the p-value is bigger than 0.05 for some coefficient and hence the null hypothesis cannot be rejected.

The parameters (1, 0, 1) are therefore chosen, considering the fact that increasing model order only leads to an increase of the log likelihood by 0.6% and also considering the principle of parsimony, stating that the lowest order should be preferred if it provides a properly fitted model.

Appendix B

Non-convexity of rank-1 constraint if lifted OPF

B.1 Non-Convexity of the Rank-1 Constraint in Unbalanced Power Flow

Let's consider a single bus with three-phase voltages represented as a complex vector:

$$V_i = \begin{bmatrix} v_{i,a} \\ v_{i,b} \\ v_{i,c} \end{bmatrix} \in \mathbb{C}^{3\times 1}$$

where:

- $v_{i,a}, v_{i,b}, v_{i,c}$ are the complex voltage vectors for phases a, b, and c.
- The interaction between phases is encoded in the Hermitian matrix W_i, defined as:

$$W_i = V_i (V_i)^H.$$

Expanding this:

$$W_i = \begin{bmatrix} v_{i,a}{v_{i,a}}^* & v_{i,a}{v_{i,b}}^* & v_{i,a}{v_{i,c}}^* \\ v_{i,b}{v_{i,a}}^* & v_{i,b}{v_{i,b}}^* & v_{i,b}{v_{i,c}}^* \\ v_{i,c}{v_{i,a}}^* & v_{i,c}{v_{i,b}}^* & v_{i,c}{v_{i,c}}^* \end{bmatrix}.$$

B.2 Two Different Rank-1 Voltage Matrices

Let's define two different possible three-phase voltage solutions.

B.2.1 First Voltage Vector

$$V_i^1 = \begin{bmatrix} 1.02 + j0.436 \\ 0.98 - j0.45 \\ 1.05 + j0.42 \end{bmatrix}$$

Computing its outer product:

$$W_i^1 = V_i^1 (V_i^1)^H = \begin{bmatrix} 1.144 & 1.087 + j0.009 & 1.177 + j0.897 \\ 1.087 - j0.009 & 1.102 & 1.182 + j0.864 \\ 1.177 - j0.897 & 1.182 - j0.864 & 1.267 \end{bmatrix}.$$

B.2.2 Second Voltage Vector

$$V_i^2 = \begin{bmatrix} 0.95 + j0.43 \\ 1.08 - j0.44 \\ 1.01 + j0.45 \end{bmatrix}$$

Computing its outer product:

$$W_i^2 = V_i^2 (V_i^2)^H = \begin{bmatrix} 0.995 & 1.026 - j0.002 & 1.017 + j0.876 \\ 1.026 + j0.002 & 1.168 & 1.093 + j0.843 \\ 1.017 - j0.876 & 1.093 - j0.843 & 1.212 \end{bmatrix}.$$

B.3 Taking a Convex Combination

We now take a convex combination:

$$\tilde{W}_i = \beta W_i^1 + (1 - \beta) W_i^2, \quad \beta = 0.5.$$

Computing element-wise:

$$\tilde{W}_i = \begin{bmatrix} 1.07 & 1.057 + j0.004 & 1.097 + j0.886 \\ 1.057 - j0.004 & 1.135 & 1.137 + j0.853 \\ 1.097 - j0.886 & 1.137 - j0.853 & 1.24 \end{bmatrix}.$$

B.4 Checking the Rank of $\tilde{W}$

Since $\tilde{W}_i$ is a combination of two rank-1 matrices, it is no longer guaranteed to be rank-1. Computing its determinant confirms that:

$$\text{rank}(\tilde{W}_i) > 1.$$

This demonstrates that the rank-1 constraint is non-convex because the convex combination of two rank-1 matrices does not necessarily remain rank-1.

B.5 Conclusion

- Each individual matrix W_i^1 and W_i^2 was rank-1, meaning they correspond to valid three-phase voltage solutions.
- Taking a convex combination resulted in a higher-rank matrix $\tilde{W}_i$, which violates physical feasibility.
- This shows why the rank-1 constraint is non-convex and why second-order cone programming (SOCP) relaxations can lead to non-physical solutions.

Bibliography

[1] J. C. Laguna, A. Moglianesi, P. Vingerhoets, W. Nijs, and P. Lodewijks. (2023) Paths 2050 - scenarios towards a carbon-neutral belgium by 2050. [Online]. Available: https://energyville.be/wp-content/uploads/2024/03/Full-Fledged-Report_1.pdf

[2] G. Deconinck, "Smart distribution systems (b-kul-h00p3a)," 2021, course offered at KU Leuven. [Online]. Available: https://www.kuleuven.be

[3] M. A. Khan and B. Hayes, "A reduced electrically-equivalent model of the ieee european low voltage test feeder," 2021, techRxiv. Preprint.

[4] W. H. Kersting, *Distribution System Modeling and Analysis*, 3rd ed. 6000 Broken Sound Parkway NW, Suite 300 Boca Raton, FL 33487-2742: CRC Press, 2012.

[5] A. Koirala, R. D'hulst, and D. V. Hertem, "Impedance modelling for european style distribution feeder," in *2019 International Conference on Smart Energy Systems and Technology (SEST)*, September 2019.

[6] B. Lacroix and R. Calvas, "Earthing systems worldwide and evolutions," Cahier Technique, Tech. Rep. 173, September 1995, available online. [Online]. Available: https://www.studiecd.dk/cahiers_techniques/System_earthings_worldwide_and_evolutions.pdf

[7] JuMP Developers, *JuMP Documentation: Getting Solvers*, 2021, accessed: 2025-01-28. [Online]. Available: https://jump.dev/JuMP.jl/v0.21.3/installation/#Getting-Solvers-1

[8] European Union, "DIRECTIVE 2009/72/EC OF THE EUROPEAN PARLIAMENT AND OF THE COUNCIL of 13 July 2009 concerning common rules for the internal market in electricity and repealing Directive 2003/54/EC," https://eur-lex.europa.eu/LexUriServ/LexUriServ.do?uri\=OJ:L:2009:211:0055:0093:en:PDF, 2009, accessed: 2024-12-02.

[9] European Commission, "Governance of the internal energy market," 2024, accessed: 2024-12-09. [Online]. Available: https://energy.ec.europa.eu/topics/markets-and-consumers/governance-internal-energy-market_en

[10] European University Institute et al., "The EU clean energy package," https://data.europa.eu/doi/10.2870/58299, 2020, accessed: 2024-3-7.

[11] European Union, "Directive (EU) 2018/2001 of the European Parliament and of the Council of 11 December 2018 on the promotion of the use of energy from renewable sources (recast)," https://eur-lex.europa.eu/legal-content/EN/TXT/?uri\=uriserv:OJ.L_.2018.328.01.0082.01.ENG\&toc\=OJ:L:2018:328:TOC, 2018, accessed: 2024-12-02.

[12] ——, "Directive (EU) 2019/944 of the European Parliament and of the Council of 5 June 2019 on common rules for the internal market for electricity and amending Directive 2012/27/EU (recast)," https://eur-lex.europa.eu/legal-content/EN/TXT/PDF/?uri\=CELEX:32019L0944, 2019, accessed: 2024-12-02.

[13] European Commission, "Repowereu: Affordable, secure and sustainable energy for europe," 2024, accessed: 2024-12-09. [Online]. Available: https://commission.europa.eu/strategy-and-policy/priorities-2019-2024/european-green-deal/repowereu-affordable-secure-and-sustainable-energy-europe_en

[14] Belgian federal parliament, "8 AOUT 1980. - Loi spéciale de réformes institutionnelles. (NOTE : Consultation des versions antérieures à partir du 13-08-1988 et mise à jour au 01-02-2024)," https://www.ejustice.just.fgov.be/cgi_loi/change_lg.pl?language\=fr\&la\=F\&cn\=1980080802\&table_name\=loi, 1980, accessed: 2024-12-02.

[15] ——, "29 AVRIL 1999. - Loi relative à l'organisation du marché de l'électricité," https://etaamb.openjustice.be/fr/loi-du-29-avril-1999_n1999011160.html, 1999, accessed: 2024-12-02.

[16] Service public fédéral de justice, "22 AVRIL 2019. - Arrêté royal établissant un règlement technique pour la gestion du réseau de transport de l'électricité et l'accès à celui-ci," https://etaamb.openjustice.be/fr/arrete-royal-du-22-avril-2019_n2019012009, 2019, accessed: 2024-12-02.

[17] CREG, "CREG - CODE DE BONNE CONDUITE ÉLECTRICITÉ," https://www.creg.be/sites/default/files/assets/Publications/Decisions/B2409Annex1.pdf, 2022, accessed: 2024-12-02.

[18] Elia, "Section 2.2.2.1. Règles applicables à chaque installation et raccordement au réseau de transport," https://www.elia.be/-/media/project/elia/elia-site/company/legal-framework/legal_framework/belgium/20231123_regles-applicables-a-chaque-installation-et-connexion-au-reseau-de-transport.pdf, 2023, accessed: 2024-12-02.

[19] Synergrid, "GUIDE DU MARCHÉ FLEXIBILITÉ –2.1," https://www.synergrid.be/images/downloads/document_release_2b/2024-Updated_Market_Guide_FLEX_v2.1-FR.pdf, 2024, accessed: 2024-12-02.

[20] ——, "C8-01 (v15) Network Flexibility Study pour la participation des URD à des Services de flexibilité," https://view.officeapps.live.com/op/view.aspx?src=https\%3A\%2F\%2Fwww.synergrid.be\%2Fimages\%2Fdownloads\%2Fdocument_release_2b\%2Fc8-01-fr-20240508-v15.docx\&wdOrigin=BROWSELINK, 2024, accessed: 2024-12-02.

[21] Parlement bruxellois, "8 FEVRIER 2022. - Projet d'ordonnance modifiant l'ordonnance du 19 juillet 2001 relative à l'organisation du marché de l'électricité en Région de BruxellesCapitale, l'ordonnance du 1er avril 2004 relative à l'organisation du marché du gaz en Région de Bruxelles-Capitale, concernant des redevances de voiries en matière de gaz et d'électricité et portant modification de l'ordonnance du 19 juillet 2001 relative à l'organisation du marché de l'électricité en Région de BruxellesCapitale et l'ordonnance du 12 décembre 1991 créant des fonds budgétaires en vue de la transposition de la directive 2018/2001 et de la directive 2019/944," http://weblex.brussels/data/crb/doc/2021-22/144302/images.pdf\#page, 2022, accessed: 2024-12-02.

[22] "Commission regulation (eu) 2017/2195 of 23 november 2017 - establishing a guideline on electricity balancing," 2017.

[23] European Commission, "Communication from the commission to the european parliament, the european council, the council, the european economic and social committee and the committee of the regions - repowereu: Joint european action for more affordable, secure and sustainable energy," 2022. [Online]. Available: https://eur-lex.europa.eu/resource.html?uri\=cellar:71767319-9f0a-11ec-83e1-01aa75ed71a1.0001.02/DOC_1\&format=PDF

[24] ——, "Communication from the commission to the european parliament, the council, the european economic and social committee and the committee of the region - sustainable and smart mobility strategy – putting european transport on track for the future," 2020. [Online]. Available: https://eur-lex.europa.eu/resource.html?uri\=cellar:5e601657-3b06-11eb-b27b-01aa75ed71a1.0001.02/DOC_1\&format\=PDF

[25] ——, "Communication from the commission to the european parliament, the council, the european economic and social committee and the committee of the regions – eu solar energy strategy," 2022. [Online]. Available: https://eur-lex.europa.eu/resource.html?uri\=cellar:516a902d-d7a0-11ec-a95f-01aa75ed71a1.0001.02/DOC_1\&format\=PDF

[26] Elia, "Solar power generation," 2024. [Online]. Available: https://www.elia.be/en/grid-data/generation-data/solar-pv-power-generation-data

[27] Meletiou, A. Vasiljevska, J., Prettico G., Vitiello, S., "Distribution System Operators observatory 2022," 2023.

[28] Council of European Energy Regulators (CEER), "7TH CEER-ECRB BENCHMARKING REPORT ON THE QUALITY OF ELECTRICITY AND GAS SUPPLY," https://www.ceer.eu/wp-content/uploads/2024/04/7th-Benchmarking-Report-2022.pdf, 2022, accessed: 2024-12-02.

[29] Sibelga, "Statistiques 2022," https://www.sibelga.be/asset/file/8febf988-1025-11ee-aac1-005056970ffd, 2022, accessed: 2024-12-02.

[30] N. Jayawarna, M. Lorentzou, and S. Papathanassiou, "Review of earthing in a micro grid," 2004.

[31] B. Li, Y. Li, and T. Ma, "Research on earthing schemes in lv microgrids," in *2011 International Conference on Advanced Power System Automation and Protection*, vol. 2, 2011, pp. 1003–1007.

[32] A. A. Sallam and O. P. Malik, *Earthing of Electric Distribution Systems*. Wiley-IEEE Press, 2019, pp. 73–109.

[33] International Electrotechnical Commission, "IEC 60364 - Electrical installations of buildings," 2009.

[34] S. Haben, S. Arora, G. Giasemidis, M. Voss, and D. Vukadinović Greetham, "Review of low voltage load forecasting: Methods, applications, and recommendations," *Applied Energy*, vol. 304, p. 117798, 2021. [Online]. Available: https://www.sciencedirect.com/science/article/pii/S0306261921011326

[35] Sibelga, "Rapport annuel," https://www.sibelga.be/asset/file/cce59666-2e0e-11ef-ad59-005056970ffd, 2023, accessed: 2024-12-02.

[36] H. de Heer, M. ven der Laan, and A. Saez Armenteros, "Usef: The framework explained," 2021. [Online]. Available: chrome-extension://efaidnbmnnnibpcajpcglclefindmkaj/https://www.usef.energy/app/uploads/2021/05/USEF-The-Framework-Explained-update-2021.pdf

[37] ENTSO-E, "Electricity balancing," 2022, accessed: https://www.entsoe.eu/network_codes/eb/.

[38] Elia, "afrr," accessed: January 2023. https://www.elia.be/en/electricity-market-and-system/system-services/keeping-the-balance/afrr.

[39] D. Zenner, "Elia student challenge presentation over frequency ancillary services considering lv assets," accessed: March 2023.

[40] Elia, "FCR Service Design Note for 2020," April 2019, accessed: 2025-01-27. [Online]. Available: https://www.elia.be/-/media/project/elia/elia-site/electricity-market-and-system---document-library/balancing---balancing-services-and-bsp/2019/2019-design-note-fcr-for-2020.pdf

[41] ——, "BSP Contract FCR - July 2020 (French Version)," June 2020, accessed: 2025-01-27. [Online]. Available: https://www.elia.be/-/media/project/elia/elia-site/electricity-market-and-system---document-library/balancing---balancing-services-and-bsp/2020/20200609_bsp-contract-fcr_jul2020_fr.pdf

[42] ——, "BSP Contract aFRR (French Version)," December 2024, accessed: 2025-01-27. [Online]. Available: https://www.elia.be/-/media/project/elia/elia-site/electricity-market-and-system/system-services/keeping-the-balance/afrr/20241204-bsp-contract-afrr_fr.pdf

[43] ——, "Rules and Processes for FCR," May 2020, accessed: 2025-01-27. [Online]. Available: https://www.elia.be/-/media/project/elia/elia-site/electricity-market-and-system/system-services/keeping-the-balance/20200518_rpp-rules-and-processes-for-fcr_en.pdf

[44] ——, "ICAROS Future Congestion Risk Indicator: Design Note," 2018, accessed: 2025-01-27. [Online]. Available: https://www.elia.be/-/media/project/elia/elia-site/electricity-market-and-system---document-library/congestion-management-and-redispatching/2018/2018-design-note-icaros-future-congestion-risk-indicator.pdf

[45] European Commission, "Commission regulation (EU) 2015/1222 of 24 july 2015 establishing a guideline on capacity allocation and congestion management (text with EEA relevance)," 2015, legislative Body: COM. [Online]. Available: http://data.europa.eu/eli/reg/2015/1222/oj/eng

[46] European Parliament, "Regulation (EU) 2019/943 of the european parliament and of the council of 5 june 2019 on the internal market for electricity (recast) (text with EEA relevance.)," 2019. [Online]. Available: http://data.europa.eu/eli/reg/2019/943/oj/eng

[47] G. Block, P. Henneaux, O. Meylan, C. Negru, and M. Petrelli, "Study on technical and legal definitions of congestions in electricity networks," 2023, accessed: 2024-12-11. [Online]. Available: https://www.acer.europa.eu/sites/default/files/documents/Publications/Study_electricity_networks_congestions_definitions.pdf

[48] ACER, "Demand response and other distributed energy resources: what barriers are holding them back? 2023 Market Monitoring Report," p. 73, 2023.

[49] A. Srivastava, D. Steen, L. A. Tuan, O. Carlson, I. Bouloumpasis, Q.-T. Tran, and L. Lemius, "Development of a DSO support tool for congestion forecast," *IET Generation, Transmission & Distribution*, vol. 15, no. 23, pp. 3345–3359, 2021, _eprint: https://onlinelibrary.wiley.com/doi/pdf/10.1049/gtd2.12266. [Online]. Available: https://onlinelibrary.wiley.com/doi/abs/10.1049/gtd2.12266

[50] A. Srivastava, D. Steen, L. A. Tuan, and O. Carlson, "A congestion forecast framework for distribution systems with high penetration of PVs and PEVs," in *2019 IEEE Milan PowerTech*, 2019-06, pp. 1–6.

[51] S. Alves, M. Bourgeois, and B. Wilkin, "Le décrochage d'onduleur, ce nuisible solaire," nov 2023. [Online]. Available: https://www.renouvelle.be/fr/le-decrochage-onduleur-ce-nuisible-solaire/

[52] DEIP - Dynamic Operating Envelopes Working Group, "Outcomes report," https://arena.gov.au/assets/2022/03/dynamic-operating-envelope-working-group-outcomes-report.pdf, 2022, accessed: 2024-10-17.

[53] Project EDGE, "Project EDGE Overview," https://electrical.eng.unimelb.edu.au/power-energy/projects/project-edge, 2021, accessed: 2024-10-17.

[54] M. Liu, L. Ochoa, P. Wong, and J. Theunissen, "Using opf-based operating envelopes to facilitate residential der services," *IEEE Transactions on Smart Grid*, vol. 13, no. 6, pp. 4494–4504, Nov. 2022.

[55] Bundesnetzagentur, "Bundesnetzagentur launches second consultation on integrating controllable consumer devices into the electricity grid," https://www.bundesnetzagentur.de/SharedDocs/Pressemitteilungen/EN/2023/20230616_Sperrfrist.html, 2023, accessed: 2024-10-17.

[56] ENTSO-E. (2019) TSO-DSO report - an integrated approach to active system management with the focus on TSO-DSO coordination in congestion management and balancing. [Online]. Available: https://eepublicdownloads.blob.core.windows.net/public-cdn-container/clean-documents/Publications/Position\%20papers\%20and\%20reports/TSO-DSO_ASM_2019_190416.pdf.

[57] Eurelectric. (2020) Recommendations on the use of flexibility in distribution networks. [Online]. Available: https://www.eurelectric.org/media/4410/recommendations-on-the-use-of-flexibility-in-distribution-networks_proof-h-86B1B173.pdf

[58] BRUGEL, "Note synthétique partie 2: Méthodologie tarifaire 2025-2029," 2023, accessed: 2025-02-28. [Online]. Available: https://brugel.brussels/publication/document/notype/2023/fr/Note-synthetique-Partie2-methodologie-Structure-tarifaire.pdf

[59] European Union, "Directive (EU) 2024/1711 of the European Parliament and of the Council of 13 June 2024 on common rules for the internal market for electricity and amending Directives (EU) 2018/2001 and (EU) 2019/944 as regards improving the Union's electricity market design," https://eur-lex.europa.eu/legal-content/EN/TXT/PDF/?uri=OJ:L_202401711, 2024, accessed: 2024-12-02.

[60] M. Z. Liu, L. Ochoa, "Project EDGE - Deliverable 1.1: Operating Envelopes Calculation Architecture," https://www.researchgate.net/publication/348176636_Deliverable_11_Operating_Envelopes_Calculation_Architecture, 2021, accessed: 2024-10-17.

[61] W. Ananduta, A. Sanjab, and L. Marques, "Ensuring grid-secure use of distributed flexibility in sequential tso-dso markets," *arXiv preprint*, vol. arXiv:2406.04889, 2024. [Online]. Available: https://arxiv.org/abs/2406.04889

[62] S. Meinecke, L. Thurner, and M. Braun, "Review of steady-state electric power distribution system datasets," *Energies*, vol. 13, no. 18, p. 4826, 2020, number: 18 Publisher: Multidisciplinary Digital Publishing Institute. [Online]. Available: https://www.mdpi.com/1996-1073/13/18/4826

[63] M. A. Khan and B. P. Hayes, "A reduced electrically-equivalent model of the ieee european low voltage test feeder," in *2022 IEEE Power and Energy Society General Meeting (PESGM)*, 2022, pp. 1–5.

[64] M. Srinivas, "Distribution load flows: a brief review," in *2000 IEEE Power Engineering Society Winter Meeting. Conference Proceedings (Cat. No.00CH37077)*, vol. 2, 2000, pp. 942–945 vol.2.

[65] D. Thukaram and H.M. Wijekoon Banda and Jovitha Jerome, "A robust three phase power flow algorithm for radial distribution systems," *Electric Power Systems Research*, vol. 50, no. 3, pp. 227–236, 1999.

[66] C. Cheng and D. Shirmohammadi, "A three-phase power flow method for real-time distribution system analysis," *IEEE Transactions on Power Systems*, vol. 10, no. 2, pp. 671–679, 1995.

[67] P. Garcia, J. Pereira, S. Carneiro, V. da Costa, and N. Martins, "Three-phase power flow calculations using the current injection method," *IEEE Transactions on Power Systems*, vol. 15, no. 2, pp. 508–514, 2000.

[68] J. Mayordomo, M. Izzeddine, S. Martinez, and R. Asensi, "A contribution for three-phase power flows using the current injection method," in *Ninth International Conference on Harmonics and Quality of Power. Proceedings (Cat. No.00EX441)*, vol. 1, 2000, pp. 295–300 vol.1.

[69] L. Sun, Y. Ju, L. Yang, S. Ge, Q. Fang, and J. Wang., "Holomorphic embedding load flow modeling of the three-phase active distribution network," in *2018 International Conference on Power System Technology (POWERCON)*, 2018, pp. 488–495.

[70] S. Boyd and L. Vandenberghe, *Convex Optimization*. Cambridge, UK: Cambridge University Press, 2009.

[71] F. Geth and H. Ergun, "Real-value power-voltage formulations of, and bounds for, three-wire unbalanced optimal power flow," *arXiv*, 2023, preprint.

[72] D. M. Fobes, S. Claeys, F. Geth, and C. Coffrin, "Powermodelsdistribution.jl: An open-source framework for exploring distribution power flow formulations," *Electric Power Systems Research*, vol. 189, p. 106664, 2020. [Online]. Available: http://www.sciencedirect.com/science/article/pii/S0378779620304673

[73] V. Rigoni and A. Keane, "Open-dsopf: an open-source optimal power flow formulation integrated with opendss," in *2020 IEEE Power & Energy Society General Meeting (PESGM)*, 2020, pp. 1–5.

[74] L. Thurner, A. Scheidler, F. Schäfer, J. Menke, J. Dollichon, F. Meier, S. Meinecke, and M. Braun, "pandapower — an open-source python tool for convenient modeling, analysis, and optimization of electric power systems," *IEEE Transactions on Power Systems*, vol. 33, no. 6, pp. 6510–6521, Nov 2018.

[75] J. R. Carson, "Wave propagation in overhead wires with ground return," *Bell System Technical Journal*, vol. 5, p. 539, 1926.

[76] W. H. Kersting and R. K. Green, "Application of carson's equations to the steady-state analysis of distribution feeders," in *IEEE Power System Conference and Exposition*, Phoenix, AZ, March 2011.

[77] G. Kron, "Tensorial analysis of integrated transmission systems, part i: The six basic reference frames," *AIEE Transactions*, vol. 71, 1952.

[78] Prettico, G., Flammini, M. G., Andreadou, N., Vitiello, S., Fulli, G., and Masera, M., "Distribution System Operators observatory 2018," https://https://setis.ec.europa.eu/distribution-system-operators-observatory-2018_en, 2018, accessed: 2023-3-21.

[79] Hitachi, "Network manager adms — hitachi energy," https://www.hitachienergy.com/offering/product-and-system/scada/network-management/network-manager-adms, accessed: 2022-09-29.

[80] Siemens, "Spectrum power advanced distribution management," https://new.siemens.com/global/en/products/energy/energy-automation-and-smart-grid/grid-control/advanced-distribution-management.html, accessed: 2022-09-29.

[81] Schneider Electric, "Adms (advanced distribution management system)," https://www.se.com/ww/en/work/solutions/for-business/electric-utilities/advanced-distribution-management-system-adms/, accessed: 2022-09-29.

[82] Y. Wang, Q. Chen, T. Hong, and C. Kang, "Review of smart meter data analytics: Applications, methodologies, and challenges," *IEEE Transactions on Smart Grid*, vol. 10, no. 3, pp. 3125–3148, 2019.

[83] T. Gneiting and M. Katzfuss, "Probabilistic forecasting," *Annual Review of Statistics and Its Application*, vol. 1, no. 1, pp. 125–151, 2014. [Online]. Available: https://ssrn.com/abstract=2405902

[84] T. Hong and S. Fan, "Probabilistic electric load forecasting: A tutorial review," *International Journal of Forecasting*, vol. 32, no. 3, pp. 914–938, 2016, number: 3. [Online]. Available: https://www.sciencedirect.com/science/article/pii/S0169207015001508

[85] B. Yildiz, J. I. Bilbao, J. Dore, and A. B. Sproul, "Recent advances in the analysis of residential electricity consumption and applications of smart meter data," *Applied Energy*, vol. 208, pp. 402–427, 2017. [Online]. Available: https://www.sciencedirect.com/science/article/pii/S0306261917314265

[86] J. Soenen, A. Yurtman, T. Becker, R. D'hulst, K. Vanthournout, W. Meert, and H. Blockeel, "Scenario generation of residential electricity consumption through sampling of historical data," *Sustainable Energy, Grids and Networks*, vol. 34, p. 100985, 2023. [Online]. Available: https://www.sciencedirect.com/science/article/pii/S2352467722002302

[87] U. H. Ramadhani *et al.*, "Probabilistic load flow analysis of electric vehicle smart charging in unbalanced lv distribution systems with residential photovoltaic generation," *Sustainable Cities and Society*, vol. 72, p. 103043, September 2021, visited on 05/08/2023. [Online]. Available: https://www.sciencedirect.com/science/article/pii/S2210670721003279

[88] J. Widén, M. Shepero, and J. Munkhammar, "Probabilistic load flow for power grids with high pv penetrations using copula-based modeling of spatially correlated solar irradiance," *IEEE Journal of Photovoltaics*, vol. 7, no. 6, pp. 1740–1745, 2017.

[89] Synergrid, "Profils - SLP-SPP-RLP," https://www.synergrid.be/fr/centre-de-documentation/statistiques-et-donnees/profils-slp-spp-rlp, 2024, accessed: 2024-10-17.

[90] U. H. Ramadhani, M. Shepero, J. Munkhammar, J. Widén, and N. Etherden, "Review of probabilistic load flow approaches for power distribution systems with photovoltaic generation and electric vehicle charging," *International Journal of Electrical Power & Energy Systems*, vol. 120, p. 106003, 2020. [Online]. Available: https://www.sciencedirect.com/science/article/pii/S0142061519341730

[91] P. Chen, Z. Chen, and B. Bak-Jensen, "Probabilistic load flow: A review," in *2008 Third International Conference on Electric Utility Deregulation and Restructuring and Power Technologies*, 2008, pp. 1586–1591.

[92] GridLAB-D Team, "Gridlab-d main page," https://gridlab-d.shoutwiki.com/wiki/Main_Page, n.d., accessed: 2025-01-20.

[93] N. Damianakis, G. R. C. Mouli, P. Bauer, and Y. Yu, "Assessing the grid impact of electric vehicles, heat pumps & pv generation in dutch lv distribution grids," *Applied Energy*, vol. 352, December 2023.

[94] R. Gupta, A. Pena-Bello, K. N. Streicher, C. Roduner, Y. Farhat, D. Thöni, M. K. Patel, and D. Parra, "Spatial analysis of distribution grid capacity and costs to enable massive deployment of pv, electric mobility and electric heating," *Applied Energy*, vol. 287, April 2021.

[95] C. Protopapadaki and D. Saelens, "Heat pump and pv impact on residential low-voltage distribution grids as a function of building and district properties," *Applied Energy*, vol. 192, April 2017.

[96] M. F. Dynge, P. C. del Granado, N. Hashemipour, and M. Korpås, "Impact of local electricity markets and peer-to-peer trading on low-voltage grid operations," *Applied Energy*, vol. 301, November 2021.

[97] M. Roos and B. Holthuizen, "Congestion of lv distribution networks by household battery energy storage systems utilized for fcr, afrr and market trading," in *2018 53rd International Universities Power Engineering Conference (UPEC)*, September 2018.

[98] A. Shahsavari *et al.*, "Distribution grid reliability versus regulation market efficiency: An analysis based on micro-pmu data," *IEEE Transactions on Smart Grid*, vol. 8, no. 6, pp. 2916–2925, November 2017.

[99] L. Delchambre, T. Carron, P. Hendrick, H. Almasalma, P. Henneaux, and A. Bathily, "Probabilistic impact analysis of residential batteries providing fcr and afrr on low voltage grid," in *27th International Conference on Electricity Distribution (CIRED 2023)*, vol. 2023, 2023, pp. 2238–2242.

[100] Elia, "Frequency and fcr demand per 10 seconds," accessed: January 2023. https://opendata.elia.be/explore/dataset/ods057/information/.

[101] A. Bolzoni, R. Todd, A. Forsyth, and R. Perini, "Real-time auto-regressive modelling of electric power network frequency," in *IECON 2019 - 45th Annual Conference of the IEEE Industrial Electronics Society*, vol. 1, 2019, pp. 515–520.

[102] W. Bang and J. W. Yoon, "Forecasting the electric network frequency signals on power grid," in *2019 International Conference on Information and Communication Technology Convergence (ICTC)*, 2019, pp. 1218–1223.

[103] M. Dey, D. Wickramarachchi, S. P. Rana, C. V. Simmons, and S. Dudley, "Power grid frequency forecasting from mpmu data using hybrid vector-output lstm network," in *2023 IEEE PES Innovative Smart Grid Technologies Europe (ISGT EUROPE)*, 2023, pp. 1–5.

[104] J. Kruse, B. Schäfer, and D. Witthaut, "Predictability of power grid frequency," *IEEE Access*, vol. 8, pp. 149 435–149 446, 2020.

[105] G. E. P. Box, G. M. Jenkins, and G. C. Reinsel, *Time Series Analysis: Forecasting and Control*. Wiley, 2008.

[106] A. Gomez-Exposito, A. J. Conejo, and C. Canizares, *Electric Energy Systems: Analysis and Operation*. CRC Press, 2017.

[107] M. Merten, F. Rücker, I. Schoeneberger, and D. U. Sauer, "Automatic frequency restoration reserve market prediction: Methodology and comparison of various approaches," *Applied Energy*, vol. 268, p. 114978, June 2020.

[108] F. Nitsch, M. Deissenroth-Uhrig, C. Schimeczek, and V. Bertsch, "Economic evaluation of battery storage systems bidding on day-ahead and automatic frequency restoration reserves markets," *Applied Energy*, vol. 298, p. 117267, September 2021.

[109] E. de Winkel, Z. Lukszo, M. Neerincx, and R. Dobbe, "A review of fairness conceptualizations in electrical distribution grid congestion management," in *IEEE PES ISGT Europe 2024*, 2024.

[110] K. Petrou, M. Liu, A. Procopiou, L. Ochoa, J. Theunissen, and J. Harding, "Operating envelopes for prosumers in lv networks: A weighted proportional fairness approach," in *2020 IEEE PES Innovative Smart Grid Technologies Europe (ISGT-Europe)*, 2020, pp. 579–583.

[111] K. Petrou *et al.*, "Ensuring distribution network integrity using dynamic operating limits for prosumers," *IEEE Transactions on Smart Grid*, vol. 12, no. 5, pp. 3877–3888, Sept. 2021.

[112] B. Liu and J. Braslavsky, "Sensitivity and robustness issues of operating envelopes in unbalanced distribution networks," *IEEE Access*, vol. 10, pp. 92 789–92 798, 2022.

[113] Y. Makarov, C. Loutan, J. Ma, and P. de Mello, "Operational impacts of wind generation on california power systems," *IEEE Transactions on Power Systems*, vol. 24, pp. 1039–1050, 2009.

[114] Y. Makarov, P. Etingov, J. Ma, Z. Huang, and K. Subbarao, "Incorporating uncertainty of wind power generation forecast into power system operation, dispatch, and unit commitment procedures," *IEEE Transactions on Sustainable Energy*, vol. 2, pp. 433–443, 2011.

[115] A. Ulbig and G. Andersson, "On operational flexibility in power systems," in *2012 IEEE Power and Energy Society General Meeting*, 2012.

[116] H. Nosair and F. Bouffard, "Flexibility envelopes for power system operational planning," *IEEE Transactions on Sustainable Energy*, vol. 6, pp. 800–809, 2015.

[117] M. Liu, L. Ochoa, T. Ting, and J. Theunissen, "Bottom-up services and network integrity: The need for operating envelopes," in *CIRED 2021 - The 26th International Conference and Exhibition on Electricity Distribution*, 2021, pp. 1944–1948.

[118] A. Procopiou *et al.*, "Integrated mv-lv network modelling for der studies," in *CIRED 2020 Berlin Workshop (CIRED 2020)*, 2020, pp. 274–277.

[119] B. Liu and J. H. Braslavsky, "Robust dynamic operating envelopes for DER integration in unbalanced distribution networks," *IEEE Transactions on Power Systems*, vol. 39, no. 2, pp. 3921–3936, 2024.

[120] D. K. Molzahn and I. A. Hiskens, *A Survey of Relaxations and Approximations of the Power Flow Equations*. now, 2019.

[121] S. H. Low, "Convex relaxation of optimal power flow—part i: Formulations and equivalence," *IEEE Transactions on Control of Network Systems*, vol. 1, no. 1, pp. 15–27, 2014.

[122] V. Bassi, L. F. Ochoa, T. Alpcan, and C. Leckie, "Deliverables 3b-4: Improved model free operating envelopes and other considerations," https://arena.gov.au/assets/2022/03/dynamic-operating-envelope-working-group-outcomes-report.pdf, 2022, accessed: 2024-10-17.

[123] ——, "Electrical model-free voltage calculations using neural networks and smart meter data," *IEEE Transactions on Smart Grid*, vol. 14, no. 4, pp. 3271–3282, 2023.

[124] C. Zhao, E. Dall'Anese, and S. H. Low, "Optimal power flow in multiphase radial networks with delta connections," in *IREP 2017 Bulk Power Systems Dynamics and Control Symposium, Preprint*, 2017.

[125] S. H. Low, "Convex relaxation of optimal power flow—part ii: Exactness," *IEEE Transactions on Control of Network Systems*, vol. 1, no. 2, pp. 177–189, 2014.

[126] M. Farivar and S. H. Low, "Branch flow model: Relaxations and convexification—part i," *IEEE Transactions on Power Systems*, vol. 28, no. 3, pp. 2554–2564, 2013.

[127] F. Geth and H. Ergun, "Real-value power-voltage formulations of, and bounds for, three-wire unbalanced optimal power flow," *arxiv*, August 2023.

[128] H. Moring and J. Mathieu, "Inexactness of second order cone relaxations for calculating operating envelopes," in *2023 IEEE International Conference on Communications, Control, and Computing Technologies for Smart Grids (SmartGridComm)*, 2023, pp. 1–6.

[129] L. Delchambre, P. Hendrick, P. Henneaux, and H. Almasalma, "Phase imbalance impact on operating envelope for low-voltage distribution grid," in *IEEE PES ISGT Europe 2024*, 2024.

[130] M. Vanin, H. Ergun, R. D'Hulst, K. Vanthournout, and D. V. Hertem, "Analysis and insights from reactive power measurements of low voltage users," in *27th International Conference on Electricity Distribution (CIRED 2023)*, 2023.

[131] Synergrid, "PDG - Flexibilité," https://www.synergrid.be/fr/concertation-du-marche/pdg-flexibilite, 2025. [Online]. Available: https://www.synergrid.be/fr/concertation-du-marche/pdg-flexibilite

[132] Sibelga, "Roadmap smart grid," 2024, accessed: 2025-01-12. [Online]. Available: https://www.sibelga.be/asset/file/477e2536-1781-11ef-81dc-005056970ffd